A UNITED STATES DEPARTMENT OF COMMERCE PUBLICATION

EASTROPAC ATLAS

U.S. DEPARTMENT OF COMMERCE
National Oceanic and Atmospheric Administration
National Marine Fisheries Service

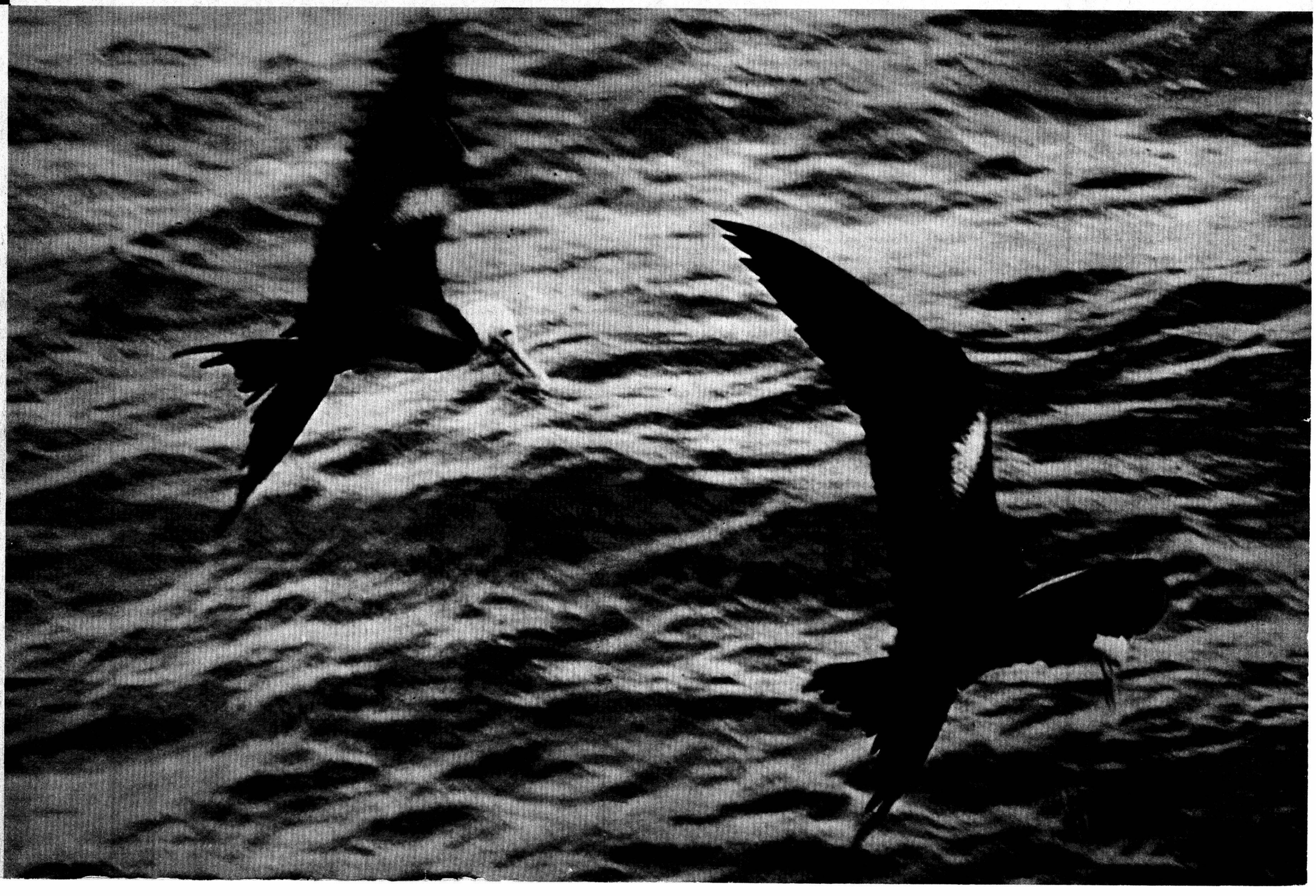

CIRCULAR
330
VOLUME 1
JUNE
1972

EASTROPAC *Atlas*

Volume 1	Physical oceanographic and meteorological data from principal participating ships, first survey cruise, February-March 1967.	Published June 1972
Volume 2	Biological and nutrient chemistry data from principal participating ships, first survey cruise, February-March 1967.	Published April 1971
Volume 3	Physical oceanographic and meteorological data from principal participating ships, first and second monitor cruises, April-July 1967.	Published September 1971
Volume 4	Biological and nutrient chemistry data from principal participating ships, first and second monitor cruises, April-July 1967.	Published November 1970
Volume 5	Physical oceanographic and meteorological data from principal participating ships, second survey cruise, August-September 1967.	In preparation
Volume 6	Biological and nutrient chemistry data from principal participating ships, second survey cruise, August-September 1967.	In preparation
Volume 7	Physical oceanographic and meteorological data from principal participating ships and *Oceanographer,* third and fourth monitor cruises, October 1967-January 1968.	In preparation
Volume 8	Biological and nutrient chemistry data from principal participating ships and *Oceanographer,* third and fourth monitor cruises, October 1967-January 1968.	In preparation
Volume 9	Physical oceanographic and meteorological data from principal participating ships, third survey cruise, February-March 1968.	In preparation
Volume 10	Biological and nutrient chemistry data from principal participating ships, third survey cruise, February-March 1968.	In preparation
Volume 11	Data from Latin American cooperating ships and ships of opportunity, all cruises, February 1967-March 1968.	In preparation

Cover. Immature magnificent frigatebirds near Cocos Island.
Photo by John H. Taylor, Scripps Institution of Oceanography.

ABSTRACT

This atlas contains charts depicting the distribution of physical, chemical, and biological oceanographic properties and associated meteorological properties observed during EASTROPAC. EASTROPAC was an international cooperative investigation of the eastern tropical Pacific Ocean (20° N. to 20° S., and from the west coasts of the American continents to 119° W.) which was intended to provide data necessary for a more effective use of the marine resources of the area, especially tropical tunas, and also to increase knowledge of the ocean circulation, air-sea interaction, and ecology. The Bureau of Commercial Fisheries (now National Marine Fisheries Service) was the coordinating agency. The field work, from February 1967 through March 1968, was divided into seven 2-month cruise periods. During each cruise period one or more ships were operating in the study area.

On completion of the field work the data seemed too numerous for a classical data report. Instead, it was decided to produce an 11-volume atlas of the results, with 5 volumes containing physical oceanographic and meteorological data from the principal participating ships, 5 volumes containing biological and nutrient chemistry data from the same ships, and 1 volume containing all data from Latin American cooperating ships and ships of opportunity. Extensive use was made of a computer and automatic plotter in preparation of the atlas charts. Methods used to collect and process the data upon which the atlas is based are described in detail by the contributors of the following categories of charts: temperature, salinity, and derived quantities; thickness of the upper mixed layer; dissolved oxygen; meteorology; nutrient chemistry; phytoplankton standing stocks and production; zooplankton and fish larvae; micronekton; birds, fish schools, and marine mammals.

U.S. DEPARTMENT OF COMMERCE
National Oceanic and Atmospheric Administration
National Marine Fisheries Service
Fishery-Oceanography Center
8604 La Jolla Shores Drive
P.O. Box 271
La Jolla, California 92037

March 1972

NOTICE TO RECIPIENTS OF THE EASTROPAC ATLAS, VOLUME 1

In an insert in the front of Volume 4, published in November 1970, I informed recipients that the Volume 1 introductory material had been included in Volume 4 so that users would have necessary information about the EASTROPAC Project, processing of the data, and preparation of the atlas in the first volume to be published. I asked the recipients when they received their copy of Volume 1 at a later date to remove the appropriate pages from Volume 4 and insert them into their proper place in Volume 1.

The atlas staff later decided, however, to reprint those Volume 1 pages and include them in their proper place during publication so that this volume will be complete as received. Please disregard my request in the Volume 4 insert.

Cuthbert M. Love
Editor, EASTROPAC Atlas

EASTROPAC *Atlas*

VOLUME 1

ERRATA Number 1

May 1972

INTRODUCTION, page 4.	The table on this page entitled "Abbreviations used in figure designation system" should be labeled as Table 4. It is referred to as such on the preceding page.
FIGURE 11-G-v4.	Caption, second sentence: The clause about dark shading should be deleted. No eastward flow is shown on this section.
FIGURE 12-T-v6.	The contour which intersects the sea surface at latitude 14.8° N. and again at 16.5° N. should be labeled 26°.
FIGURE 12-G-v5.	Caption, second sentence: The clause about dark shading should be deleted. No flow toward northeast is shown on this section.
FIGURE 13-G-v3.	Caption, second sentence: The clause about light shading should be deleted. No southward flow is shown on this section.
FIGURE 13-G-v5.	Caption, second sentence: The clause about light shading should be deleted. No flow toward the northwest is shown on this section.
FIGURE 13-O_2-v3.	The legend "DEPTH (METERS)" should be added along the left edge.

FIGURE 14-O_2-v21. The contours in the depth range 40-140 m. should be labeled as shown below:

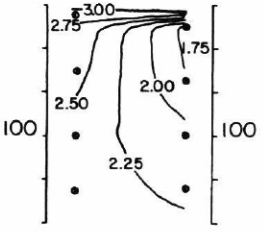

FIGURE 14-O_2-v24. The number zero on the latitude scale should be added.

EASTROPAC Atlas

VOLUME 1

ERRATA Number 2

November 1972

FIGURE 10-O_2Sa-10.	An area of less than 100% saturation centered at 8.5° N., 88° W. should be shaded.
FIGURE 11-T-v5. FIGURE 11-S-v5. FIGURE 11-δ-v5.	The index maps are incorrect. These sections extend only to 13° S. instead of 20° S. as shown.
FIGURE 12-G-v2.	Caption, second sentence: The clause about light shading should be deleted. No flow toward the northwest is shown in this section.

EASTROPAC *Atlas*

VOLUME 7

ERRATA Number 2

December 1973

FIGURE 50-S-v5. The closed heavy contour at a depth of 50-100m in the vicinity of 1°-2°S should be labeled 35.0. The heavy contour which intersects the sea surface at 2.2°N and 4.3°N should be labeled 34.0.

FIGURE 50-S-v6. The heavy contour which intersects the sea surface at 6.8°N and 7.7°N should be labeled 33.0.

FIGURE OP-S-v4. The dot at the sea surface near 10° N is not a contour and should be disregarded.

FIGURE OP-O_2-v1.
FIGURE OP-O_2-v3.
FIGURE OP-O_2-v4. The whole numbered contours (1.00, 2.00, etc.) on these charts have not been accented with heavier lines as is the case with other oxygen sections in this and other volumes.

FIGURE OP-O_2-v1. The contour at the top center of the chart should be labeled 5.50 instead of 55.0.

FIGURE OP-O_2-v3. Some of the contours near the surface are incorrectly labeled. The short contour at the very top, in the vicinity of 2°S should be labeled 5.25. The contour immediately below it should be labeled 5.00. The next contour down (the first one to extend across the whole section) should be labeled 4.75 instead of 4.50.

FIGURE 60-S-v3. The small heavy contour which intersects the sea surface twice in the vicinity of 15.6°N should be labeled 33.5.

VOLUME 1

INTRODUCTION ---- Page 9, Paragraph 2, Line 1 now reads ". . . 20 cm diameter Secchi disc.", this should read ". . . 30 cm diameter Secchi disc."

UNITED STATES DEPARTMENT OF COMMERCE
Peter G. Peterson, *Secretary*

NATIONAL OCEANIC AND ATMOSPHERIC ADMINISTRATION
Robert M. White, *Administrator*

NATIONAL MARINE FISHERIES SERVICE
Philip M. Roedel, *Director*

EASTROPAC ATLAS

VOLUME 1

PHYSICAL OCEANOGRAPHIC AND METEOROLOGICAL DATA FROM
PRINCIPAL PARTICIPATING SHIPS
FIRST SURVEY CRUISE, FEBRUARY-MARCH 1967

CUTHBERT M. LOVE, *Editor*

CIRCULAR 330
WASHINGTON, D.C.
JUNE 1972

For sale by the Superintendent of Documents, U.S. Government Printing Office, Washington, D.C. 20402—Price $4.75 per volume

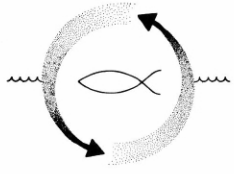

COORDINATOR, EASTROPAC PROJECT

WARREN S. WOOSTER, Scripps Institution of Oceanography, June 27, 1966-May 15, 1967
ALAN R. LONGHURST, National Marine Fisheries Service, May 15, 1967-June 30, 1970

ATLAS CONTRIBUTORS

ELBERT H. AHLSTROM—National Marine Fisheries Service, Fish Larvae
MAURICE BLACKBURN—Scripps Institution of Oceanography, Micronekton
WITOLD L. KLAWE—Inter-American Tropical Tuna Commission, Scombroid Larvae
R. MICHAEL LAURS—National Marine Fisheries Service, Zooplankton, Micronekton, Bird and Mammal Observations
FORREST R. MILLER—Inter-American Tropical Tuna Commission, Meteorology
ROBERT W. OWEN, Jr.—National Marine Fisheries Service, Phytoplankton, Oxygen, Mixed Layer Depth
BRUCE A. TAFT—Scripps Institution of Oceanography, Physical Oceanography
WILLIAM H. THOMAS—Scripps Institution of Oceanography, Nutrient Chemistry
MIZUKI TSUCHIYA—Scripps Institution of Oceanography, Physical Oceanography
BERNT ZEITZSCHEL—Scripps Institution of Oceanography, Phytoplankton

EDITORIAL COMMITTEE

CUTHBERT M. LOVE, National Marine Fisheries Service
BRUCE A. TAFT, Scripps Institution of Oceanography
R. MICHAEL LAURS, National Marine Fisheries Service

National Marine Fisheries Service
Southwest Fisheries Center
La Jolla, California 92037

Scripps Institution of Oceanography
University of California, San Diego
La Jolla, California 92037

Inter-American Tropical Tuna Commission
% Scripps Institution of Oceanography
La Jolla, California 92037

CONTENTS

LIST OF FIGURES

FIGURE 10-AP-8300.—Acceleration potential (j./kg.), relative to 500 db., on the surface where $\delta_\pi = 300$ cl./t., February-March 1967. The heavy dashed line near the coast of Peru, in the vicinity of 15°S., indicates the intersection of this surface with the sea surface. For computing acceleration potential, thermosteric anomaly, δ_T, was used instead of specific volume anomaly, δ.

FIGURE 10-O_2-8300.—Oxygen (ml./l.) on the surface where $\delta_\pi = 300$ cl./t., February-March 1967. The heavy dashed line near the coast of Peru, in the vicinity of 15°S., indicates the intersection of this surface with the sea surface.

FIGURE 10-8250-z.—Depth (m.) of the surface where $\delta_\pi = 250$ cl./t., February-March 1967. The zero contour near the coast of Peru, in the vicinity of 15°S., indicates the intersection of this surface with the sea surface.

FIGURE 10-S-8250.—Salinity (‰) on the surface where $\delta_\pi = 250$ cl./t., February-March 1967. The heavy dashed line near the coast of Peru, in the vicinity of 15°S., indicates the intersection of this surface with the sea surface. The table shows the temperature corresponding to each isohaline on the chart.

FIGURE 10-AP-8250.—Acceleration potential (j./kg.), relative to 500 db., on the surface where $\delta_\pi = 250$ cl./t., February-March 1967. The heavy dashed line near the coast of Peru, in the vicinity of 15° S., indicates the intersection of this surface with the sea surface. For computing acceleration potential, thermosteric anomaly, δ_T, was used instead of specific volume anomaly, δ.

FIGURE 10-O_2-8250.—Oxygen (ml./l.) on the surface where $\delta_\pi = 250$ cl./t., February-March 1967. The heavy dashed line near the coast of Peru, in the vicinity of 15°S., indicates the intersection of this surface with the sea surface.

FIGURE 10-8200-z.—Depth (m.) of the surface where $\delta_\pi = 200$ cl./t., February-March 1967.

FIGURE 10-S-8200.—Salinity (‰) on the surface where $\delta_\pi = 200$ cl./t., February-March 1967. The table shows the temperature corresponding to each isohaline on the chart.

FIGURE 10-AP-8200.—Acceleration potential (j./kg.), relative to 500 db., on the surface where $\delta_\pi = 200$ cl./t., February-March 1967. For computing acceleration potential, thermosteric anomaly, δ_T, was used instead of specific volume anomaly, δ.

FIGURE 10-O_2-8200.—Oxygen (ml./l.) on the surface where $\delta_\pi = 200$ cl./t., February-March 1967.

FIGURE 10-8160-z.—Depth (m.) of the surface where $\delta_\pi = 160$ cl./t., February-March 1967.

FIGURE 10-S-8160.—Salinity (‰) on the surface where $\delta_\pi = 160$ cl./t., February-March 1967. The table shows the temperature corresponding to each isohaline on the chart.

FIGURE 10-AP-8160.—Acceleration potential (j./kg.), relative to 500 db., on the surface where $\delta_\pi = 160$ cl./t., February-March 1967. For computing acceleration potential, thermosteric anomaly, δ_T, was used instead of specific volume anomaly, δ.

FIGURE 10-O_2-8160.—Oxygen (ml./l.) on the surface where $\delta_\pi = 160$ cl./t., February-March 1967.

Meteorology—Blue pages

FIGURE 10-MW-1.—Analyses of the surface air pressure and surface winds from all available ship observations, averaged over 2-degree (latitude-longitude) squares for the period February 1-14, 1967. Heavy dashed lines are isobars. Solid lines are streamlines showing the mean resultant direction of wind flow. Light dash-dot lines are isotachs indicating mean resultant wind speed (kn.). Pressure (mb.) averaged for 5-degree squares is plotted above the mean position of the square, and resultant wind direction followed by speed (kn.) is plotted below. The monthly climatological position of the intertropical convergence zone is shown by a wide dashed band.

FIGURE 10-MW-2.—Analyses of the surface air pressure and surface winds from all available ship observations, averaged over 2-degree (latitude-longitude) squares for the period February 15-28, 1967. Heavy dashed lines are isobars. Solid lines are streamlines showing the mean resultant direction of wind flow. Light dash-dot lines are isotachs indicating mean resultant wind speed (kn.). Pressure (mb.) averaged for 5-degree squares is plotted above the mean position of the square, and resultant wind direction followed by speed (kn.) is plotted below. The monthly climatological position of the intertropical convergence zone is shown by a wide dashed band.

FIGURE 10-MW-3.—Analyses of the surface air pressure and surface winds from all available ship observations, averaged over 2-degree (latitude-longitude) squares for the period March 1-17, 1967. Heavy dashed lines are isobars. Solid lines are streamlines showing the mean resultant direction of wind flow. Light dash-dot lines are isotachs indicating mean resultant wind speed (kn.). Pressure (mb.) averaged for 5-degree squares is plotted above the mean position of the square, and resultant wind direction followed by speed (kn.) is plotted below. The monthly climatological position of the intertropical convergence zone is shown by a wide dashed band.

FIGURE 10-MW-4.—Analyses of the surface air pressure and surface winds from all available ship observations, averaged over 2-degree (latitude-longitude) squares for the period March 18-31, 1967. Heavy dashed lines are isobars. Solid lines are streamlines showing the mean resultant direction of wind flow. Light dash-dot lines are isotachs indicating mean resultant wind speed (kn.). Pressure (mb.) averaged for 5-degree squares is plotted above the mean position of the square, and resultant wind direction followed by speed (kn.) is plotted below. The monthly climatological position of the intertropical convergence zone is shown by a wide dashed band.

FIGURE 10-MT-1.—Analysis of sea surface temperatures based on averages for 2-degree (latitude-longitude) squares from all available ship observations for the period February 1-14, 1967. Solid lines are sea surface isotherms (°C.); the isotherms are dashed where data are sparse. Dark hatching outlines areas with positive temperature anomalies (computed from mean sea surface temperatures averaged over 22 years) greater than 1°C.; light hatching shows areas with negative anomalies greater than 1°C. Sea surface temperature (°C. x 10) averaged for 5-degree squares is plotted above the mean position of the square; sea temperature minus air temperature difference (°C. x 10) is plotted below the symbol.

FIGURE 10-MT-2.—Analysis of sea surface temperatures based on averages for 2-degree (latitude-longitude) squares from all available ship observations for the period February 15-28, 1967. Solid lines are sea surface isotherms (°C.); the isotherms are dashed where data are sparse. Dark hatching outlines areas with positive temperature anomalies (computed from mean sea surface temperatures averaged over 22 years) greater than 1°C.; light hatching shows areas with negative anomalies greater than 1°C. Sea surface temperature (°C. x 10) averaged for 5-degree squares is plotted above the mean position of the square; sea temperature minus air temperature difference (°C. x 10) is plotted below the symbol.

FIGURE 10-MT-3.—Analysis of sea surface temperatures based on averages for 2-degree (latitude-longitude) squares from all available ship observations for the period March 1-17, 1967. Solid lines are sea surface isotherms (°C.); the isotherms are dashed where data are sparse. Dark hatching outlines areas with positive temperature anomalies (computed from mean sea surface temperatures averaged over 22 years) greater than 1°C.; light hatching shows areas with negative anomalies greater than 1°C. Sea surface temperature (°C. x 10) averaged for 5-degree squares is plotted above the mean position of the square; sea temperature minus air temperature difference (°C. x 10) is plotted below the symbol.

FIGURE 10-MT-4.—Analysis of sea surface temperatures based on averages for 2-degree (latitude-longitude) squares from all available ship observations for the period March 18-31, 1967. Solid lines are sea surface isotherms (°C.); the isotherms are dashed where data are sparse. Dark hatching outlines areas with positive temperature anomalies (computed from mean sea surface temperatures averaged over 22 years) greater than 1°C.; light hatching shows areas with negative anomalies greater than 1°C. Sea surface temperature (°C. x 10) averaged for 5-degree squares is plotted above the mean position of the square; sea temperature minus air temperature difference (°C. x 10) is plotted below the symbol.

FIGURE 10-MC-1.—Analyses of the surface dew-point temperature of the air and total cloud cover based on 2-degree (latitude-longitude) averages from all available ship observations for the month of February 1967. Solid lines depict the monthly mean total cloud cover in oktas; the lines are dashed where data are sparse. Dash-dot lines are isotherms of the mean monthly dew-point temperature at 2-degree (C.) intervals. Areas where 15 percent or more of the ships reported rain of any type at or within sight of the ship are shaded. Dew-point temperature (°C. x 10) averaged for 5-degree squares is plotted above the mean position of the square, with total cloud cover (oktas) below and rainfall frequency (%) to the right of the symbol.

FIGURE 10-MC-2.—Analyses of the surface dew-point temperature of the air and total cloud cover based on 2-degree (latitude-longitude) averages from all available ship observations for the month of March 1967. Solid lines depict the monthly mean total cloud cover in oktas; the lines are dashed where data are sparse. Dash-dot lines are isotherms of the mean monthly dew-point temperature at 2-degree (C.) intervals. Areas where 15 percent or more of the ships reported rain of any type at or within sight of the ship are shaded. Dew-point temperature (°C. x 10) averaged for 5-degree squares is plotted above the mean position of the square, with total cloud cover (oktas) below and rainfall frequency (%) to the right of the symbol.

Temperature and salinity—White pages

FIGURE 11-T-v1.—Vertical distribution of temperature (°C.) along 119° W. from 28°36′ N. to 6°21′ S., January 25-February 9, 1967. The data from Stations 1-24 were not calibrated against Nansen cast data.

FIGURE 11-T-v2.—Vertical distribution of temperature (°C.) along 119° W. from 1°14′ S. to 20°00′ S., February 7-14, 1967.

FIGURE 11-T-v3.—Vertical distribution of temperature (°C.) along 20° S., February 14-16, 1967.

FIGURE 11-T-v4.—Vertical distribution of temperature (°C.) along 126° W. from 19°59′ S. to 6°38′ S., February 16-21, 1967.

FIGURE 11-T-v5.—Vertical distribution of temperature (°C.) along 126° W. from 12°42′ S. to 22°33′ N., February 19-March 3, 1967.

FIGURE 11-S-v1.—Vertical distribution of salinity (‰) along 119° W. from 28°36′ N. to 6°21′ S., January 25-February 9, 1967. The data from Stations 1-24 were not calibrated against Nansen cast data.

FIGURE 11-S-v2.—Vertical distribution of salinity (‰) along 119° W. from 1°14′ S. to 20°00′ S., February 7-14, 1967.

FIGURE 11-S-v3.—Vertical distribution of salinity (‰) along 20° S., February 14-16, 1967.

FIGURE 11-S-v4.—Vertical distribution of salinity (‰) along 126° W. from 19°59′ S. to 6°38′ S., February 16-21, 1967.

FIGURE 11-S-v5.—Vertical distribution of salinity (‰) along 126° W. from 12°42′ S. to 22°33′ N., February 19-March 3, 1967.

Thermosteric anomaly and geostrophic velocity—Yellow pages

FIGURE 11-δ-v1.—Vertical distribution of thermosteric anomaly, δ_T, (cl./t.) along 119° W. from 28°36′ N. to 6° 21′ S., January 25-February 9, 1967. The temperature and salinity data from stations 1-24 were not calibrated against Nansen cast data.

FIGURE 11-δ-v2.—Vertical distribution of thermosteric anomaly, δ_T, (cl./t.) along 119° W. from 1°14′ S. to 20°00′ S., February 7-14, 1967.

FIGURE 11-δ-v3.—Vertical distribution of thermosteric anomaly, δ_T, (cl./t.) along 20° S., February 14-16, 1967.

FIGURE 11-δ-v4.—Vertical distribution of thermosteric anomaly, δ_T, (cl./t.) along 126° W. from 19°59′ S. to 6°38′ S., February 16-21, 1967.

FIGURE 11-δ-v5.—Vertical distribution of thermosteric anomaly, δ_T, (cl./t.) along 126° W. from 12°42′ S. to 22°33′ N., February 19-March 3, 1967.

FIGURE 11-G-v1.—Vertical distribution of the zonal component of geostrophic velocity (cm./sec.), relative to 500 db., along 119° W. from 20°00′ N. to 6°21′ S., January 28-February 9, 1967. Dark shading indicates eastward flow with a velocity greater than 5 cm./sec.; light shading indicates westward flow with a velocity greater than 5 cm./sec.

FIGURE 11-G-v2.—Vertical distribution of the zonal component of geostrophic velocity (cm./sec.), relative to 500 db., along 119° W. from 1°14′ S. to 20°00′ S., February 7-14, 1967. Dark shading indicates eastward flow with a velocity greater than 5 cm./sec.; light shading indicates westward flow with a velocity greater than 5 cm./sec.

FIGURE 11-G-v3.—Vertical distribution of the meridional component of geostrophic velocity (cm./sec.), relative to 500 db., along 20° S., February 14-16, 1967. Dark shading indicates northward flow with a velocity greater than 5 cm./sec.; light shading indicates southward flow with a velocity greater than 5 cm./sec.

FIGURE 11-G-v4.—Vertical distribution of the zonal component of geostrophic velocity (cm./sec.), relative to 500 db., along 126° W. from 19°59′ S. to 6°38′ S., February 16-21, 1967. Dark shading indicates eastward flow with a velocity greater than 5 cm./sec.; light shading indicates westward flow with a velocity greater than 5 cm./sec.

FIGURE 11-G-v5.—Vertical distribution of the zonal component of geostrophic velocity (cm./sec.), relative to 500 db., along 126° W. from 12°42′ S. to 20°01′ N., February 19-March 2, 1967. Dark shading indicates eastward flow with a velocity greater than 5 cm./sec.; light shading indicates westward flow with a velocity greater than 5 cm./sec.

Oxygen—Green pages

FIGURE 11-O_2-v1.—Vertical distribution of oxygen (ml./l.) along 119° W. from 20°00′ N. to 6°21′ S., January 28-February 9, 1967.

FIGURE 11-O_2-v2.—Vertical distribution of oxygen (ml./l.) along 119° W. from 1°14′ S. to 20°00′ S., February 7-14, 1967.

FIGURE 11-O_2-v3.—Vertical distribution of oxygen (ml./l.) along 20° S., February 14-16, 1967.

FIGURE 11-O_2-v4.—Vertical distribution of oxygen (ml./l.) along 126° W. from 19°59′ S. to 6°38′ S., February 16-21, 1967.

FIGURE 11-O_2-v5.—Vertical distribution of oxygen (ml./l.) along 126° W. from 12°42′ S. to 20°01′ N., February 19-March 2, 1967.

Temperature and salinity—White pages

FIGURE 12-T-v1.—Vertical distribution of temperature (°C.) along a section from 29° N. near the coast of Baja California to 12° N., 112° W., February 8-12, 1967. These data were not calibrated against Nansen cast data.

FIGURE 12-T-v2.—Vertical distribution of temperature (°C.) along a section from 12° N., 112° W. to Manzanillo, February 12-16, 1967.

FIGURE 12-T-v3.—Vertical distribution of temperature (°C.) along a section from Acapulco to 12° N., 105° W., February 19-21, 1967.

FIGURE 12-T-v4.—Vertical distribution of temperature (°C.) along 105° W., February 21-March 6, 1967.

FIGURE 12-T-v5.—Vertical distribution of temperature (°C.) along a southeast-northwest section from 20° S., 105° W. to 10° S., 112° W., March 6-9, 1967.

FIGURE 12-T-v6.—Vertical distribution of temperature (°C.) along 112° W., March 9-21, 1967.

FIGURE 12-S-v1.—Vertical distribution of salinity (‰) along a section from 29° N. near the coast of Baja California to 12° N., 112° W., February 8-12, 1967. These data were not calibrated against Nansen cast data.

FIGURE 12-S-v2.—Vertical distribution of salinity (‰) along a section from 12° N., 112° W. to Manzanillo, February 12-16, 1967.

FIGURE 12-S-v3.—Vertical distribution of salinity (‰) along a section from Acapulco to 12° N., 105° W., February 19-21, 1967.

FIGURE 12-S-v4.—Vertical distribution of salinity (‰) along 105° W., February 21-March 6, 1967.

FIGURE 12-S-v5.—Vertical distribution of salinity (‰) along a southeast-northwest section from 20° S., 105° W. to 10° S., 112° W., March 6-9, 1967.

FIGURE 12-S-v6.—Vertical distribution of salinity (‰) along 112° W., March 9-21, 1967.

Thermosteric anomaly and geostrophic velocity—Yellow pages

FIGURE 12-δ-v1.—Vertical distribution of thermosteric anomaly, δ_T, (cl./t.) along a section from 29° N. near the coast of Baja California to 12° N., 112° W., February 8-12, 1967. The temperature and salinity data from these stations were not calibrated against Nansen cast data.

FIGURE 12-δ-v2.—Vertical distribution of thermosteric anomaly, δ_T, (cl./t.) along a section from 12° N., 112° W. to Manzanillo, February 12-16, 1967.

FIGURE 12-δ-v3.—Vertical distribution of thermosteric anomaly, δ_T, (cl./t.) along a section from Acapulco to 12° N., 105° W., February 19-21, 1967.

FIGURE 12-δ-v4.—Vertical distribution of thermosteric anomaly, δ_T, (cl./t.) along 105° W., February 21-March 6, 1967.

FIGURE 12-δ-v5.—Vertical distribution of thermosteric anomaly, δ_T, (cl./t.) along a southeast-northwest section from 20° S., 105° W. to 10° S., 112° W., March 6-9, 1967.

FIGURE 12-δ-v6.—Vertical distribution of thermosteric anomaly, δ_T, (cl./t.) along 112° W., March 9-12, 1967.

FIGURE 12-G-v2.—Vertical distribution of the component of geostrophic velocity (cm./sec.), relative to 500 db., normal to a section from 12° N., 112° W. to Manzanillo, February 12-16, 1967. Dark shading indicates flow toward the southeast with a velocity greater than 5 cm./sec.; light shading indicates flow toward the northwest with a velocity greater than 5 cm./sec.

FIGURE 12-G-v3.—Vertical distribution of the component of geostrophic velocity (cm./sec.), relative to 500 db., normal to a section from Acapulco to 12° N., 105° W., February 19-21, 1967. Dark shading indicates flow toward the southeast with a velocity greater than 5 cm./sec.; light shading indicates flow toward the northwest with a velocity greater than 5 cm./sec.

FIGURE 12-G-v4.—Vertical distribution of the zonal component of geostrophic velocity (cm./sec.), relative to 500 db., along 105° W., February 21-March 6, 1967. Dark shading indicates eastward flow with a velocity greater than 5 cm./sec.; light shading indicates westward flow with a velocity greater than 5 cm./sec.

FIGURE 12-G-v5.—Vertical distribution of the component of geostrophic velocity (cm./sec.), relative to 500 db., normal to a section from 20° S., 105° W. to 10° S., 112° W., March 6-9, 1967. Dark shading indicates flow toward the northeast with a velocity greater than 5 cm./sec.; light shading indicates flow toward the southwest with a velocity greater than 5 cm./sec.

FIGURE 12-G-v6.—Vertical distribution of the zonal component of geostrophic velocity (cm./sec.), relative to 500 db., along 112° W., March 9-21, 1967. Dark shading indicates eastward flow with a velocity greater than 5 cm./sec.; light shading indicates westward flow with a velocity greater than 5 cm./sec.

Oxygen—Green pages

FIGURE 12-O_2-v2.—Vertical distribution of oxygen (ml./l.) along a section from 12° N., 112° W. to Manzanillo, February 12-16, 1967.

FIGURE 12-O_2-v3.—Vertical distribution of oxygen (ml./l.) along a section from Acapulco to 12° N., 105° W., February 19-21, 1967.

FIGURE 12-O_2-v4.—Vertical distribution of oxygen (ml./l.) along 105° W., February 21-March 6, 1967.

FIGURE 12-O_2-v6.—Vertical distribution of oxygen (ml./l.) along 112° W., March 9-21, 1967.

Temperature and salinity—White pages

FIGURE 13-T-v1.—Vertical distribution of temperature (°C.) along 88° W., February 1-4, 1967. These contours are based on STD data read from analog traces.

FIGURE 13-T-v2.—Vertical distribution of temperature (°C.) along 92° W., February 7-21, 1967. These contours are based on STD data read from analog traces.

FIGURE 13-T-v3.—Vertical distribution of temperature (°C.) along 20° S., February 21-23, 1967. These contours are based on STD data read from analog traces.

FIGURE 13-T-v4.—Vertical distribution of temperature (°C.) along 98° W., February 23-March 8, 1967. These contours are based on STD data read from analog traces.

FIGURE 13-T-v5.—Vertical distribution of temperature (°C.) along a section from Acapulco to 12° N., 105° W., March 13-15, 1967. These contours are based on STD data read from analog traces.

FIGURE 13-T-v6.—Vertical distribution of temperature (°C.) along 95° W., March 17-20, 1967. These contours are based on STD data read from analog traces.

FIGURE 13-S-v1.—Vertical distribution of salinity (‰) along 88° W., February 1-4, 1967. These contours are based on STD data read from analog traces.

FIGURE 13-S-v2.—Vertical distribution of salinity (‰) along 92° W., February 7-21, 1967. These contours are based on STD data read from analog traces.

FIGURE 13-S-v3.—Vertical distribution of salinity (‰) along 20° S., February 21-23, 1967. These contours are based on STD data read from analog traces.

FIGURE 13-S-v4.—Vertical distribution of salinity (‰) along 98° W., February 23-March 8, 1967. These contours are based on STD data read from analog traces.

FIGURE 13-S-v5.—Vertical distribution of salinity (‰) along a section from Acapulco to 12° N., 105° W., March 13-15, 1967. These contours are based on STD data read from analog traces.

FIGURE 13-S-v6.—Vertical distribution of salinity (‰) along 95° W., March 17-20, 1967. These contours are based on STD data read from analog traces.

Thermosteric anomaly and geostrophic velocity—Yellow pages

FIGURE 13-δ-v1.—Vertical distribution of thermosteric anomaly, $\delta_{s,t}$ (cl./t.) along 88° W., February 1-4, 1967. These contours are based on STD data read from analog traces.

FIGURE 13-δ-v2.—Vertical distribution of thermosteric anomaly, $\delta_{s,t}$ (cl./t.) along 92° W., February 7-21, 1967. These contours are based on STD data read from analog traces.

FIGURE 13-δ-v3.—Vertical distribution of thermosteric anomaly, $\delta_{s,t}$ (cl./t.) along 20° S., February 21-23, 1967. These contours are based on STD data read from analog traces.

FIGURE 13-δ-v4.—Vertical distribution of thermosteric anomaly, $\delta_{s,t}$ (cl./t.) along 98° W., February 23-March 8, 1967. These contours are based on STD data read from analog traces.

FIGURE 13-δ-v5.—Vertical distribution of thermosteric anomaly, $\delta_{s,t}$ (cl./t.) along a section from Acapulco to 12° N., 105° W., March 13-15, 1967. These contours are based on STD data read from analog traces.

FIGURE 13-δ-v6.—Vertical distribution of thermosteric anomaly, $\delta_{s,t}$ (cl./t.) along 95° W., March 17-20, 1967. These contours are based on STD data read from analog traces.

FIGURE 13 G-v1.—Vertical distribution of the zonal component of geostrophic velocity (cm./sec.), relative to 500 db., along 88° W., February 1-4, 1967. Dark shading indicates eastward flow with a velocity greater than 5 cm./sec.; light shading indicates westward flow with a velocity greater than 5 cm./sec.

FIGURE 13-G-v2.—Vertical distribution of the zonal component of geostrophic velocity (cm./sec.), relative to 500 db., along 92° W., February 7-21, 1967. Dark shading indicates eastward flow with a velocity greater than 5 cm./sec.; light shading indicates westward flow with a velocity greater than 5 cm./ sec.

FIGURE 13-G-v3.—Vertical distribution of the meridional component of geostrophic velocity (cm./sec.), relative to 500 db., along 20° S., February 21-23, 1967. Dark shading indicates northward flow with a velocity greater than 5 cm./sec.; light shading indicates southward flow with a velocity greater than 5 cm./sec.

FIGURE 13-G-v4.—Vertical distribution of the zonal component of geostrophic velocity (cm./sec.), relative to 500 db., along 98° W., February 23-March 8, 1967. Dark shading indicates eastward flow with a velocity greater than 5 cm./sec.; light shading indicates westward flow with a velocity greater than 5 cm./sec.

FIGURE 13-G-v5.—Vertical distribution of the component of geostrophic velocity (cm./sec.), relative to 500 db., normal to a section from Acapulco to 12° N., 105° W., March 13-15, 1967. Dark shading indicates flow toward the southeast with a velocity greater than 5 cm./sec.; light shading indicates flow toward the northwest with a velocity greater than 5 cm./sec.

FIGURE 13-G-v6.—Vertical distribution of the zonal component of geostrophic velocity (cm./sec.), relative to 500 db., along 95° W., March 17-20, 1967. Dark shading indicates eastward flow with a velocity greater than 5 cm./sec.; light shading indicates westward flow with a velocity greater than 5 cm./sec.

Oxygen—Green pages

FIGURE 13-O_2-v1.—Vertical distribution of oxygen (ml./l.) along 88° W., February 1-4, 1967.

FIGURE 13-O_2-v2.—Vertical distribution of oxygen (ml./l.) along 92° W., February 7-21, 1967.

FIGURE 13 O_2-v3.—Vertical distribution of oxygen (ml./l.) along 20° S., February 21-23, 1967.

FIGURE 13-O_2-v4.—Vertical distribution of oxygen (ml./l.) along 98° W., February 23-March 8, 1967.

FIGURE 13-O_2-v5.—Vertical distribution of oxygen (ml./l.) along a section from Acapulco to 12° N., 105° W., March 13-15, 1967.

FIGURE 13 O_2-v6.—Vertical distribution of oxygen (ml./l.) along 95° W., March 17-20, 1967.

Meteorology—Blue pages

FIGURE 13-UA-v2.—Vertical section of the atmosphere along 92° W., February 8-22, 1967. Solid lines are isotherms of air temperature (°C.) Dashed lines are isopleths of mixing ratio of the air (g./kg.). Surface air temperature is plotted above surface mixing ratio and below a base line representing the surface pressure (mb.) The computed height (m.) of each standard pressure surface is plotted for the northernmost radiosonde station of the section. At other stations the difference of computed height minus the corresponding height at the northern station is shown at each standard level.

FIGURE 13-UA-v4.—Vertical section of the atmosphere along 98° W., February 23-March 8, 1967. Solid lines are isotherms of air temperature (°C.). Dashed lines are isopleths of mixing ratio of the air (g./kg.). Surface air temperature is plotted above surface mixing ratio and below a base line representing the surface pressure (mb.) The computed height (m.) of each standard pressure surface is plotted for the northernmost radiosonde station of the section. At other stations the difference of computed height minus the corresponding height at the northern station is shown at each standard level.

FIGURE 13-UA-v5.—Vertical section of the atmosphere along a line from Acapulco to 12° N., 105 W., March 9 and 13-15, 1967. Solid lines are isotherms of air temperature (°C.). Dashed lines are isopleths of mixing ratio of the air (g./kg.). Surface air temperature is plotted above surface mixing ratio and below a base line representing the surface pressure (mb.). The computed height (m.) of each standard pressure surface is plotted for the northernmost radiosonde station of the section. At other stations the difference of computed height minus the corresponding height at the northern station is shown at each standard level.

FIGURE 13-UA-v6.—Vertical section of the atmosphere along 95° W., March 16-20, 1967. Solid lines are isotherms of air temperature (°C.). Dashed lines are isopleths of mixing ratio of the air (g./kg.). Surface air temperature is plotted above surface mixing ratio and below a base line representing the surface pressure (mb.). The computed height (m.) of each standard pressure surface is plotted for the northernmost radiosonde station of the section. At other stations the difference of computed height minus the corresponding height at the northern station is shown at each standard level.

Temperature and salinity—White pages

FIGURE 14-T-v1.—Vertical distribution of temperature (°C.) along a southwest-northeast section in the northern portion of the Panama Bight from 79°44′ W. to 78°43′ W., January 31, 1967. These contours are based on STD data read principally from analog traces.

FIGURE 14-T-v2.—Vertical distribution of temperature (°C.) along a section in the Panama Bight near the coasts of Panama and Colombia from 7°35′ N. to 6°58′ N., January 31-February 1, 1967. These contours are based on STD data read principally from analog traces.

FIGURE 14-T-v3.—Vertical distribution of temperature (°C.) along northeast-southwest section in the Panama Bight from the coast of Colombia to 5°43′ N., 79°22′ W., February 1, 1967. These contours are based on STD read principally from analog traces.

FIGURE 14-T-v4.—Vertical distribution of temperature (°C.) along a northwest-southeast section in the central portion of the Panama Bight from 5°43′ N., 79°22′ W. to the coast of Colombia, February 1-2, 1967. These contours are based on STD data read principally from analog traces.

FIGURE 14-T-v5.—Vertical distribution of temperature (°C.) along a section in the Panama Bight near the coast of Colombia from 4°10′ N. to 2°45′ N., February 2-3, 1967. These contours are based on STD data read principally from analog traces.

FIGURE 14-T-v6.—Vertical distribution of temperature (°C.) along a southeast-northwest section across the Panama Bight from the coast of Colombia to Peninsula de Azuero, Panama, February 3-5, 1967. These contours are based on STD data read principally from analog traces.

FIGURE 14-T-v7.—Vertical distribution of temperature (°C.) along a northeast-southwest section from Isla Coiba, Panama to 5°03′ N., 82°18′ W., February 5-6, 1967. These contours are based on STD data read principally from analog traces.

FIGURE 14-T-v8.—Vertical distribution of temperature (°C.) along a northwest-southeast section from 5°03′ N., 82°18′ W. to the coast of Ecuador, February 6-8, 1967. These contours are based on STD data read principally from analog traces.

FIGURE 14-T-v9.—Vertical distribution of temperature (°C.) along the Equator from the coast of Ecuador to 81°54′ W., February 8-9, 1967. These contours are based on STD data read principally from analog traces.

FIGURE 14-T-v10.—Vertical distribution of temperature (°C.) along 82° W. from 0°18′ S. to 7°27′ S., February 9-11, 1967. These contours are based on STD data read principally from analog traces.

FIGURE 14-T-v11.—Vertical distribution of temperature (°C.) along 7°15′ S. from 81°50′ W. to the coast of Peru, February 11-12, 1967. These contours are based on STD data read principally from analog traces.

FIGURE 14-T-v12.—Vertical distribution of temperature (°C.) along a northeast-southwest section from the coast of Peru to 11° S., 81°46′ W., February 13-14, 1967. These contours are based on STD data read principally from analog traces.

FIGURE 14-T-v13.—Vertical distribution of temperature (°C.) along 81°46′ W. from 11°02′ S. to 14°37′ S., February 14-15, 1967. These contours are based on STD data read principally from analog traces.

FIGURE 14-T-v14.—Vertical distribution of temperature (°C.) along 15° S. from 81°46′ W. to the coast of Peru, February 15-17, 1967. These contours are based on STD data read principally from analog traces.

FIGURE 14-T-v15.—Vertical distribution of temperature (°C.) along the coast of Peru from 15°07′ S. to 12°27′ S., February 17-24, 1967. These contours are based on STD data read principally from analog traces.

FIGURE 14-T-v16.—Vertical distribution of temperature (°C.) along a northeast-southwest section from the coast of Peru to 14°30′ S., 81°43′ W., February 24-25, 1967. These contours are based on STD data read principally from analog traces.

FIGURE 14-T-v17.—Vertical distribution of temperature (°C.) along 14°30′ S. from 81°43′ W. to 88°17′ W., February 25-27, 1967. These contours are based on STD data read principally from analog traces.

FIGURE 14-T-v18.—Vertical distribution of temperature (°C.) along 88°46′ W., February 27-March 4, 1967. These contours are based on STD data read principally from analog traces.

FIGURE 14-T-v19.—Vertical distribution of temperature (°C.) along 92° W., west of the Galapagos Islands, March 8-9, 1967. These contours are based on STD data read principally from analog traces.

FIGURE 14-T-v20.—Vertical distribution of temperature (°C.) along a section north of the Galapagos Islands, from 0°16′ N., 91°47′ W. to 2°01′ N., 90°03′ W., March 9-10, 1967. These contours are based on STD data read principally from analog traces.

FIGURE 14-T-v21.—Vertical distribution of temperature (°C.) along a section northeast of the Galapagos Islands, from 2°01′ N., 90°03′ W. to the Equator at 89°03′ W., March 11, 1967. These contours are based on STD data read principally from analog traces.

FIGURE 14-T-v22.—Vertical distribution of temperature (°C.) along a southwest-northeast section from the Equator at 89°03′ W. to Puntarenas, March 11-15, 1967. These contours are based on STD data read principally from analog traces.

FIGURE 14-T-v23.—Vertical distribution of temperature (°C.) along a northeast-southwest section from the coast of Costa Rica to 3°52′ N., 85°57′ W., March 18-20, 1967. These contours are based on STD data read principally from analog traces.

FIGURE 14-T-v24.—Vertical distribution of temperature (°C.) along 86°19′ W., March 20-25, 1967. These contours are based on STD data read principally from analog traces.

FIGURE 14-T-v25.—Vertical distribution of temperature (°C.) along 12° S., March 25-26, 1967. These contours are based on STD data read principally from analog traces.

FIGURE 14-T-v26.—Vertical distribution of temperature (°C.) along 84° W., March 26-31, 1967. These contours are based on STD data read principally from analog traces.

FIGURE 14-T-v27.—Vertical distribution of temperature (°C.) along a southwest-northeast section from 3°45′ N., 83°48′ W. to Punta Burica, Costa Rica-Panama, March 31-April 2, 1967. These contours are based on STD data read principally from analog traces.

FIGURE 14-T-v28.—Vertical distribution of temperature (°C.) along the coast of Panama from 82°50′ W. to 81°28′ W., April 2, 1967. These contours are based on STD data read principally from analog traces.

FIGURE 14-T-v29.—Vertical distribution of temperature (°C.) along the coast of Panama from 81°28′ W. to 79°38′ W., April 2-3, 1967. These contours are based on STD data read principally from analog traces.

FIGURE 14-S-v1.—Vertical distribution of salinity (‰) along a southwest-northeast section in the northern portion of the Panama Bight from 79°44′ W. to 78°43′ W., January 31, 1967. These contours are based on STD data read principally from analog traces.

FIGURE 14-S-v2.—Vertical distribution of salinity (‰) along a section in the Panama Bight near the coasts of Panama and Colombia from 7°35′ N. to 6°58′ N., January 31-February 1, 1967. These contours are based on STD data read principally from analog traces.

FIGURE 14-S-v3.—Vertical distribution of salinity (‰) along a northeast-southwest section in the Panama Bight from the coast of Colombia to 5°43′ N., 79°22′ W., February 1, 1967. These contours are based on STD data read principally from analog traces.

FIGURE 14-S-v4.—Vertical distribution of salinity (‰) along a northwest-southeast section in the central portion of the Panama Bight from 5°43′ N., 79°22′ W. to the coast of Colombia, February 1-2, 1967. These contours are based on STD data read principally from analog traces.

FIGURE 14-S-v5.—Vertical distribution of salinity (‰) along a section in the Panama Bight near the coast of Colombia from 4°10′ N. to 2°45′ N., February 2-3, 1967. These contours are based on STD data read principally from analog traces.

FIGURE 14-S-v6.—Vertical distribution of salinity (‰) along a southeast-northwest section across the Panama Bight from the coast of Colombia to Peninsula de Azuero, Panama, February 3-5, 1967.

FIGURE 14-S-v7.—Vertical distribution of salinity (‰) along a northeast-southwest section from Isla Coiba, Panama to 5°03′ N., 82°18′ W., February 5-6, 1967. These contours are based on STD data read principally from analog traces.

FIGURE 14-S-v8.—Vertical distribution of salinity (‰) along a northwest-southeast section from 5°03′ N., 82°18′ W. to the coast of Ecuador, February 6-8, 1967. These contours are based on STD data read principally from analog traces.

FIGURE 14-S-v9.—Vertical distribution of salinity (‰) along the Equator from the coast of Ecuador to 81°54′ W., February 8-9, 1967. These contours are based on STD data read principally from analog traces.

FIGURE 14-S-v10.—Vertical distribution of salinity (‰) along 82° W. from 0°18′ S. to 7°27′ S., February 9-11, 1967. These contours are based on STD data read principally from analog traces.

FIGURE 14-S-v11.—Vertical distribution of salinity (‰) along 7°15′ S. from 81°50′ W. to the coast of Peru, February 11-12, 1967. These contours are based on STD data read principally from analog traces.

FIGURE 14-S-v12.—Vertical distribution of salinity (‰) along a northeast-southwest section from the coast of Peru to 11° S., 81°46′ W., February 13-14, 1967. These contours are based on STD data read principally from analog traces.

FIGURE 14-S-v13.—Vertical distribution of salinity (‰) along 81°46′ W. from 11°02′ S. to 14°37′ S., February 14-15, 1967. These contours are based on STD data read principally from analog traces.

FIGURE 14-S-v14.—Vertical distribution of salinity (‰) along 15° S. from 81°46′ W. to the coast of Peru, February 15-17, 1967. These contours are based on STD data read principally from analog traces.

FIGURE 14-S-v15.—Vertical distribution of salinity (‰) along the coast of Peru from 15°07′ S. to 12°27′ S., February 17-24, 1967. These contours are based on STD data read principally from analog traces.

FIGURE 14-S-v16.—Vertical distribution of salinity (‰) along a northeast-southwest section from the coast of Peru to 14°30′ S., 81°43′ W., February 24-25, 1967. These contours are based on STD data read principally from analog traces.

FIGURE 14-S-v17.—Vertical distribution of salinity (‰) along 14°30′ S. from 81°43′ W. to 88°17′ W., February 25-27, 1967. These contours are based on STD data read principally from analog traces.

FIGURE 14-S-v18.—Vertical distribution of salinity (‰) along 88°46′ W., February 27-March 4, 1967. These contours are based on STD data read principally from analog traces.

FIGURE 14-S-v19.—Vertical distribution of salinity (‰) along 92° W., west of the Galapagos Islands, March 8-9, 1967. These contours are based on STD data read principally from analog traces.

FIGURE 14-S-v20.—Vertical distribution of salinity (‰) along a section north of the Galapagos Islands, from 0°16′ N., 91°47′ W. to 2°01′ N., 90°03′ W., March 9-10, 1967. These contours are based on STD data read principally from analog traces.

FIGURE 14-S-v21.—Vertical distribution of salinity (‰) along a section northeast of the Galapagos Islands, from 2°01′ N., 90°03′ W. to the Equator at 89°03′ W., March 11, 1967. These contours are based on STD data read principally from analog traces.

FIGURE 14-S-v22.—Vertical distribution of salinity (‰) along a southwest-northeast section from the Equator at 89°03′ W. to Puntarenas, March 11-15, 1967. These contours are based on STD data read principally from analog traces.

FIGURE 14-S-v23.—Vertical distribution of salinity (‰) along a northeast-southwest section from the coast of Costa Rica to 3°52′ N., 85°57′ W., March 18-20, 1967. These contours are based on STD data read principally from analog traces.

FIGURE 14-S-v24.—Vertical distribution of salinity (‰) along 86°19′ W., March 20-25, 1967. These contours are based on STD data read principally from analog traces.

FIGURE 14-S-v25.—Vertical distribution of salinity (‰)along 12° S., March 25-26, 1967. These contours are based on STD data read principally from analog traces.

FIGURE 14-S-v26.—Vertical distribution of salinity (‰) along 84° W., March 26-31, 1967. These contours are based on STD data read principally from analog traces.

FIGURE 14-S-v27.—Vertical distribution of salinity (‰) along a southwest-northeast section from 3°45′ N., 83°48′ W. to Punta Burica, Costa Rica-Panama, March 31-April 2, 1967. These contours are based on STD data read principally from analog traces.

FIGURE 14-S-v28.—Vertical distribution of salinity (‰) along the coast of Panama from 82°50′ W. to 81°28′ W., April 2, 1967. These contours are based on STD data read principally from analog traces.

FIGURE 14-S-v29.—Vertical distribution of salinity (‰) along the coast of Panama from 81°28′ W. to 79°38′ W., April 2-3, 1967. These contours are based on STD data read principally from analog traces.

Thermosteric anomaly and geostrophic velocity—Yellow pages

FIGURE 14-δ-v1.—Vertical distribution of thermosteric anomaly, δ_T, (cl./t.) along a southwest-northeast section in the northern portion of the Panama Bight from 79°44′ W. to 78°43′ W., January 31, 1967. These contours are based on STD data read principally from analog traces.

FIGURE 14-δ-v2.—Vertical distribution of thermosteric anomaly, δ_T, (cl./t.) along a section in the Panama Bight near the coasts of Panama and Colombia from 7°35′ N. to 6°58′ N., January 31-February 1, 1967. These contours are based on STD data read principally from analog traces.

FIGURE 14-δ-v3.—Vertical distribution of thermosteric anomaly, δ_T, (cl./t.) along a northeast-southwest section in the Panama Bight from the coast of Colombia to 5°43′ N., 79°22′ W., February 1, 1967. These contours are based on STD data read principally from analog traces.

FIGURE 14-δ-v4.—Vertical distribution of thermosteric anomaly, δ_T, (cl./t.) along a northwest-southeast section in the central portion of the Panama Bight from 5°43′ N., 79°22′ W. to the coast of Colombia, February 1-2, 1967. These contours are based on STD data read principally from analog traces.

FIGURE 14-δ-v5.—Vertical distribution of thermosteric anomaly, δ_T, (cl./t.) along a section in the Panama Bight near the coast of Colombia from 4°10′ N. to 2°45′ N., February 2-3, 1967. These contours are based on STD data read principally from analog traces.

FIGURE 14-δ-v6.—Vertical distribution of thermosteric anomaly, δ_T, (cl./t.) along a southeast-northwest section across the Panama Bight from the coast of Colombia to Peninsula de Azuero, Panama, February 3-5, 1967. These contours are based on STD data read principally from analog traces.

FIGURE 14-δ-v7.—Vertical distribution of thermosteric anomaly, δ_T, (cl./t.) along a northeast-southwest section from Isla Coiba, Panama to 5°03′ N., 82°18′ W., February 5-6, 1967. These contours are based on STD data read principally from analog traces.

FIGURE 14-δ-v8.—Vertical distribution of thermosteric anomaly, δ_T, (cl./t.) along a northwest-southeast section from 5°03′ N., 82°18′ W. to the coast of Ecuador, February 6-8, 1967. These contours are based on STD data read principally from analog traces.

FIGURE 14-δ-v9.—Vertical distribution of thermosteric anomaly, δ_T, (cl./t.) along the Equator from the coast of Ecuador to 81°54′ W., February 8-9, 1967. These contours are based on STD data read principally from analog traces.

FIGURE 14-δ-v10.—Vertical distribution of thermosteric anomaly, δ_T, (cl./t.) along 82° W. from 0°18′ S. to 7°27′ S., February 9-11, 1967. These contours are based on STD data read principally from analog traces.

FIGURE 14-δ-v11.—Vertical distribution of thermosteric anomaly, δ_T, (cl./t.) along 7°15′ S. from 81°50′ W. to the coast of Peru, February 11-12, 1967. These contours are based on STD data read principally from analog traces.

FIGURE 14-δ-v12.—Vertical distribution of thermosteric anomaly, δ_T, (cl./t.) along a northeast-southwest section from the coast of Peru to 11° S., 81°46′ W., February 13-14, 1967. These contours are based on STD data read principally from analog traces.

FIGURE 14-δ-v13.—Vertical distribution of thermosteric anomaly, δ_T, (cl./t.) along 81°46′ W. from 11°02′ S. to 14°37′S., February 14-15, 1967. These contours are based on STD data read principally from analog traces.

FIGURE 14-δ-v14.—Vertical distribution of thermosteric anomaly, δ_T, (cl./t.) along 15° S. from 81°46′ W. to the coast of Peru, February 15-16, 1967. These contours are based on STD data read principally from analog traces.

FIGURE 14-δ-v15.—Vertical distribution of thermosteric anomaly, δ_T, (cl./t.) along the coast of Peru from 15°07′ S. to 12°27′ S., February 17-24, 1967. These contours are based on STD data read principally from analog traces.

FIGURE 14-δ-v16.—Vertical distribution of thermosteric anomaly, δ_T, (cl./t.) along a northeast-southwest section from the coast of Peru to 14°30′ S., 81°43′ W., February 24-25, 1967. These contours are based on STD data read principally from analog traces.

FIGURE 14-δ-v17.—Vertical distribution of thermosteric anomaly, δ_T, (cl./t.) along 14°30′ S. from 81°43′ W. to 88°17′ W., February 25-27, 1967. These contours are based on STD data read principally from analog traces.

FIGURE 14-δ-v18.—Vertical distribution of thermosteric anomaly, δ_T, (cl./t.) along 88°46′ W., February 27-March 4, 1967. These contours are based on STD data read principally from analog traces.

FIGURE 14-δ-v19.—Vertical distribution of thermosteric anomaly, δ_T, (cl./t.) along 92° W., west of the Galapagos Islands, March 8-9, 1967. These contours are based on STD data read principally from analog traces.

FIGURE 14-δ-v20.—Vertical distribution of thermosteric anomaly, δ_T, (cl./t.) along a section north of the Galapagos Islands, from 0°16′ N., 91°47′ W. to 2°01′ N., 90°03′ W., March 9-10, 1967. These contours are based on STD data read principally from analog traces.

FIGURE 14-δ-v21.—Vertical distribution of thermosteric anomaly, δ_T, (cl./t.) along a section northeast of the Galapagos Islands, from 2°01′ N., 90°03′ W. to the Equator at 89°03′ W., March 11, 1967. These contours are based on STD data read principally from analog traces.

FIGURE 14-δ-v22.—Vertical distribution of thermosteric anomaly, δ_T, (cl./t.) along a southwest-northeast section from the Equator at 89°03′ W. to Puntarenas, March 11-15, 1967. These contours are based on STD data read principally from analog traces.

FIGURE 14-δ-v23.—Vertical distribution of thermosteric anomaly, δ_T, (cl./t.) along a northeast-southwest section from the coast of Costa Rica to 3°52′ N., 85°57′ W., March 18-20, 1967. These contours are based on STD data read principally from analog traces.

FIGURE 14-δ-v24.—Vertical distribution of thermosteric anomaly, δ_T, (cl./t.) along 86°19′ W., March 20-25, 1967. These contours are based on STD data read principally from analog traces.

FIGURE 14-δ-v25.—Vertical distribution of thermosteric anomaly, δ_T, (cl./t.) along 12° S., March 25-26, 1967. These contours are based on STD data read principally from analog traces.

FIGURE 14-8-v26.—Vertical distribution of thermosteric anomaly, δ_T, (cl./t.) along 84° W., March 26-31, 1967. These contours are based on STD data read principally from analog traces.

FIGURE 14-8-v27.—Vertical distribution of thermosteric anomaly, δ_T, (cl./t.) along a southwest-northeast section from 3°45′ N., 83°48′ W. to Punta Burica, Costa Rica-Panama, March 31-April 2, 1967. These contours are based on STD data read principally from analog traces.

FIGURE 14-8-v28.—Vertical distribution of thermosteric anomaly, δ_T, (cl./t.) along the coast of Panama from 82°50′ W. to 81°28′ W., April 2, 1967. These contours are based on STD data read principally from analog traces.

FIGURE 14-8-v29.—Vertical distribution of thermosteric anomaly, δ_T, (cl./t.) along the coast of Panama from 81°28′W. to 79°38′ W., April 2-3, 1967. These contours are based on STD data read principally from analog traces.

FIGURE 14-G-v4.—Vertical distribution of the component of geostrophic velocity (cm./sec.), relative to 500 db., normal to a northwest-southeast section in the central portion of the Panama Bight from 5°43′ N., 79°22′ W. to the coast of Colombia, February 1-2, 1967. Dark shading indicates flow toward the northeast with a velocity greater than 5 cm./sec.; light shading indicates flow toward the southwest with a velocity greater than 5 cm./sec.

FIGURE 14-G-v6.—Vertical distribution of the component of geostrophic velocity (cm./sec.), relative to 500 db., normal to a southeast-northwest section across the Panama Bight from the coast of Colombia to Peninsula de Azuero, Panama, February 3-5, 1967. Dark shading indicates flow toward the northeast with a velocity greater than 5 cm./sec.; light shading indicates flow toward the southwest with a velocity greater than 5 cm./sec.

FIGURE 14-G-v8.—Vertical distribution of the component of geostrophic velocity (cm./sec.), relative to 500 db., normal to a northwest-southeast section from 5°03′ N., 82°18′ W. to the coast of Equador, February 6-7, 1967. Dark shading indicates flow toward the northeast with a velocity greater than 5 cm./sec.; light shading indicates flow toward the southwest with a velocity greater than 5 cm./sec.

FIGURE 14-G-v10.—Vertical distribution of the zonal component of geostrophic velocity (cm./sec.), relative to 500 db., along 82° W. from 1°35′ S. to 7°07′ S., February 9-11, 1967. Dark shading indicates eastward flow with a velocity greater than 5 cm./sec.; light shading indicates westward flow with a velocity greater than 5 cm./sec.

FIGURE 14-G-v13.—Vertical distribution of the zonal component of geostrophic velocity (cm./sec.), relative to 500 db., along 81°46′ W. from 11°02′ S. to 13°42′ S., February 14-15, 1967. Dark shading indicates eastward flow with a velocity greater than 5 cm./sec.

FIGURE 14-G-v14.—Vertical distribution of the meridional component of geostrophic velocity (cm./sec.), relative to 500 db., along 15° S. from 81°46′ W. to the coast of Peru, February 15-17, 1967. Dark shading indicates northward flow with a velocity greater than 5 cm./sec.; light shading indicates southward flow with a velocity greater than 5 cm./sec.

FIGURE 14-G-v16.—Vertical distribution of the component of geostrophic velocity (cm./sec.), relative to 500 db., normal to a northeast-southwest section from the coast of Peru to 14°30′ S., 81°43′ W., February 24-25, 1967. Dark shading indicates flow toward the southeast with a velocity greater than 5 cm./sec.; light shading indicates flow toward the northwest with a velocity greater than 5 cm./sec.

FIGURE 14-G-v17.—Vertical distribution of the meridional component of geostrophic velocity (cm./sec.), relative to 500 db., along 14°30′ S. from 81°43′ W. to 88°17′ W., February 25-27, 1967. Dark shading indicates northward flow with a velocity greater than 5 cm./sec.

FIGURE 14-G-v18.—Vertical distribution of the zonal component of geostrophic velocity (cm./sec.) relative to 500 db., along 88°46′ W., February 27-March 4, 1967. Dark shading indicates eastward flow with a velocity greater than 5 cm./sec.; light shading indicates westward flow with a velocity greater than 5 cm./sec.

FIGURE 14-G-v22.—Vertical distribution of the component of geostrophic velocity (cm./sec.), relative to 500 db., normal to a southwest-northeast section from 1°22′ N., 89°02′ W. to Puntarenas, March 12-15, 1967. Dark shading indicates flow toward the southeast with a velocity greater than 5 cm./sec.; light shading indicates a flow toward the northwest with a velocity greater than 5 cm./sec.

FIGURE 14-G-v23.—Vertical distribution of the component of geostrophic velocity (cm./sec.), relative to 500 db., normal to a northeast-southwest section from the coast of Costa Rica to 4°25′ N., 85°47′ W., March 18-19, 1967. Dark shading indicates flow toward the southeast with a velocity greater than 5 cm./sec.; light shading indicates flow toward the northwest with a velocity greater than 5 cm./sec.

FIGURE 14-G-v24.—Vertical distribution of the zonal component of geostrophic velocity (cm./sec.), relative to 500 db., along 86°19′ W., March 20-24, 1967. Dark shading indicates eastward flow with a velocity greater than 5 cm./sec.; light shading indicates westward flow with a velocity greater than 5 cm./sec.

Oxygen—Green pages

FIGURE 14-O_2-v1.—Vertical distribution of oxygen (ml./l.) along a southwest-northeast section in the northern portion of the Panama Bight from 79°44′ W. to 78°43′ W., January 31, 1967.

FIGURE 14-O_2-v2.—Vertical distribution of oxygen (ml./l.) along a section in the Panama Bight near the coasts of Panama and Colombia from 7°35′ N. to 6°58′ N., January 31-February 1, 1967.

FIGURE 14-O_2-v3.—Vertical distribution of oxygen (ml./l.) along a northeast-southwest section in the Panama Bight from the coast of Colombia to 5°43′ N., 79°22′ W., February 1, 1967.

FIGURE 14-O_2-v4.—Vertical distribution of oxygen (ml./l.) along a northwest-southeast section in the central portion of the Panama Bight from 5°43′ N., 79°22′ W. to the coast of Colombia, February 1-2, 1967.

FIGURE 14-O_2-v5.—Vertical distribution of oxygen (ml./l.) along a section in the Panama Bight near the coast of Colombia from 4°10′ N. to 2°45′ N., February 2-3, 1967.

FIGURE 14-O_2-v6.—Vertical distribution of oxygen (ml./l.) along a southeast-northwest section across the Panama Bight from the coast of Colombia to Peninsula de Azuero, Panama, February 3-5, 1967.

FIGURE 14-O_2-v7.—Vertical distribution of oxygen (ml./l.) along a northeast-southwest section from Isla Coiba, Panama to 5°03′ N., 82°18′ W., February 5-6, 1967.

FIGURE 14-O_2-v8.—Vertical distribution of oxygen (ml./l.) along a northwest-southeast section from 5°03′ N., 82°18′ W. to the coast of Ecuador, February 6-8, 1967.

FIGURE 14-O_2-v9.—Vertical distribution of oxygen (ml./l.) along the Equator from the coast of Ecuador to 81°54′ W., February 8-9, 1967.

FIGURE 14-O_2-v10.—Vertical distribution of oxygen (ml./l.) along 82° W. from 0°18′ S. to 7°27′ S., February 9-11, 1967.

FIGURE 14-O_2-v11.—Vertical distribution of oxygen (ml./l.) along 7°15′ S. from 81°50′ W. to the coast of Peru, February 11-12, 1967.

FIGURE 14-O_2-v12.—Vertical distribution of oxygen (ml./l.) along a northeast-southwest section from the coast of Peru to 11° S., 81°46′ W., February 13-14, 1967.

FIGURE 14-O_2-v13.—Vertical distribution of oxygen (ml./l.) along 81°46′ W. from 11°02′ S. to 14°37′ S., February 14-15, 1967.

FIGURE 14-O_2-v14.—Vertical distribution of oxygen (ml./l.) along 15° S. from 81°46′ W. to the coast of Peru, February 15-17, 1967.

FIGURE 14-O_2-v15.—Vertical distribution of oxygen (ml./l.) along the coast of Peru from 15°07′ S. to 12°27′ S., February 17-24, 1967.

FIGURE 14-O_2-v16.—Vertical distribution of oxygen (ml./l.) along a northeast-southwest section from the coast of Peru to 14°30′ S., 81°43′ W., February 24-25, 1967.

FIGURE 14-O_2-v17.—Vertical distribution of oxygen (ml./l.) along 14°30′ S. from 81°43′ W. to 88°17′ W., February 25-27, 1967.

FIGURE 14-O_2-v18.—Vertical distribution of oxygen (ml./l.) along 88°46′ W., February 27-March 4, 1967.

FIGURE 14-O_2-v19.—Vertical distribution of oxygen (ml./l.) along 92° W., west of the Galapagos Islands, March 8-9, 1967.

FIGURE 14-O_2-v21.—Vertical distribution of oxygen (ml./l.) along a section northeast of the Galapagos Islands, from 1°33′ N., 89°44′ W., to the Equator at 89°03′ W., March 11, 1967.

FIGURE 14-O_2-v22.—Vertical distribution of oxygen (ml./l.) along a southwest-northeast section from the Equator at 89°03′ W. to Puntarenas, March 11-15, 1967.

FIGURE 14-O_2-v23.—Vertical distribution of oxygen (ml./l.) along a northeast-southwest section from the coast of Costa Rica to 3°52′ N., 85°57′ W., March 18-20, 1967.

FIGURE 14-O_2-v24.—Vertical distribution of oxygen (ml./l.) along 86°19′ W., March 20-25, 1967.

FIGURE 14-O_2-v25.—Vertical distribution of oxygen (ml./l.) along 12° S., March 25-26, 1967.

FIGURE 14-O_2-v26.—Vertical distribution of oxygen (ml./l.) along 84° W., March 26-31, 1967.

FIGURE 14-O_2-v27.—Vertical distribution of oxygen (ml./l.) along a southwest-northeast section from 3°45′ N., 83°48′ W. to Punta Burica, Costa Rica-Panama, March 31-April 2, 1967.

PREFACE

During the last two decades a number of expeditions have worked in the eastern tropical Pacific Ocean, so that the general features of its circulation and biology have been described. (References to such investigations are to be found in the two reports of the Eastern Pacific Oceanic Conference — EPOC, cited below.) However, the accumulated observations are too poorly arranged in time and space to describe, in an adequate fashion, the monthly or seasonal variation in the distribution of physical or biological properties. Large-scale changes in the atmospheric circulation clearly lead to changes in mass transport within major components of the circulation, as well as causing variation in the intensity of vertical motion on the equator and along the continental margin. In order to understand and to predict the nature of such variation it was evident from the data of previous studies in the eastern tropical Pacific Ocean that a more solid data base for modeling circulation and biotic production in this region was necessary.

Many of the members of the EPOC are engaged in research in the eastern tropical Pacific, and a proposal for a detailed and comprehensive study of the upper ocean in this area originated in 1960 at the Seventh Annual Meeting of EPOC. The Conference appointed a Committee, chaired by Gerald V. Howard of the Bureau of Commercial Fisheries (BCF)[1] to consider the desirability, feasibility, and possible scope of a cooperative program of oceanic survey and research in the eastern tropical Pacific Ocean. This Committee reported the results of its study to the Eighth EPOC, held in September 1961, and published these as the *Report of EPOC on a Cooperative Program of Study of the Eastern Tropical Pacific Ocean.*

The recommendations called for a $20-million oceanography program to begin in 1963 and run for a period of 8 years to encompass general survey work and special research in meteorology; physical, chemical, and biological oceanography (including fisheries); geology; and geophysics. It noted that such a program would not only greatly advance the marine sciences and provide opportunities for significant new understanding of the ocean, but would also be of value in providing the scientific basis for increasing the harvest of the fisheries of the region, forecasting weather, and improving shipping and navigation. It recommended that the U.S. Interagency Committee on Oceanography (ICO) and the individual agencies of the government should begin planning for support of the program. It also recommended that international participation and aid should be sought through appropriate international agencies and from Latin American institutions with oceanographic capabilities. The program then received the approval of the Intergovernmental Oceanographic Commission at its meeting in Paris in September 1961.

However, for various reasons, 4 years elapsed and little progress was made before implementation of the EPOC plan. Between the fall of 1963 and the spring of 1964, a group of scientists from several agencies engaged in oceanography in the eastern Pacific met to consider the EPOC program in the light of developments, or lack thereof, towards its implementation during the intervening years. This ad hoc group agreed that two major factors were deterrents to the program. The funding agencies appeared to consider the proposed survey and research too costly, and some parts of the program had not attracted the scientists who would be required to carry them out.

The ad hoc group decided to revise and trim the EPOC program as originally recommended in the hope of overcoming major obstacles apparently blocking its implementation. It took into consideration recent developments, especially in the fisheries of the eastern tropical Pacific and the present and potential manpower and facilities of the scientific community. It concluded that the geological-geophysical portion could be deleted because it dealt with time-independent properties not closely related to the rest of the program, and that the detailed meteorological program could be reduced. Also, it was decided that the research cruises and special research projects could be omitted from the basic plan since these would follow as people recognized their possibilities and importance. What remained of the original proposal, then, was the hard core of the field survey program for physical, chemical, and biological oceanography and essentials of the meteorological program, although even these efforts were reduced to coincide with reductions in research ship time. While trimming the overall oceanographic program as originally conceived, the ad hoc group recognized a need to include fishery surveys in the plan to insure that the fishing industries would obtain maximum benefit from the proposed work in descriptive oceanography. The revised program was now labeled EASTROPAC *A Cooperative Effort Towards Understanding of the Oceanography of the Eastern Tropical Pacific Ocean.*

The ad hoc group prepared estimates of the total funds that would be required to launch the field operations associated with EASTROPAC, process the data collected, analyze the data, and prepare reports on the results. In making the estimates, the group took into account the existing capabilities — available scientific personnel and oceanographic programs underway in the laboratories already engaged in studies of the eastern tropical Pacific Ocean — that were available for the EASTROPAC expeditions. Thus, the major share of the budget prepared was for the support of ship operations and unmanned buoys.

EASTROPAC finally became a reality with the first cruise scheduled for February-March 1967. The investigations were to be coordinated by the Bureau of Commercial Fisheries through its laboratory in La Jolla, and in June 1966 a Coordinator, Dr. Warren S. Wooster, Scripps Institution of Oceanography (SIO), was appointed; in May 1967, Dr. Alan R. Longhurst, then of SIO, replaced Dr. Wooster. As his first task, Dr. Wooster enlisted the support of various Federal agencies and scientific institutions in providing ships and personnel. Mexico and a number of South American countries were also asked to participate because of the importance of these expeditions to Latin American fisheries.

By the time the first expedition was due to sail, an impressive number of agencies had pledged their support in one way or another; these included international and foreign organizations as well as United States universities and Federal agencies.

The organizations involved in EASTROPAC, and the nature of their involvement, were as follows:

International:

Inter-American Tropical Tuna Commission (IATTC), La Jolla, California. Participation of biological and physical oceanographers and technicians aboard U.S. and Latin American research vessels. Performed analysis of meteorological data and sorting of zooplankton samples under contract to Bureau of Commercial Fisheries. Provided computer programming services and assistance in reduction and analysis of some Latin American data.

Foreign:

Chile—Instituto Hidrográfico de la Armada. Organization and manning of research cruises off Chile on Chilean research vessel *Yelcho* and through tropical area by *Esmeralda.*

Ecuador—Instituto Nacional de Pesca. Organization and manning (with IATTC) of research cruises off Ecuador with Ecuadorian research vessel *Huayaipe.*

Peru—Instituto del Mar. Organization and manning of research cruises off Peru with Peruvian research vessel *Unanue.*

Mexico—Dirección General de Pesca e Industrias Conexas. Organization and manning (with IATTC) of research cruises off Mexico with Mexican vessels *Yolanda* and *Tuxpan* and a chartered U. S. vessel, *Defiance* (with IATTC and the U. S. Bureau of Sport Fisheries and Wildlife).

United States:

U.S. Coast Guard. Provision of USCG research vessel *Rockaway* for three major cruises off Central America and partial provision of her scientific party, the rest supplied by other agencies. Provided financial support for atlas publication.

U. S. Department of Commerce (ESSA). Provision on some of the major cruises of Weather Bureau personnel and equipment for taking surface and upper air observations. Designated one leg of the inaugural voyage of U.S. Coast and Geodetic Survey Ship *Oceanographer* for EASTROPAC participation.

U. S. Department of the Navy (ONR). Provision of funding in support of some of the university research vessels participating and of processing and analysis of data obtained. *(NAVOCEANO).* Designated a portion of a research cruise of the USNS *Charles H. Davis* for EASTROPAC participation.

National Oceanographic Data Center (NODC). Consultation and cooperation concerning standardization of observational and data-recording techniques. Sent one oceanographer to La Jolla for 6 months to assist in processing of physical oceanographic data. Provided financial support for atlas publication.

[1] Now National Marine Fisheries Service.

National Science Foundation (NSF). Funds in support of some university personnel and research ships.

Smithsonian Institution. Provision of ornithologists trained in sea-bird and fish-school observations for most of the major cruises.

Stanford University. Supplied data from research vessel *Te Vega* which operated concurrently in the survey area.

University of California (Scripps Institution of Oceanography). Provision of research vessels *Thomas Washington* and *Argo,* and partial provision of their scientific parties. Provision of two instrumented buoys to be moored in the survey area. Assistance subsequent to the expeditions in reduction and analysis of data.

Texas A & M University. Provision of research vessel *Alaminos* and partial provision of her scientific party. Supply of meteorological instruments for other vessels.

U. S. Department of the Interior (Bureau of Commercial Fisheries). Provision of coordination unit at La Jolla, of research vessels *David Starr Jordan* and *Undaunted* and their scientific parties; post-expedition reduction and analysis of data. Provided financial support for atlas publication.

The EASTROPAC expeditions were unique in their scope and in the degree of coordinated planning of the cruises. In size of area and number of observations, EASTROPAC was comparable with such major international efforts as the International Indian Ocean Expedition, yet, unlike IIOE, all participating ships worked tracks designated prior to the expeditions to survey comprehensively the designated area in space and time; all participating ships undertook to perform a standard and basic suite of physical and biological observations, using standardized gear and conforming to standards laid down by the EASTROPAC *Manual of Observations* (Staff EASTROPAC, 1967) issued before the first cruise and modified only very slightly during the 14 months the expeditions occupied. Such routine observations formed a very large part of the effort of each participating ship and other scientific activities were performed only on a "not to interfere" basis.

The expeditions were extremely fortunate in the small number of medical emergencies and ship breakdowns which disrupted planned observational patterns, and only minor modifications had to be made to planned cruise tracks. This was due in no small part to the enthusiasm of the individual participants aboard the expedition ships, whose dedication to the idea behind the series of expeditions must be recognized and acknowledged by those involved in its planning.

It was decided by a meeting of the EASTROPAC Coordinating Committee in April 1968, that the data derived from the expeditions were so numerous as to render classical data reports impractical, and it was decided that all data should be archived on magnetic tape at the National Oceanographic Data Center after they had been used for production of a comprehensive atlas of the physical and biological results of the expeditions. It was also decided, in view of the volume of the data and the consequent number of sheets in the atlas, the preliminary data processing and chart analyses would be performed entirely by computer. Therefore only minimum hand computation and limited drafting were needed in this atlas. Only in this way could it have been produced in the short time available and as economically as it has been; the presentation may not be as aesthetically pleasing as in more classical atlases but it is hoped that our charts and sections will be equally as useful as hand-drawn ones.

In accepting the role of coordinating agency for EASTROPAC, the Bureau of Commercial Fisheries recognized that the expeditions were a necessary preliminary to fishery development in the eastern tropical Pacific Ocean to the west of the present-day tuna fisheries. A second-phase operation was visualized after data reduction, analysis, and presentation were completed for the original series of EASTROPAC expeditions. This second phase would consist of (1) stock assessment of oceanic tunas and determination of their availability to a fishery, in areas and at seasons indicted by analysis of EASTROPAC data; (2) further investigations of phenomena, physical or biological, demonstrated by the initial data to be interesting yet improperly understood; and (3) a determination from the initial expedition data, what way these data and later monitoring operations (surface ships, buoys, or remote sensors) might be used to develop fisheries advisory services for the tropical tuna fleet.

At the time of writing, in early 1970, the Bureau of Commercial Fisheries is moving towards these second-phase objectives.

ALAN R. LONGHURST
EASTROPAC Coordinator

INTRODUCTION

EASTROPAC CRUISES

The EASTROPAC field work was divided into seven, 2-month cruise periods. During each period there was a single- or multi-ship cruise. Each cruise was planned to last about 50 days; in practice some lasted longer. There were two types of cruises—survey and monitor. Survey cruises were multi-ship operations designed to provide simultaneous coverage of as much of the study area as possible. The study area was defined as latitude 20° N. to latitude 20° S. and from the coast of the American continents westward to longitude 119° W. There were three such surveys, 6 months apart. In each interval between survey cruises there were two, single-ship monitor cruises, making a total of four. The area covered by monitor cruises was determined partly by oceanographic considerations and partly by time and logistic constraints placed on a vessel operating from San Diego, but the purpose was to monitor changes in oceanographic conditions taking place between survey cruises.

Cruises by Latin American cooperating vessels were usually timed to coincide with survey cruises, and their coverage designed to supplement the survey cruises.

In addition to the major EASTROPAC cruises and Latin American cooperating vessels, certain ships of opportunity presented themselves. In some cases, such as *Te Vega*, the ship was operating in the same area and at the same time, and the data were made available to EASTROPAC. In other cases, such as *Oceanographer* and *Charles H. Davis*, the observations made during a portion of each of their cruises were planned to be part of EASTROPAC. EASTROPAC personnel were aboard *Oceanographer* during that portion of her cruise.

The cruises are designated in the atlas by a two-digit numbering system. The first number, from 1 through 7, designates one of the seven, 2-month cruise periods beginning with February-March 1967. The second number indicates the track followed or area covered within that cruise period. The monitor cruise track is designated by 0. For the first survey cruise (4 ships) the tracks are designated 1 to 4 with the westernmost track having the lowest number. For the second and third survey cruises (3 ships each) the tracks are numbered 5, 6, and 7 with, again, the westernmost track carrying the lowest number. Thus, cruise 12 represents track 2 of the first survey cruise; 30 designates the second monitor cruise; 77 refers to track 7 (the easternmost track) of the third survey cruise. Local practice has been to include the name of the ship when referring to a cruise, e.g., *Jordan* 12, but it is not necessary for complete identification of the cruise. There has also been some use of the expressions "10-series cruises," "40-series cruises," etc., to refer to cruises made during the first survey cruise period, second survey cruise period, etc. Cruises of foreign cooperating vessels or ships of opportunity have been identified by the expedition names or cruise numbers assigned by the operating agency.

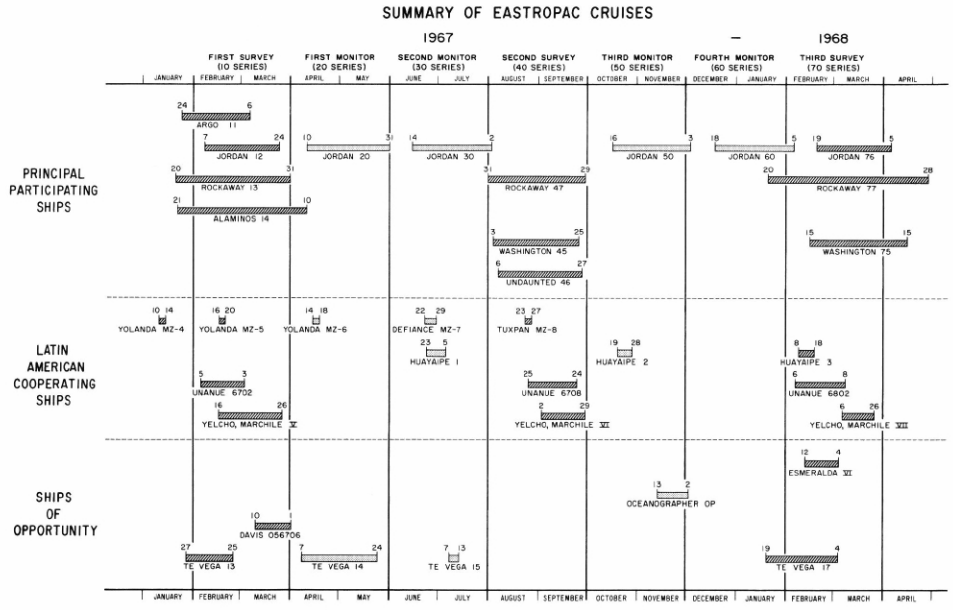

FIGURE 1. — Summary of EASTROPAC cruises.

Figure 1 is a graphical summary of EASTROPAC cruises. The affiliations of the participating ships are shown in the accompanying table (table 1).

TABLE 1.—Affiliations of ships participating in EASTROPAC (1967-68).

Category and ship	Country	Agency or institution
Principal participating ships:		
Alaminos	U.S.A.	Department of Oceanography, Texas A & M University
Argo	U.S.A.	Scripps Institution of Oceanography, University of California
David Starr Jordan	U.S.A.	Bureau of Commercial Fisheries, La Jolla
Rockaway	U.S.A.	U.S. Coast Guard
Undaunted	U.S.A.	Bureau of Commercial Fisheries, Miami
Thomas Washington	U.S.A.	Scripps Institution of Oceanography, University of California
Latin American cooperating ships:		
Defiance	Mexico & U.S.A.	Dirección General de Pesca e Industrias Conexas, Mexico, and U.S. Bureau of Sport Fisheries and Wildlife
Huayaipe	Ecuador	Instituto Nacional de Pesca
Tuxpan	Mexico	Dirección General de Pesca e Industrias Conexas
Unanue	Peru	Instituto del Mar
Yelcho	Chile	Instituto Hidrográfico de la Armada
Yolanda	Mexico	Dirección General de Pesca e Industrias Conexas
Ships of opportunity:		
Charles H. Davis	U.S.A.	U.S. Naval Oceanographic Office
Esmeralda	Chile	Instituto Hidrográfico de la Armada
Oceanographer	U.S.A.	Environmental Science Services Administration, U.S. Coast & Geodetic Survey
Te Vega	U.S.A.	Stanford Oceanographic Expeditions, Stanford University

The field work began with the first survey cruise (10-series cruises) in February-March 1967 (figs. 10-TC-a, 10-TC-b). Major coverage was by four ships: *Argo* of the Scripps Institution of Oceanography, University of California, San Diego, and *David Starr Jordan* of the Bureau of Commercial Fisheries, Fishery-Oceanography Center in La Jolla, both operating from San Diego, and the U.S. Coast Guard Cutter *Rockaway* from New York, and *Alaminos* from the Department of Oceanography, Texas A & M University, which began their EASTROPAC operations after entering the Pacific from the Canal Zone. The area covered was from 20° N. to 20° S. and from the coast westward to longitude 126° W. It should be noted that this was the only cruise in which there was coverage on 126° W. Subsequent cruises only extended westward to 119° W. Additional coverage along the coast of cooperating nations was provided by *Yolanda* of the Dirección General de Pesca e Industrias Conexas, Mexico, (DGPIC) operating out of Mazatlán in a joint project with the Inter-American Tropical Tuna Commission (IATTC), *Unanue* of the Instituto del Mar of Peru (IMP) from Callao, and the MARCHILE V cruise run by *Yelcho* of the Instituto Hidrográfico de la Armada, Chile, (IHA) from Valparaiso. Ships of opportunity operating during the period were the USNS *Charles H. Davis* of the U.S. Naval Oceanographic Office from San Diego, which ran a north-south section on 85° W., and *Te Vega* of Stanford Oceanographic Expeditions, Stanford University, from Pacific Grove, which operated on a line from Cape San Lucas to the Galápagos.

Two monitor cruises by *David Starr Jordan*, cruise 20 in April-May (fig. 20-TC) and cruise 30 in June-July (fig. 30-TC), followed. During the first monitor period, *Yolanda* again operated from Mazatlán and *Te Vega* was working off the coast of Mexico between 13° and 24° N. During the second monitor cruise, *Defiance*, a chartered U.S. fishing vessel, operated out of Mazatlán instead of *Yolanda* for a joint cruise sponsored by DGPIC, the U.S. Bureau of Sport Fisheries and Wildlife, and the IATTC; *Huayaipe* of the Instituto Nacional de Pesca, Ecuador (INPE), in conjunction with IATTC, operated in the waters between Guayaquil and the Galápagos; and *Te Vega* occupied stations in the entrance to the Gulf of California.

The second survey cruise (40-series) took place in August-September 1967 (figs. 40-TC-a, 40-TC-b). Only three ships were available for the principal coverage: *Thomas Washington*, SIO, *Undaunted* from the BCF Tropical Atlantic Biological Laboratory in Miami, and *Rockaway*. It was necessary to rearrange the cruise tracks, especially in the eastern portion of the area, and the extent of the southward coverage was reduced. Other vessels operating during this period were *Tuxpan* of DGPIC and IATTC from Mazatlán, *Unanue*, and *Yelcho* (MARCHILE VI).

The third and fourth monitor cruises were run by *David Starr Jordan*, cruise 50 in October-November (fig. 50-TC) and cruise 60 in December 1967-January 1968 (fig. 60-TC). During the third monitor period, the U.S. Coast and Geodetic Survey Ship *Oceanographer* made observations during part of her track between Callao and San Diego. This portion of her inaugural, round-the-world voyage had been designated for EASTROPAC participation. Also during this period *Huayaipe* made a second cruise in the area between Guayaquil and the Galápagos. *Te Vega* ran a north-south line on 100° W. and some stations in the vicinity of the Galápagos in a time period which overlapped between the fourth monitor and third survey cruise periods.

The principal observations during the third survey cruise (70-series) in February-March 1968 (figs. 70-TC-a, 70-TC-b) were made by three ships: *Thomas Washington*, *David Starr Jordan*, and *Rockaway*. The cruise tracks were similar to those of the second survey except that some of the north-south lines extended to 20° S. and there was no coverage along 92° W. Cooperating ships operating at the same time were *Huayaipe*, *Unanue*, *Yelcho* (MARCHILE VII), and *Esmeralda*. The latter, a training ship of the Chilean Navy, made a series of mechanical bathythermograph observations during a run from Valparaiso to Panama.

PROGRAM OF OBSERVATIONS

The program of observations followed during principal EASTROPAC cruises was based on three types of stations, designated A, B, and C, which were arranged by the time of day. At A stations there was a Nansen bottle cast to 500 m., a lowering of the salinity-temperature-depth recorder (STD) to 500 m., a lexan bottle cast for primary production and plant pigment samples, an oblique plankton haul from 200 m. to the surface using paired 1-m. and 50-cm. nets along with a simultaneous surface haul with a 1-m. net, and a micronekton haul from 200 m. to the surface using a 5-ft.-square net. A stations were made twice daily at approximately 0000 and 1200 local time. B stations were taken at approximately 0400 and 1600 local time and consisted of a 1,000-m. Nansen cast, 1,000-m. STD lowering, and oblique plankton haul and surface haul as on A stations. The original program of observations called for a 1,000-m. Nansen and STD cast at A stations and 500-m. casts of both types at B stations. This system was changed in the course of the project in order to make the time on station at A and B stations more equal. On one monitor cruise, cruise 30, a 500-m. Nansen cast was paired with a 1,000-m. STD cast on A stations and vice versa on B stations. There were four C stations each day, scheduled approximately at mid-time between departure from an A station and arrival at a following B station or vice versa. C stations usually consisted of expendable bathythermograph (XBT) drops underway although sometimes STD lowerings to 300 m. or 500 m. were substituted. This made the sequence of stations for a 12-hour period starting at midnight as follows: A (0000)-C-B-C-A (1200). On principal cruises all stations were numbered consecutively regardless of type. The two-digit cruise number described previously was combined with a three-digit consecutive number to form a five-digit number that uniquely identifies each station; thus station 12.025 indicates the 25th consecutive station of *Jordan* cruise 12.

There were modifications to this routine of observations, and other types of observations were made which also contributed information to this atlas. Within 5° of latitude on each side of the equator most ships ran the so-called "equatorial detail" pattern where additional C stations, either XBT or shallow STD lowerings, were run in between the stations mentioned above. These made a 12-hour sequence: A-C-C-C-B-C-C-C-A. Bird observations by observers from the Smithsonian Institution were made on cruises 11, 12, 13, 30, 45, 46, 50, 75, and 76. The observers were usually stationed on the ship's bow or flying bridge during daylight hours. Equipped with binoculars and cameras, they attempted to identify and count all birds seen. A few birds were collected for study specimens. In addition, they made valuable observations of fish schools and marine mammals. Weather observers from the Weather Bureau, ESSA, were aboard during cruises 13, 20, 30, 47, and 77, and on *Oceanographer*, where they made twice daily radiosonde observations to measure upper air conditions. Table 2 is a summary of observations made on EASTROPAC cruises.

TABLE 2.—Summary of types of observations made on EASTROPAC cruises.

Item	Category of ships			Total
	Principal participating ships	Latin American cooperating ships	Ships of opportunity	
STD casts	2,683	.....	128	2,811
Total Nansen casts	1,833	685	155	2,673
Nansen casts below 1,000 m.	137	109	61	307
XBT lowerings	2,266	.....	222	2,488
Mechanical BT lowerings	386	879	81	1,346
Meteorology:				
Surface observations	3,820	440	200	4,460
Upper air observations	382	.....	28	410
Lexan casts:				
Primary production experiments	451	299	83	833
Plant pigment determinations	926	292	105	1,323
Plankton hauls:				
Oblique with paired nets	1,744	132	50	1,926
Surface	1,600	141	49	1,790
Vertical	.....	425	.....	425
Micronekton hauls	810	.....	39	849

The information presented in this atlas is based primarily on the observations described above. There were a number of other measurements and observations made during EASTROPAC. Some were made on several cruises and others only on one. Some of the former are described below. Continuous recordings of bottom depths were made on most of the major cruises. In fact, the north-south portions of the monitor cruise tracks were shifted each time a few miles either to the east or west of the base meridians of 98° W., 105° W., 112° W., 119° W., so as to provide different bathymetric coverage. Table 3 shows the longitudes covered during monitor cruises. Sounding information from San Diego-based EASTROPAC ships has been turned over to the Department of Earth Sciences, SIO, for analysis. Although the data shown in this atlas extended only to 1,000-m. depth, there were 163 stations occupied during the project where Nansen casts deeper than 1,000 m. were made. In some cases these casts extended to within 100 m. of the bottom. There are tentative plans for these deep-station data to be published in a separate data report, but in any case, they will be sent to the National Oceanographic Data

TABLE 3.—Longitudes covered on north-south lines during EASTROPAC monitor cruises.

Cruise	Base meridians			
	119° W	112° W.	105° W.	98° W.
20	119°20′ W.	112°20′ W.	105°20′ W.	98°20′ W.
30	118°30′ W.	111°30′ W.	104°30′ W.	97°30′ W.
50	119°10′ W.	112°10′ W.	105°10′ W.	98°10′ W.
60	118°45′ W.	111°45′ W.	104°45′ W.	97°45′ W.

Center. The Scripps Institution of Oceanography provided two instrument platforms (buoys) to be moored in the study area during the period of EASTROPAC. These buoys were set out during the first survey cruise at two locations on longitude 119° W. in the Equatorial Counter Current, at approximately 6° N. and 9.5° N. They were equipped to measure and record subsurface temperatures at seven depths as well as surface water temperature and meteorological properties. The buoys were visited during each subsequent voyage to service the equipment. The buoy at 6° N. was not found in August 1967, during cruise 45, apparently having been swept away by bad weather. The one at 9.5° N. was located in October on cruise 50, but all sensors except one were inoperative so the instrument package was removed from the buoy. The buoy itself had disappeared when the area was searched in December during cruise 60. A preliminary data report issued by SIO (Evans, Schwartzlose, and Isaacs, 1968) showed that a maximum of 3307 hours of observations was obtained from the 6° N. buoy and 2369 hours from the one at 9.5° N.

Details of the observations made during the EASTROPAC cruises will be found in the various EASTROPAC Information Papers (Wooster, 1966a, 1966b, 1966c; Wooster and Love, 1967; Longhurst and Love, 1967; Longhurst, 1967a, 1967b, 1968, 1969a, 1969b; Love, 1969). In particular, Numbers 6, 8, and 9 of this series contain lists of stations occupied on all cruises showing date, time, position, and observations made. It is intended that most of the information collected, whether or not it appears in the atlas, will be made the subject of detailed research reports by the various investigators concerned.

Some of the Latin American cooperating ships and ships of opportunity followed the EASTROPAC routine of observations as well as their equipment, personnel, and time schedules would permit, while others followed their own routines. During the EASTROPAC portion of the *Oceanographer* voyage the prescribed routine was followed. Plans for the *Unanue* and *Yelcho* cruises called for the three types of stations previously mentioned and also for station spacing based on time of day. These ships were not equipped with an STD, however, nor were they able to make all the specified plankton or micronekton collections. *Charles H. Davis* ran the extra detail requested in equatorial regions during her transit on 85° W.

PREPARATION OF ATLAS CHARTS

The processing of almost all the data mentioned in the preceding section involved the use of automatic data processing (ADP) equipment at some stage. The data were therefore already stored on punched cards or magnetic tape and readily available for plotting in various forms by computer-driven plotter.

The vertical sections of physical properties, dissolved oxygen, and nutrient chemicals were prepared almost entirely by computer plotter, including drawing of the contours. Hand work included accenting certain contours and the addition of contour labels. For phytoplankton properties and upper atmosphere sections the outline of the section and depths, or heights, of sampling were plotter-drawn, and then hand-drawn contours were traced onto the section from a preliminary contoured version.

There was more variety in the methods used to prepare the charts of horizontal distributions. The options open to the contributors included hand or machine plotting of station positions and the data to be contoured, and then hand or machine drawing of the contours. Copies of the standard base map on which to plot data were available to all contributors. The base map was adapted from two U.S. Naval Oceanographic Office charts and is a Mercator projection. Some charts were plotted and contoured by hand; others were plotted automatically and contoured by hand. This latter was the most popular method of chart preparation. In either of the above methods the draftsman overlaid the preliminary version with a clean base map and copied the contours and station positions and applied shading as necessary. The charts showing zooplankton standing stock were plotted and contoured automatically. Drafting work on these charts was limited to touch-up work and application of shading.

ORGANIZATION OF THE ATLAS

Arrangement of Volumes

The EASTROPAC Atlas consists of 11 volumes. There are 10 volumes containing data from the principal participating ships plus *Oceanographer* and 1 volume containing data from the Latin American cooperating ships and other ships of opportunity. The first 10 volumes are arranged chronologically and by two general subject headings; 5 volumes contain physical oceanography and meteorology, and 5 volumes contain biological properties and nutrient chemistry. The following table indicates the arrangement. It should be noted that charts of horizontal distribution of properties which appear in the first 10 volumes do contain data from the Latin American ships and ships of opportunity as well as principal ship data. It is the vertical sections based on Latin American and ships of opportunity data which are found in volume 11.

Volume number	Contents	Ships and cruise period(s)	Dates
1	Physical properties and meteorology	Principal ships—First survey cruise (10-series)	February-March 1967
2	Biological properties and nutrient chemistry		
3	Physical properties and meteorology	Principal ships—First and second monitor cruises (20, 30 series)	April-May, June-July 1967
4	Biological properties and nutrient chemistry		
5	Physical properties and meteorology	Principal ships—Second survey cruise (40-series)	August-September 1967
6	Biological properties and nutrient chemistry		
7	Physical properties and meteorology	Principal ships and *Oceanographer*—Third and fourth monitor cruises (50, 60-series)	October-November 1967, December 1967-January 1968
8	Biological properties and nutrient chemistry		
9	Physical properties and meteorology	Principal ships—Third survey cruise (70-series)	February-March 1968
10	Biological properties and nutrient chemistry		
11	All properties	Latin American cooperating ships and ships of opportunity—All cruises	February 1967-March 1968

Color of Pages

In order to assist users to find the pages they want, pages showing different groups of properties have been printed on differently colored paper. Five colors have been used in each type of volume according to the following scheme:

Physical Oceanography and Meteorology (odd-numbered volumes):
- Temperature, salinity ..... White
- Computed quantities (thermosteric anomaly, geostrophic velocity, acceleration potential) ..... Yellow
- Oxygen ..... Green
- Depth of surfaces, including mixed layer depth ..... Buff
- Meteorological charts ..... Blue

Biological Properties and Nutrient Chemistry (even-numbered volumes and volume 11):
- Nutrient chemistry ..... White
- Phytoplankton ..... Green
- Zooplankton and micronekton ..... Blue
- Fish larvae ..... Yellow
- Sightings of birds, tuna schools, mammals ..... Buff

Figure Designation System

Although the atlas will initially be published in volumes arranged chronologically, as explained above, looseleaf binding permits users to rearrange the pages to suit their own needs. It was necessary to devise a figure designation system compatible with this flexibility. The system used consists of a series of numbers and letters or symbols which indicate the cruise or cruise period, the property represented, and whether it is a vertical section or horizontal distribution. In the latter case the designator further indicates whether the property is shown at a constant depth (phosphate-phosphorus at 10 m.), integrated over a layer (chlorophyll-a integrated over the euphotic layer), on a surface of constant thermosteric anomaly (salinity on the 300 cl./t. surface), or whether the contours represent numbers collected or observed per station, per day, etc. (total *Auxis* larvae taken in 1-m. oblique hauls). Sample figure designators and a complete list of abbreviations used are shown below. It should be noted that each figure bears a caption and each vertical section is also accompanied by a small index map to indicate its location so that the reader does not have to rely on the figure designator alone for a description of what the figure represents.

The following sample designators will illustrate the system:

12-T-v1 — First vertical section from cruise 12 showing distribution of temperature.

45-P-v2 — Second vertical section from cruise 45 showing distribution of phosphate-phosphorous.

The vertical sections are assigned consecutive numbers, v1, v2, etc., within each cruise which follow the chronological order in which the ship ran the sections.

40-NO_3-10 — Distribution of nitrate-nitrogen at 10-m. during second survey cruise (40-series).

20-δ300-z — Depth of 300 cl./t. thermosteric anomaly surface during the first monitor period.

30-O_2-δ160 — Distribution of oxygen on the 160 cl./t. thermosteric anomaly surface during second monitor period.

50-Ch-ei — Distribution of chlorophyll-a integrated over the euphotic layer during third monitor period.

70-ZhN — Standing stock of zooplankton taken in 50-cm. net hauls at night during third survey cruise period.

Table 4 shows all the abbreviations used in figure designators.

Remarks Concerning the Charts

The editorial policy of the atlas allowed each contributor to decide whether or not he wanted to use shading to enhance his presentation. A uniform shading scheme was adopted and was followed on all charts where shading was used. Shading scales are not shown on most charts in the belief that the combination

Abbreviations used in figure designation system

Cruise or cruise period	Property represented	Mnemonic to explain choice of letters	Indicator for vertical sections or type of horizontal surface
Numbers 11, 12, 13, etc., indicate principal cruises. See figure 1.	T Temperature		v1, v2, etc., indicate vertical sections.
Letters or letter-number combinations indicate cruises of Latin American cooperating ships or ships of opportunity, as follows:	S Salinity		Vertical sections are assigned consecutive numbers within each cruise which follow the chronological order in which the ship ran the sections.
MZ-4 *Yolanda*, MZ-4	δ Thermosteric anomaly (δ_T)		
MZ-5 *Yolanda*, MZ-5	G Geostrophic velocity		
MZ-6 *Yolanda*, MZ-6	O_2 Oxygen concentration		
MZ-7 *Defiance*, MZ-7	O_2Sa Oxygen saturation		
MZ-8 *Tuxpan*, MZ-8	ML Thickness of the mixed layer		
	δ300 300 cl./t. thermosteric anomaly surface		Number 10 or 100 following O_2Sa or horizontal P, Si, NO_2, NO_2, or NH_3 charts indicates distribution at that depth (m.).
H1 *Huayaipe*-1	AP Acceleration Potential		
H2 *Huayaipe*-2			
H3 *Huayaipe*-3	P Phosphate-phosphorus		
	Si Silicate-silicon		
U1 *Unanue* 6702	NO_3 Nitrate-nitrogen		
U2 *Unanue* 6708	NO_2 Nitrite-nitrogen		
U3 *Unanue* 6802	NH_3 Ammonia-nitrogen		
	Ch Chlorophyll-a		
Y5 *Yelcho* MARCHILE V	Ph Phaeophytin		s Distribution at the sea surface
Y6 *Yelcho* MARCHILE VI	PP Primary production		δ300 Distribution on the surface where δ_T=300 cl./t.
Y7 *Yelcho* MARCHILE VII	EL Thickness of the euphotic layer		ei Distribution integrated over the euphotic layer
E6 *Esmeralda* BE VI	FCγ Fish and cephalopod standing stock		150i Distribution integrated to 150 m. depth
OP *Oceanographer*	Cr Crustacean standing stock		z Depth of a surface
CD *Charles H. Davis*	Nk Total micronekton standing stock		
	ZhN Zooplankton standing stock from 50-cm. net hauls, night	Zooplankton, half-meter, Night	Number 1 or 2 following SP or SW charts indicates one of two 6-month periods into which those observations were divided.
T3 *Te Vega* 13	Z1N Zooplankton standing stock from 1-m. net hauls, night	Zooplankton, 1-meter, Night	
T4 *Te Vega* 14	ZhD Zooplankton standing stock from 50-cm. net hauls, day	Zooplankton, half-meter, Day	
T5 *Te Vega* 15	Z1D Zooplankton standing stock from 1-m. net hauls, day	Zooplankton, 1-meter, Day	Numbers 1 to 4 or 1 to 6 following MT or MW charts indicate one of the approximate 2-week periods into which those observations were divided. For all cruise periods except 40, the MT and MW charts were drawn for four 2-week periods. For the 40 cruise period these charts were drawn for six periods ranging from 12 to 16 days in length, but with several days overlap between some periods. Number 1 or 2 following MC charts indicates one of the monthly periods for which those charts were drawn.
T6 *Te Vega* 16	FLN Total fish larvae, night hauls	Fish Larvae, Night	
T7 *Te Vega* 17	FLD Total fish larvae, day hauls	Fish Larvae, Day	
	FE Total fish eggs		
	FS Total skipjack tuna larvae	Fish, Skipjack	
Numbers 10, 20, 30, 40, 50, 60, 70, indicate 2-month cruise periods.	FA Total *Auxis* larvae	Fish, *Auxis*	
	FC Total *Coryphaena* larvae	Fish, *Coryphaena*	
	FMN Total myctophid larvae, night hauls	Fish, Myctophid, Night	
	FMD Total myctophid larvae, day hauls	Fish, Myctophid, Day	
	FGN Total gonostomatid and sternoptychid larvae, night hauls	Fish, Gonostomatid, Night	
	FGD Total gonostomatid and sternoptychid larvae, day hauls	Fish, Gonostomatid, Day	
	BP Relative abundance of plankton-feeding birds	Birds, Plankton-feeding	
	BF Relative abundance of fish and cephalopod-feeding birds	Birds, Fish-feeding	
	SP Porpoise sightings	Sightings, Porpoise	
	SW Whale sightings	Sightings, Whales	
	ST Tuna school sightings, all cruises	Sightings, Tuna	
	UA Upper atmosphere meteorology		
	MW Surface meteorological analysis, winds and pressure	Meteorology, Winds	
	MC Surface meteorological analysis, clouds, dewpoint, temperature	Meteorology, Clouds	
	MT Surface meteorological analysis, sea temperature, sea-air temperature difference, sea temperature anomaly	Meteorology, Temperature	
	RM Reference map		
	TC Track chart		

of shading and contours is self-explanatory. In cases where it was not considered so, a shading scale is used or an explanatory remark placed in the caption.

Since the atlas is in effect serving as a data report for the EASTROPAC field work, the editors decided that the charts should be as objective as possible. To this end, an effort was made not to extend contours or shading across areas where there were no data even though the trend of the truncated contours and their relation to other contours in the vicinity might indicate a logical extension across such an area. The principal lines of observations on most cruises ran north-south; in the case of the lines run on all monitor cruises and most survey cruises, these lines were 7° of longitude, or less, apart. For horizontal distributions it was decided not to extend contours or shading between north-south lines which were more than 7° of longitude apart. It was difficult to make definite rules for other lines of observations, and decisions where to end contours and shading in such areas were made by the contributors and the editor. An effort was also made not to extend the shading up to the coastline. EASTROPAC was a deepwater project, and the EASTROPAC *Manual of Observations* (Staff, EASTROPAC, 1967) specified that when leaving the coast, observations should not be begun until a water depth of at least 500 m. was reached. There were some exceptions made to this rule, but in general, shallow nearshore waters were not sampled.

Vertical sections extending to a depth greater than 300 m. have been divided into two panels, with the depth scale in the upper panel twice that of the lower panel. The sections showing geostrophic velocity components are an exception. They consist of one panel extending to 500 m., with no change of depth scale. Since the original versions of the vertical sections were drawn with a horizontal scale of 3 cm. equal to 1° of latitude or 60 nautical miles (111.2 km.) and a vertical scale of 1 cm. equals 10-m. depth on the upper panel or 1 cm. equals 20-m. depth on the lower panel, the vertical exaggeration of the upper panel is 3707 times and that of the lower panel 1853 times. Tick marks showing the location of all stations used in preparing the section are shown in the space between the top and bottom panels. In addition, location marks and numbers of all stations which were sampled to 1,000 m. or deeper appear along the bottom of the section. On sections based on Nansen or lexan cast observations (oxygen, nutrient chemicals, phytoplankton) the station numbers of all stations used in the section also appear in the space between panels. Because STD observations were made more often than Nansen casts in some areas, it was found to be impossible to show all the STD station numbers in the space between panels. Therefore, sections of temperature, salinity, etc., do not have this latter feature. If a user wants to identify a particular station in one of the STD sections, it is believed that the information on the figure plus the listings of station positions and observations given in the previously cited Information Papers will enable him to do so. On sections which extend only to 500 m., all station numbers appear in the space between panels.

Vertical sections of temperature, salinity, thermosteric anomaly, and geostrophic velocity components from all principal cruises as well as *Oceanographer* are based on STD observations. Since the STD is a continuous sampling instrument, no sampling depths at each station need be shown. Sections of temperature, salinity, etc. from ships not equipped with an STD as well as sections of oxygen, nutrient chemicals, and phytoplankton properties are based on data collected with Nansen or lexan bottles. On these sections dots indicate the sampling depths in the conventional manner. On some sections the deepest sampling depth at each station is indicated by an inverted T symbol superimposed on the dot.

On STD sections some small, enclosed contours are not labeled. This should cause no confusion as generally such contours have the same value as the nearest continuous contour. Also, some of these contours are accented or dashed indicating they have the same value as the nearest continuous contour similarly marked.

On north-south sections the station location marks are positioned by latitude, and on the few east-west sections they are positioned by longitude. On sections which run in a direction which is neither north-south nor east-west, or close to those directions, both latitude and longitude scales are shown. Since lines of

oceanographic stations rarely lie in a straight line, a combination graphical-computational method was used to project the position of each station onto a base line drawn between the first and last station of the section. Thus, the station location marks indicate the distance along the base line between the projected station positions, and the latitude and longitude marks appear where the parallels and meridians cross the base line.

As was explained above, the vertical sections have been numbered consecutively (v1, v2, etc.) within each cruise in the chronological order in which the ship ran the sections. Section v1 of cruise 11, for instance, represents the same geographical location regardless of the property represented. On some sections of some cruises, there were STD observations but no Nansen or lexan bottle casts. In these cases there are sections showing temperature, salinity, thermosteric anomaly etc., but no corresponding sections of oxygen, nutrient chemicals, or phytoplankton properties.

ACKNOWLEDGMENTS

A number of people were involved in the preliminary processing of the various types of data and samples brought back from EASTROPAC cruises, but a smaller group carried through the advanced data preparation, computer programming, preparation of charts and copy, and the drafting which contributed directly to the production of this atlas. It is to this latter group that the editor and contributors first wish to extend their special thanks as follows:

From the EASTROPAC operations staff at BCF, La Jolla: Kenneth A. Bliss, who worked with all the temperature and salinity data—checking, preparing for computer operations, editing preliminary charts, and programming; Michael G. Kruse, who prepared all the phytoplankton data—checking, preparing for computer operations, and contouring and editing preliminary charts; Tapuni S. Mulitauaopele, who worked with the oxygen data—checking, preparing for computer operations, and editing preliminary charts; and Robert N. Nishimoto, who worked with zooplankton and bird sighting data.

From the Scripps Tuna Oceanography Research (STOR) group: Dorothy L. Burgess, who at various times worked with nutrient chemistry and oxygen data, digitized STD traces, and read off mixed layer depths; Edward H. Renger, who prepared the nutrient chemistry data—checking all cruises, preparing for computer operations, and editing preliminary charts from earlier cruises; and Don L. R. Seibert, who performed similar functions with the nutrient chemistry data from later cruises.

From the Oceanic Research Division, SIO: Miriam K. Oleinik, who worked with temperature and salinity data—checking, preparing for computer operations, editing, and programming; and Ruth W. Opdycke, who also worked with temperature and salinity data—checking, and hand-digitizing STD traces from some cruises.

Forrest R. Miller, IATTC, wrote all of the computer programs for drawing and contouring vertical sections and horizontal plots as well as some of the programs used for processing various data. Without his excellent contouring programs and his generous assistance with all phases of computer operations, this atlas would have taken a much longer time to prepare. He was assisted by Thomas A. Knight, BCF, in the development of horizontal contouring programs. These programs have been described by Miller and Bliss.[1] James H. Jones, SIO, wrote the series of programs for processing STD data up to the stage of preparing the final STD data tape (Jones, 1969) . Other computer programs used in data processing or preliminary chart preparation were written by Kenneth A. Bliss, BCF. Miriam K. Oleinik, SIO, wrote the isentropic analysis program as well as assisting with others. The program for calculating oxygen saturation is by Manley L. W. Young, SIO.

Drafting was done by Roy M. Allen, Michael J. Griffith, Frank W. Lyall, Dale B. Mann, Stuart M. Peace, and Kenneth S. Raymond, all of BCF; J. Duane Anderson and Joann S. Anderson, under contract with BCF; Judith M. Shepard, IATTC; and Miriam K. Oleinik and Howard G. Shirley, SIO.

The following groups were involved in preliminary data processing: The staff of the IATTC plankton sorting group who sorted the 1-m. net oblique samples—Kathleen S. Anderson, Jo A. Bauerschmidt, Georgene Bauld, Diane L. Berry, Kimberlie Boyd, Barbara C. Burris, Eleanor W. Clark, Diane M. de Sonia, Katherine E. Dice, Betty C. Duchow, Lorraine M. Fischer, Rosemary Gonzales, Donna E. Kidd, Donna J. Koudelka, Dorothy D. Normark, Viola G. Olsen, Gina M. Pournelle, Idea M. Robbins, Susan L. Toy, Mary J. Tucker, Carol A. Tyre, and Nancy K. Wiley; those who sorted the micronekton samples—Mary E. Farrell, K. Gopalakrishnan, Fay B. Hendricks, and Barbara Symroski of STOR and Svata M. Louda, BCF; the members of the Senior Scientist's Unit, BCF, who identified fish larvae—Elizabeth G. Stevens and Mary J. Kalin; those who processed the Nansen cast data—the staff of the Data Collection and Processing Group, SIO, supervised by Frances C. Wilkes.

Individuals who are due thanks include: Enid D. Duffield, BCF, for preparing tables for the introduction, composing and proofreading captions, and other indispensable clerical assistance; David Kramer, BCF, for editing and for many helpful suggestions concerning format; Nelson C. Ross, Jr., NODC, for his assistance in the early stages of processing the STD data; James R. Thrailkill, BCF, for contouring the fish larvae charts; John J. Dickenson, Timothy Geiser, Janet Rehm, and Stephanie M. Williams, STOR, for assistance with the nutrient chemistry data; David W. Asbury and Stephen T. Semegen, STOR, and Richard A. MacIntosh, BCF, for assistance with phytoplankton data; Robert C. Counts, BCF, and John del Pescaio and Jay Toumey of the NSF summer student program for running plankton volumes; Walter Lenz, SIO, for preliminary work on mixed layer depths; Maureen A. Knight, BCF, for assistance with physical oceanographic data and computer operations; and Frank W. Lyall and George M. Mattson of BCF for the cover design.

Acknowledgment is due to the participating agencies not located in La Jolla who performed the preliminary processing of their own cruise data and furnished the results to the EASTROPAC staff: Centro Nacional de Datos Oceanográficos, Chile; Coast Guard Oceanographic Unit; Instituto del Mar, Peru; Instituto Nacional de Pesca, Ecuador, which worked in conjunction with IATTC; Pacific Support Group of the Naval Oceanographic Office; Stanford Oceanographic Expeditions of Stanford University; Department of Oceanography, Texas A & M University; and Inter-American Tropical Tuna Commission, which processed the data from Mexican cruises. The preliminary data on bird observations were worked up at the Smithsonian Institution.

Cuthbert M. Love
Editor

[1]Miller, Forrest R, and Kenneth A. Bliss. 1970. Processing STD data and the construction of vertical temperature and salinity sections by computer. Bureau of Commercial Fisheries Fishery-Oceanography Center, La Jolla, California. Unpublished manuscript.

COLLECTION AND PROCESSING OF THE DATA

TEMPERATURE, SALINITY, AND DERIVED QUANTITIES

The in situ salinometer (STD) was the principal source of temperature and salinity data on EASTROPAC. On most EASTROPAC cruises temperature and salinity data from Nansen casts were used as a check on the STD. Nansen cast data were used to draw profiles only when an STD instrument was unavailable or was not working properly. Foreign cooperating vessels and some ships of opportunity did not have STD instruments so that all of their sections are based on Nansen casts. Unless otherwise indicated atlas charts showing distributions of temperature, salinity, thermosteric anomaly, and geostrophic velocity components are based on STD data. Sections of temperature, salinity, and thermosteric anomaly which are based on Nansen cast data can be identified by the presence of small circles indicating the discrete sampling depths.

On many cruises STD data were recorded on magnetic tape in digital form on a data-logger. Processing of these data was carried out with techniques and computer programs described by Jones (1969). The programs smooth the data and produce vertical profiles of temperature and salinity with values interpolated at 1-m. intervals. The interpolated data were written on magnetic tape which was then used as a data input for a program to contour vertical sections.

When a data-logger instrument was not available, the STD analog record was hand-digitized. Inflection points on the salinity and temperature traces were read, and the data were punched on cards. A linear interpolation program was used to produce values at 1-m. intervals, and the interpolated values were written on tape as the input to the computer program which draws the sections.

Temperature measurements on Nansen casts were made with reversing thermometers. Two protected thermometers were used on each Nansen bottle, and their results averaged if the values were within 0.10° C. above 300 m. depth or within 0.05° C. below 300 m. Depths of Nansen bottles were determined with pairs of protected and unprotected reversing thermometers. Depths for the observations were obtained by drawing L-Z curves and reading off the accepted depths. Salinity samples were analyzed on a Hytech Model 6220[2] laboratory salinometer or a University of Washington conductivity bridge aboard *Alaminos*. Samples from *Unanue*, *Yelcho*, and *Huayaipe* cruises were analyzed with an Autolab inductive salinometer. As a preliminary check on the quality of the Nansen cast data, salinity-thermosteric anomaly characteristic curves were plotted, and the suspicious values were eliminated before the data were punched on cards. The Nansen bottle temperature, salinity, and depth data were punched on cards, and a linear interpolation program was used to produce data at 1-m. intervals on magnetic tape.

All STD profiles were calibrated by comparing the STD output with Nansen cast temperatures and salinities. Differences between Nansen cast temperatures and salinities at approximately 400 m. and the STD temperatures and salinities at the corresponding depth were computed and plotted. At 400 m. the water is relatively isothermal and isohaline, and the offset in the STD can be determined without errors in depth strongly influencing the determination of the calibration factor. Least-square lines were fitted to the data by eye, and a set of average calibration factors was derived to make the STD and Nansen cast data compatible. In general, the calibration factors were less than 0.03 ‰ in salinity and 0.10° C. in temperature.

Vertical sections of temperature, salinity, and thermosteric anomaly were plotted by computer. The input data to the computer consisted of one magnetic tape for each cruise containing the corrected STD data at 1-m. intervals. Each file (station) of STD data was preceded by an information record giving date, time, and location of the station.

The program read temperatures and salinities for selected stations to be included in a vertical section into a two-dimensional array. For the upper 500 m. the data were selected at 2-m. intervals beginning at the surface; intervals of 5 m. were used between 500 and 1,000 m. The array of salinity data to be contoured was stored temporarily on magnetic tapes or on disk file while the contour analysis was being performed on the temperature data.

[2]References to trade names in this publication do not imply endorsement of commercial products by the Bureau of Commercial Fisheries.

The location of the preselected isotherms within the data array which were to be contoured was determined by a search routine which, initially, scanned the entire boundary of the array looking for the point to start the contour. From there the placement of the contour was determined by searching inward from the boundaries between adjacent points of data and locating a four point subset in which the isotherm lay. The exact placement of an isotherm within a subset was obtained by linear interpolation between adjacent points and also a linear interpolation along the diagonal between opposite corner points of the subset. This process was continued until all subsets of temperature data were searched for a particular isotherm. The grid points defining the location of an isotherm were scaled to inches (distance) from a specified plot origin, and they were written on tape together with the plotter commands. The location of all other isotherms followed by repeatedly searching the array. After all coordinates of the isotherms were located, scaled, and written on the plotter tape, the entire process was repeated with the salinity data. The preparation of STD data and the contouring routines were described in greater detail by Miller and Bliss (see footnote 1).

Because STD stations were not uniformly spaced along the cruise tracks, horizontal scaling factors were precomputed before running the contour program. The horizontal scaling information consists of assigned station numbers and distances (inches) between STD stations. These distances were based only on latitude for north-south sections and only on longitude for east-west sections; for all other sections they were based on both latitude and longitude. The scales for the vertical sections are: 3 cm. equals 60 miles horizontal distance; and 1 cm. equals 10 m. in depth for the 0 m. to 300 m. portion of the section, and 1 cm. equals 20 m. for the 300 m. to 1,000 m. portion of the section.

The STD contour program was written in FORTRAN-63 computer language for a Control Data Corporation (CDC) 3600 computer with a 32,000 (48 bit) word core memory. Some CDC type logic statements were used, but these were convertible to FORTRAN IV type statements. A minimum of two magnetic tape units was required during execution of the program. As many as 55 STD stations to a depth of 500 m. could be used during a single run of the program. Owing to the limitation of core memory size, the program allowed for only 38 stations with depths to 1,000 m. on a single run.

The electronic plotter used was a CALCOMP (model 763) 30-inch drum type with zip mode of operation. It has a plot resolution of 100 increments per inch. All EASTROPAC plots were made with a 0.2 size plotting pen using CALCOMP black ink. Plotter commands and data points references were written in FORTRAN language with calls to CALCOMP plot subroutines stored on a library tape at the University of California, San Diego (UCSD) Computer Center.

Geostrophic velocity computations were done relative to 500 db. Data for the computations were selected in the following ways. The computer went along the section and selected successive stations whose separation was greater than 110 km. (approximately 1° of latitude). The geopotential anomaly was computed at these two stations, and the difference in geopotential was used to compute the geostrophic velocity component. The sections represent the average geostrophic velocity component over distances that usually lie between 110 and 138 km. For example, on the north-south sections only rarely did the distance between stations exceed 1.25° of latitude. The same contouring program was used for drawing vertical sections of geostrophic velocity that was used for the temperature, salinity, and thermosteric anomaly fields. Since the geostrophic velocity is an average velocity between two points, it is only continuous in the vertical. Montgomery and Stroup (1962) discussed the choice of a method of representation of geostrophic velocity and argued against the advisability of representing the geostrophic velocity with isotach (equal velocity) contours. As they pointed out, this type of representation is only appropriate to a field which is continuous vertically and laterally. The isotach representation was chosen to present the geostrophic computations in order to expedite the processing of the EASTROPAC data. It was felt that the programming effort required to develop a different representation for geostrophic computations was not justified. The main distortion

of the field of geostrophic velocity by the contouring program is the linear interpolation of the contours between average velocities. The average geostrophic velocity field is basically discrete and not continuous. Lateral gradients of velocity are certainly distorted and should not be read directly from the contours.

Bruce A. Taft
Forrest R. Miller

THICKNESS OF THE UPPER MIXED LAYER

The bottom of the upper mixed layer was defined somewhat arbitrarily by the depth where the vertical temperature gradient first exceeded 1° C./m. To eliminate consideration of transient gradients, this criterion gradient was required to hold over a reasonable depth interval, usually 10 m. Though seldom violated, the condition also was imposed that no portion of a major halocline should overlie the depth found to represent the bottom of the mixed layers by the thermal criterion.

Most of the processing work was done from analog traces of the Bissett-Berman Salinity-Temperature-Depth (STD) system and the General Motors (cruise 11 only) expendable bathythermograph (XBT) systems, rather than from digital results. Where disagreement between STD and XBT series occurred, the STD results were used.

Plots of mixed layer thickness were made along cruise track lines and a smoothing line was eye-fitted to each track line segment to reduce the effect of internal waves and other sources of variation on scales too small to have been sampled adequately. The smoothing lines then were used to construct the charts showing the thickness of the upper mixed layer during each of the seven cruise periods of EASTROPAC.

Robert W. Owen, Jr.

DISSOLVED OXYGEN

The Carpenter (1965) modification of the Winkler method of oxygen determination was used without further change with the exception that calibrated biochemical oxygen demand (B.O.D.) bottles were used rather than the Erlenmeyer flasks specified by Carpenter.

Upon return to shore, the data were processed at La Jolla in the following manner. With due regard to when reagents were changed, standard and blank titration values were plotted against time (days) for each cruise, and eye-fitted averaging lines were drawn through the points to establish computing values. Next, analyst's comments were scanned to rid the data of obvious errors, and the remaining titration values were computed, tabulated, and profiled using the CDC 3600 computer. Tabulations and profiles then were individually scanned and compared with neighboring station values: where "rogue" points were encountered, the analyst's original comments were referred to and the value was discarded either if the comments or departure from the normal pattern warranted rejection. Values which received an analyst's comment of uncertainity were retained if no departure from the normal profile could be discerned.

Edited card decks then were submitted to the computer facilities at the UCSD to be machine-contoured (vertical sections) or machine-plotted for hand contouring (horizontal fields). Vertical sections then were inspected, re-edited and rerun for the final version.

Closed contours isolating single observed values in the vertical sections were eliminated if the difference between the contour value and the observed value was less than 0.05 ml./l. By comparison, the smallest contour interval used was 0.25 ml./l.

Horizontal charts of oxygen at 10-m. depth are presented in the form of percent saturation rather than oxygen concentration because it was felt that percent saturation was a better measure of oceanographic sources of variation (vertical mixing, plant production) and was a better measure of oxygen conditions in the surface mixed layer than was oxygen concentration itself. The 10-m. depth was chosen because surface values were erratic, possibly because of ship's influence, and because the 10-m. values do in fact represent surface conditions.

Saturation values were computed using a program which employs a polynomial fitted to the tables of saturation as a function of temperaure and salinity given by Gilbert, Pawley, and Park (1967).

Robert W. Owen, Jr.

METEOROLOGY

General

The meteorology described in this atlas consists primarily of surface analyses and data plots of selected sea surface meteorological elements observed over the oceanic areas of the eastern tropical Pacific (ETP) as defined below. On *Jordan* 20 and 30 cruises and on the *Oceanographer* cruise, U.S. Weather Bureau, ESSA, personnel, who were on board the vessels, observed upper air temperature (by radiosonde) and humidity. On the *Rockaway* cruises, they observed the upper air winds, too. Upper air vertical sections are included in the atlas only along cruise tracks because of the sparsity of data elsewhere over the eastern tropical Pacific. Surface meteorological observations (International ship weather code: FM 22.D) were taken at 3- to 6-hour intervals along cruise tracks by U.S. Weather Bureau personnel when aboard or by the bridge crew on American vessels. Mexican and South American ships participating in EASTROPAC recorded weather on the bathythermograph logs in most cases.

In order to fill in as much of the eastern tropical Pacific, 30° N. to 25° S. and 70° W. to 130° W., as possible, all other maritime weather observations (International ship weather codes: FM 22.D, FM 23.D, and FM 26.D) collected and made available by the Bureau of Commercial Fisheries, La Jolla, California, were included in the preparation of the meteorological data for the atlas.

Wherever data permitted, analyses were extended to the boundaries of the EASTROPAC base chart rather than restricting them to the areas along the cruise tracks. This permitted a more accurate and definitive presentation of the meteorology in areas over and adjacent to cruise tracks. Furthermore, the larger scale meteorological analyses provided background information which may be directly related to physical and biological environmental features of the oceans.

Meteorological observations were never uniformly distributed over the eastern tropical Pacific; but most of the data were distributed along EASTROPAC cruise tracks and over the shipping lanes into and out of the Panama Canal and along the coastlines of the Americas. In order to provide detailed analyses, observations were averaged over squares of 2° latitude and longitude. In regions of sparse data, particularly south of 10° S., between 70° W. and 110° W., climatology combined with averaged observations along the shipping lanes formed the only data base for extending the analyses. Reasonable analyses were possible over sparse data areas because the temporal and spatial distribution of ship's observations covered the period of analysis. Because of the relatively slow-changing weather patterns over the eastern tropical Pacific during most of EASTROPAC, data were composited into sets covering periods of 12 to 16 days. In general, these meteorological periods were centered around the dates when the research vessels were sailing along the principal cruise tracks. However, because of rapidly changing weather patterns north of the equator during the August-September summer survey (40-series cruises) the analytical periods were reduced to 8 to 10 days with a 3- to 4-day overlap for those cruises.

In order to present the meteorology of the eastern tropical Pacific in a manner which is most useful to the study of atmospheric (marine layer) conditions as they relate to the oceans and fishery ecology, three basic series of charts are presented: one series depicts the surface air flow in terms of surface winds and pressure; another series represents surface sea and air temperature conditions, and the third series displays the clouds and moisture distribution over the eastern tropical Pacific with the total cloud cover, dew point temperature, and frequency of precipitation reported from ships. The first and second series cover semimonthly periods. The third series has one chart per month because of the great variability in clouds and moisture and because there were insufficient data to obtain representative averages for periods less than a month over most of the ETP area.

Processing the Observations

All of the meteorological observations taken aboard research vessels participating in EASTROPAC were punched on cards in the international ship weather code. Each observation was quality-checked with a computer program which set acceptance limits based on the climatology of each element reported. An observation considered erroneous was printed out and hand-checked for possible correction. After errors were corrected, wherever possible, selected elements were averaged by 2° and by 5° of latitude and longitude (referred to hereafter as 2° and 5° squares). The results were printed out and punched on cards by the computer. The processing of research vessel data was performed in subsets by cruise periods. Computer plots of 2° averaged data were made and analyzed for each cruise period. These analyses and data plots formed the composite sets which served as key or control analyses for coordinating the analyses of the larger data sets covering the entire EASTROPAC area.

The charts in the atlas are constructed from all observations available from research and merchant vessels sailing in the eastern tropical Pacific. The Bureau of Commercial Fisheries in La Jolla maintains punch card files of all available weather observations taken by ships in the Pacific Ocean. Merchant ship observations were processed for this atlas by computer and averaged by 2° squares in the same manner as described for research vessels. There were approximately 2,500 merchant ship observations available for each month, and about 10 percent of these contained one or more errors. Approximately 80 percent of the erroneous observations could be corrected and inserted back into the data files. These observations were well distributed diurnally and throughout the month so that daily or semimonthly biases were minimized.

Because of the general sparsity of data over much of the eastern tropical Pacific, all merchant ship observations were combined with those from research vessels into composite sets. Preliminary analyses of each meteorological element were prepared from computer plots of the 2° averaged data. The atlas charts contain analyses based on 2° averages superimposed on plots of data averaged by 5° squares. The data plots show the large scale distribution of observations. The limitations in, and preparation of, averaged values of each meteorological element used in constructing the series of charts are described in the following paragraphs.

Surface Winds

Surface wind observations on all research ships, and increasingly on merchant ships, are measured accurately by anemometer. Winds estimated from the state of the sea also are accurate enough to be used in the analysis when speeds are greater than 5 kn.

Surface winds represent the air flow in the marine layer of the tropical atmosphere more accurately than does the pressure field. Therefore, streamline and isotach analyses have been emphasized in representing the composite low level direction and speed of air flow over the eastern tropical Pacific. Streamlines are drawn parallel to mean resultant winds which are computed from the east-west and north-south components of wind direction and averaged by 2° and 5° squares. Isotach analyses are based on the mean resultant wind speeds which are obtained from averaged components of observed winds. A detailed discussion of wind analysis by the streamline-isotach method can be found in several textbooks on

tropical meteorology, including Riehl (1954). A good estimate of the mean wind speed, without regard to direction, can be obtained by multiplying the mean steadiness of the wind for a particular location and month, obtained from marine meteorological atlases (Marine Division of the Meteorological Office, 1965; U.S. Navy, 1959), by the mean resultant wind speed obtained from the appropriate chart in this atlas designated MW.

Streamlines and isotachs were not extended into areas where observations were not available. However, where winds were observed along shipping lanes for at least part of a month, the extended streamlines and isotachs reflect an estimate based on climatology modified by the available data over sparse data areas.

Sea Surface Pressure

Surface pressures are usually observed aboard ships with precision aneroid barometers. They are reported more frequently than winds, especially during very light wind conditions. All surface pressure observations were checked for gross errors in reporting. Corrections for diurnal variation in pressure were applied as required, but because of the uniform distributions of observations (except in sparse data areas), the averaging over 2° squares eliminated most of the diurnal bias. The pressure field as depicted by isobars on charts designated MW reflects the general state of the atmosphere.

Intertropical Convergence Zone

The intertropical convergence zone (ITCZ) is also displayed on each chart that depicts surface wind flow and pressure. The climatological position of the ITCZ for each month is based on 77 years of ship observations obtained from the National Weather Records Center and prepared at Goddard Space Flight Center, NASA (Allison, Kreins, Godshall, and Warnecke, 1969).

In the atlas the climatological position of the ITCZ can be compared with the average position of the ITCZ for the specified EASTROPAC period. The ITCZ is found where the winds (streamlines) of both hemispheres converge asymptotically, where surface pressures are lowest (approximately 1010 mb.), and where wind speeds are generally under 10 kn. This area is also referred to as the "doldrums."

Sea Surface Temperature

Sea surface temperatures measured aboard research vessels participating in EASTROPAC were based on bucket thermometer or thermograph measurements. On most of the merchant ships sea surface temperatures were measured in the sea chest of the water injection system. Because of the accuracy of research vessel data, sea surface temperature analyses were completed from composite sets of these data to include an entire survey or monitor period. These analyses, which included surface temperatures from STD casts, provided the required quality control needed for checking the larger ETP area analyses based on all available sea surface temperatures averaged over 2° squares.

All sea surface temperatures were quality checked against a climatology derived from bathythermograph surface temperatures for the eastern tropical Pacific compiled by Scripps Institution of Oceanography and analyzed for each month (Wyrtki, 1964). The climatological sea surface temperatures provided a data base for computing sea surface temperature anomalies and for quality control checking the observations. The anomalies were useful also in constructing the sea surface temperature charts because accurately averaged temperatures usually showed consistent anomaly patterns. The temperature data which passed the initial computer checks but had small errors showed up on the charts as unusually large anomalies. Since significant anomaly patterns of sea temperature may be related to significant physical or biological changes in the ocean, the anomaly patterns have been superimposed on the isotherms (1° C. intervals) in charts designated MT. These patterns delineate areas which experienced anomalies in the sea surface temperatures of ± 1° C. or more.

Surface Air Temperature

Surface air temperatures observed on all ships reflect large diurnal and areal variations. Heating of the ship during the day is often reflected in high temperatures, and ship observations taken near the Americas are affected frequently by the hot or cold temperatures advected seaward from land. However, most of the averaged air temperatures observed away from continental influence did not reflect diurnal bias.

In the chart series designated MT, the difference between sea surface and surface air temperatures, averaged over 5° squares, is plotted. This difference is not reliable in sparse data areas. However, it reflects the stability of the marine layer of the atmosphere, i.e., colder sea temperatures in upwelling areas are associated with a stable lower atmosphere. Air temperatures derived from the sea surface temperatures and sea-air temperature differences provide reasonable values of air temperature, except near coastlines and over sparse data areas. Sea-air surface temperature differences and the air temperatures averaged for 2° squares are available in the EASTROPAC data file.

Dew Point Temperature

The surface dew point temperature is one of the elements which can be measured accurately at sea and reflects existing moisture or humidity conditions in the marine layer with less diurnal variation than the air temperature. This temperature is important also in determining the vapor pressure gradients between the sea surface and the lower atmosphere for energy budget computations.

Dew point temperature analyses appear in the cloud and moisture series of charts designated MC. The dew point isotherms are based on averages for 2° squares. They are superimposed over plots of dew points averaged over 5° squares. In the eastern tropical Pacific, high values of dew point temperatures are closely associated with extensive low and middle level cloudiness and the intertropical convergence zone. In areas of upwelling, dew point temperatures are usually lower than sea surface temperatures so that fog is seldom found over open ocean areas. The low surface dew point temperatures also reflect the general dryness of the tropical atmosphere above a shallow marine layer.

Cloudiness

Clouds, their types and amounts, constitute one of the most variable meteorological elements observed over the eastern tropical Pacific. For the past several years weather satellite photographs have revealed this variability as well as the complexity in cloud structure over the eastern tropical Pacific.

Surface marine observations included fairly accurate estimates of the total cloudiness (sky cover). However, there were seldom enough observations which accurately report the vertical cloud structure. Because of the difficulty in accurately depicting the three-dimensional cloud patterns, analyses of total cloud amounts (low, middle, and high clouds combined and reported in eighths of the sky covered) were prepared. In sparse data areas total cloud cover analyses were based on satellite data from two sources: (1) photographs on 35-mm. film available from ESSA (Environmental Data Service, 1967, 1968a, 1968b), and (2) mean monthly total cloud cover charts derived from weather satellite nephanalysis by Sadler (1969). An estimate of the predominant cloud type, associated with the cloud cover charts in the EASTROPAC Atlas, can be obtained by referring to marine meteorological atlases referenced in the section on surface winds.

Precipitation

Observations of precipation in the tropics show greater variability than any other observed element. Rainfall amounts cannot be accurately measured from a moving ship; therefore, the frequency of rainfall reported at or near a ship provides the only information available over oceanic areas of the eastern tropical Pacific.

Because of the relatively short period of EASTROPAC no attempt has been made to interpret in detail the percentage frequency of rainfall reported from ships. Rather, the average percentage frequency of all types of rainfall (within sight of a ship) taken over 5° squares was plotted on the charts designated MC. In addition, areas where ships reported rainfall for 15 percent or more of the time were outlined for quick reference to the more rainy areas of the eastern tropical Pacific. The large-scale precipitation patterns of the EASTROPAC period have not reflected unusually large deviations from those based on long-term means and displayed in meteorological atlases. Although the schematic presentation of rainfall frequencies in this atlas agrees well with the other meteorological elements that indicate bad weather for each chart period, the results should be reviewed with caution.

Forrest R. Miller

NUTRIENT CHEMISTRY

Water samples drawn from Nansen bottles were analyzed aboard ship for the following phytoplankton nutrients: inorganic phosphate-phosphorus, nitrate-nitrogen, nitrite-nitrogen, and silicate-silicon. On survey cruises 11, 12, 45, 46, 75, and 76 and on monitoring cruises 20, 30, 50, and 60 the Technicon auto-analyzer was used with the methods of Armstrong, Stearns, and Strickland (1967), which are also described by Strickland and Parsons (1968). On other cruises nutrients were determined manually by the methods outlined by Strickland and Parsons (1968). The methods were standardized by running known concentrations of each nutrient along with samples from each Nansen cast.

Peak values of absorbance were read from the autoanalyzer charts or with a Beckman Model DU spectrophotometer; these were used to calculate nutrient concentration either at sea or ashore. Some calculations were done with desk calculators; others were done by computer. For each station, profiles or concentration vs. depth were plotted by computer plotter and checked for obvious errors by visual inspection. Errors that escaped this preliminary check were detected later when vertical sections were drawn.

For each cruise period, maps of the horizontal distribution of phosphate, nitrate, and silicate were drawn for depths of 10 and 100 m. Values were entered either by hand or by computer plotter and were contoured by visual inspection. The horizontal distribution of nitrite at 100 m. proved to be highly irregular and has not been shown in the atlas. All vertical sections were drawn by computer plotter using programs described by Miller and Bliss (see footnote 1).

On some cruises, samples for ammonia analysis were frozen and analyzed ashore at La Jolla. The method of Richards and Kletsch (1964), which includes some labile amino nitrogen along with ammonia, was used. Ammonia values were low (generally <1 μg.-at. N/l.) and were distributed irregularly so that vertical sections and horizontal maps could not be contoured. Values at 10 and 100 m. were entered on maps of the area so that the general magnitude of the ammonia concentration could be shown in the atlas.

William H. Thomas

PHYTOPLANKTON STANDING STOCKS AND PRODUCTION

Sample Collection

Samples were taken from special casts on two stations per day, at noon and midnight. Production and phytoplankton pigments were measured from the noon samples, and plant pigments alone were measured from the samples collected at night. Reversing bottles made of biologically inert lexan plastic were most generally used, supplanted on occasion by bottles made of polyvinyl chloride (PVC) plastic. In either case there was no contact of sample water with known ionic contaminants. Sampling bottles were scrubbed routinely to reduce biological contamination.

Sampling depths were calculated from the depth of disappearance of a 20-cm.-diameter Secchi disk. This depth was taken to represent the depth where green light was 16 percent of that at the surface at each noon station. The depth where light intensity corresponded to that in each of seven bottle spaces in the production experiment incubators then was selected off a semilogarithmic plot of transmittance vs. depth. These depths spanned the euphotic zone, as defined by the layer of water lying above the depth where light was 1 percent of surface intensity. At night stations, the depths sampled were those of the previous noon station. Additional depths below the euphotic layer generally were sampled for plant pigment analysis at both types of station.

The translucent sampling bottles were taken into the laboratory directly upon recovery to reduce the adverse effect of direct exposure to full sunlight on noon stations. Water was drawn soon after collection to minimize sedimentation of cells. Samples for plant pigments were drawn into rinsed 270-ml. plastic bottles and placed out of direct light until filtration. Samples for production experiments were drawn into scrubbed and rinsed 270-ml. glass bottles and stored dark until incubation.

Shipboard Sample Processing

Pigments.—Samples in 270-ml. plastic bottles were filtered under low vacuum (not exceeding –7 p.s.i.g.) through Whatman GF/C glass fiber filters (2.4-cm. diameter) having a thin magnesium carbonate coating. Filtration was nearly always completed within a half hour after sample collection.

Filters then were placed in 90 percent-v/v-spectral-quality acetone, ground for 30 seconds in a motor-driven tissue grinder and stored dark for 10 minutes to permit full extraction of the pigments. Filters and extract were separated by centrifuging for 10 minutes. Extract volume was brought up to 10.0 ml.; about 5 ml. was placed in a cuvette and submitted to a Turner fluorometer, Model 111, for fluorometric analysis by the method of Holm-Hansen, Lorenzen, Holmes, and Strickland (1965). A blue-pass Corning 5-60 primary filter and a red-pass Corning 2-64 secondary filter were used in conjunction with the light source and the detector, a red-sensitive multiplier phototube (Hamamatsu R 136).

Production.—Samples in 270-ml. glass bottles received 1.00 ml. of sterile $NaH^{14}CO_2$ solution buffered at pH 9.0. Activity was usually 20 μc./ml., but in the richer waters of the easternmost part of the survey region, solutions having 10 μc./ml. were sometimes used. Directly after inoculation, samples were loaded into two cylindrical incubators, one completely opaque and the other made to transmit 100, 50, 25, 12, 6, 3, and 1 percent of incident sunlight across discrete segments along its length to accommodate one sample in each segment with sufficient room between samples to insert opaque bumpers. The body of the light incubator was of lucite plastic wrapped with neutral density fabric screens which in turn were protected by an outer sheath of lucite plastic tubing. The opaque incubator was constructed of PVC plastic.

When loaded with inoculated samples the incubators were placed on deck under full exposure to sun and sky radiation. Timing of sample collection and inoculation was such that deck incubation could be started at local apparent noon. Incubation continued until local sunset, when the samples were recovered for filtration.

Filtration was conducted in subdued light at vacuum not ordinarily exceeding –7 inches of mercury using Gelman membrane filters (2.5-cm. diameter) with 0.45-μm. pore diameters. Filters then were glued lightly to identified copper planchets, placed in perforated pill boxes, and stored in desiccators until their return to shore for radioassay.

Sample Processing Ashore

Pigments.—As mentioned previously, plant pigments usually were analyzed at sea. On occasion, however, a fluorometer failure occurred and sample filters were folded, stored dark in a freezer, and analyzed later if the instrument could be repaired, or returned frozen to La Jolla for analysis. Values so obtained were multiplied by 1.1 to account for the consistent 10 percent loss that occurs when samples are stored for more than a day. Data on file to which this correction has been made are identified by asterisks.

Production.—Upon their return to shore for radioassay, membrane filters from production experiments were fumed over concentrated HCl for 10 minutes, sorted by station and returned to their desiccators to await beta-assay. As soon as possible after fuming, samples were turned over to Gulf General Atomic Corporation, La Jolla, where by contract agreement samples were counted in their radiological laboratories on Beckman wide-beta gas flow counters. Detector end windows were of 80-μg./cm.^{2} Mylar with 5.72-cm. diameters. Samples were counted for 3 minutes. Background counts, subtracted from each sample count, were determined each day and usually did not exceed three counts per minute. Counter efficiencies were 27.0 and 34.0 percent during the entire period of analyses of EASTROPAC samples, as determined from point-source standards calibrated against those maintained by the National Bureau of Standards.

Computation

All phytoplankton data were card punched, verified, and submitted to the CDC 3600 computer at UCSD for calculation of basic phytoplankton parameters. Computed and listed by cruise, station, and depth were chlorophyll *a* concentration, phaeo-pigment concentration,[3] total pigment concentration, phytoplankton production per unit volume, and several parameters for use in editing and interpreting these basic values. Also printed were interpolations and vertical profiles of pigment and production values.

Pigment concentrations were calculated from the equations given by Lorenzen (1966):

$$\text{chlorophyll } a\,(\text{mgm}^{-3}) = \frac{\frac{Fo/Fa_{\max}}{(Fo/Fa_{\max})-1}(k_x)(Fo-Fa)}{\text{liters filtered}}$$

$$\text{phaeophytin } a\,(\text{mgm}^{-3}) = \frac{\frac{Fo/Fa_{\max}}{(Fo/Fa_{\max})-1}(k_x)[Fo/Fa_{\max}(Fa)-Fo]}{\text{liters filtered}}$$

where: Fo = fluorescence before acidification
Fa = fluorescence after acidification
$Fo/Fa_{\max}$ = maximum acid factor which can be expected in the absence of phaeophytin
k_x = calibration constant for a specific sensitivity scale.

The k_x factors were determined by submitting known concentrations of chlorophyll *a* to each fluorometer and observing fluorescence units. Linearity of each instrument was checked by serial dilution of pigment extracts. The $Fo/Fa_{\max}$ factor was determined by observing fluorescence before and after acidification of extracts of diatom and dinoflagellate cultures sampled in logarithmic phase of growth; phaeo-pigments thus were absent.

Production rate of the phytoplankton was calculated from the equation:

$$\text{Production (mg. C/m.}^3\text{/day)} = (L - D)\left\{\frac{W}{A \times E}\right\} \times 1.05 \times 1.51 \times 2$$

where: L = counting rate (counts per minute) of the phytoplankton in the light bottle

D = counting rate (counts per minute) of the phytoplankton in the dark bottle

W = weight of carbonate carbon in the water assumed to be 25,000 mg./m.^{3}

A = discharges per minute by the radiocarbon added to each sample; usually 4.44×10^7 d.p.m.

E = counter efficiency, 0.270 and 0.340 for the two counters used

1.05 = factor to allow for difference in uptake rate of ^{14}C as compared with that of ^{12}C

1.51 = correction to bring incubator values close to those found by true in situ incubation (Doty, Jitts, Koblentz-Mishke, and Saijo, 1965)

2 = correction from the half day incubation period to full day.

Editing

Pigments.—Values were examined station by station. Constancy of the shape of each vertical profile was considered and in the few cases where a deep maximum occurred that was defined by a single observation, a scale reading error was presumed to have occurred and the value was rejected. In addition, the profile of the acid factor, the proportional change of pigment fluorescence upon acidification of the extract, was examined. This factor normally decreased monotonically from surface layer values near 2 to deep (150 to 200 m.) values near 1. Where single significant departures from this pattern occurred, sample values either were justified from the basic data, or, if no simple change of values could be supported in terms of analyst error, the observation was rejected. Apparent errors and rejections both were rare, never exceeding 0.1 percent on most cruises.

Production.—Predictably, plant production experiment results required more editing than did those of pigment analyses. One batch of ^{14}C solution, provided by a commercial source in sterilized ampoules, later proved to have been contaminated by fungus. Because the strands, or hyphae, were "hot" and because they were deposited on filters in varying concentrations, much of the production data obtained on the first set of survey cruises (10-series) and on part of the first monitor cruise (20) had to be rejected. Neither fuming nor autoradiography proved of value in salvaging data.

Criteria for rejection of production values with good ^{14}C stocks were developed after samples from all cruises were processed to provide uniform applicability. We first rejected values for which the corresponding dark count exceeded 100 counts per minute except when the production value was consistent with others in the same vertical profile.

Next, production/chlorophyll ratios were examined statistically for each cruise at each light level. In nitrate-deficient waters, production values were rejected when this ratio exceeded two standard deviations of the mean value for the light level and cruise in question. We felt this necessary in view of the occasional erratic values encountered that were due to unidentifiable errors in experimental procedure or contamination of the sample. Values obtained from

[3] Phaeo-pigments are degradation products of chlorophyll *a* and represent detrital pigment.

richer waters were rejected only if they exhibited a radical departure from the normal vertical profile pattern.

Values for entire stations were rejected when the vertical profile was so erratic as to indicate light leaks in the incubator, inadvertent exposure to ambient light during filtration, or contamination of the sample.

Integration Over Depth

Integrations with respect to depth were performed on both plant pigment and production data using computer programs written for the CDC 3600. The programs were based on Simpson's Rule for irregular areas and therefore use a linear interpolation between observations.

Plant pigments, both chlorophyll *a* and phaeo-pigment concentrations, were integrated to 150 m. to express the total pigment under a square meter of sea surface. Except in the extreme southern portion of the survey tracks (south of about 16° S.), there exist only minute quantities of plant pigments below 150 m. Where observations did not reach 150 m., the fraction below the last observed depth was estimated from other stations in the vicinity (sometimes from other cruises to the same area) and added to the observed integral.

Plant production and chlorophyll *a* were computer integrated to the euphotic depth at each station to express total production per unit of sea surface area and total pigments involved in photosynthesis.

Mapping

Horizontal distributions of surface and integrated values of phytoplankton parameters were hand-plotted and contoured. The resulting charts are somewhat smoother than would have resulted from computer contouring because some interpretive selection was used, e.g., at saddle points or at two closely spaced values.

Vertical sections were computer-plotted and hand-contoured.

Shading of plots is arbitrary and serves only to impart a more immediate sense of the field of values than do labeled contours alone. The shading scheme for each parameter is, however, consistent throughout the atlas.

Robert W. Owen, Jr.
Bernt Zeitzschel

ZOOPLANKTON AND FISH LARVAE

During EASTROPAC cruises zooplankton hauls were routinely taken with three types of nets four times daily at the prime oceanographic stations. Oblique hauls between about 200 m. and the surface were made with 50-cm. and 1-m. mouth diameter nets in a paired-frame, and a horizontal haul at the surface was made with a 1-m. mouth diameter net. Collections taken with the 50-cm. net were for zooplankton biomass studies and with the 1-m. nets for fish eggs and larvae studies. In addition special zooplankton collections were taken with a Longhurst-Hardy Plankton Recorder and submerged pump on selected cruises; these will be discussed in future research papers. Only collections taken in the oblique hauls are considered in this atlas.

The 50-cm. net has a length of 3.5 m. and is constructed throughout of 333 Nitex nylon mesh (mesh aperture 0.333 mm.). It is fixed to a hoop in a frame assembly which also contains a hoop for the 1-m. net. The 1-m. net has a body 4.3 m. long which is constructed of 505 Nitex nylon mesh (mesh aperture 0.505 mm.), and a cod-end 0.35 m. long which is constructed of 333 Nitex nylon mesh. The frame assembly holding the two nets was attached to the towing wire by a short four-lead bridle preceded by a rope 3 to 4 m. long. The rope was clamped to the towing wire about 3 m. above a 45-kg. weight attached to the end of the wire. The haul was taken with the ship steaming slowly in an attempt to maintain a wire angle of 45°; the speed of the ship was usually about 1.5 to 2 kn. To make the haul, 300 m. of towing wire was payed out at 50 m. per minute, held at maximum depth for 30 seconds, and retrieved at 20 m. per minute. A wire angle reading was taken at each ½-minute interval during the retrieval of the net.

The depth of towing was estimated from wire angle and length of wire out, assuming that the wire described a straight line in the water during the haul (Ahlstrom, 1952). A maximum depth of 200 m. was desired, but estimated depths ranged from 75 to 254 m. The mean estimated depth for all hauls was 204 m. with a standard deviation of 13.21 m. A mechanical depth gauge was attached to the net frame on one cruise for 88 hauls to compare estimated and measured maximum depths. In many cases the measured maximum depth of sampling varied considerably from the estimated depth. The estimated maximum depth was deeper than the measured depth in 98 percent of the hauls (range 1 to 120 m.) and shallower in 2 percent of the hauls (range 16 to 27 m.). The differences between estimated and measured depths were especially pronounced at stations near the equator, where surface and subsurface currents often flow in opposite directions.

The amount of water strained during each haul was measured by a TSK flowmeter suspended in the mouth of each net. The flowmeters were calibrated before and after each cruise, and the average of these calibrations was used to compute the volume of water in cubic meters for each haul. The zooplankton collections were preserved at sea in buffered 10-percent Formalin sea water.

The standing stock of zooplankton taken with the 50-cm. net is expressed as milliliters of displacement volume of the catch of small organisms per 1,000 $m.^3$ of water strained; organisms greater than 5 cm. in length or greater than 5 ml. in volume are excluded in the displacement volume measurements. The method of measuring displacement volume is described by Ahlstrom and Thrailkill (1963). Standardization calculations were done by computer.

Analysis of variance and analysis of covariance indicated that night-day differences in the zooplankton standing stock were highly significant. Various methods of combining night and day hauls by time-adjustment were attempted, including the method of King and Hida (1954), running mean, and night/day ratio, but none appeared to be satisfactory. Instead, night and day hauls are treated separately, and separate charts are presented for night and day samples. Examination of Simrad echo-sounding profiles indicated that the greatest rate of change in depth and configuration of scattering layers occurred between about 1 hour before and 1 hour after sunrise and sunset. Hauls taken between 1 hour after sunrise and 1 hour before sunset were regarded as day hauls, and hauls taken between 1 hour after sunset and 1 hour before sunrise were regarded as night hauls. Hauls taken during twilight, i.e., between 1 hour before and after sunrise and sunset, are not included in the analyses.

Estimates of sampling variability were obtained from a series of 17 zooplankton hauls made with the 50-cm. and 1-m. nets over a 24-hour period at roughly the same geographical position. Hauls made during darkness and daylight were regarded as replicates for night and day, respectively. The coefficients of variation were smaller for replicate collections made with the 1-m. net (night 17 and day 24 percent) than with the 50-cm. net (night 37 and day 63 percent).

The charts of zooplankton standing stock presented in the atlas were generated by computer with only minor alterations and drafting done by hand. In practice, the value of the standardized zooplankton displacement volume at each station for each cruise period was plotted by computer plotter, and a separate plot of the contours of the data field and station position markers for each cruise period was also generated. The contour plot was quality checked by overlaying it on the plot showing the displacement volume for each station. Sometimes minor corrections of the contour plot were necessary at the edge of the data field or in locations of sharp gradients, and these changes were made by hand. The labels on the contours were hand-drafted and values greater than 200 ml./1,000 $m.^3$, which indicate areas of high standing stock of zooplankton, were shaded. The circular symbols on the charts show the location of stations where data were collected.

All fish eggs and larvae were sorted from the total sample of each 1-m. oblique net haul collection. The larvae were identified to species or to whatever taxon practicable. Fish larvae other than tuna were identified by E. H. Ahlstrom and tuna larvae were identified by W. L. Klawe. Because of the large number of fish larvae species identified, it was necessary to limit charts in the atlas to the selected categories mentioned below. Distributional studies of fish larvae will be discussed in detail in future research reports. The computer was used to plot the number of larvae of each species or category collected at each station for each cruise period, and the data were contoured by hand. Separate day and night charts were prepared for total fish larvae and the larvae of the gonostomatids and sternoptychids and myctophids. Also a single diel chart was prepared for larvae of skipjack tuna, *Katsuwonus pelamis*, frigate mackerel, *Auxis*, and dolphin (fish), *Coryphaena*, and total fish eggs.

R. Michael Laurs

MICRONEKTON

Micronekton consists of organisms including fishes, cephalopods, and crustaceans between about 1 and 10 cm. in size. It was collected in oblique hauls of the large net, 1.5 m. square at the mouth, described by Blackburn (1968). The net is of uniform mesh, approximately 5.5 x 2.5 mm., which retains animals greater than or equal to 1 cm., but not smaller (Jerde, 1967). On most EASTROPAC cruises usually two micronekton hauls were made per diel, one near local noon and one near local midnight. The daytime catches were of the order of one-tenth the size of the night catches as expected, an effect of net avoidance and diel vertical migration of many kinds of animals. Thus, the data on day catches underestimate the standing stock of micronekton and are not considered in this atlas, although they will be used in a research report on distribution of tuna forage. The hauls were made at ships speeds that were estimated at 5.0 kn. for *Argo, David Starr Jordan, Alaminos, Thomas Washington,* and *Oceanographer,* 4.0 kn. for *Undaunted* and 6.4 kn. for *Rockaway*. The other EASTROPAC ships did not make micronekton hauls. *Rockaway* did not make micronekton hauls on cruise 13.

The method used for micronekton hauls was to pay out 800 m. of towing cable at 50 m. per minute and then retrieve it immediately at 30 m. per minute. The maximum depth of the net on each haul was expected to be about 200 m. at a ship speed of 5 kn. For 294 hauls on which maximum depth was measured by a depth sensor the arithmetic mean and standard deviation were 197 m. and 36.4 m., the range was 100 to 348 m., and the coefficient of variation was 18.5 percent. The collections were preserved at sea in buffered 10-percent Formalin sea water.

An estimate of sampling variability for night hauls is given by a series of 11 hauls made during one night at approximately the same geographical position. The coefficient of variation of the catch volumes was 20 percent.

All the night micronekton catches were sorted in the laboratory into the following groups: (1) *Vinciguerria* spp., (2) other epipelagic fish, (3) *Pleuroncodes* spp., (4) other crustaceans, (5) cephalopods, (6) other mesopelagic fish, and (7) leptocephali. Other animals in the catches, mainly large zooplankters such as tunicates and medusae, were not considered as micronekton and were ignored. The displacement volume of each group was measured in milliliters. The preserving fluid was removed from the animals by placing them on screens and allowing them to drain, and then measuring their displacement volume in water. The crustaceans were sorted further, approximately to family level, and displacement volumes were measured for those groups after removing the preserving fluid with a vacuum pump. This gave a check on the displacement volume of total crustaceans, which is more difficult to measure than that of fishes or cephalopods; some fluid tends to be retained between the appendages of crustaceans while the preservative drains off them, so that it is hard to tell when filtration is complete. In general the agreement beween the two measurements of crustacean volume was good, which indicates that the displacement volumes of the other groups are probably accurate.

The displacement volume for each of the groups 1 through 7 was expressed as ml./1,000 $m.^3$ water strained (standardized volume). The amount of water strained by the net on each haul was estimated from the duration of the haul, ship

speed, mouth area of net, and an assumed filtration coefficient of 0.80. The filtration coefficient was approximately the mean of three observed values, namely 0.74, 0.76, and 0.88. Blackburn (1968) described the procedure by which the first two observations were made; the third was made later in the same way. The calculations were made by computer with a program that printed all seven standardized volumes for each haul together with date, time (start and end of haul), position, and observed maximum depth. These volumes were totalled in different combinations to yield volumes of total fish and cephalopods (groups 1, 2, 5, 6, and 7), total crustaceans (groups 3 and 4), and total micronekton (all groups), each standardized in ml./1,000 m.^{3}, for each haul. Charts were prepared showing the distribution of each of these three volumes in each of the seven cruise periods. The values were computer-plotted on blank maps and then contoured by hand.

Maurice Blackburn

BIRDS, FISH SCHOOLS, AND MARINE MAMMALS

The observations of pelagic birds, marine mammals, and fish schools were based on sightings made by personnel from the Smithsonian Institution Pacific Ocean Biological Survey Program.[4] Usually observations were conducted on an average of 8 hours each day in the time from sunrise to sunset, except when the ship was stopped for oceanographic station work. Most observations were made from the flying bridge, although some were made from the bow or other locations on the ship, depending on what position gave the best view of the surrounding ocean and the type of avifauna present. In most instances bird sightings were largely of birds which could be seen with the unaided eye and with binoculars if necessary for identification.

Emphasis was placed on data for birds. As a result, more information is available on the geographical and seasonal variations in the abundance of birds than for the marine mammals or fish schools. About 63,000 birds representing 83 species were observed. For convenience sake, species of birds were lumped into two categories based on their general feeding habits as determined from the literature, from stomach analyses, and from actual observations of feeding.

The two categories of birds selected were fish-and-cephalopod feeders and zooplankton feeders. The most important species included in the fish-and-cephalopod-feeding group were the sooty tern, the Manx shearwater, the wedgetailed shearwater, and the Juan Fernandez petrel. Of moderate importance were the brown, red-footed, and blue-faced boobies and the black tern. Of lesser importance were the white-winged petrel and the great frigatebird. The most abundant species in the zooplankton-feeding group were the northern phalarope, Leach's storm petrel, and Galápagos storm petrel.

The numbers of birds in each category were standardized on the basis of the number of birds observed per nautical mile and the percent of birds in flocks; five or more individuals observed together were considered a flock. On the atlas charts showing pelagic bird observations, the abundance of birds is indicated by the size of the circle, and X's indicate that observations were made but no birds were sighted. There is one symbol for each day's observations. The percentage of bird flocks is denoted by the amount that a circle is shaded.

Charts showing the distributions of porpoise sightings in northern hemisphere winter (October-March) and summer (April-September) are shown in the atlas. On the charts each circle represents the sighting of one or more porpoises and the numbers to the side of the circles indicate the month and year of the sighting; cruise tracks along which observations were made are indicated by lines. It is emphasized here that the observations of porpoise reported are only sightings which do not include data on their abundance.

The distribution of whale sightings made during northern hemisphere winter (October-March) and summer months (April-September) is also shown. On the charts each symbol represents the sighting of one or more whales and the numbers at the side of the symbols indicate the month and year of the sighting; cruise tracks along which observations were made are indicated by lines. Except for pilot whales, which often approached the ship, there were few instances when it was possible to make specific identifications since often only the spout of a whale was observed and so recorded. When specific identifications were possible, most in the oceanic waters were sperm whales. Along the coast of Baja California they were California gray whales.

Sightings of tuna schools made on EASTROPAC cruises are summarized in one figure. In addition to those sighted by the bird observers, some tuna schools were sighted by officers aboard the research vessels and are included on the chart. The circles on the chart indicate tuna schools which were identified as skipjack and the squares indicate schools of yellowfin, black skipjack, or tuna which were not identified. The numbers at the side of each symbol indicate the month and year that the school was sighted. The stippled lines indicate cruise tracks along which the sightings were made. A total of 59 tuna schools were sighted of which 22 were skipjack. Since the effort to observe tuna schools was not uniform and the observations were not made by skilled observers, the records must be considered only as sightings and can not be used to infer distribution patterns. The fact that no tuna were observed in a given area does not necessarily indicate that they were not present.

R. Michael Laurs

[4]The charts portraying bird observations should be considered as Paper Number 55, Pacific Ocean Biological Survey Program, Smithsonian Institution, Washington, D.C. 20560.

LITERATURE CITED

AHLSTROM, ELBERT H.
1952. Pilchard eggs and larvae and other fish larvae, Pacific coast, 1950. U.S. Fish Wildl. Serv., Spec. Sci. Rep. Fish. 80, 58 pp.

AHLSTROM, ELBERT H., and JAMES R. THRAILKILL.
1963. Plankton volume loss with time of preservation. Calif. Coop. Oceanic Fish. Invest. Rep. 9: 57-73.

ALLISON, LEWIS J., EARL R. KREINS, FREDRIC A. GODSHALL, and GUENTER WARNECKE.
1969. Examples of the usefulness of satellite data in general atmospheric circulation research—Part I, Monthly global atmospheric circulation characteristics as reflected in TIROS VII radiometric measurements. NASA (Nat. Aeronaut. Space Admin.) Tech. Note D-5630, iv + 75 pp.

ARMSTRONG, F. A. J., C. R. STEARNS, and J. D. H. STRICKLAND.
1967. The measurement of upwelling and subsequent biological processes by means of the Technicon Autoanalyzer and associated equipment. Deep-Sea Res. Oceanogr. Abstr. 14: 381-389.

BLACKBURN, MAURICE.
1968. Micronekton of the eastern tropical Pacific Ocean: family composition, distribution, abundance, and relations to tuna. U.S. Fish Wildl. Serv., Fish. Bull. 67: 71-115.

CARPENTER, JAMES H.
1965. The Chesapeake Bay Institute technique for the Winkler dissolved oxygen method. Limnol. Oceanogr. 10: 141-143.

DOTY, MAXWELL S., HARRY R. JITTS, OLGA J. KOBLENTZ-MISHKE, and YATSUKE SAIJO.
1965. Intercalibration of marine plankton primary productivity techniques. Limnol. Oceanogr. 10: 282-286.

ENVIRONMENTAL DATA SERVICE.
1967. Catalog of meteorological satellite data-ESSA 3 television cloud photography, Part 2. January 1,-March 31, 1967. ESSA (Environ. Sci. Serv. Admin.) Key to Meteorological Records Documentation No. 5.313, 29 pp. + 2 figs. + 178 pl.
1968a. Catalog of meteorological satellite data—ESSA 3 and ESSA 5 television cloud photography, April 4-June 30, 1967. ESSA (Environ. Sci. Serv. Admin.) Key to Meteorological Records Documentation No. 5.314, 21 pp. + 180 pl.
1968b. Catalog of meteorological satellite data-ESSA 3 and ESSA 5 television cloud photography, July 1-September 30, 1967. ESSA (Environ, Sci. Serv. Admin.) Key to Meteorological Records Documentation No. 5.315, 21 pp. + 182 pl.

EVANS, MARTHA W., RICHARD A. SCHWARTZLOSE, and JOHN D. ISAACS.
1968. Data from deep-moored instrument stations. Scripps Inst. Oceanogr., Univ. Calif. SIO Ref. 68-17, ii + 145 pp.

GILBERT, WILLIAM E., WALTER M. PAWLEY, and KILHO PARK.
1967. Carpenter's oxygen solubility table and nomograph for seawater as a function of temperature and salinity. J. Oceanogr. Soc. Jap. 23(5): 32-35.

HOLM-HANSEN, OSMUND, CARL J. LORENZEN, ROBERT W. HOLMES, and JOHN D. H. STRICKLAND.
1965. Fluorometric determination of chlorophyll. J. Cons, 30: 3-15.

JERDE, CHARLES W.
1967. A comparison of euphausiid shrimp collections made with a micronekton net and a one-meter plankton net. Pac. Sci. 21: 178-181.

JONES, JAMES H.
1969. Processing of digital data logger STD tapes at the Scripps Institution of Oceanography and the Bureau of Commercial Fisheries, La Jolla, California. U.S. Fish Wildl. Serv., Spec. Sci. Rep. Fish. 588, iii + 25 pp.

KING, J. E., and T. S. HIDA.
1954. Variations in zooplankton abundance in Hawaiian waters, 1950-52. U.S. Fish Wildl. Serv., Spec. Sci. Rep. Fish. 118, vi + 66 pp.

LONGHURST, ALAN R.
1967a. EASTROPAC information paper No. 6. [U.S.] Bur. Commer. Fish., Fish. Oceanogr. Cent., La Jolla, Calif., 88 pp.
1967b. EASTROPAC information paper No. 7. [U.S.] Bur. Commer. Fish., Fish. Oceanogr. Cent., La Jolla, Calif., 22 pp.
1968. EASTROPAC information paper No. 8. [U.S.] Bur. Commer. Fish., Fish. Oceanogr. Cent., La Jolla, Calif., 1 p. + 6 maps + 112 charts.
1969a. EASTROPAC information paper No. 9. [U.S.] Bur. Commer. Fish., Fish. Oceanogr. Cent., La Jolla, Calif., 1 p. + 12 maps + 101 charts.
1969b. EASTROPAC information paper No. 10 (EASTROPAC Colloquium, La Jolla, Calif., 9 June 1969). [U.S.] Bur. Commer. Fish., Fish. Oceanogr. Cent., La Jolla, Calif., ii + 77 pp. + 1 map.

LONGHURST, ALAN R., and CUTHBERT M. LOVE.
1967. EASTROPAC information paper No. 5. [U.S.] Bur. Comm. Fish. Fish. Oceanogr. Cent., La Jolla, Calif., 9 pp. + 2 maps + 4 charts.

LORENZEN, CARL J.
1966. A method for the continuous measurement of *in vivo* chlorophyll concentration. Deep-Sea Res. Oceanogr. Abstr. 13: 223-227.

LOVE, CUTHBERT.
1969. EASTROPAC information paper No. 11. [U.S.] Bur. Commer. Fish., Fish. Oceanogr. Cent., La Jolla, Calif., 5 pp. + append.

MARINE DIVISION OF THE METEOROLOGICAL OFFICE.
1956. Monthly meteorological charts of the eastern Pacific Ocean. Air Ministry, London, Mar. Div. Meteor. Off., M.O. 518, 122 pp. [Reprinted formerly M.O.M. 446.]

MONTGOMERY, R. B., and E. D. STROUP.
1962. Equatorial waters and currents in 150° W. in July-August 1952. Johns Hopkins Oceanogr. Stud. 1, 68 pp.

RICHARDS, FRANCIS A., and RICHARD A. KLETSCH.
1964. The spectrophotometric determination of ammonia and labile amino compounds in fresh and sea water by oxidation to nitrite. *In* Yasuo Miyake and Tadashiro Koyama (editors), Recent researches in the fields of hydrosphere, atmosphere and nuclear geochemistry, pp. 65-81. Maruzen, Tokyo.

RIEHL, HERBERT.
1954. Tropical meteorology. McGraw-Hill Book Co., New York, vii + 392 pp.

SADLER, JAMES C.
1969. Average cloudiness in the tropics from satellite observations. Int. Indian Ocean Exped. Meteorol. Monogr. 2, 22 pp. + 12 pls.

STAFF, EASTROPAC.
1967. Manual of EASTROPAC observations. [U.S.] Bur. Commer. Fish., Fish. Oceanogr. Cent., La Jolla, Calif., 24 pp. + 19 annexes.

STRICKLAND, J. D. H., and T. R. PARSONS.
1968. A practical handbook of seawater analysis. Fish. Res. Bd. Can. Bull. 167, 311 pp.

U.S. NAVY.
1959. Marine climatic atlas of the world. Volume V, South Pacific Ocean. NAVAER 50-1C-532, Washington, D.C., xvi + 267 charts.

WOOSTER, WARREN S.
1966a. EASTROPAC information paper No. 1. [U.S.] Bur. Commer. Fish., Fish. Oceanogr. Cent., La Jolla, Calif., 4 pp + 2 maps.
1966b. EASTROPAC information paper No. 2. [U.S.] Bur. Commer. Fish., Fish. Oceanogr. Cent., La Jolla, Calif., 6 pp. + 2 maps.
1966c. EASTROPAC information paper No. 3 [U.S.] Bur. Commer. Fish., Fish. Oceanogr. Cent., La Jolla, Calif., 4 pp.

WOOSTER, WARREN S., and CUTHBERT M. LOVE.
1967. EASTROPAC information paper No. 4. [U.S.] Bur. Commer. Fish., Fish. Oceanogr. Cent., La Jolla, Calif., 7 pp. + 4 maps.

WYRTKI, KLAUS.
1964. The thermal structure of the eastern Pacific Ocean. Deut. Hydrogr. Z. Ergänzungsh. A6: 6-84.

MS #1937

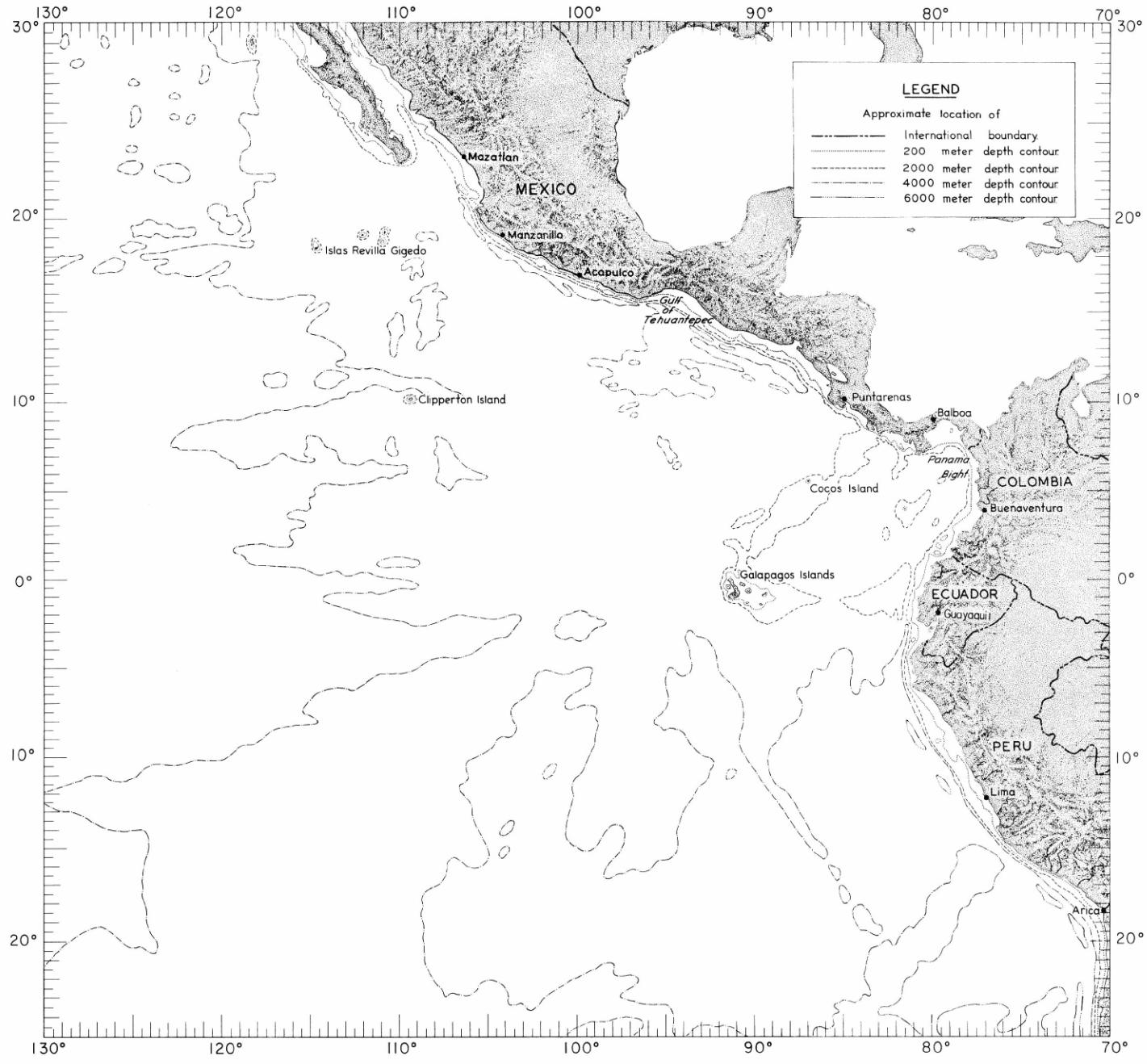

RM-a.

FIGURE RM-a. — Reference map of the main portion of the EASTROPAC area. The topographic shading and bathymetric contours are approximate only and should not be considered as portraying the latest available information.

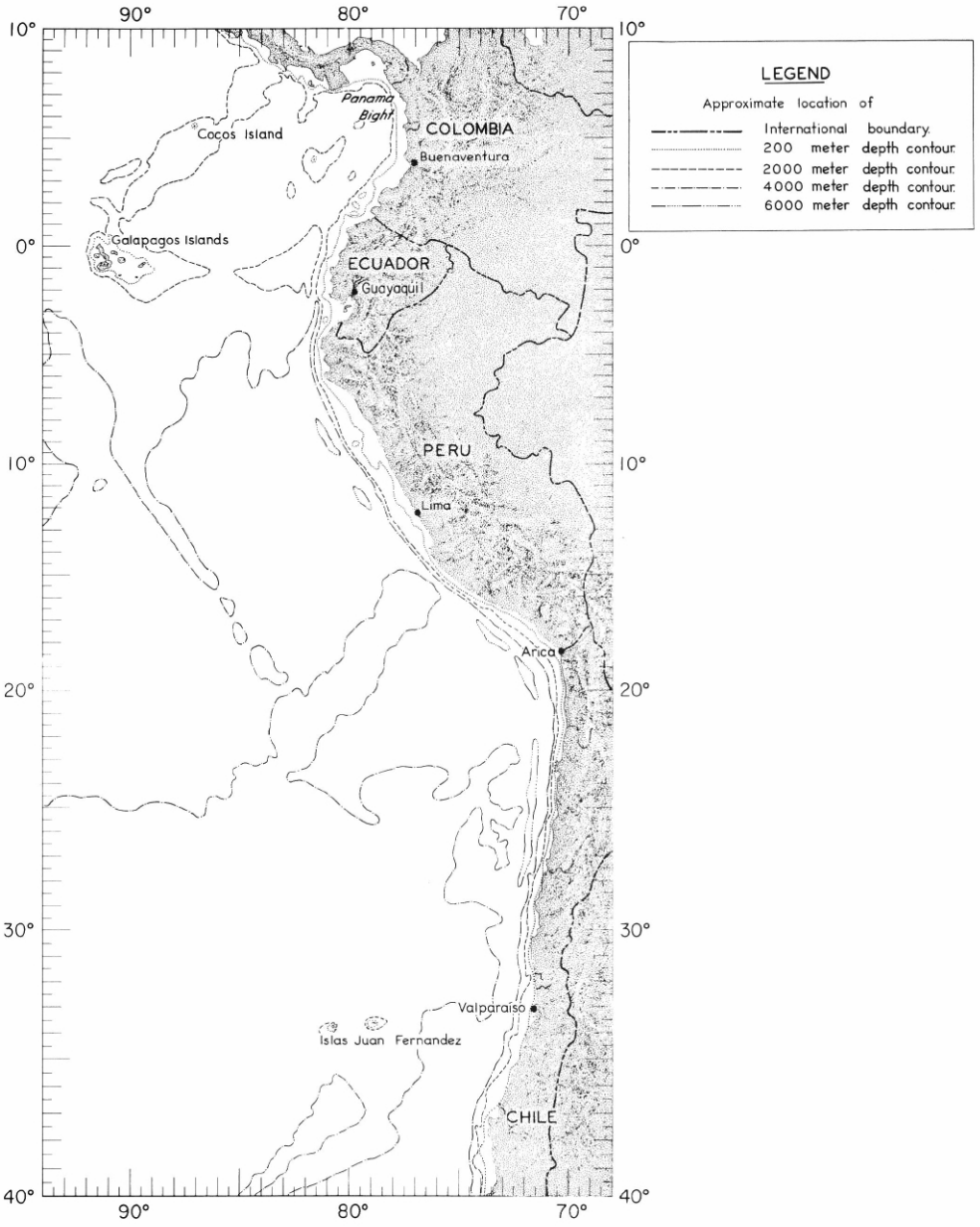

FIGURE RM-b — Reference map of the southern coastal portion of the EASTROPAC area. The topographic shading and bathymetric contours are approximate only and should not be considered as portraying the latest available information.

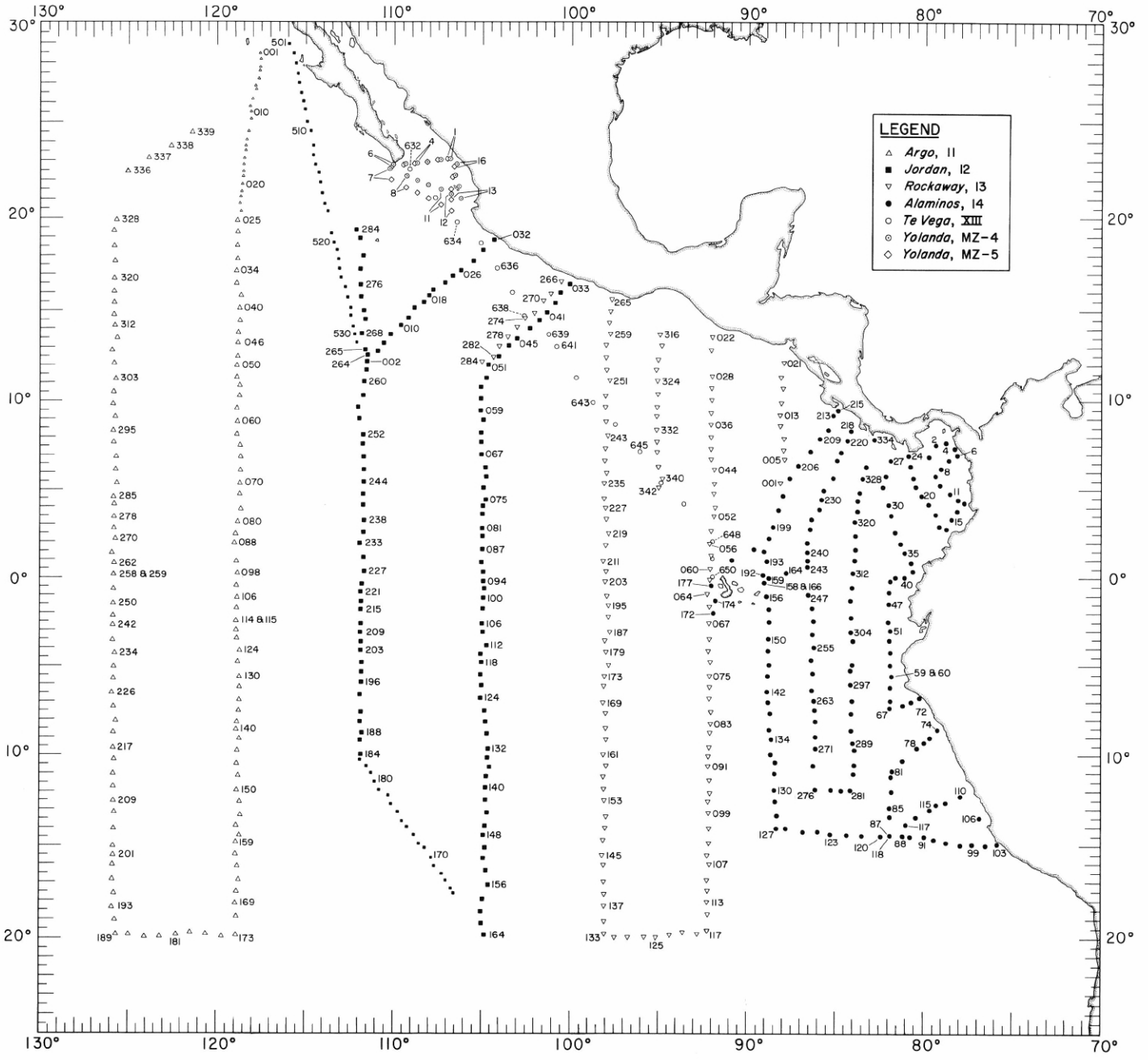

FIGURE 10-TC-a. — Locations of stations occupied by participating ships in the main portion of the EASTROPAC area during the first survey period, February-March 1967.

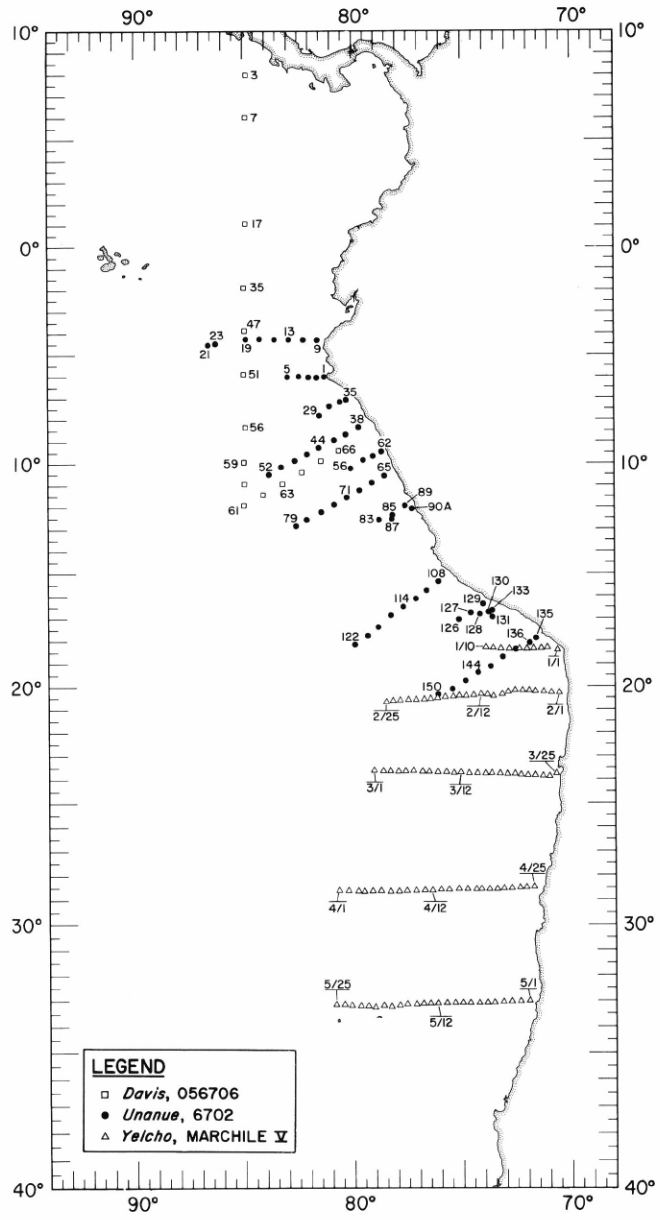

10-TC-b.

FIGURE 10-TC-b. — Locations of stations occupied by participating ships in the southern coastal portion of the EASTROPAC area during the first survey period, February-March 1967.

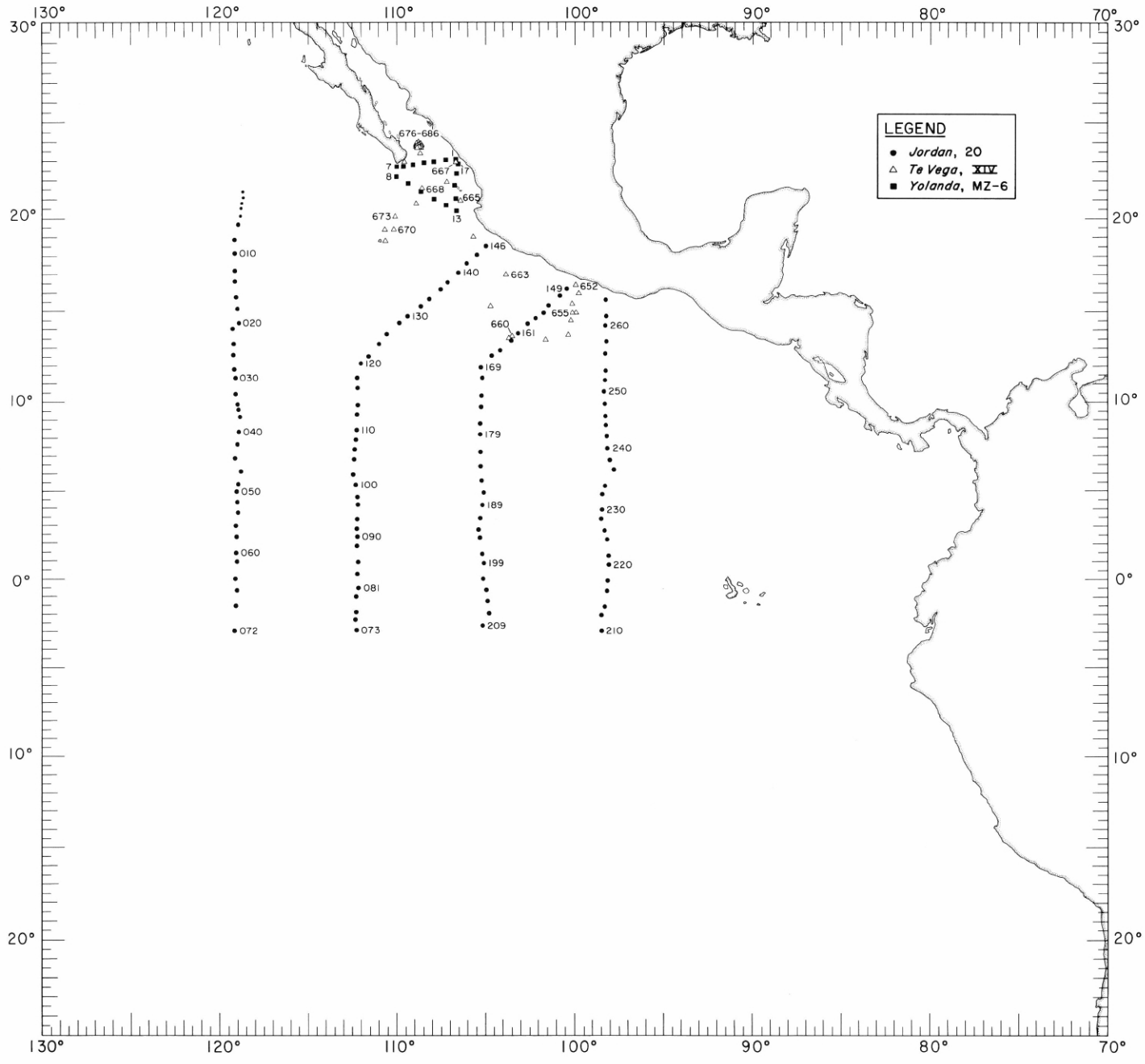

FIGURE 20-TC. — Locations of stations occupied by participating ships during the first monitor period, April-May 1967.

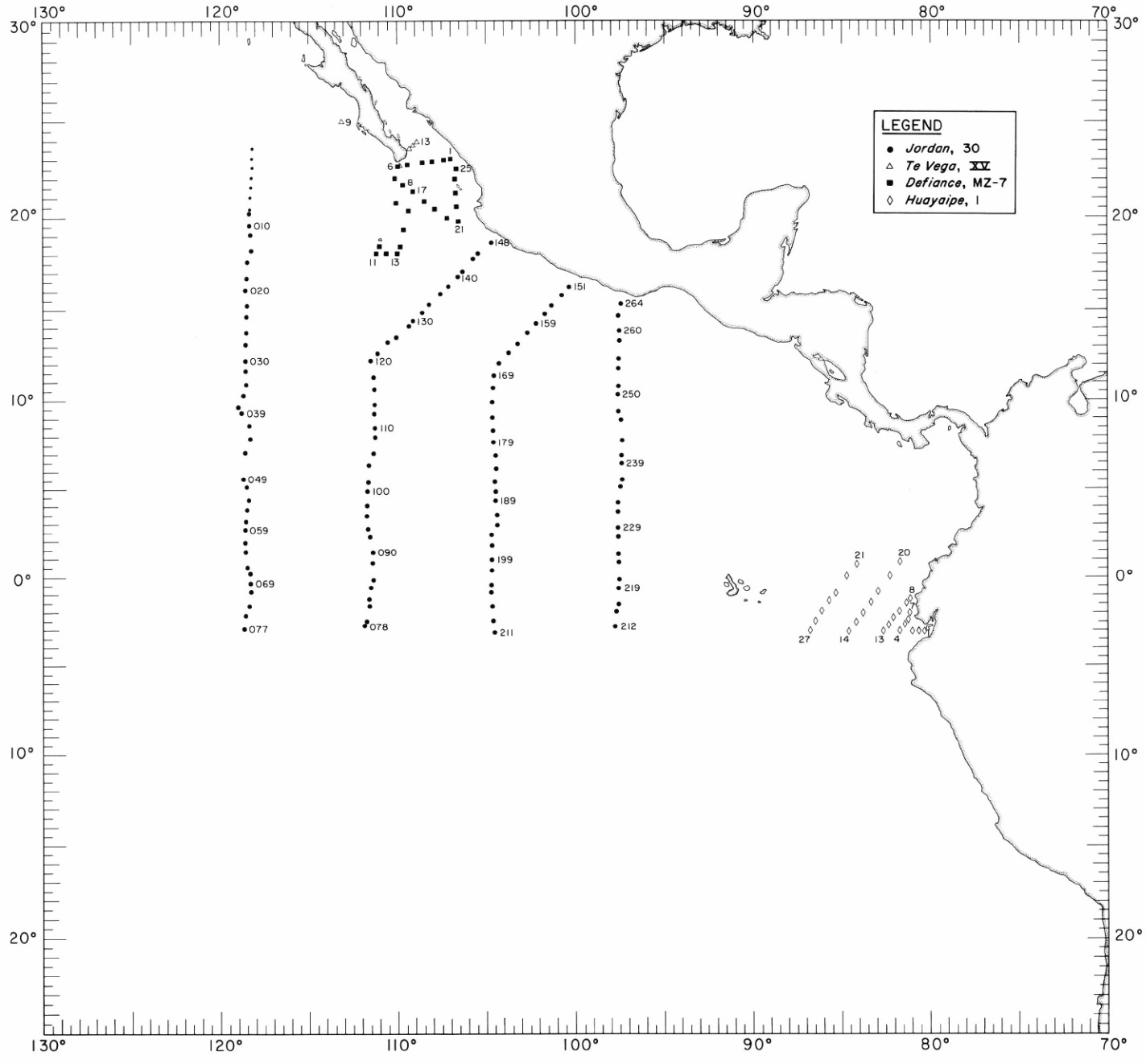

FIGURE 30-TC. — Locations of stations occupied by participating ships during the second monitor period, June-July 1967.

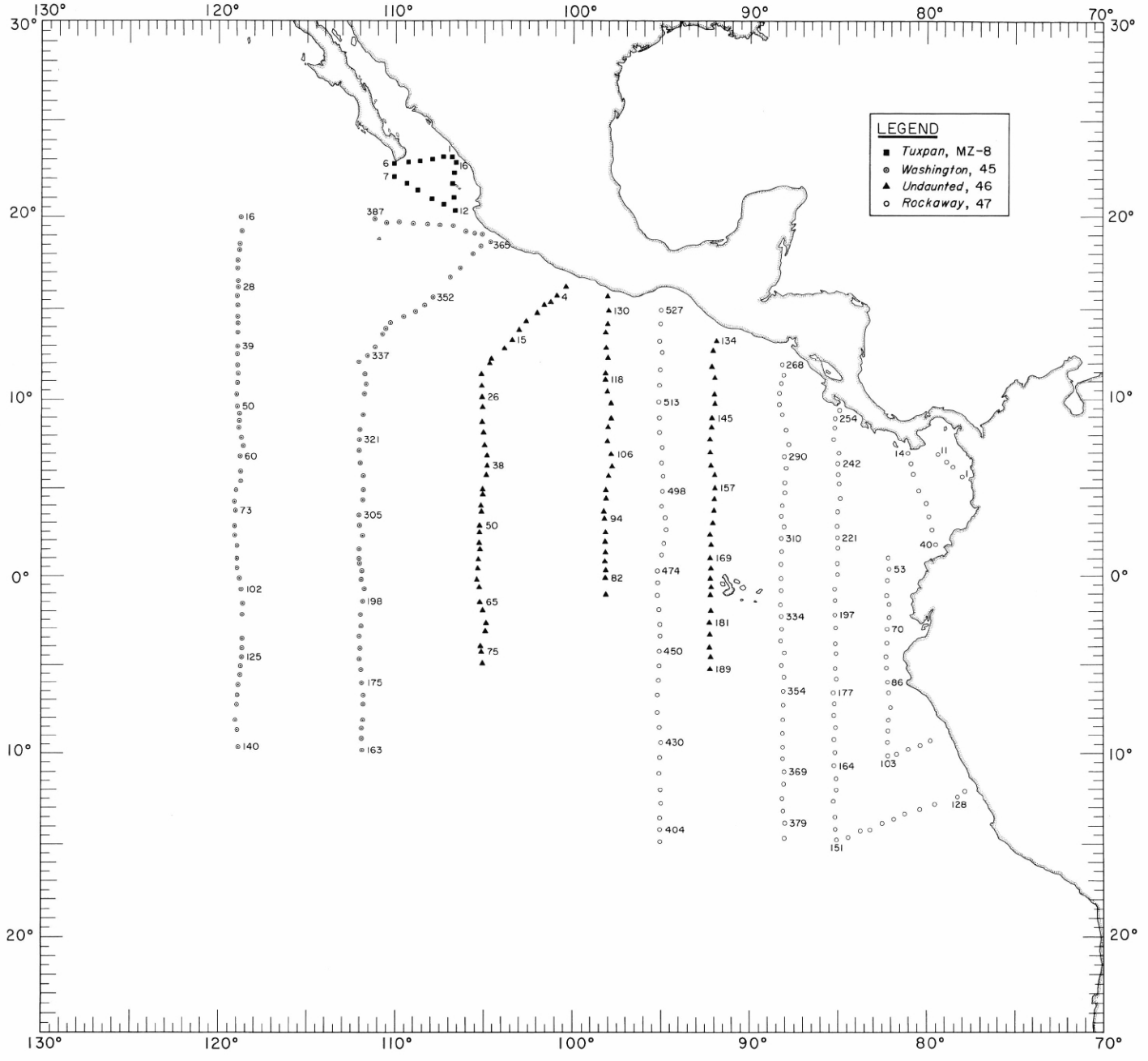

40-TC-a.

FIGURE 40-TC-a. — Locations of stations occupied by participating ships in the main portion of the EASTROPAC area during the second survey period, August-September 1967.

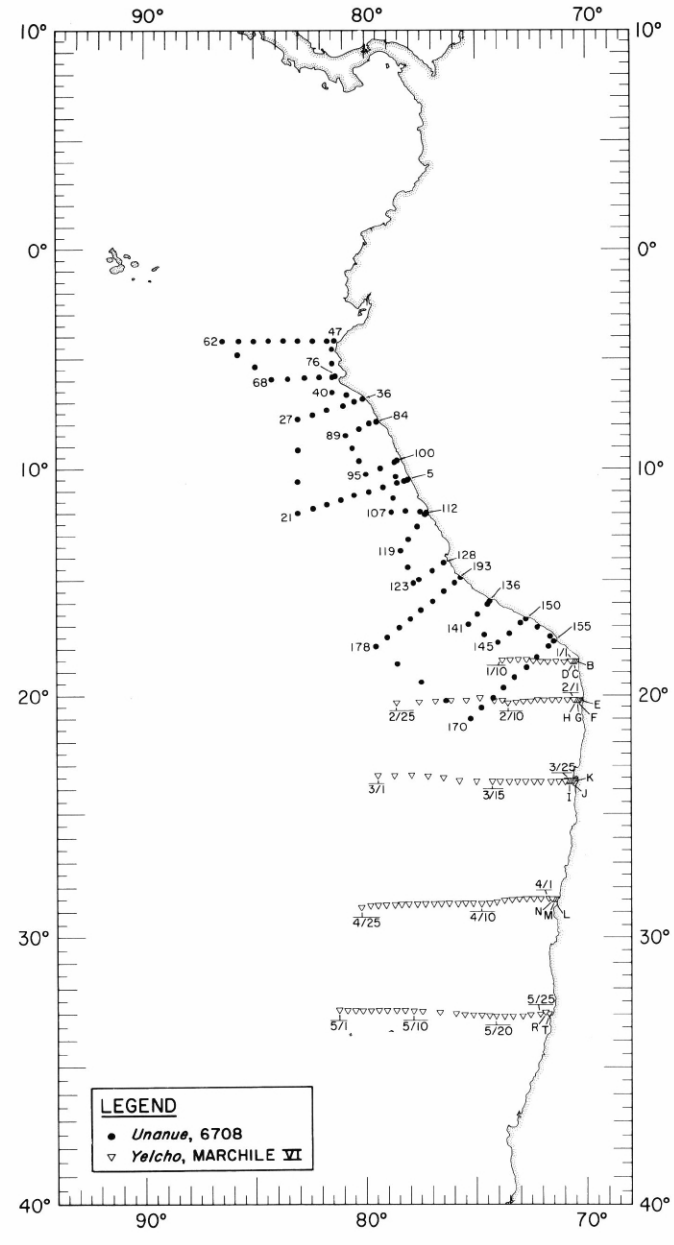

40-TC-b.

FIGURE 40-TC-b. — Locations of stations occupied by participating ships in the southern coastal portion of the EASTROPAC area during the second survey period, August-September 1967.

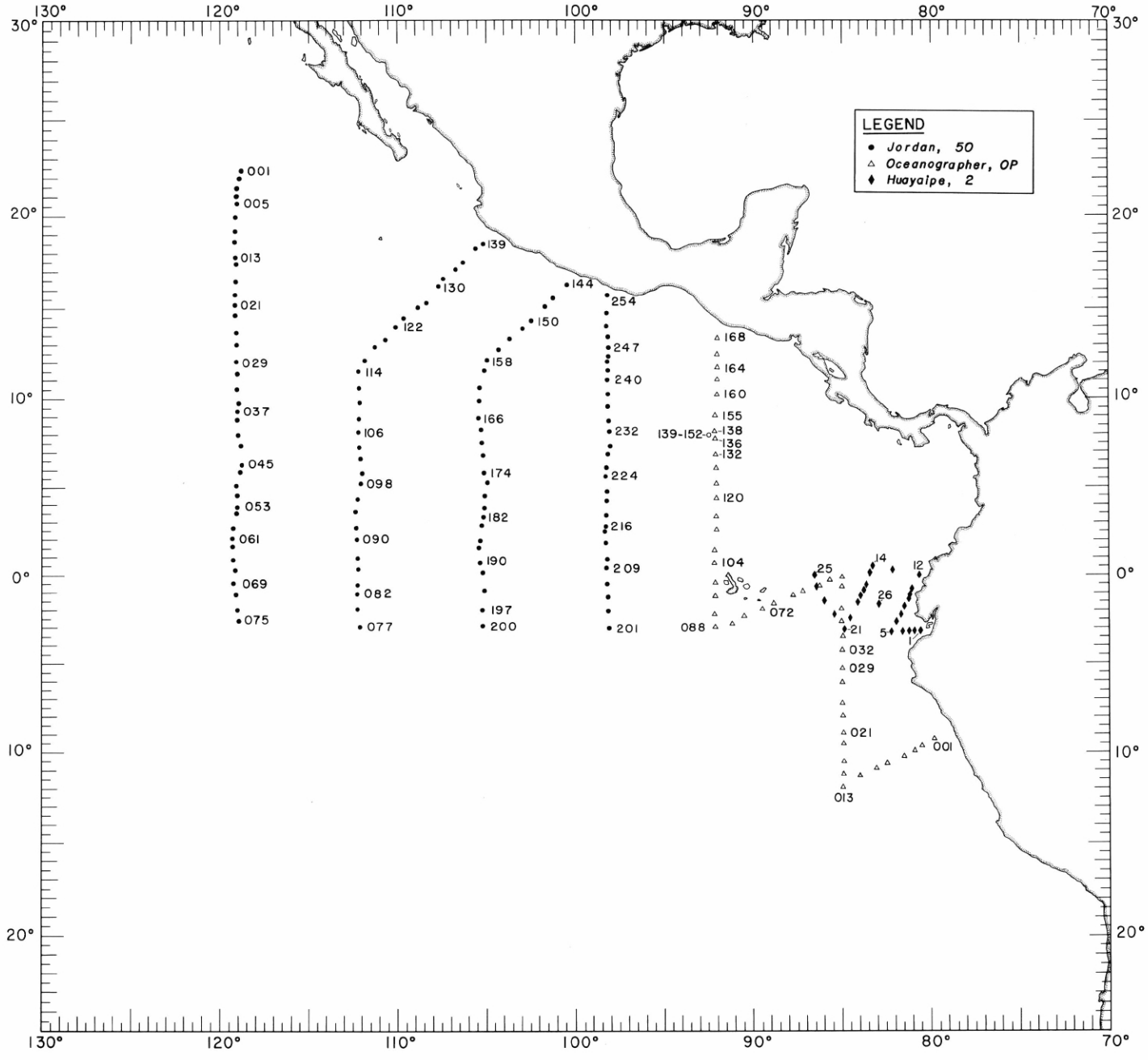

50-TC.

FIGURE 50-TC. — Locations of stations occupied by participating ships during the third monitor period, October-November 1967.

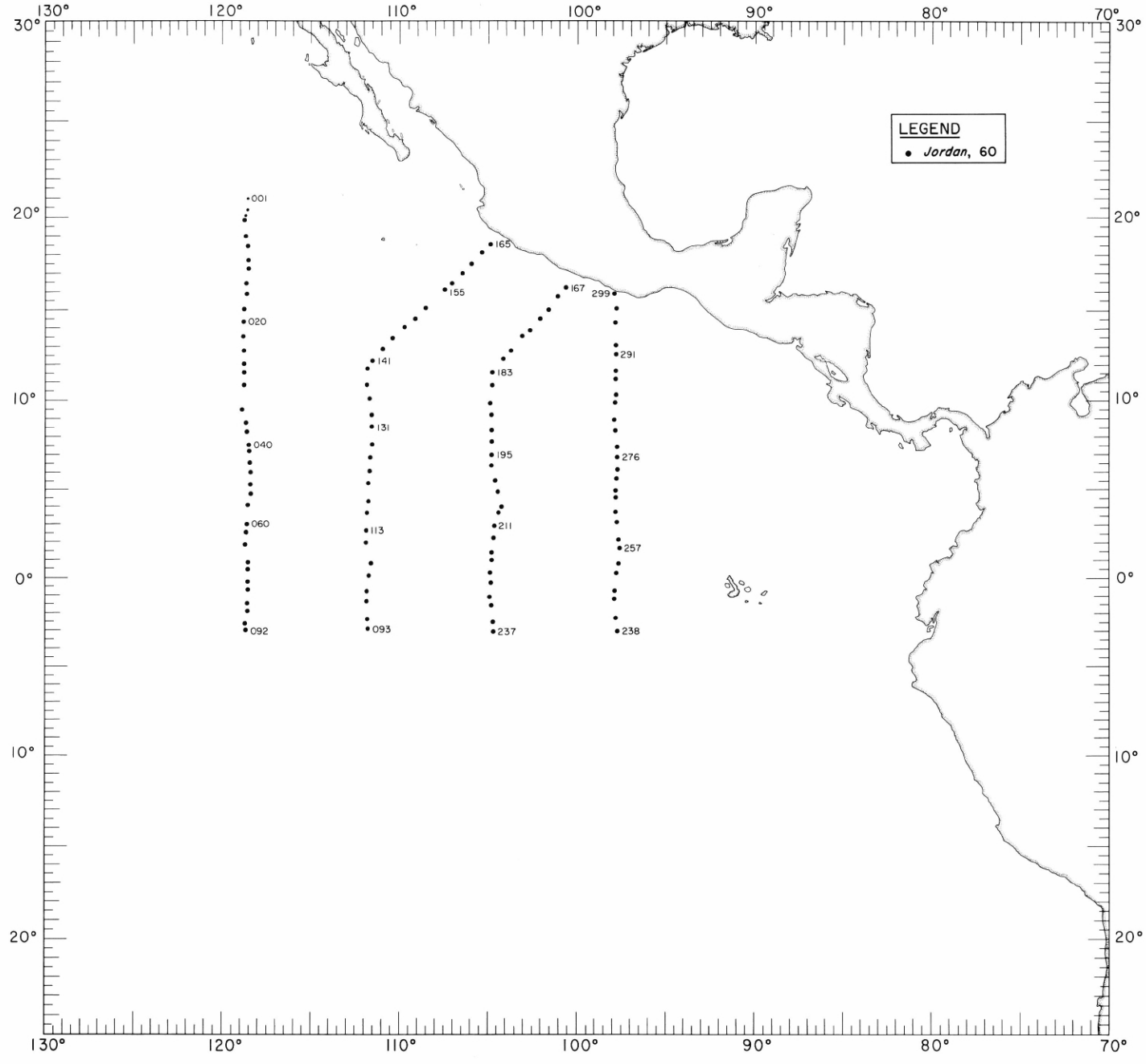

60-TC.

FIGURE 60-TC. — Locations of stations occupied by participating ships during the fourth monitor period, December 1967-January 1968.

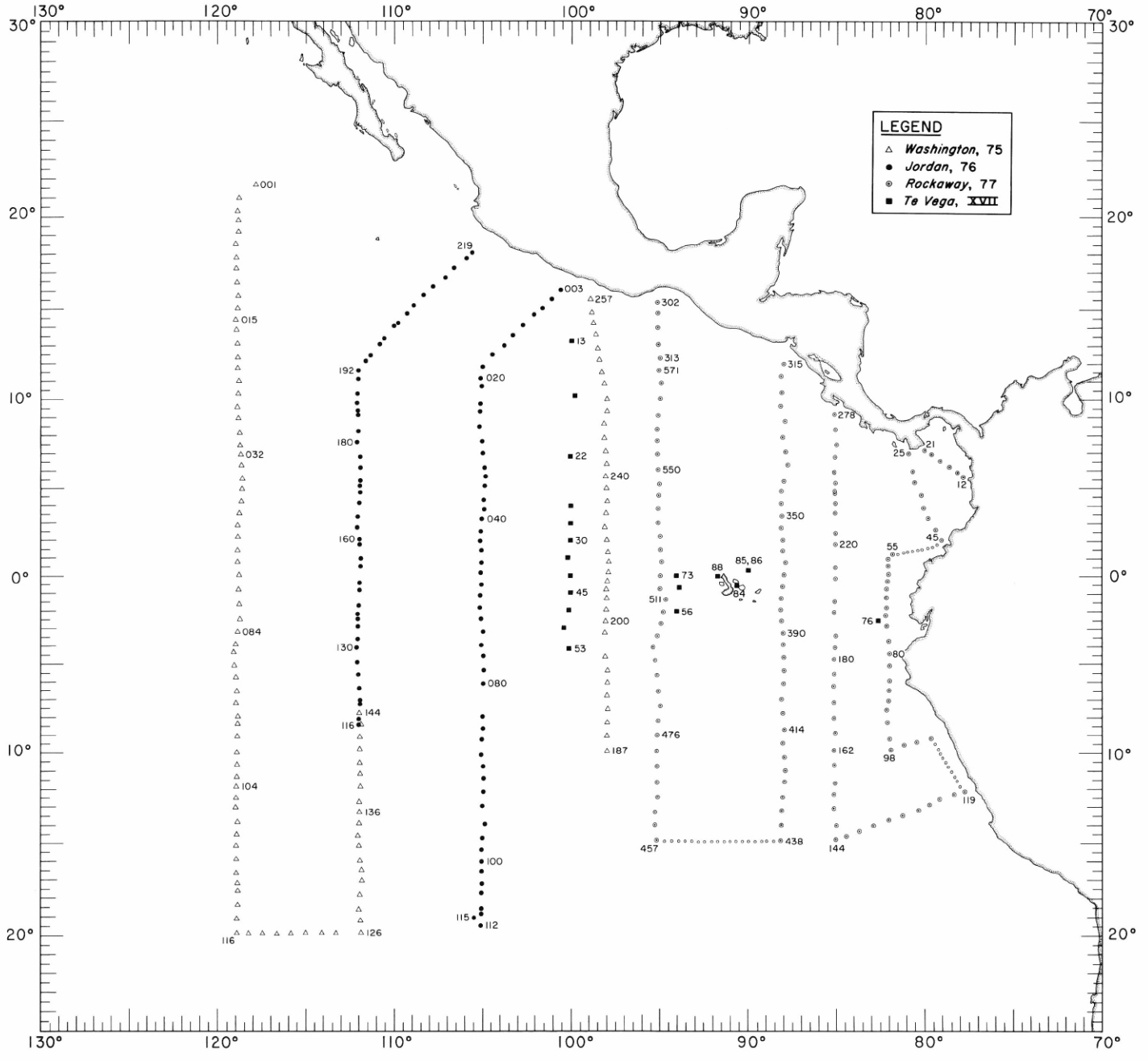

70-TC-a.

FIGURE 70-TC-a. — Locations of stations occupied by participating ships in the main portion of the EASTROPAC area during the third survey period, February-March 1968.

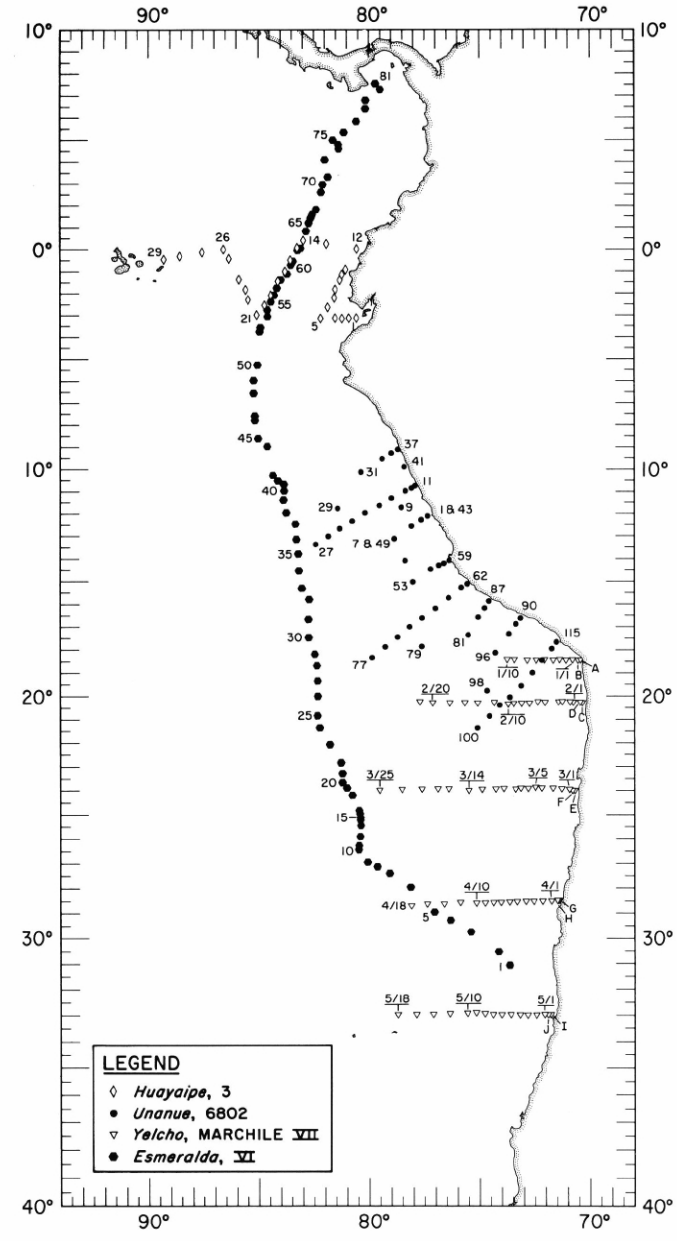

70-TC-b.

FIGURE 70-TC-b. — Locations of stations occupied by participating ships in the southern coastal portion of the EASTROPAC area during the third survey period, February-March 1968.

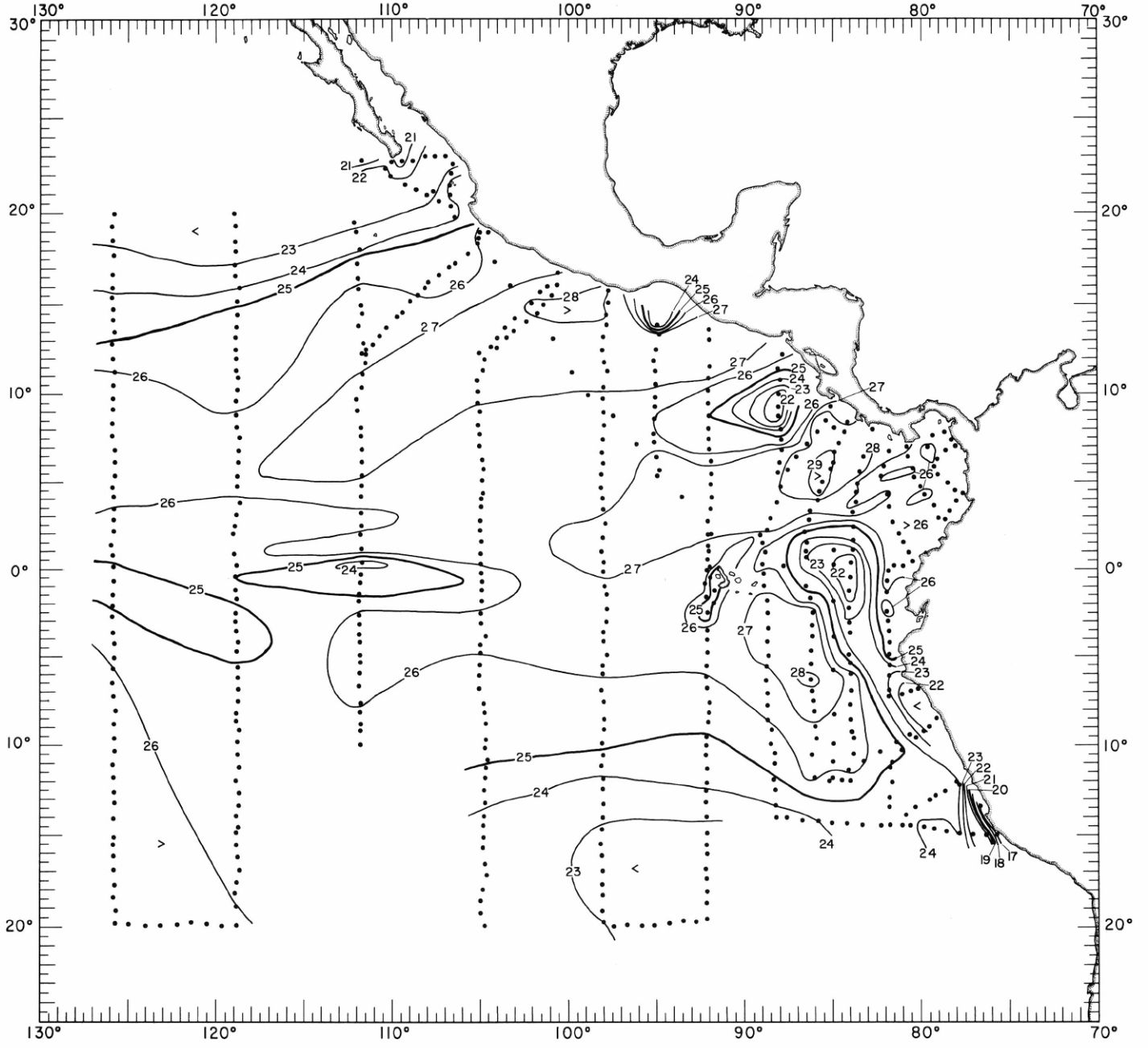

10-T-s(a).

FIGURE 10-T-s(a).—Temperature (°C.) at the sea surface in the main portion of the EASTROPAC area, February-March 1967. These contours are based on Nansen cast data from all cruises except *Alaminos* 14, for which STD data were used. The *Alaminos* stations are, in general, those in the eastern part of the area, from the coast to 88° W.; see figure 10-TC-a for more exact station locations.

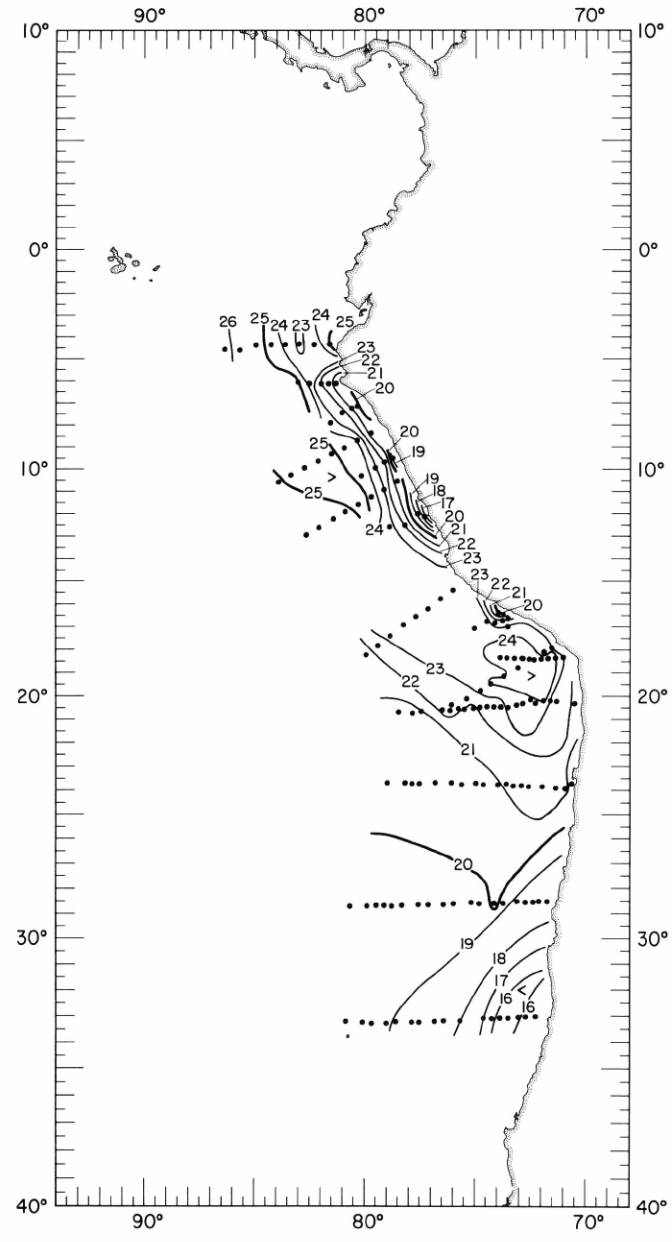

10-T-s(b).

FIGURE 10-T-s(b).—Temperature (°C.) at the sea surface in the southern coastal portion of the EASTROPAC area, February-March 1967. These contours are based on Nansen cast data.

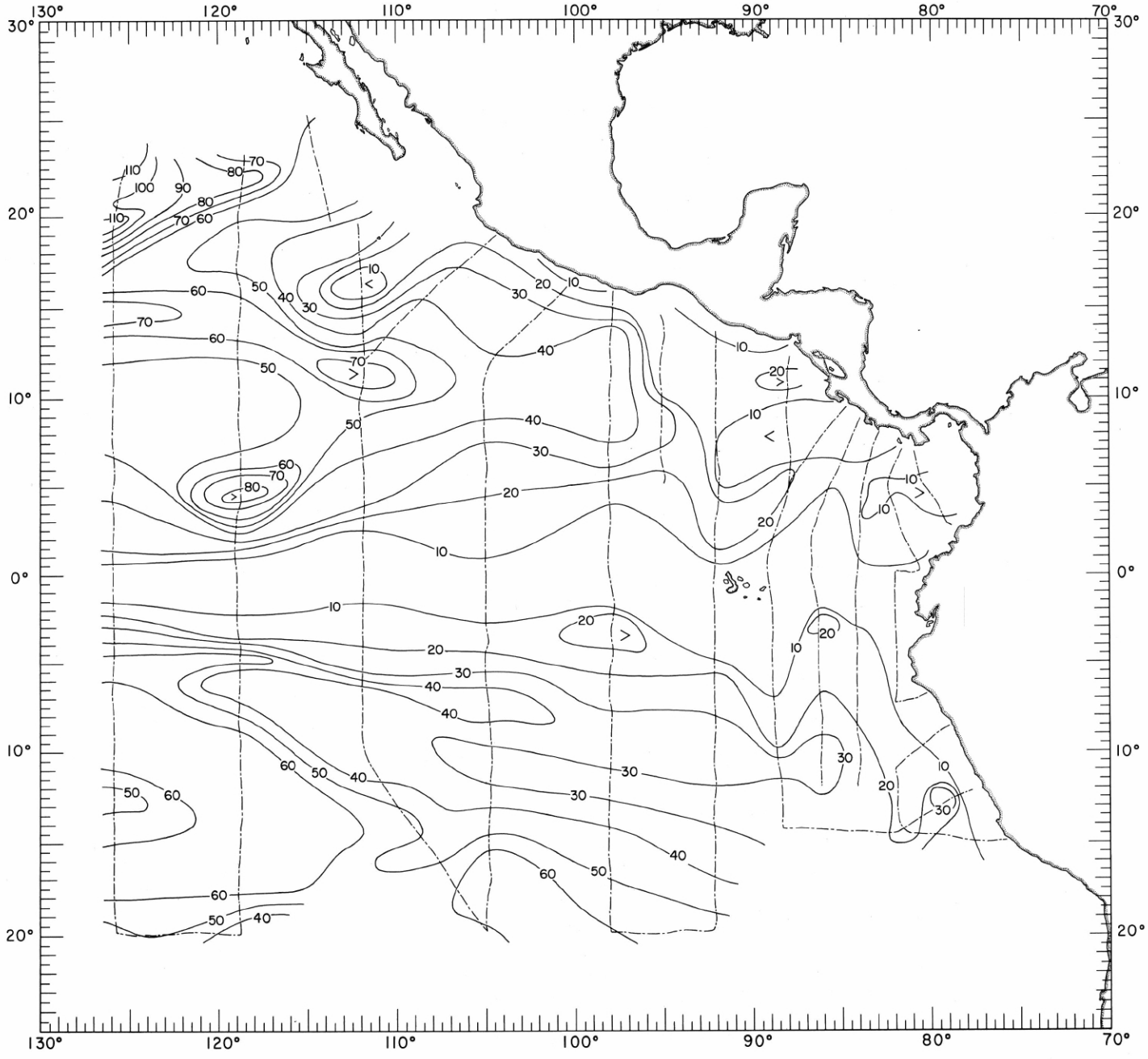

FIGURE 10-ML.—Thickness of the mixed layer in meters, February-March 1967. Dashed lines indicate portions of the cruise tracks where such data were collected.

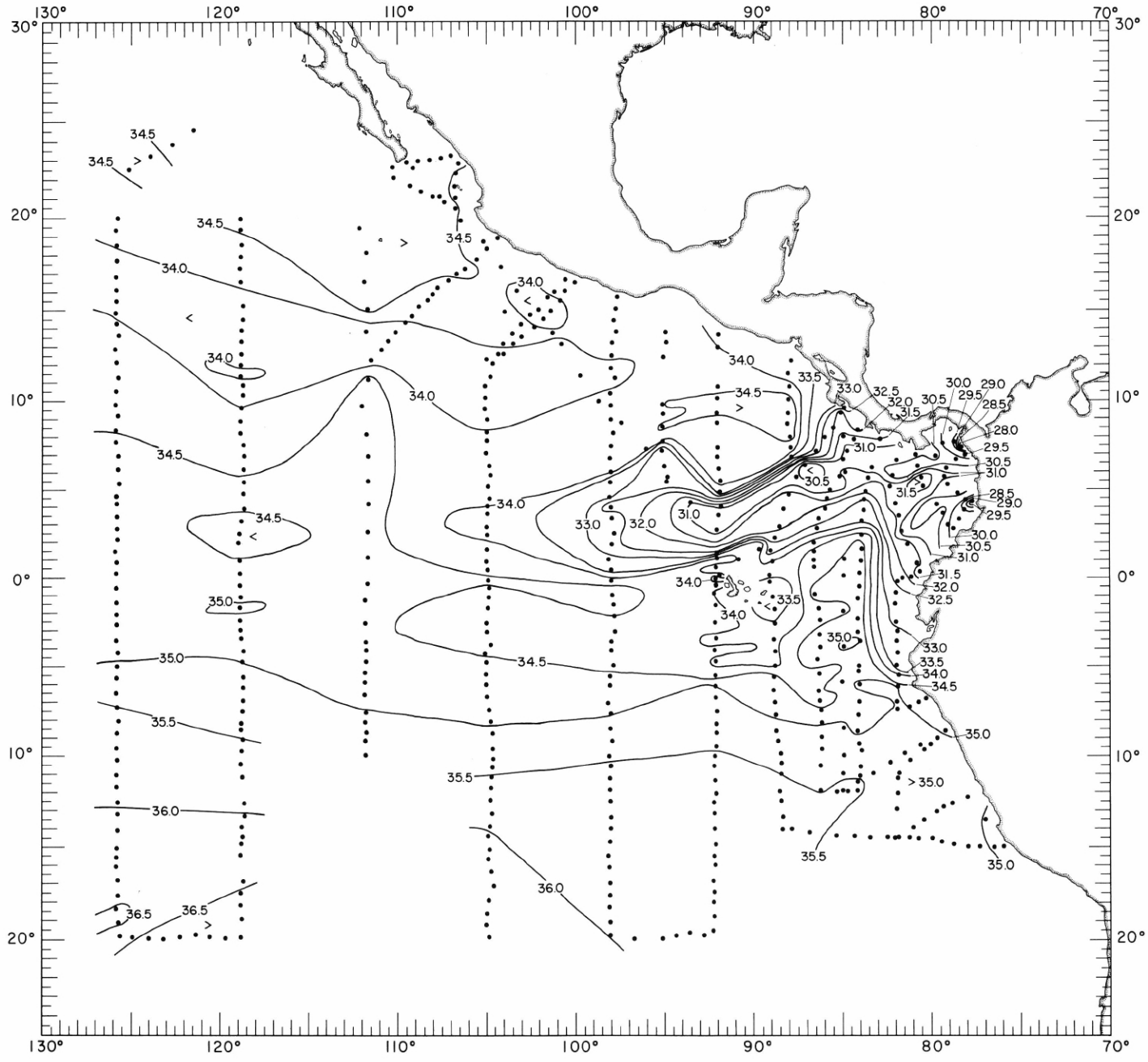

10-S-s(a).

FIGURE 10-S-s(a).—Salinity (‰) at the sea surface in the main portion of the EASTROPAC area, February-March 1967. These contours are based on Nansen cast data.

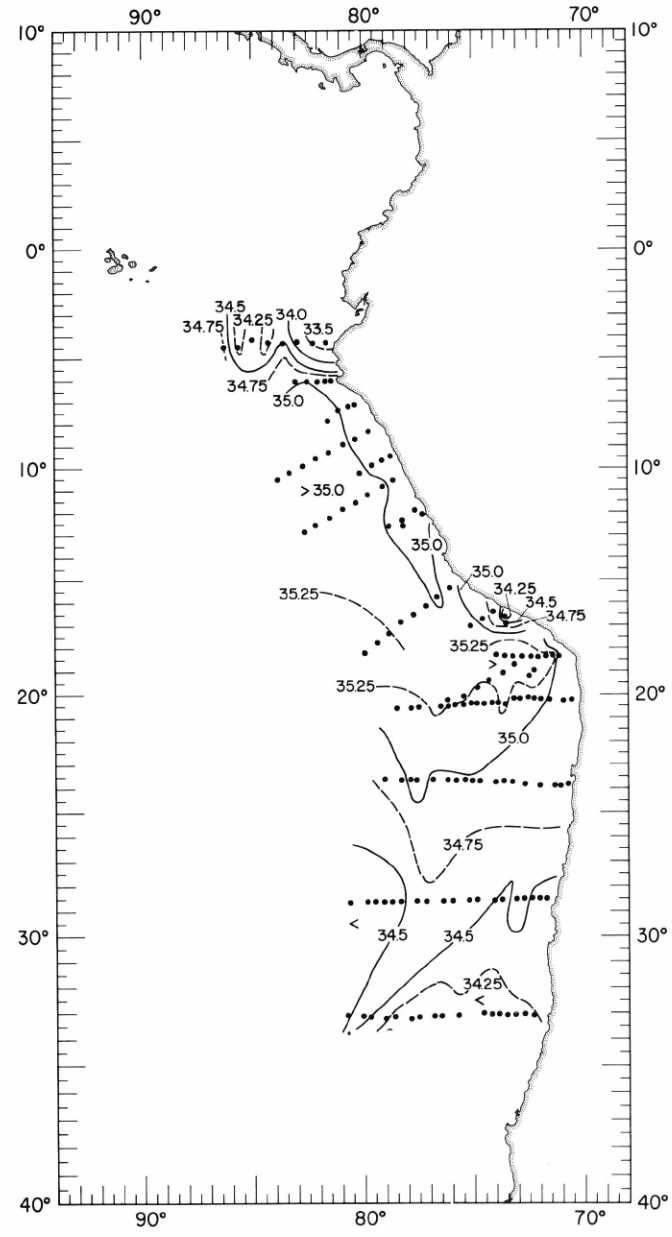

10-S-s(b).

FIGURE 10-S-s(b).—Salinity (‰) at the sea surface in the southern coastal portion of the EASTROPAC area, February-March 1967. These contours are based on Nansen cast data.

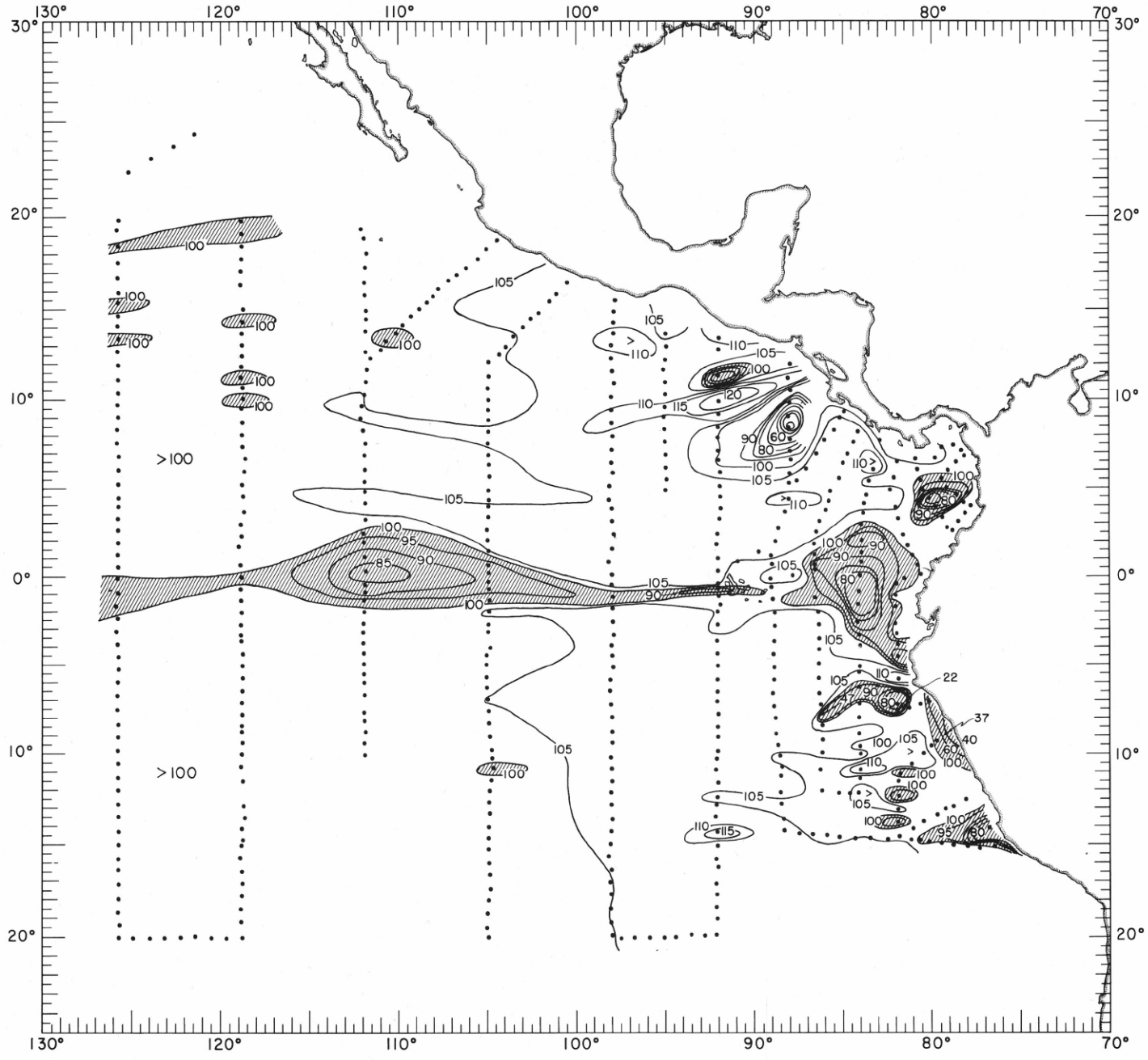

10-O2Sa-10.

FIGURE 10-O2Sa-10.—Oxygen saturation (%) at 10 meters, February-March 1967. Areas with less than 100% saturation are shaded.

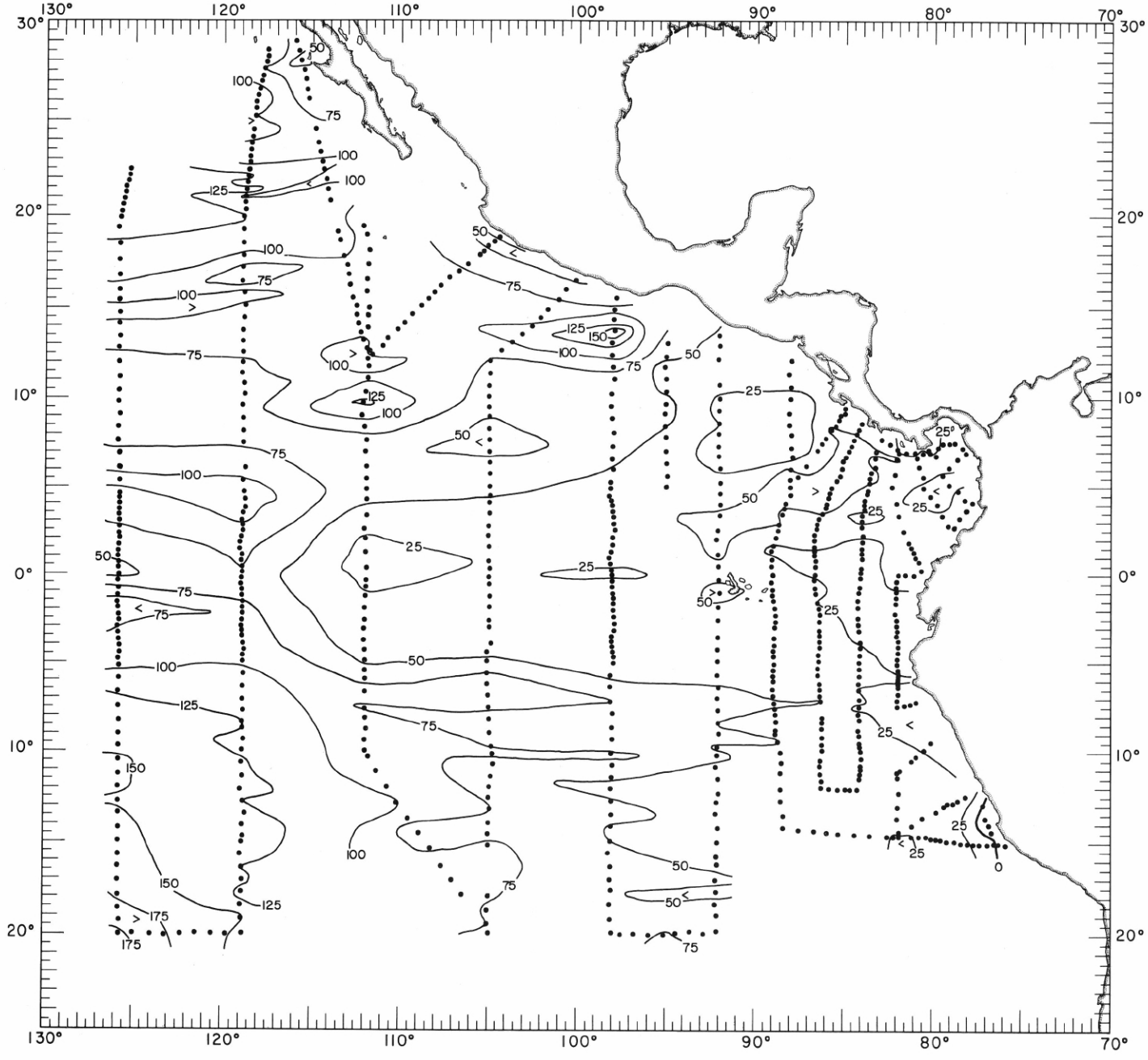

FIGURE 10-δ300-z.—Depth (m.) of the surface where $\delta_T = 300$ cl./t., February-March 1967. The zero contour near the coast of Peru, in the vicinity of 15° S., indicates the intersection of this surface with the sea surface.

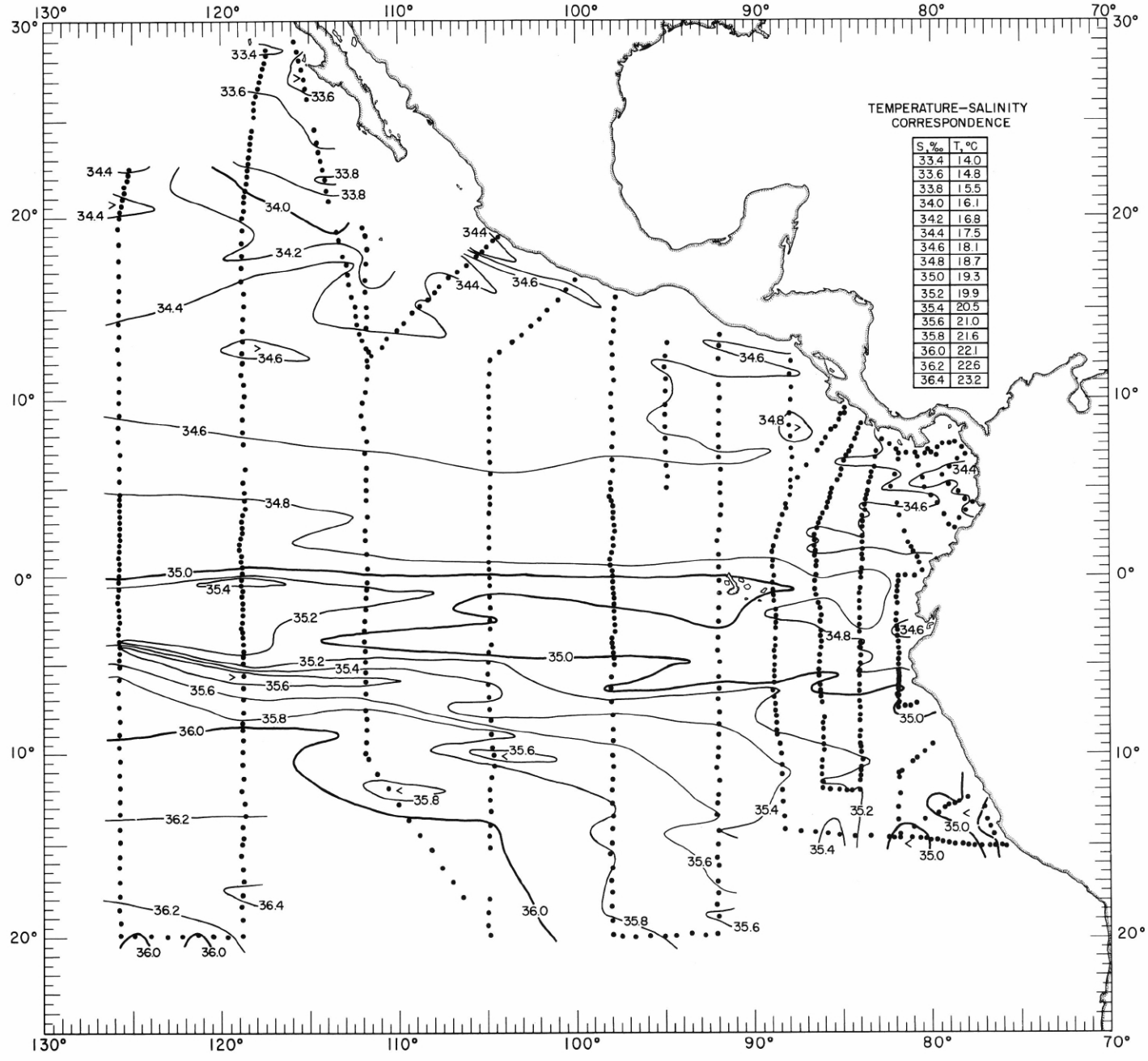

10-S-δ300.

FIGURE 10-S-δ300.—Salinity (‰) on the surface where $\delta_T = 300$ cl./t., February-March 1967. The heavy dashed line near the coast of Peru, in the vicinity of 15° S., indicates the intersection of this surface with the sea surface. The table shows the temperature corresponding to each isohaline on the chart.

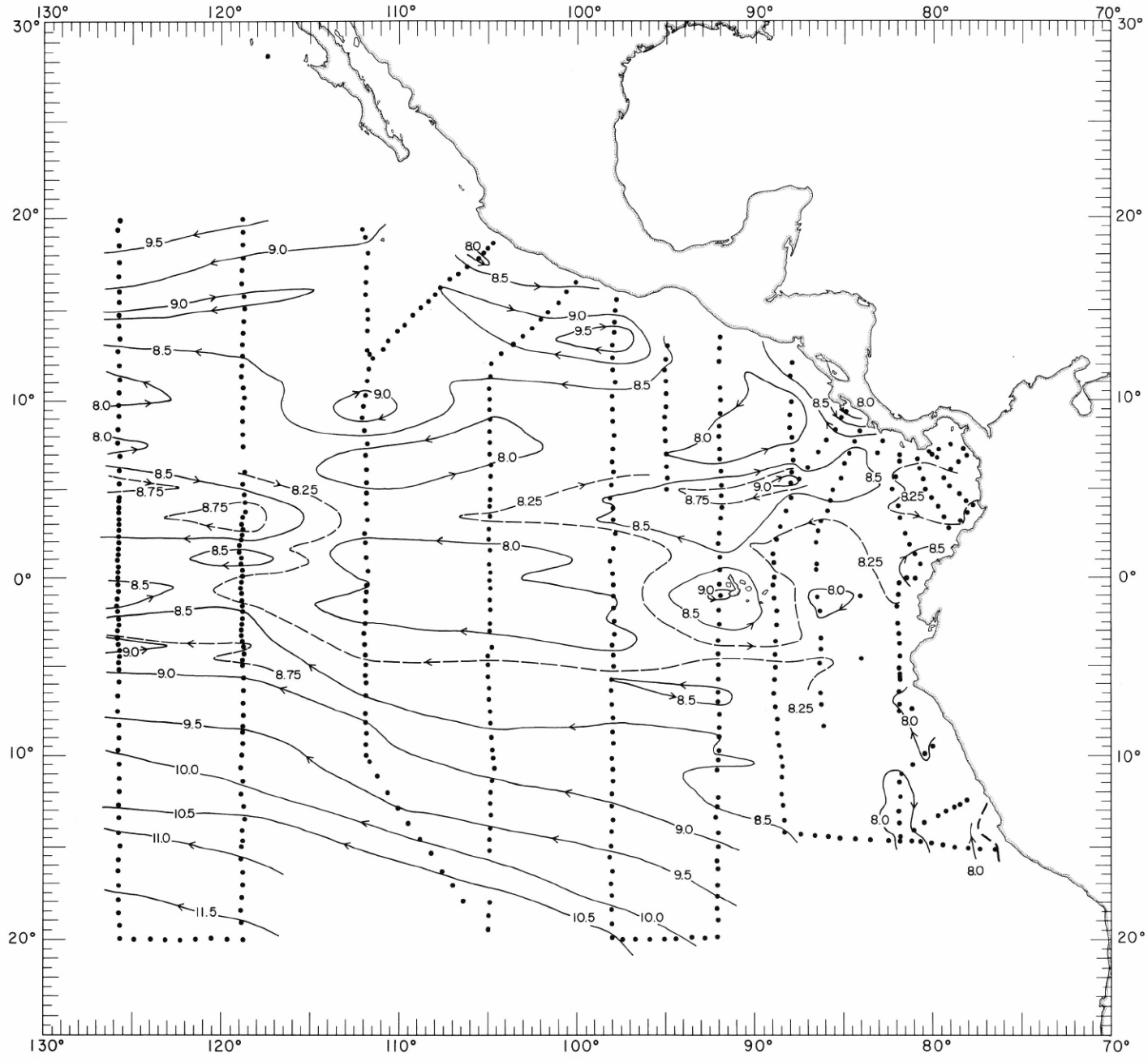

10-AP-δ300.

FIGURE 10-AP-δ300.—Acceleration potential (j./kg.), relative to 500 db., on the surface where $\delta_T = 300$ cl./t., February-March 1967. The heavy dashed line near the coast of Peru, in the vicinity of 15° S., indicates the intersection of this surface with the sea surface. For computing acceleration potential, thermosteric anomaly, δ_T, was used instead of specific volume anomaly, δ.

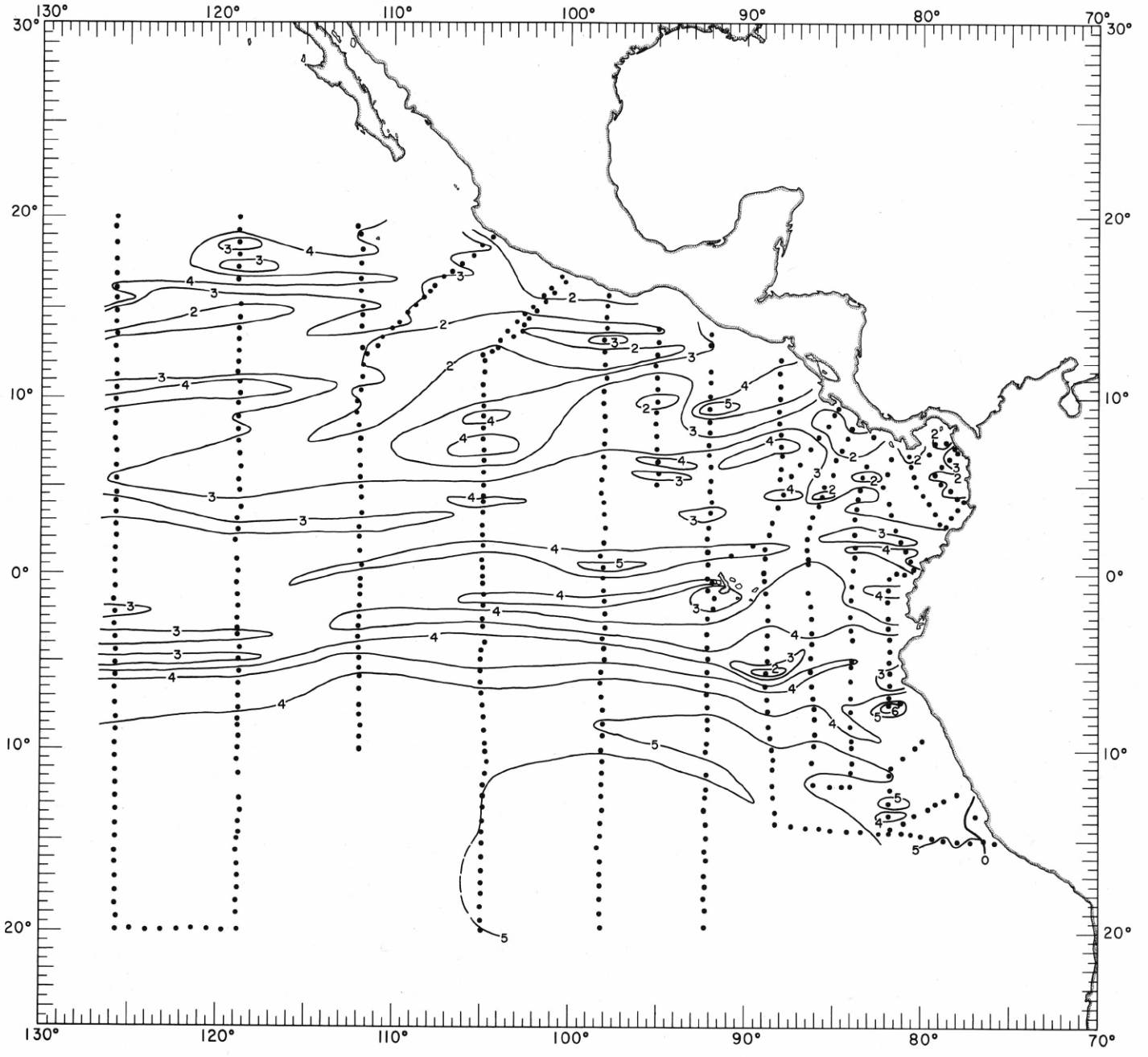

10-O_2-δ300.

FIGURE 10-O_2-δ300.—Oxygen (ml./l.) on the surface where $\delta_T = 300$ cl./t., February-March 1967. The heavy dashed line near the coast of Peru, in the vicinity of 15° S., indicates the intersection of this surface with the sea surface.

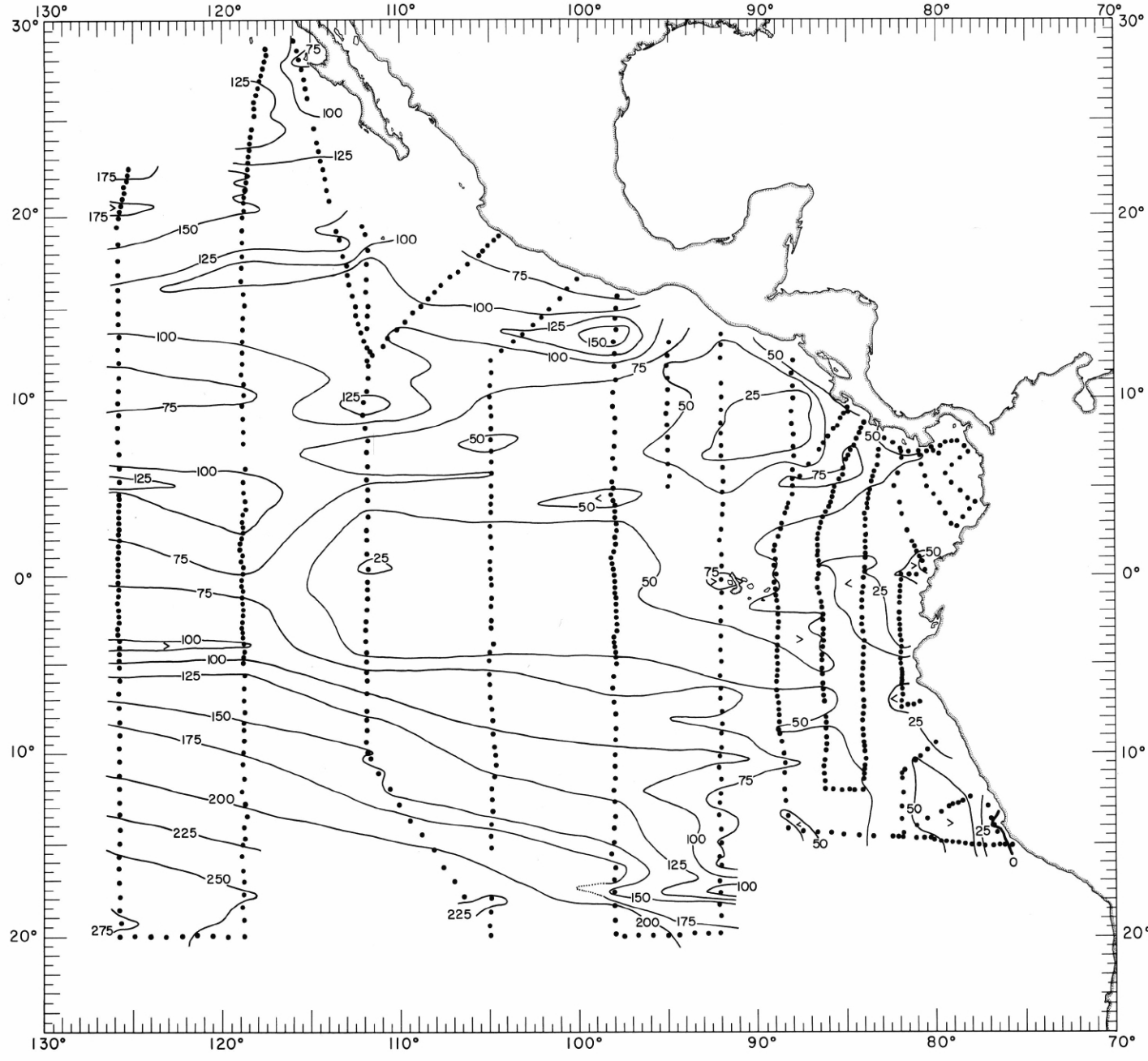

FIGURE 10-δ250-z.—Depth (m.) of the surface where $\delta_T = 250$ cl./t., February-March 1967. The zero contour near the coast of Peru, in the vicinity of 15° S., indicates the intersection of this surface with the sea surface.

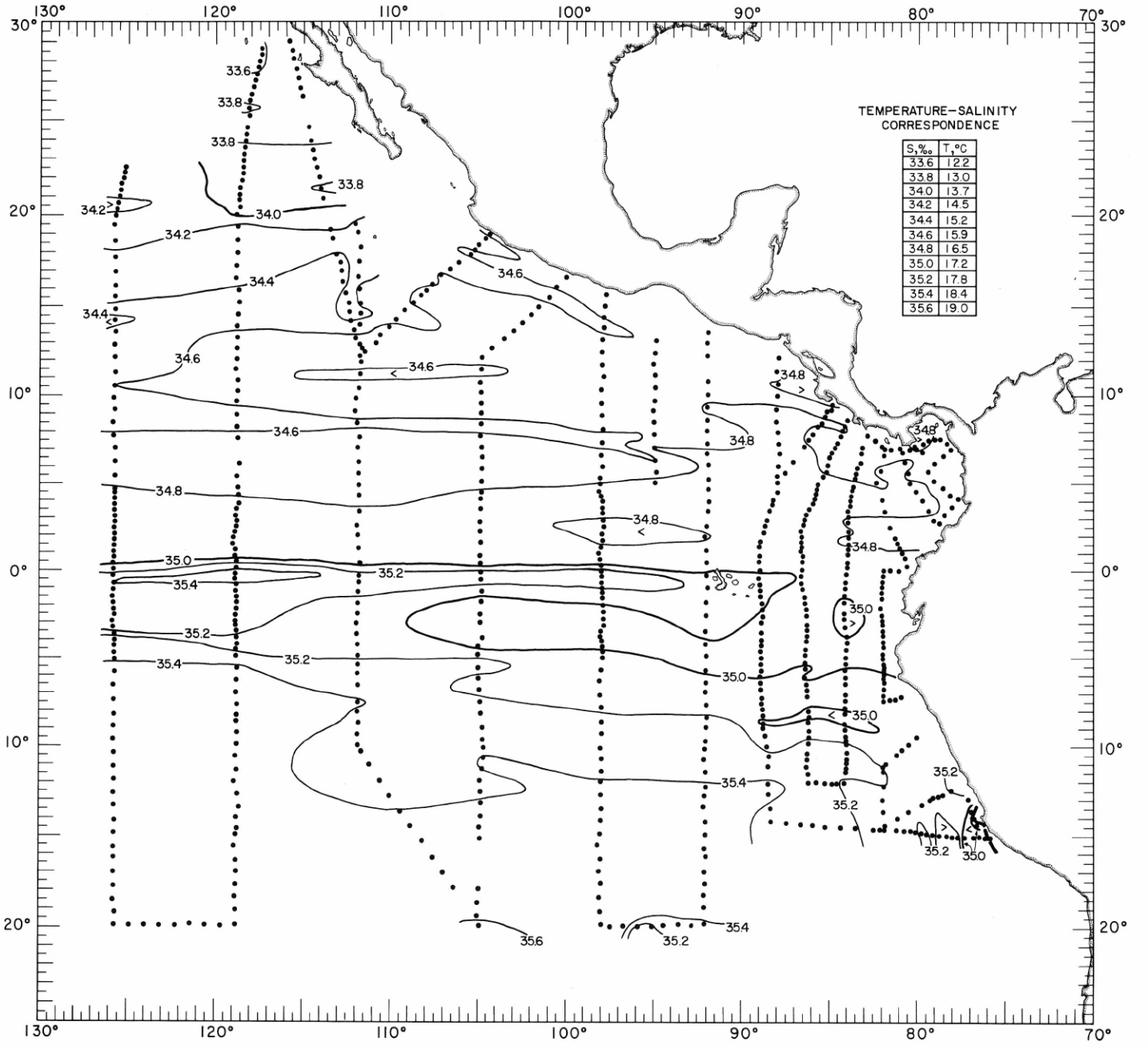

10-S-δ250.

FIGURE 10-S-δ250.—Salinity (‰) on the surface where $\delta_T = 250$ cl./t., February-March 1967. The heavy dashed line near the coast of Peru, in the vicinity of 15° S., indicates the intersection of this surface with the sea surface. The table shows the temperature corresponding to each isohaline on the chart.

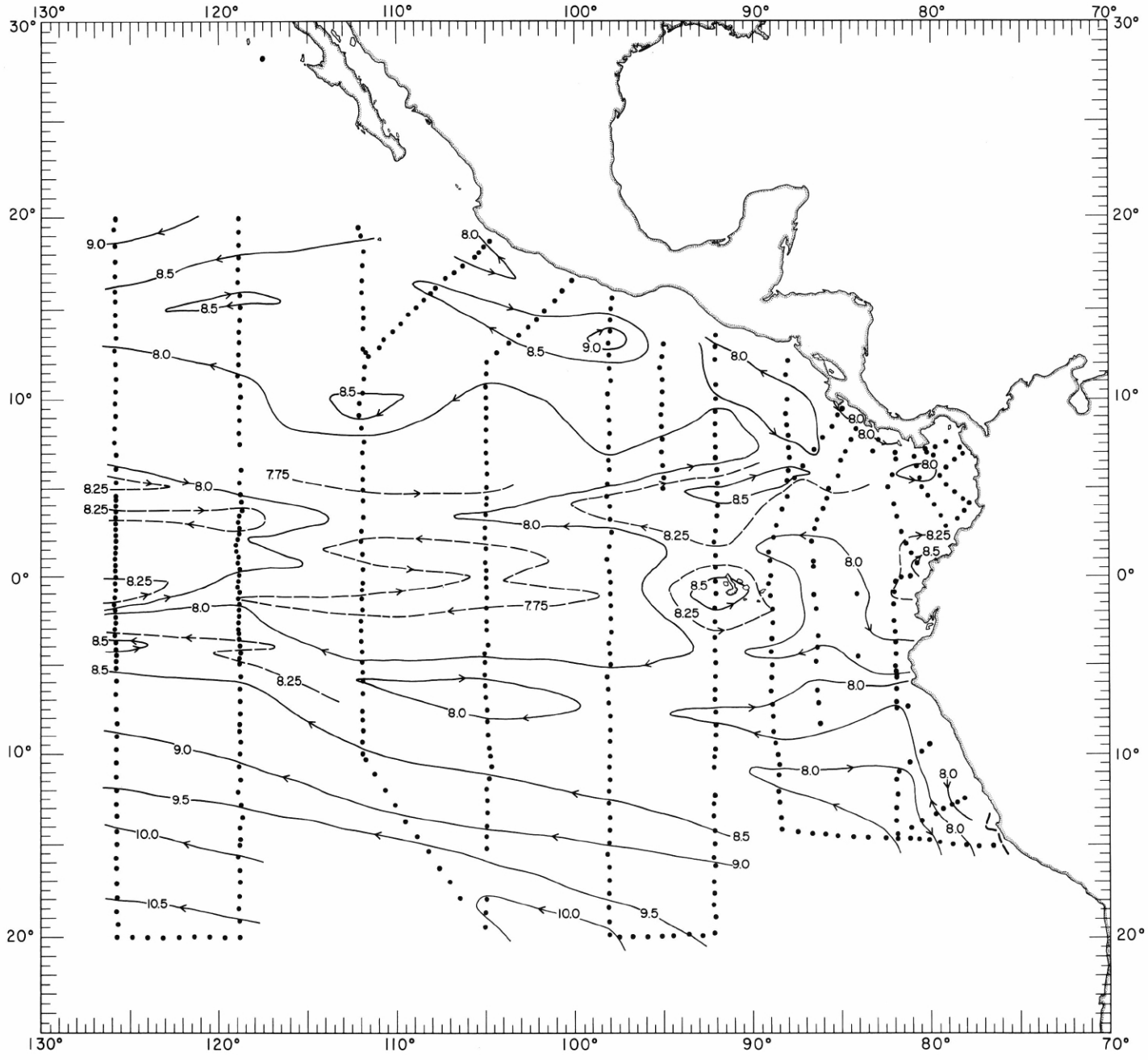

10-AP-δ250.

FIGURE 10-AP-δ250.—Acceleration potential (j./kg.), relative to 500 db., on the surface where $\delta_T = 250$ cl./t., February-March 1967. The heavy dashed line near the coast of Peru, in the vicinity of 15° S., indicates the intersection of this surface with the sea surface. For computing acceleration potential, thermosteric anomaly, δ_T, was used instead of specific volume anomaly, δ.

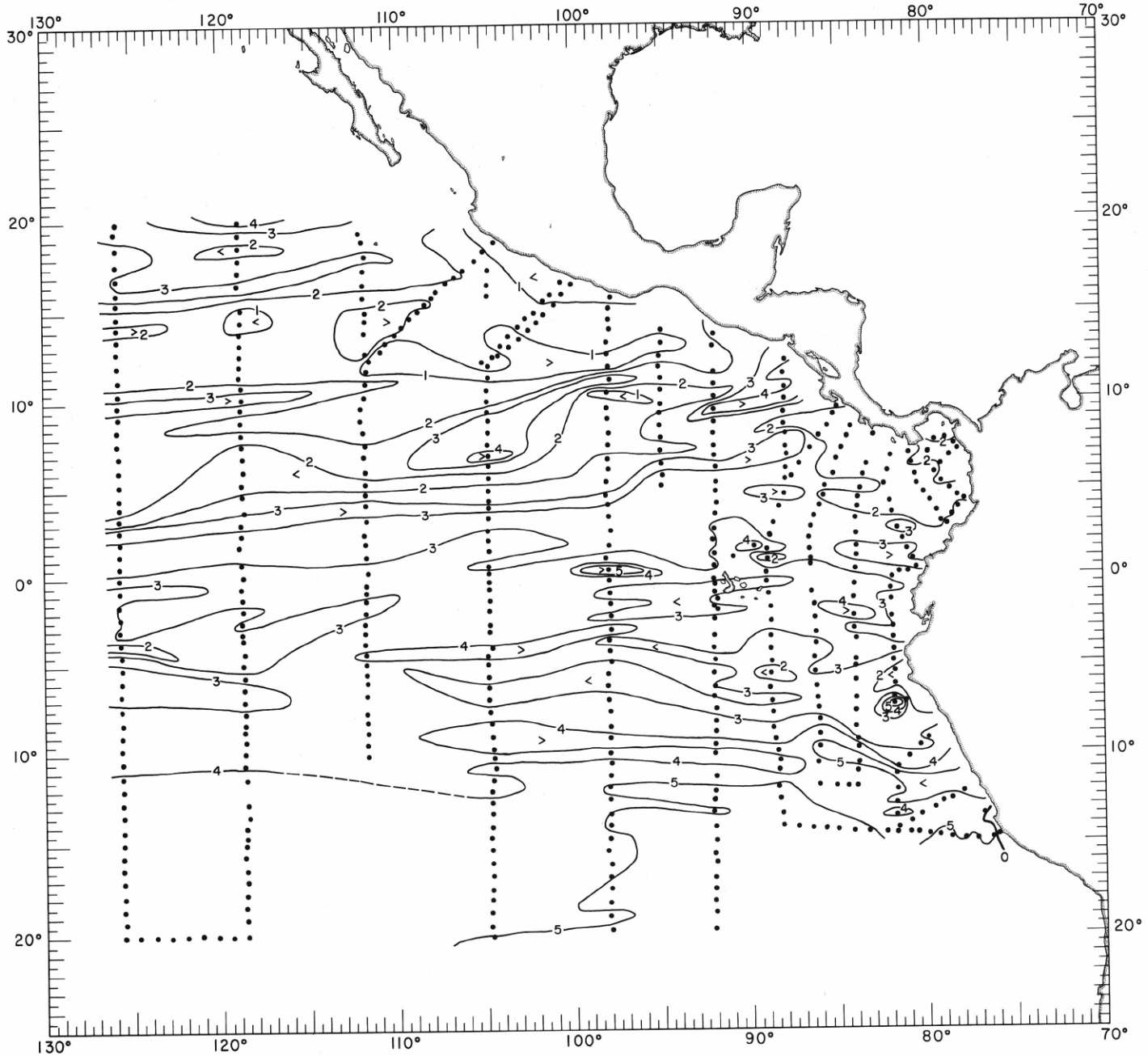

10-O_2-δ250.

FIGURE 10-O_2-δ250.—Oxygen (ml./l.) on the surface where $\delta_T = 250$ cl./t., February-March 1967. The heavy dashed line near the coast of Peru, in the vicinity of 15° S., indicates the intersection of this surface with the sea surface.

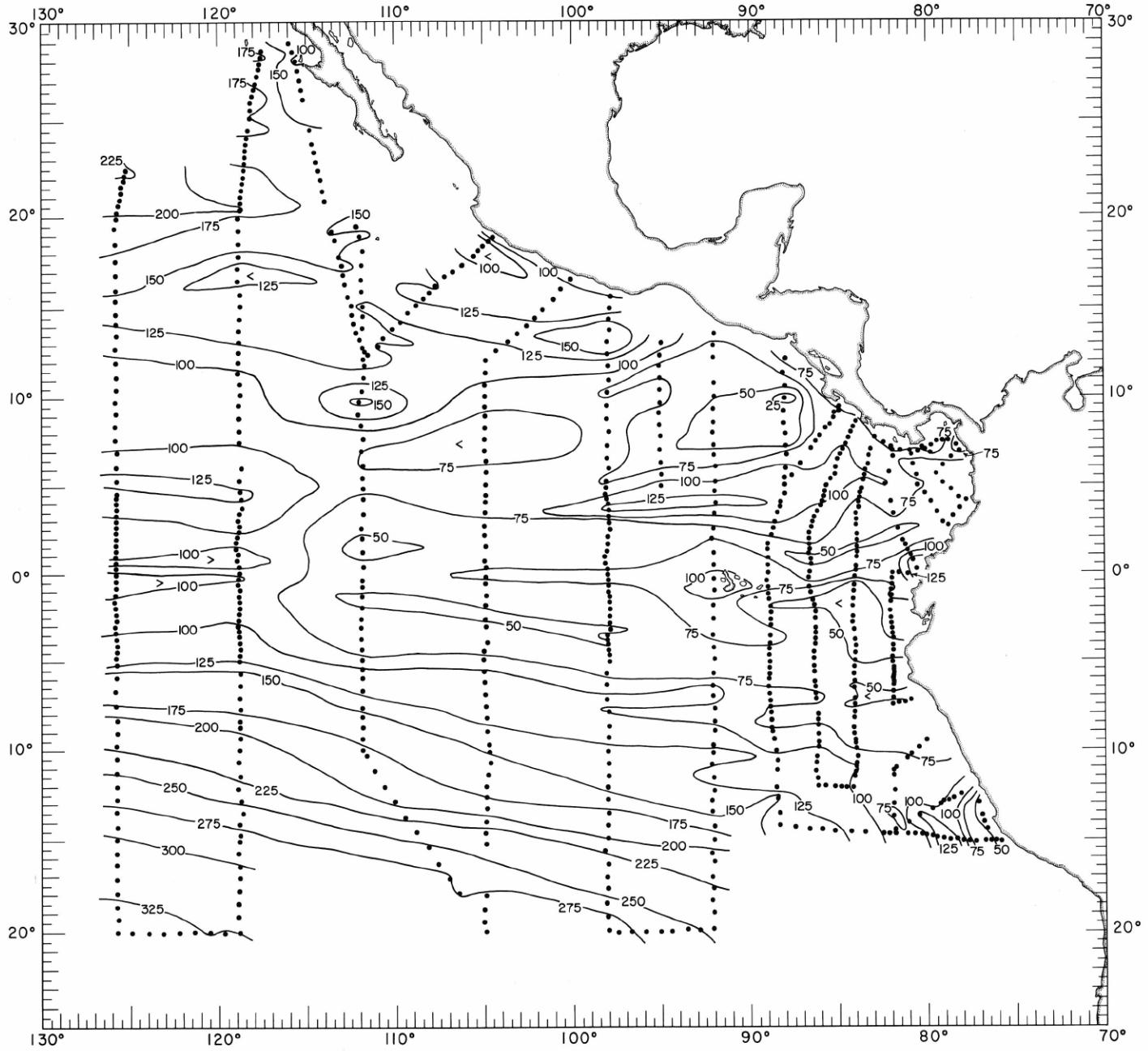

FIGURE 10-δ200-z.—Depth (m.) of the surface where $\delta_T = 200$ cl./t., February-March 1967.

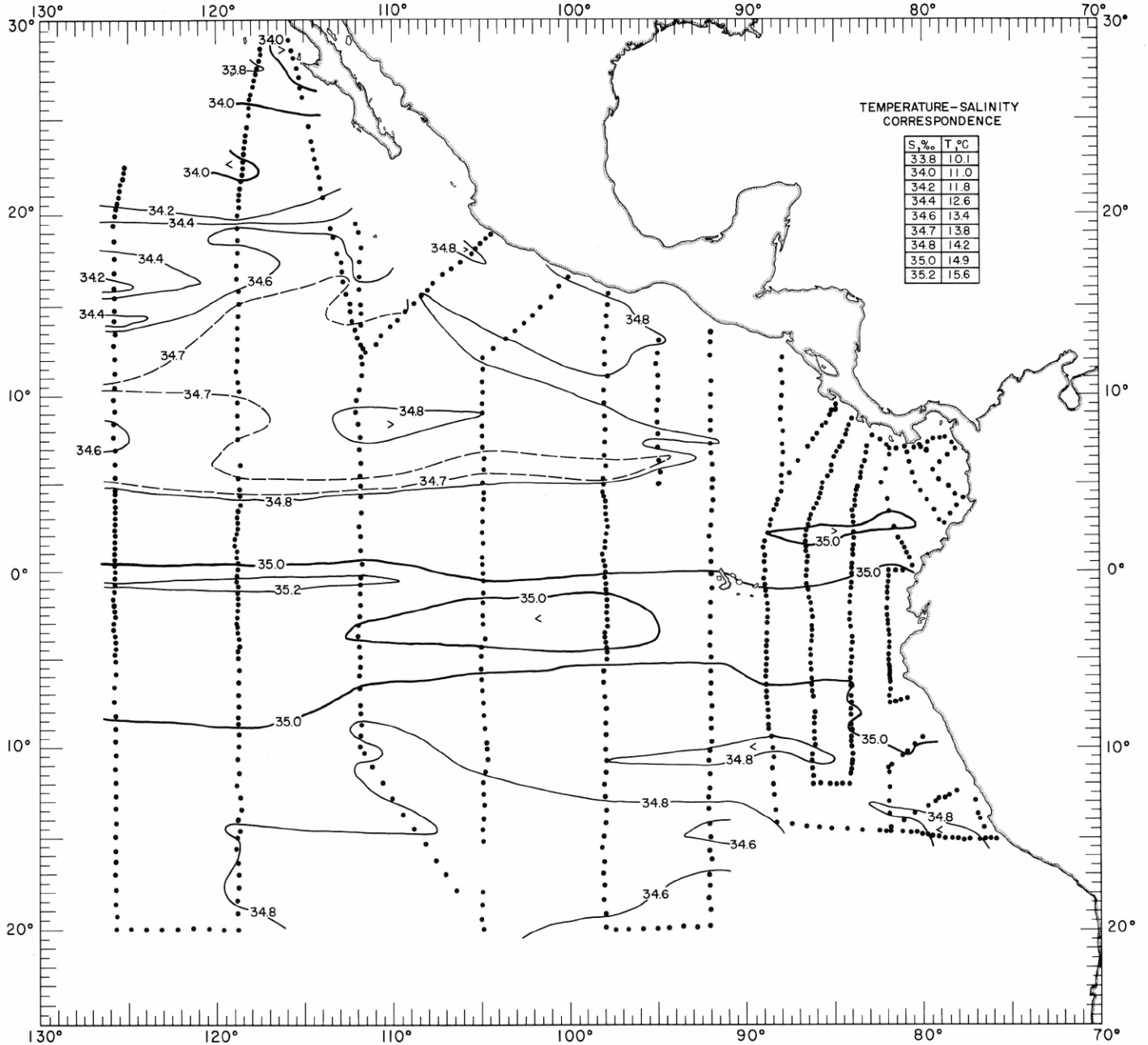

10-S-δ200.

FIGURE 10-S-δ200.—Salinity (‰) on the surface where $\delta_T = 200$ cl./t., February-March 1967. The table shows the temperature corresponding to each isohaline on the chart.

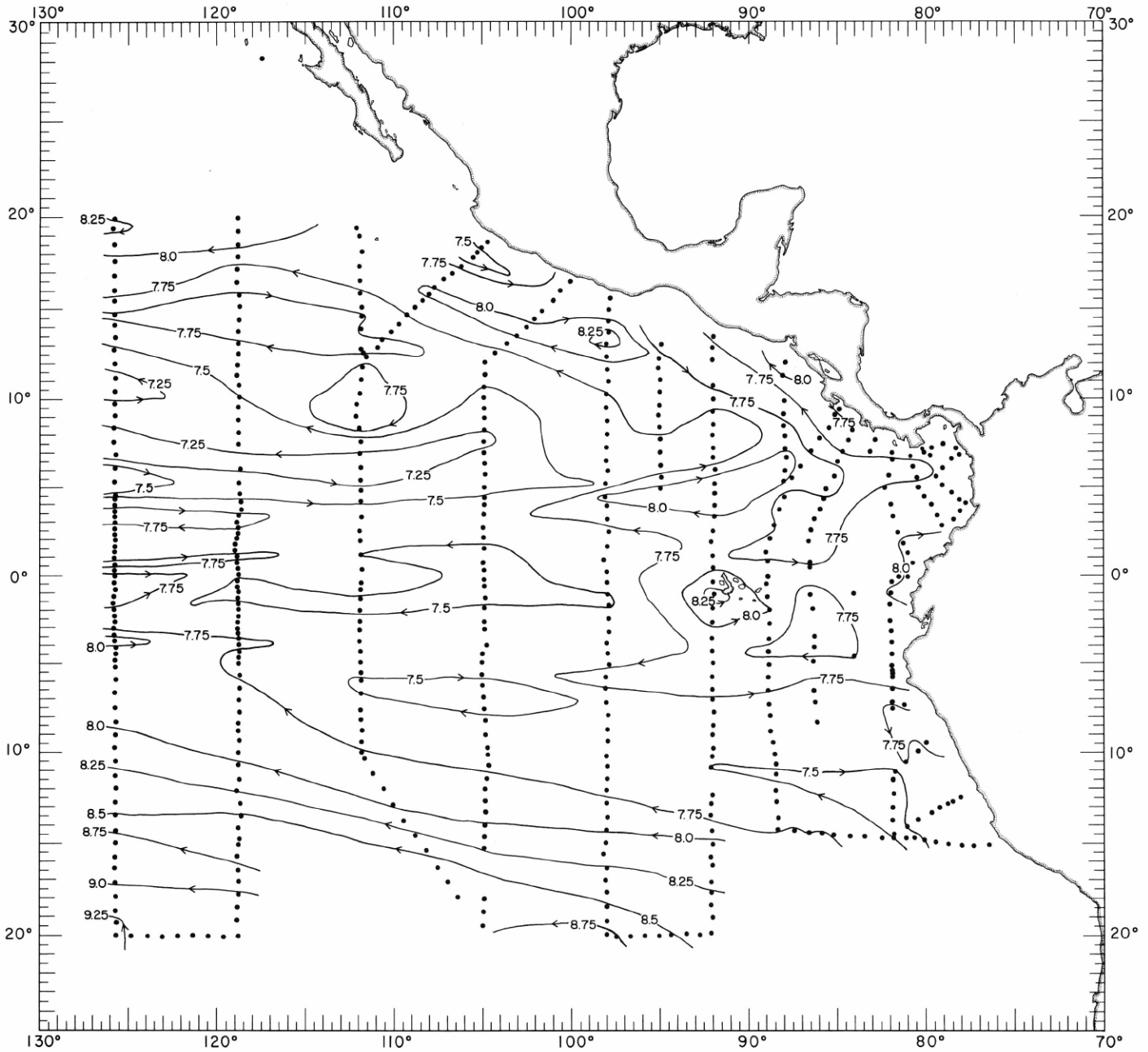

10-AP-δ200.

FIGURE 10-AP-δ200.—Acceleration potential (j./kg.), relative to 500 db., on the surface where $\delta_T = 200$ cl./t., February-March 1967. For computing acceleration potential, thermosteric anomaly, δ_T, was used instead of specific volume anomaly, δ.

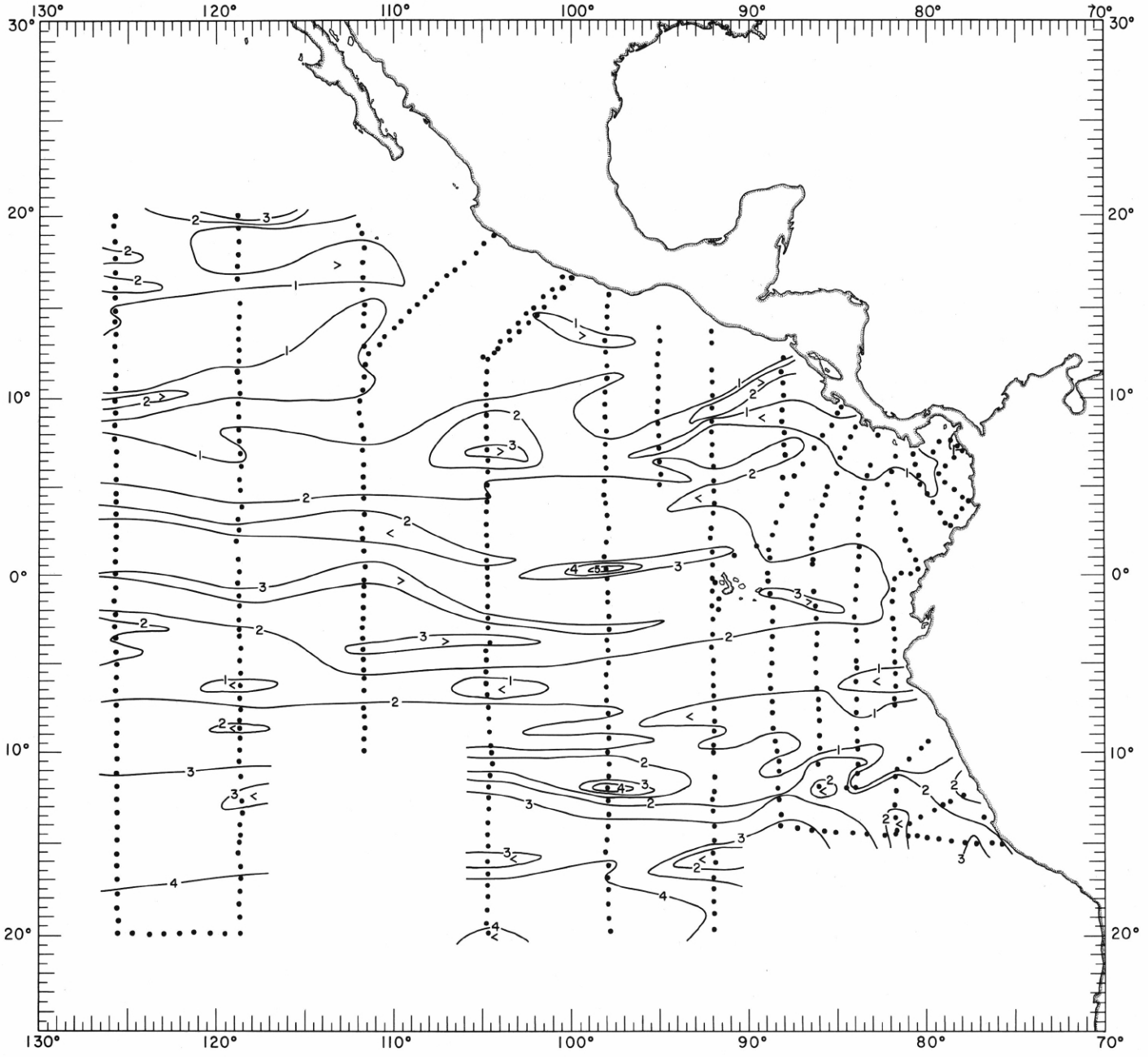

FIGURE 10-O_2-δ200.—Oxygen (ml./l.) on the surface where $\delta_T = 200$ cl./t., February-March 1967.

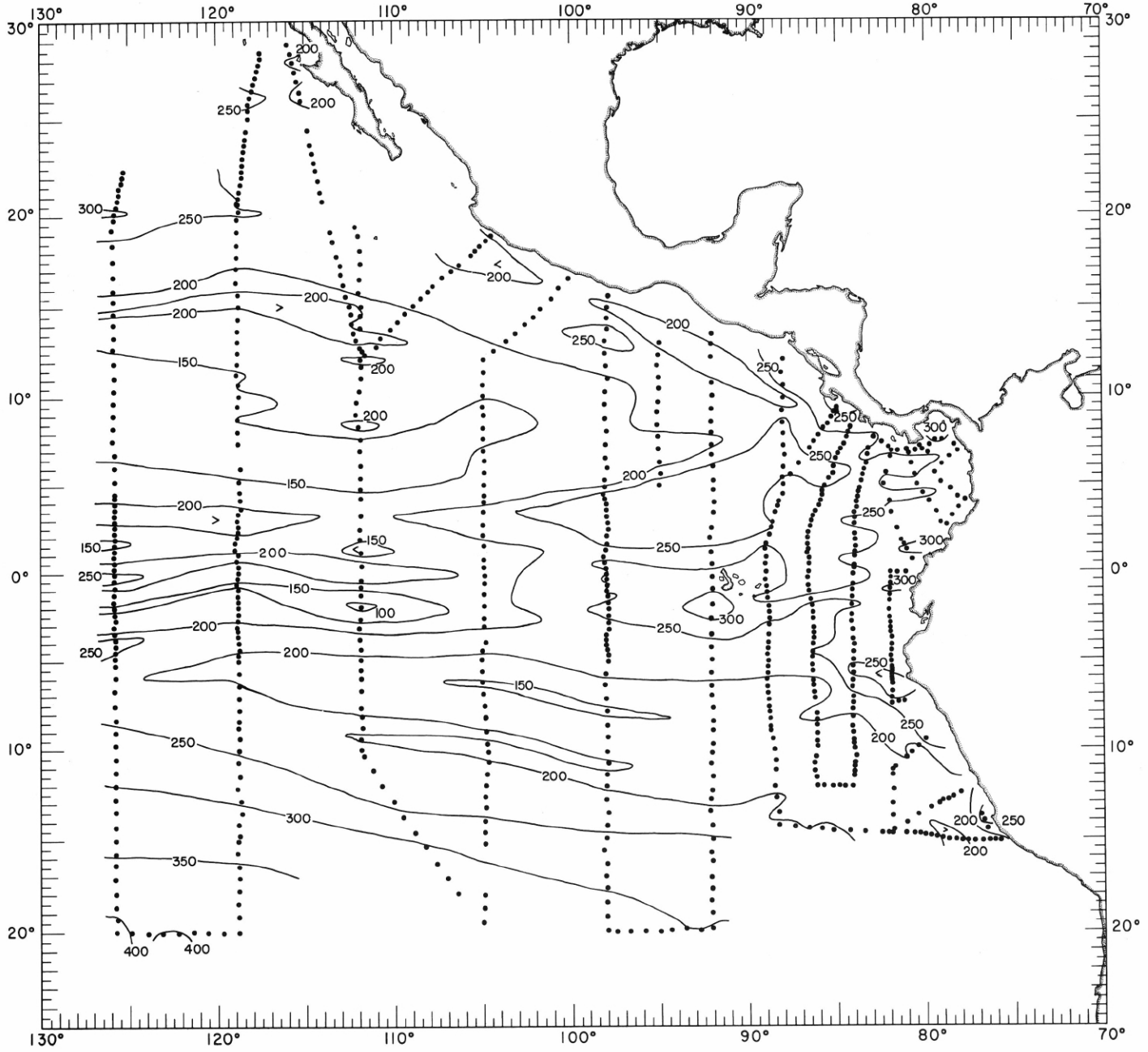

10-δ160-z.

FIGURE 10-δ160-z.—Depth (m.) of the surface where $\delta_T = 160$ cl./t., February-March 1967.

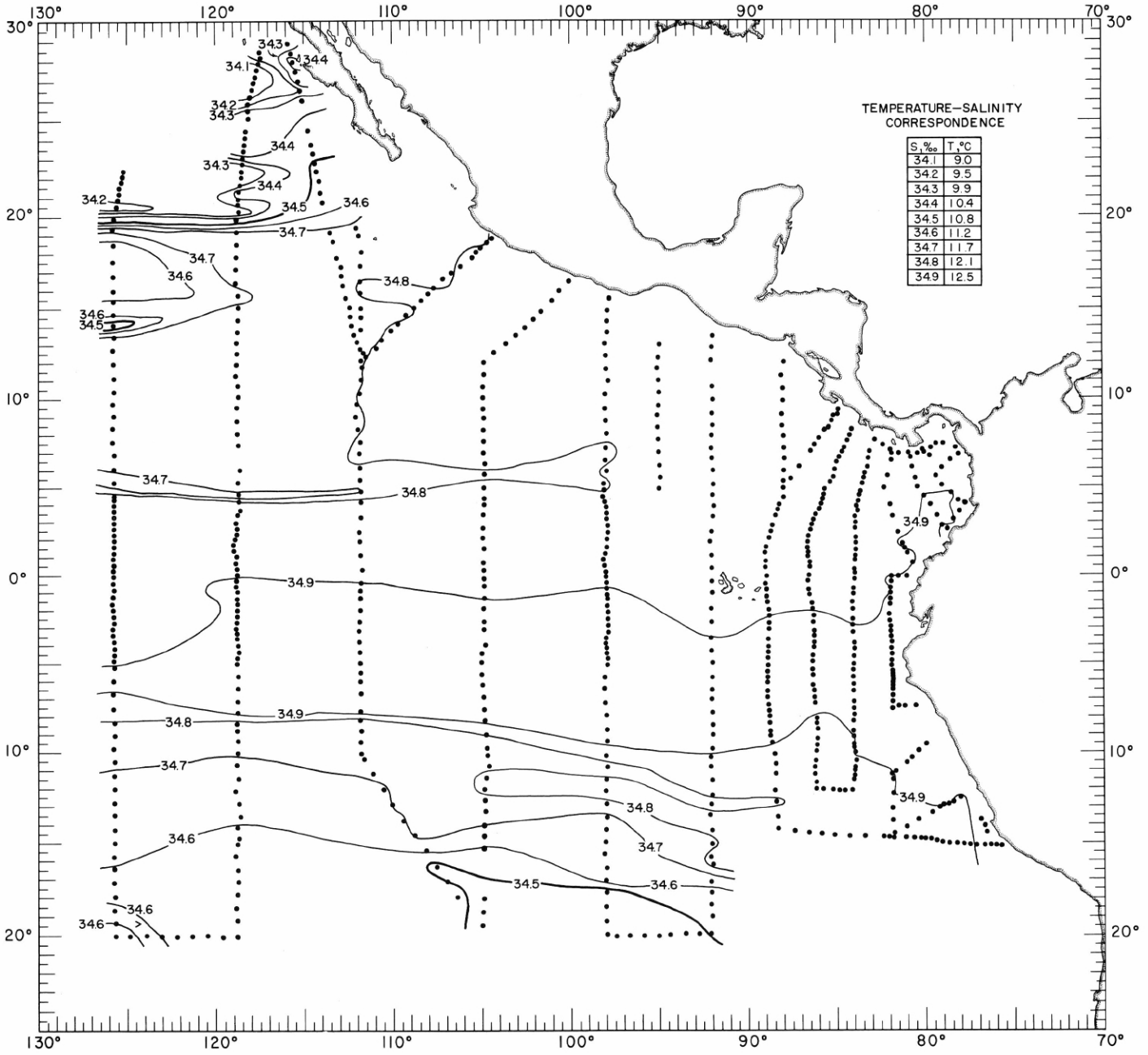

FIGURE 10-S-δ160.—Salinity (‰) on the surface where $\delta_T = 160$ cl./t., February-March 1967. The table shows the temperature corresponding to each isohaline on the chart.

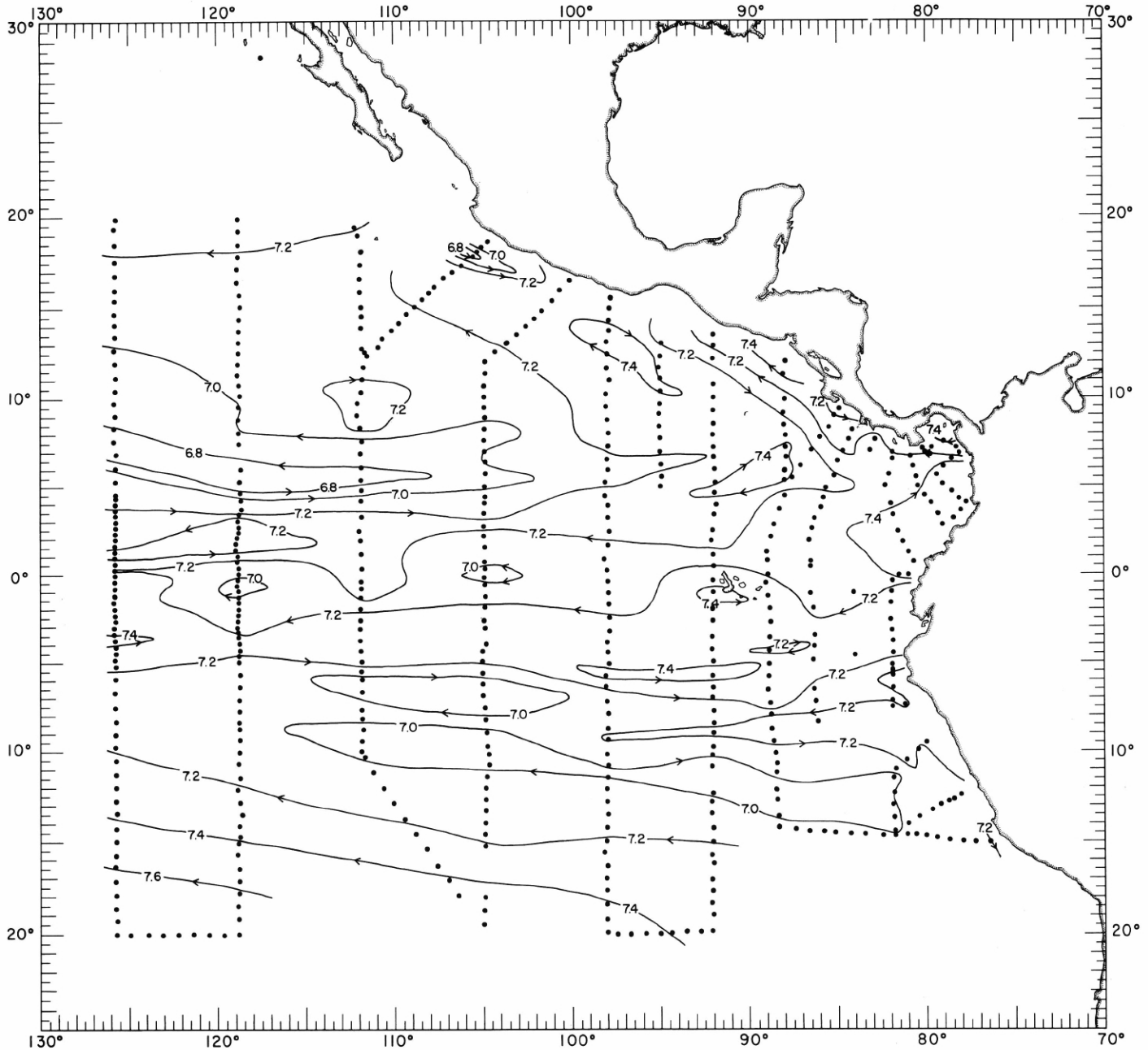

FIGURE 10-AP-δ160.—Acceleration potential (j./kg.), relative to 500 db., on the surface where $\delta_T = 160$ cl./t., February-March 1967. For computing acceleration potential, thermosteric anomaly, δ_T, was used instead of specific volume anomaly, δ.

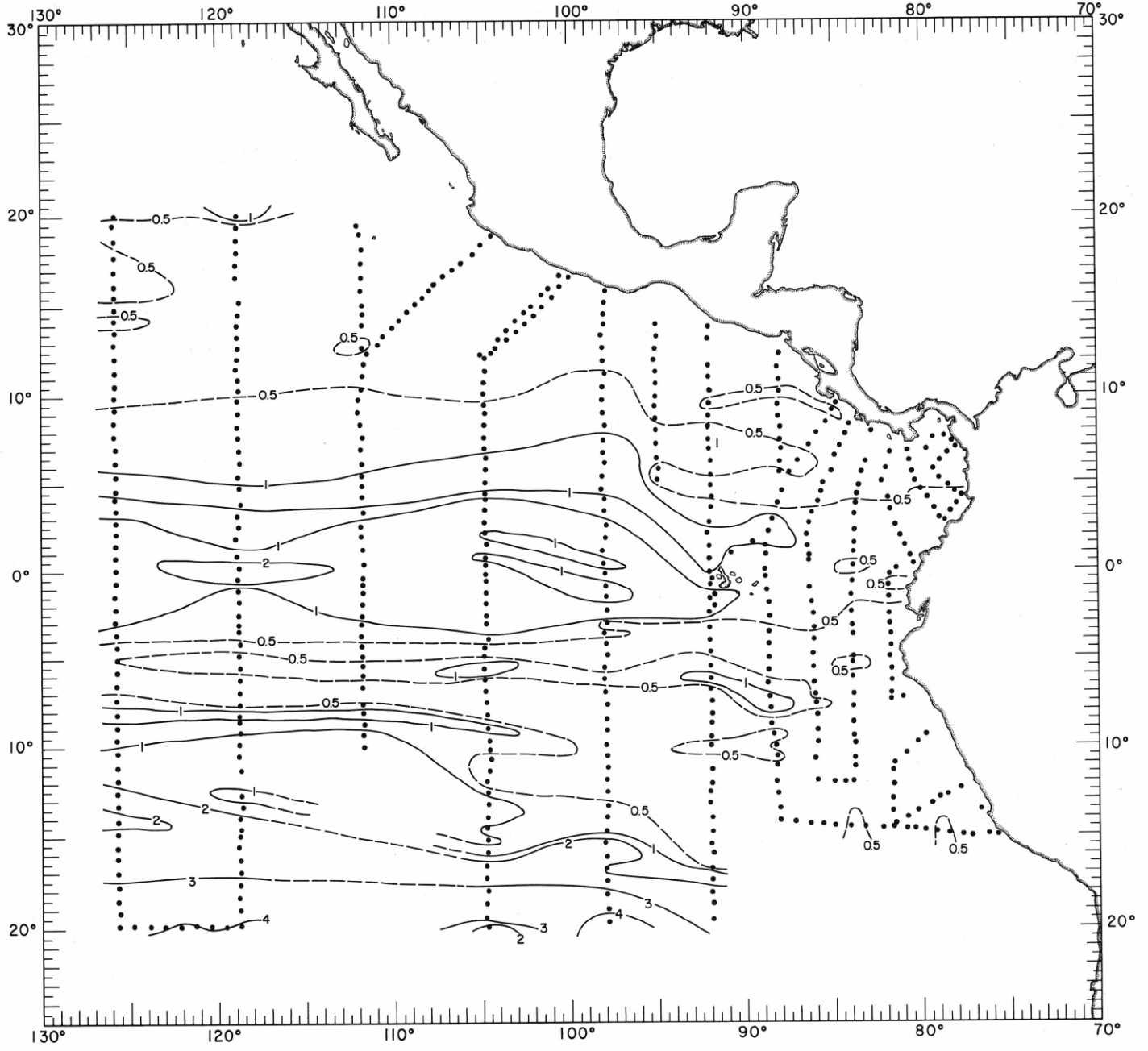

10-O_2-δ160.

FIGURE 10-O_2-δ160.—Oxygen (ml./l.) on the surface where $\delta_T = 160$ cl./t., February-March 1967.

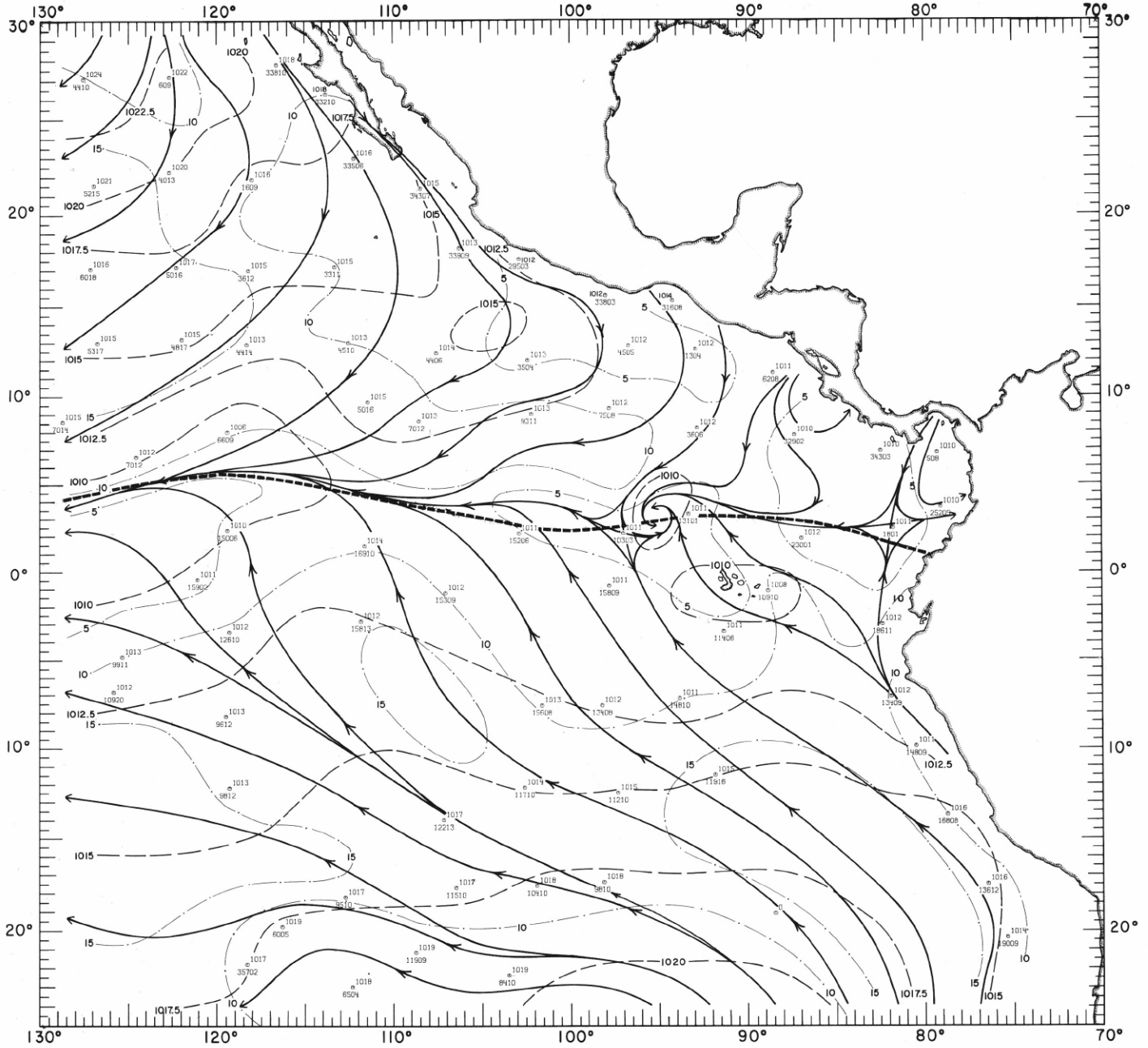

FIGURE 10-MW-1. —Analyses of the surface air pressure and surface winds from all available ship observations, averaged over 2-degree (latitude-longitude) squares for the period February 1-14, 1967. Heavy dashed lines are isobars. Solid lines are streamlines showing the mean resultant direction of wind flow. Light dash-dot lines are isotachs indicating mean resultant wind speed (kn.). Pressure (mb.) averaged for 5-degree squares is plotted above the mean position of the square, and resultant wind direction followed by speed (kn.) is plotted below. The monthly climatological position of the intertropical convergence zone is shown by a wide dashed band.

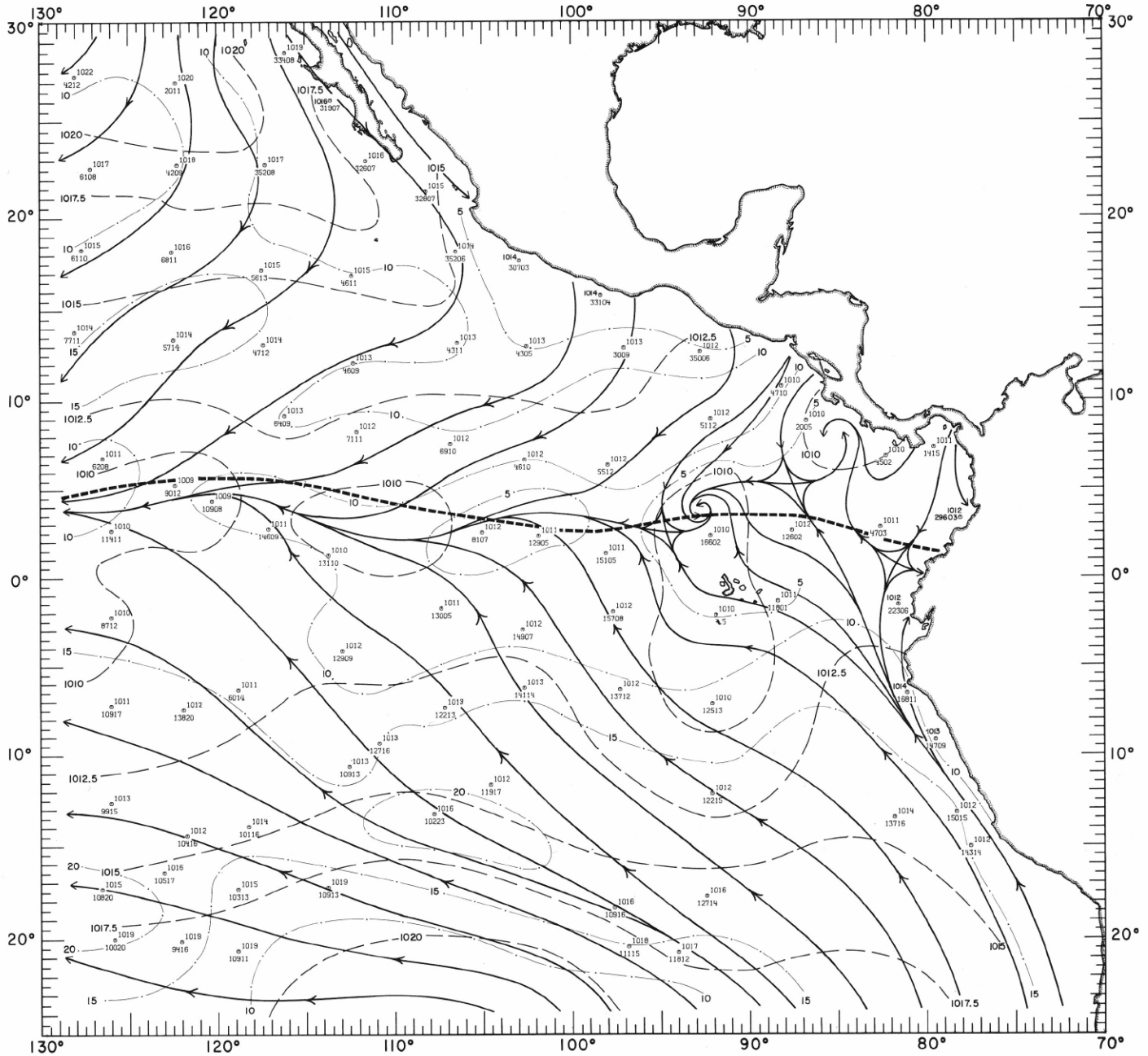

FIGURE 10-MW-2. —Analyses of the surface air pressure and surface winds from all available ship observations, averaged over 2-degree (latitude-longitude) squares for the period February 15-28, 1967. Heavy dashed lines are isobars. Solid lines are streamlines showing the mean resultant direction of wind flow. Light dash-dot lines are isotachs indicating mean resultant wind speed (kn.). Pressure (mb.) averaged for 5-degree squares is plotted above the mean position of the square, and resultant wind direction followed by speed (kn,) is plotted below. The monthly climatological position of the intertropical convergence zone is shown by a wide dashed band.

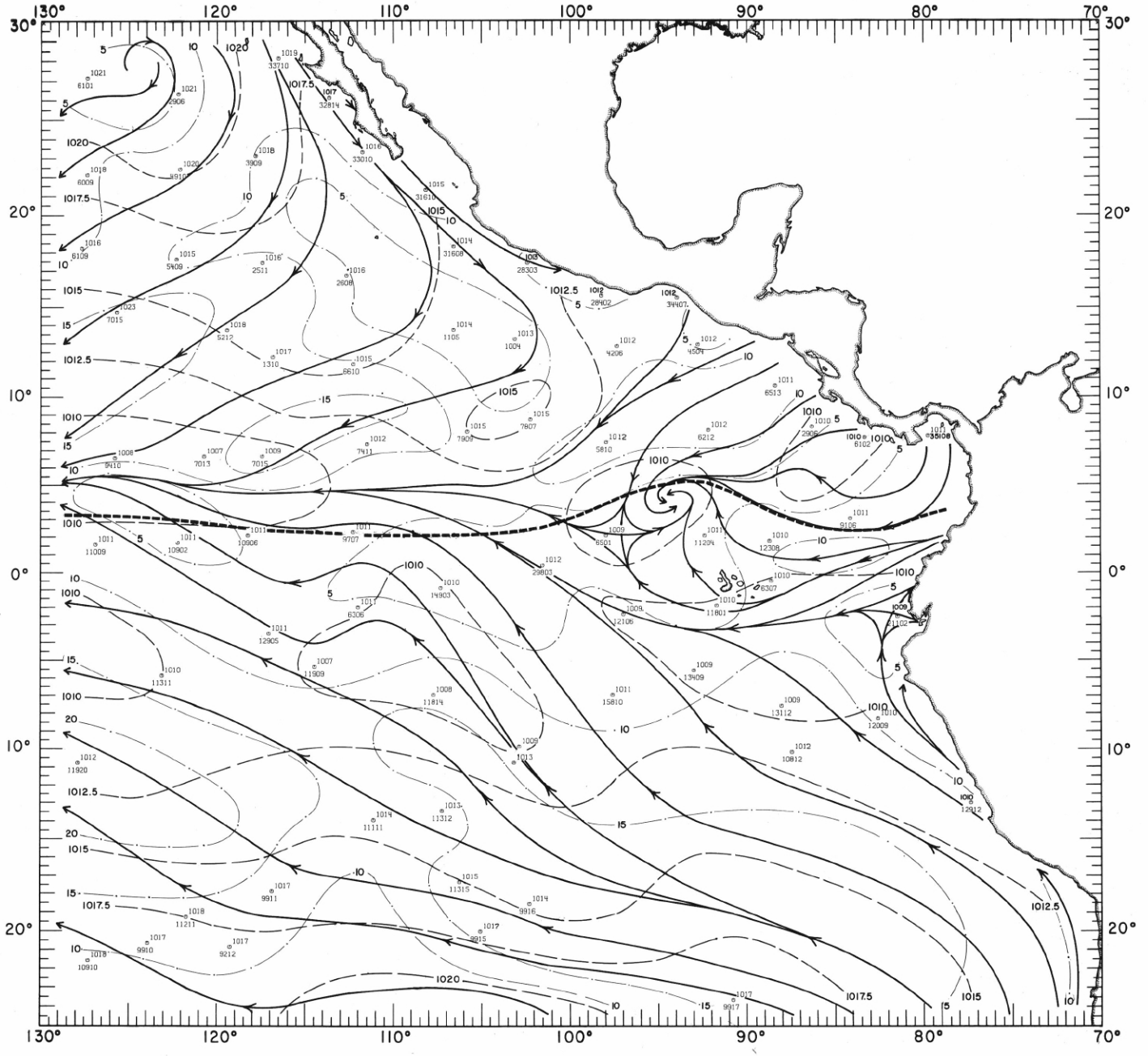

FIGURE 10-MW-3. —Analyses of the surface air pressure and surface winds from all available ship observations, averaged over 2-degree (latitude-longitude) squares for the period March 1-17, 1967. Heavy dashed lines are isobars. Solid lines are streamlines showing the mean resultant direction of wind flow. Light dash-dot lines are isotachs indicating mean resultant wind speed (kn.). Pressure (mb.) averaged for 5-degree squares is plotted above the mean position of the square, and resultant wind direction followed by speed (kn.) is plotted below. The monthly climatological position of the intertropical convergence zone is shown by a wide dashed band.

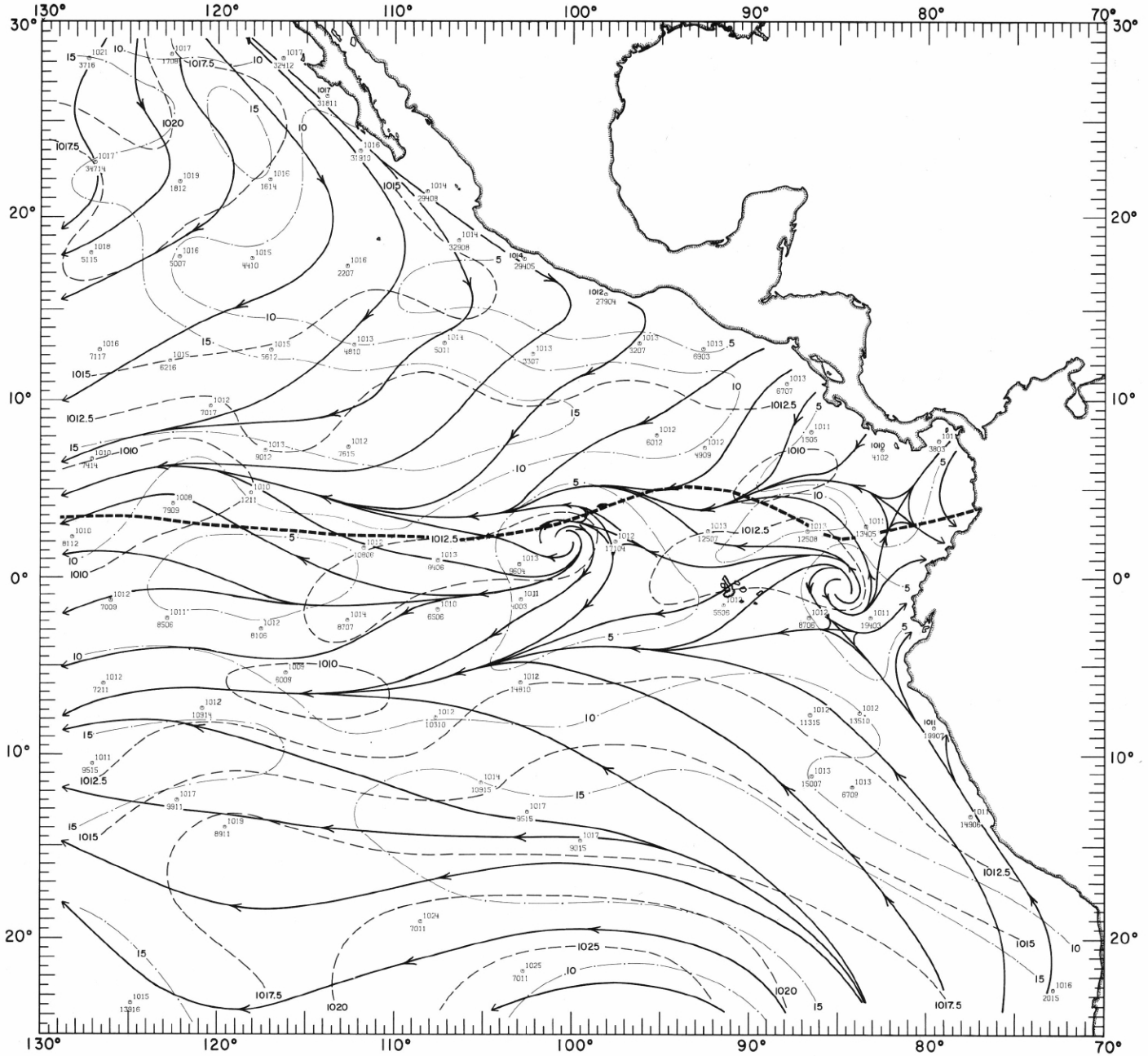

FIGURE 10-MW-4. —Analyses of the surface air pressure and surface winds from all available ship observations, averaged over 2-degree (latitude-longitude) squares for the period March 18-31, 1967. Heavy dashed lines are isobars. Solid lines are streamlines showing the mean resultant direction of wind flow. Light dash-dot lines are isotachs indicating mean resultant wind speed (kn.). Pressure (mb.) averaged for 5-degree squares is plotted above the mean position of the square, and resultant wind direction followed by speed (kn.) is plotted below. The monthly climatological position of the intertropical convergence zone is shown by a wide dashed band.

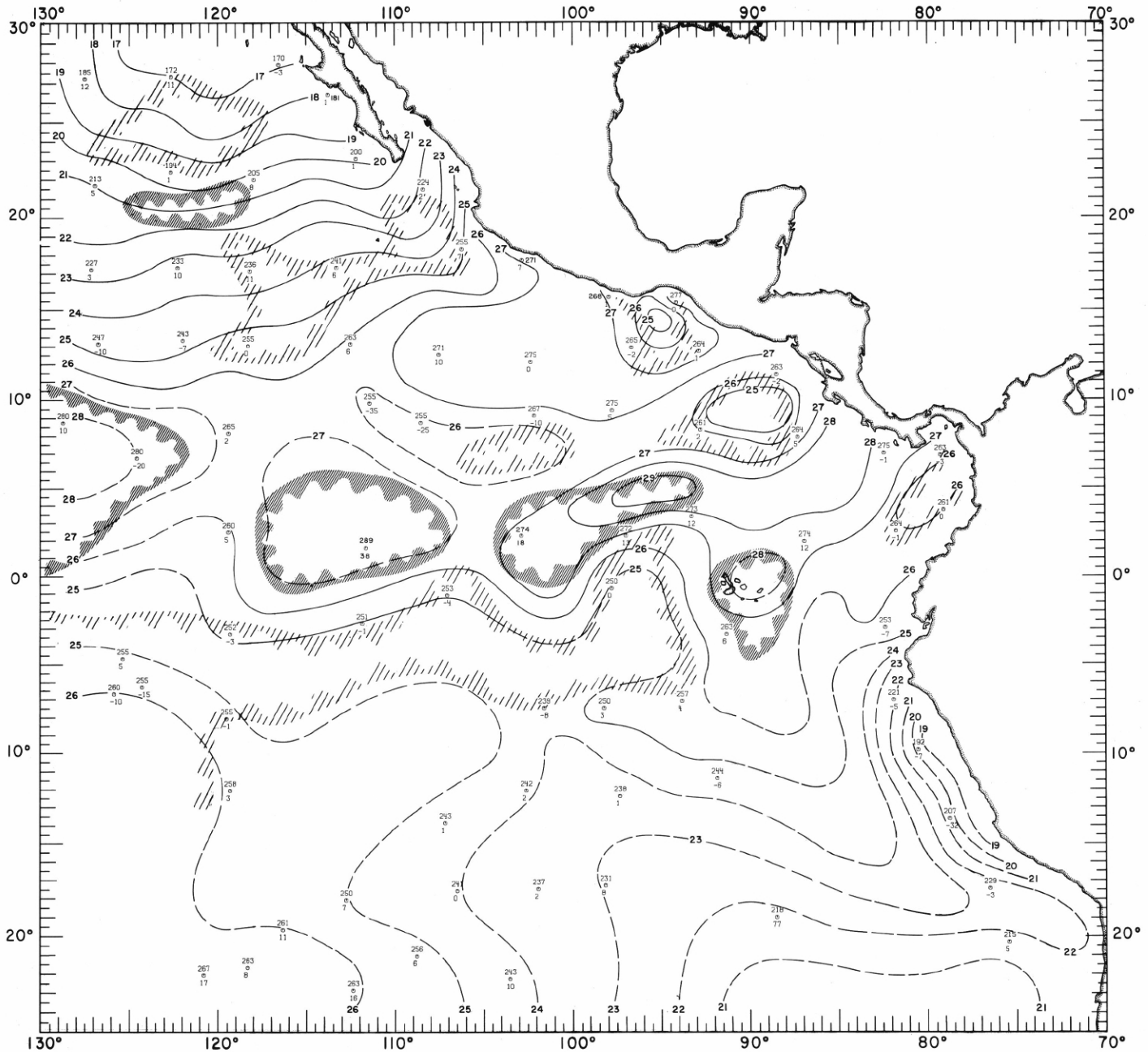

10-MT-1.

FIGURE 10-MT-1. — Analysis of sea surface temperatures based on averages for 2-degree (latitude-longitude) squares from all available ship observations for the period February 1-14, 1967. Solid lines are sea surface isotherms (°C.); the isotherms are dashed where data are sparse. Dark hatching outlines areas with positive temperature anomalies greater than 1 °C.; light hatching shows areas with negative anomalies greater than 1 °C. Sea surface temperature (°C. x 10) averaged for 5-degree squares is plotted above the mean position of the square; sea temperature minus air temperature difference (°C. x 10) is plotted below the symbol.

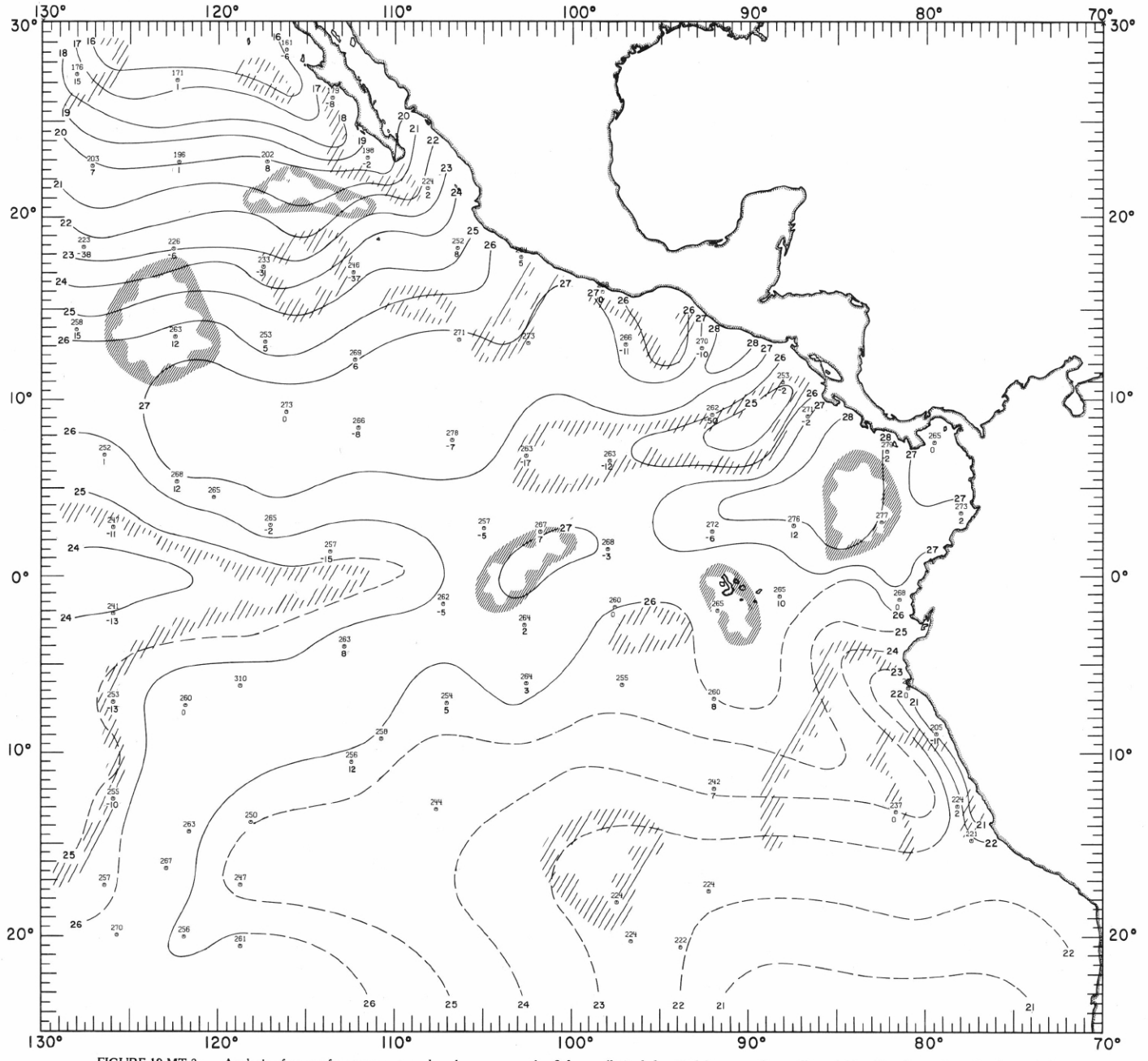

FIGURE 10-MT-2. — Analysis of sea surface temperatures based on averages for 2-degree (latitude-longitude) squares from all available ship observations for the period February 15-28, 1967. Solid lines are sea surface isotherms (°C.); the isotherms are dashed where data are sparse. Dark hatching outlines areas with positive temperature anomalies greater than 1 °C.; light hatching shows areas with negative anomalies greater than 1 °C. Sea surface temperature (°C. x 10) averaged for 5-degree squares is plotted above the mean position of the square; sea temperature minus air temperature difference (°C. x 10) is plotted below the symbol.

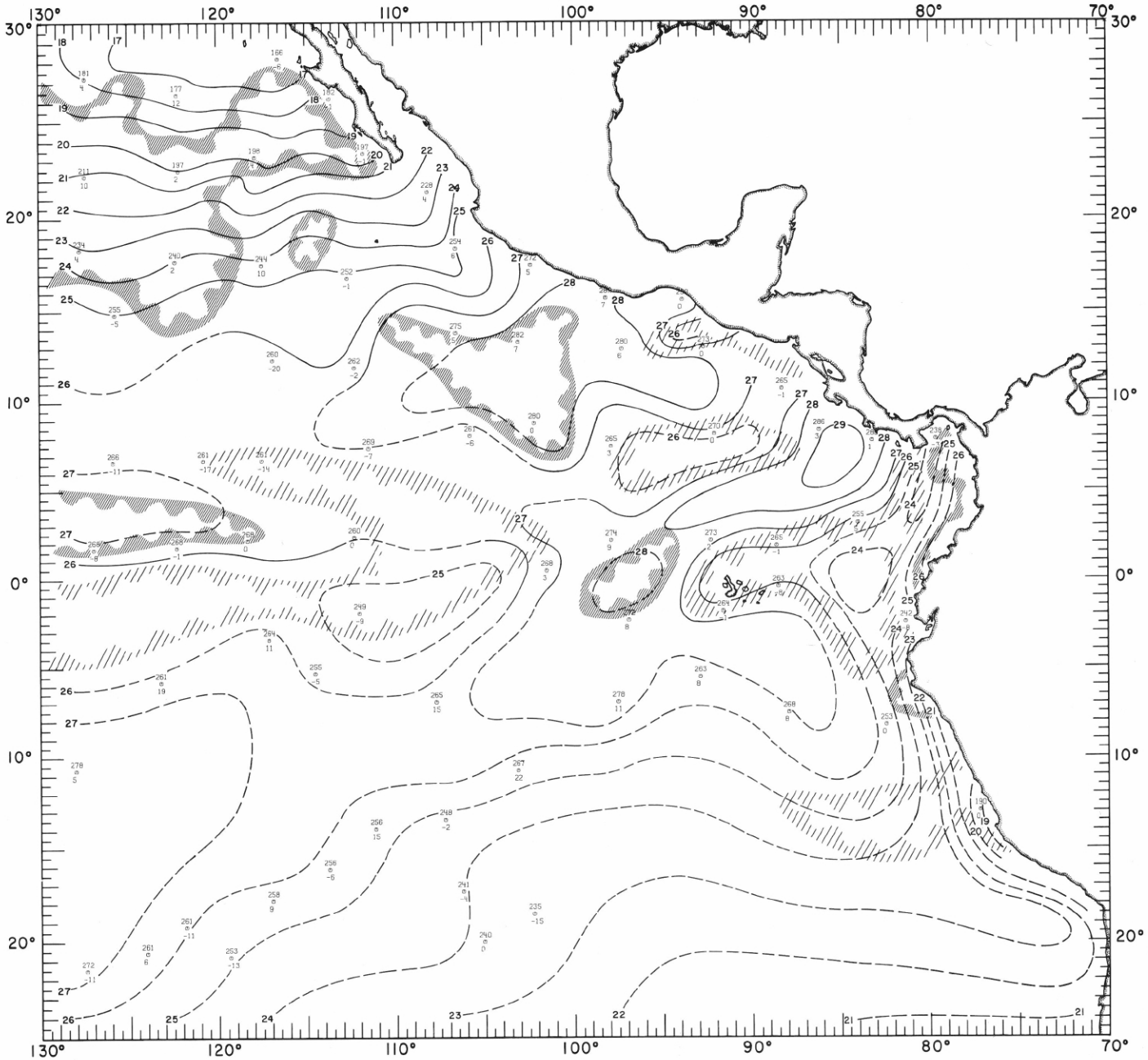

FIGURE 10-MT-3. — Analysis of sea surface temperatures based on averages for 2-degree (latitude-longitude) squares from all available ship observations for the period March 1-17, 1967. Solid lines are sea surface isotherms (°C.); the isotherms are dashed where data are sparse. Dark hatching outlines areas with positive temperature anomalies greater than 1 °C.; light hatching shows areas with negative anomalies greater than 1 °C. Sea surface temperature (°C. x 10) averaged for 5-degree squares is plotted above the mean position of the square; sea temperature minus air temperature difference (°C. x 10) is plotted below the symbol.

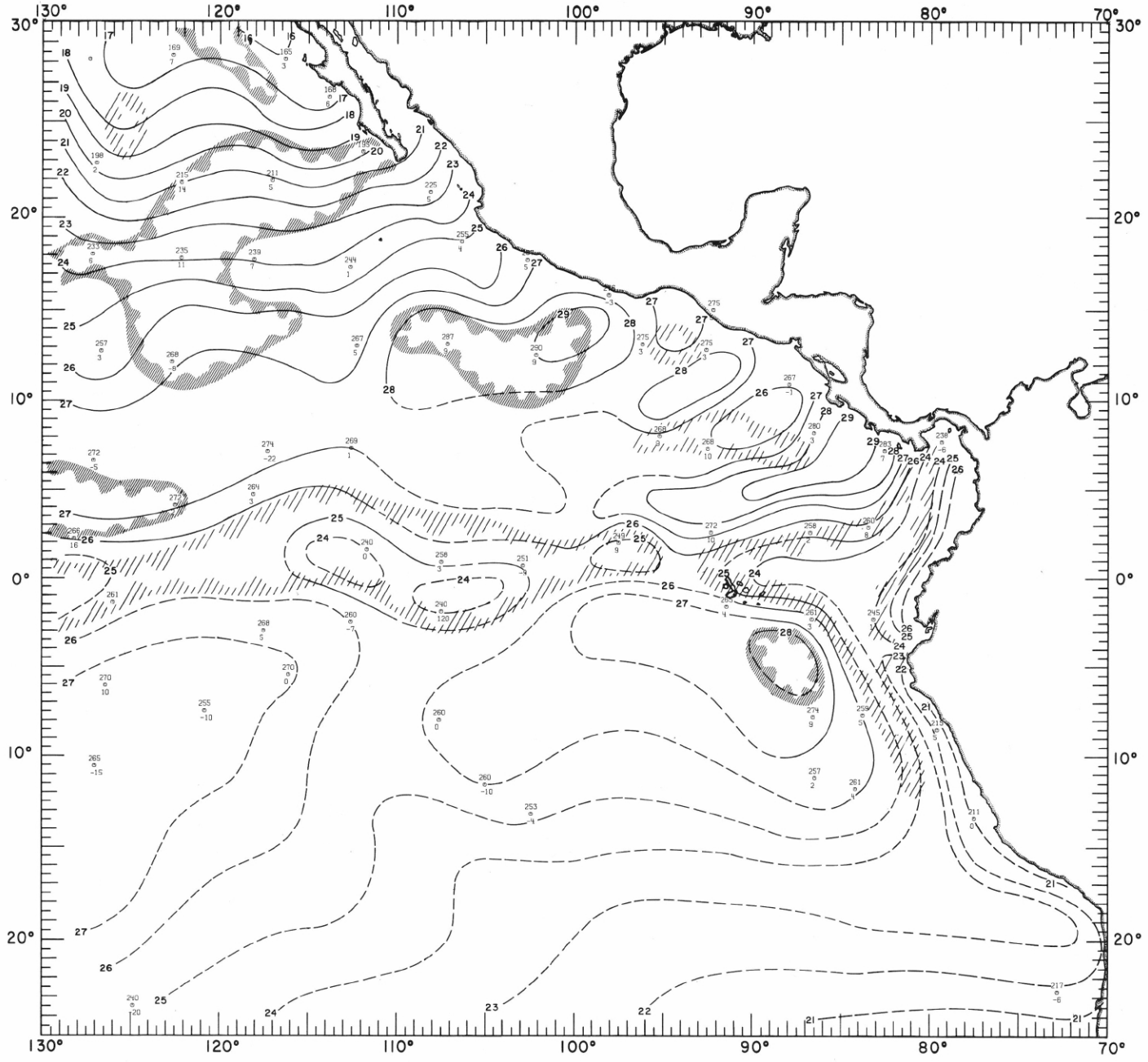

10-MT-4.

FIGURE 10-MT-4. — Analysis of sea surface temperatures based on averages for 2-degree (latitude-longitude) squares from all available ship observations for the period March 18-31, 1967. Solid lines are sea surface isotherms (°C.); the isotherms are dashed where data are sparse. Dark hatching outlines areas with positive temperature anomalies greater than 1 °C.; light hatching shows areas with negative anomalies greater than 1 °C. Sea surface temperature (°C. x 10) averaged for 5-degree squares is plotted above the mean position of the square; sea temperature minus air temperature difference (°C. x 10) is plotted below the symbol.

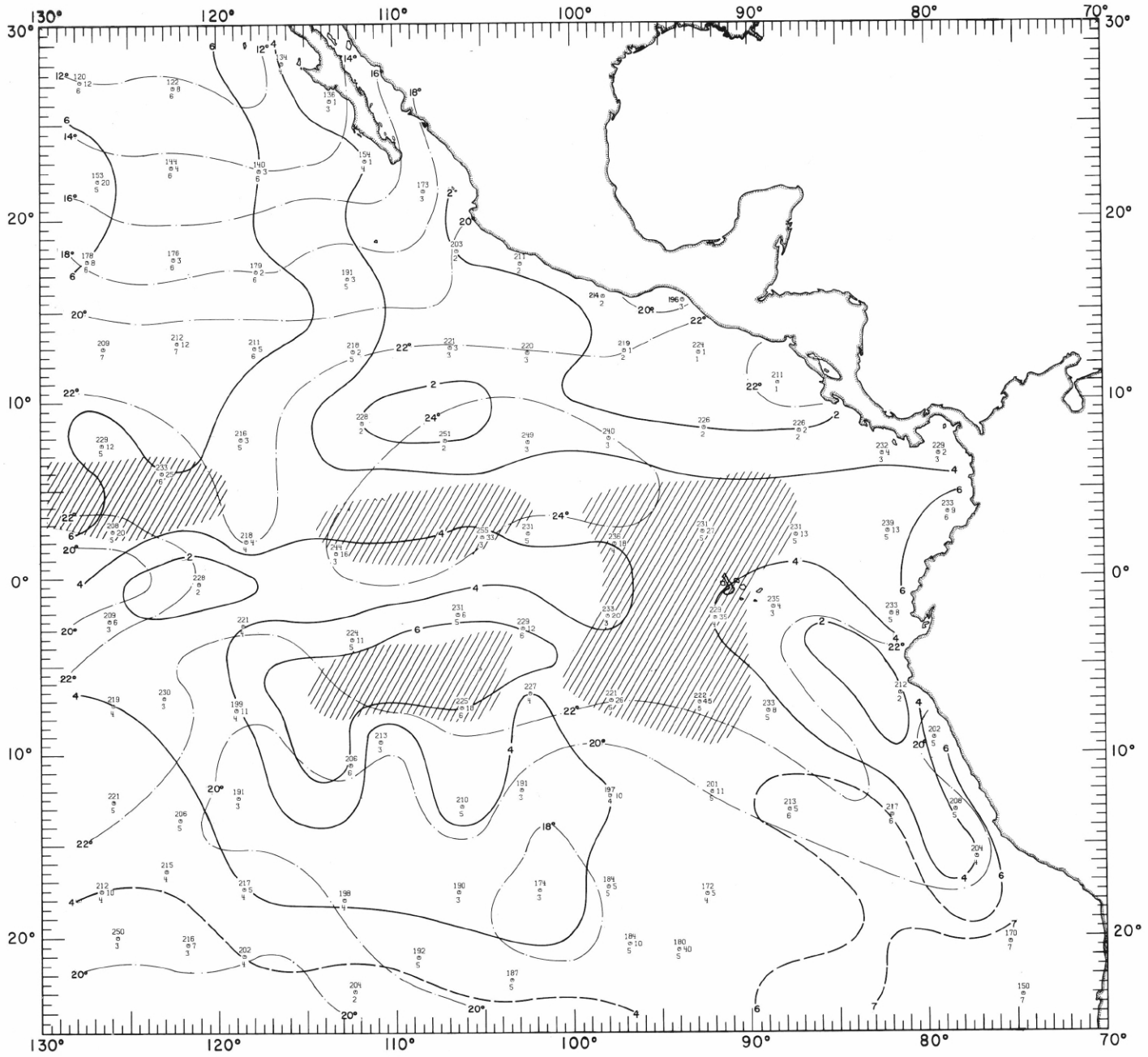

10-MC-1.

FIGURE 10-MC-1.—Analyses of the surface dew-point temperature of the air and total cloud cover based on 2-degree (latitude-longitude) averages from all available ship observations for the month of February 1967. Solid lines depict the monthly mean total cloud cover in oktas; the lines are dashed where data are sparse. Dash-dot lines are isotherms of the mean monthly dew-point temperature at 2-degree (°C.) intervals. Areas where 15 percent or more of the ships reported rain of any type at or within sight of the ship are shaded. Dew-point temperature (°C. x 10) averaged for 5-degree squares is plotted above the mean position of the square, with total cloud cover (oktas) below and rainfall frequency (%) to the right of the symbol.

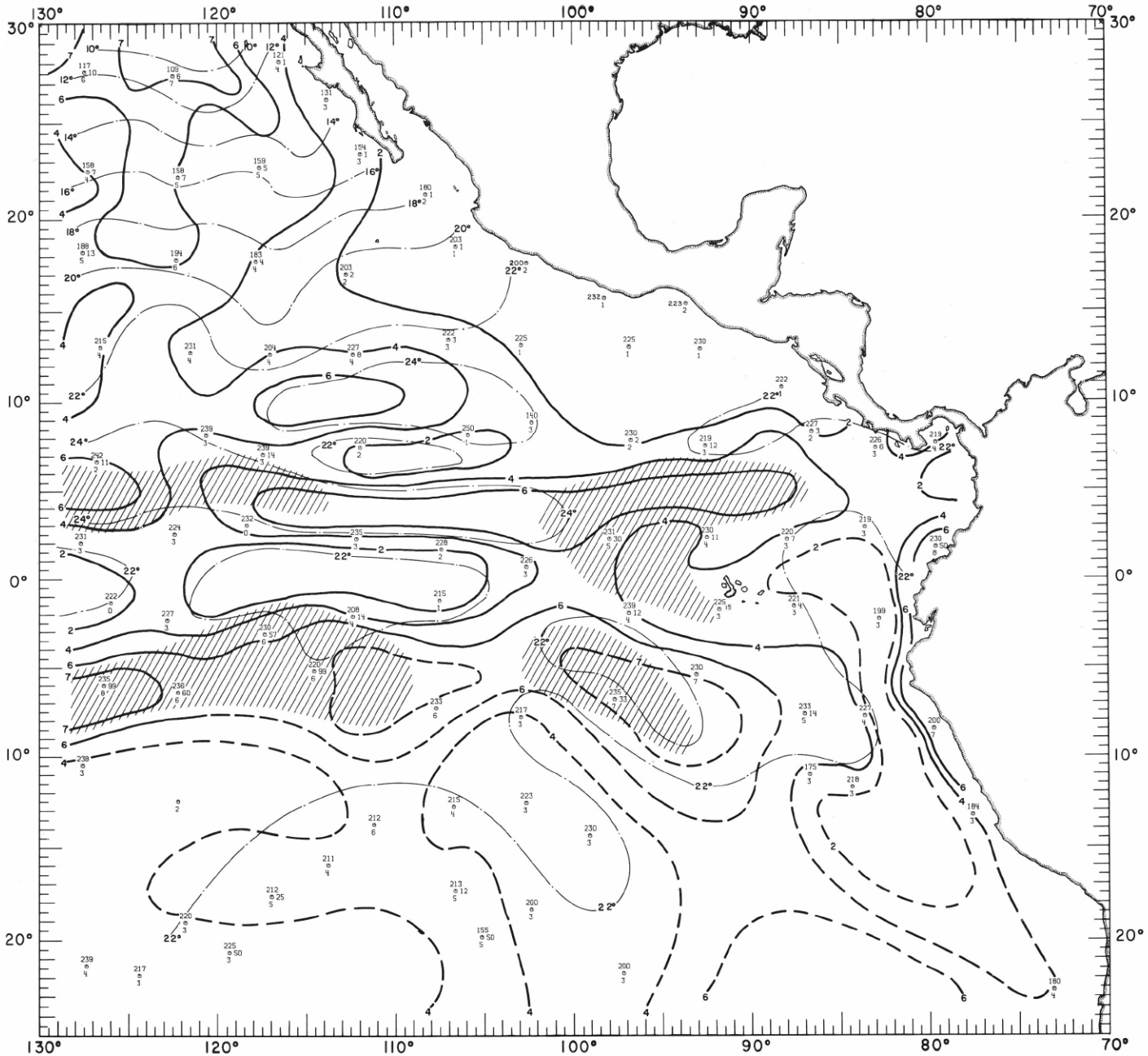

10-MC-2.

FIGURE 10-MC-2.—Analyses of the surface dew-point temperature of the air and total cloud cover based on 2-degree (latitude-longitude) averages from all available ship observations for the month of March 1967. Solid lines depict the monthly mean total cloud cover in oktas; the lines are dashed where data are sparse. Dash-dot lines are isotherms of the mean monthly dew-point temperature at 2-degree (°C.) intervals. Areas where 15 percent or more of the ships reported rain of any type at or within sight of the ship are shaded. Dew-point temperature (°C. x 10) averaged for 5-degree squares is plotted above the mean position of the square, with total cloud cover (oktas) below and rainfall frequency (%) to the right of the symbol.

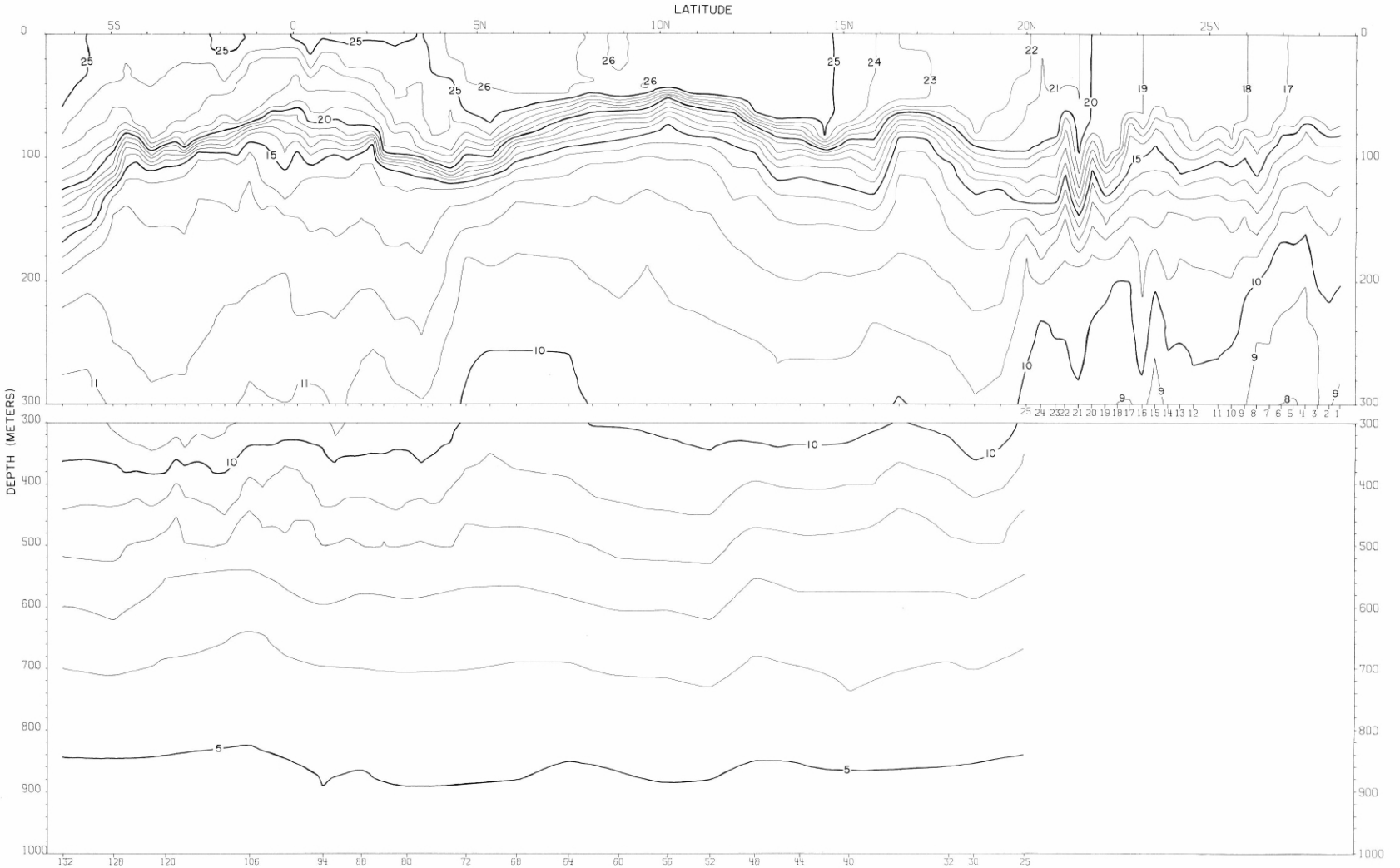

FIGURE 11-T-v1.—Vertical distribution of temperature (°C.) along 119° W. from 28°36′ N. to 6°21′ S., January 25-February 9, 1967. The data from Stations 1-24 were not calibrated against Nansen cast data.

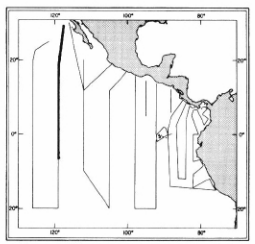

11-T-v1.

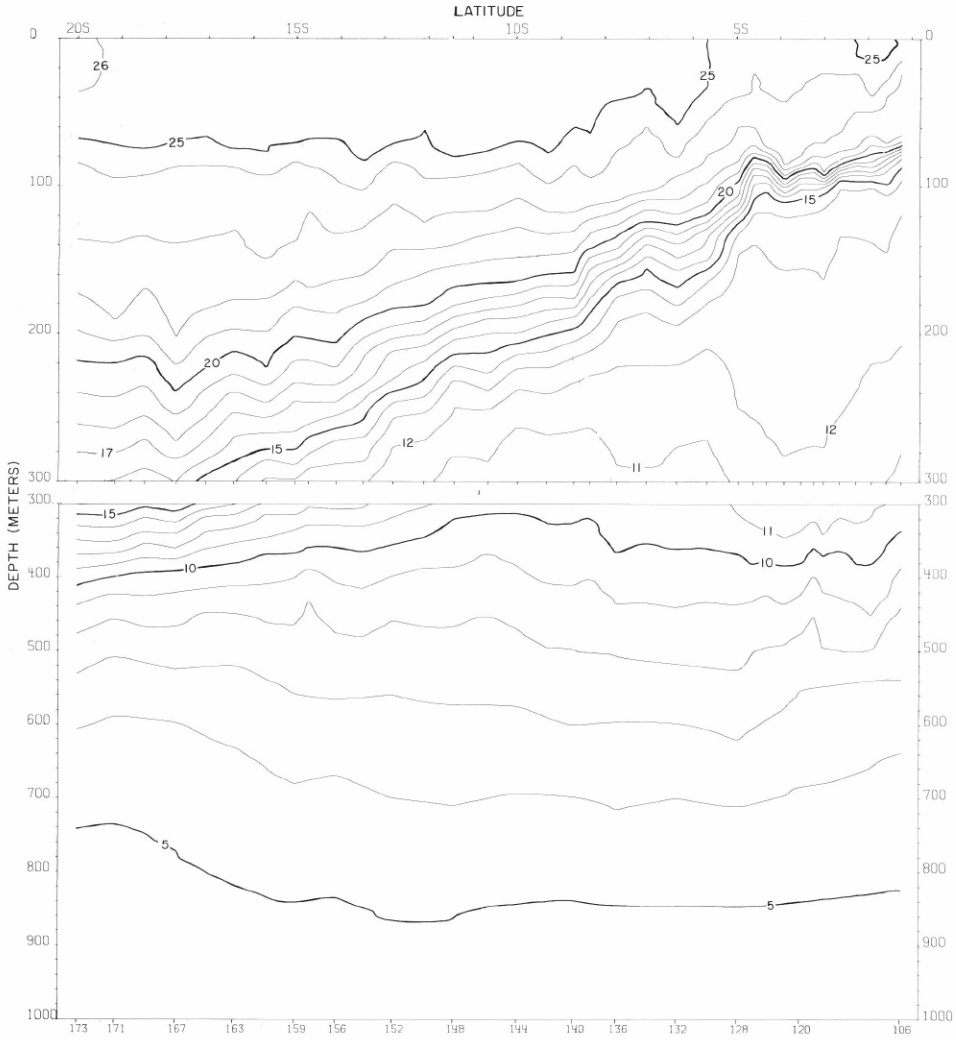

FIGURE 11-T-v2.—Vertical distribution of temperature (°C.) along 119° W. from 1°14′ S. to 20°00′ S., February 7-14, 1967.

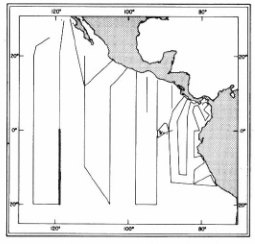

11-T-v2.

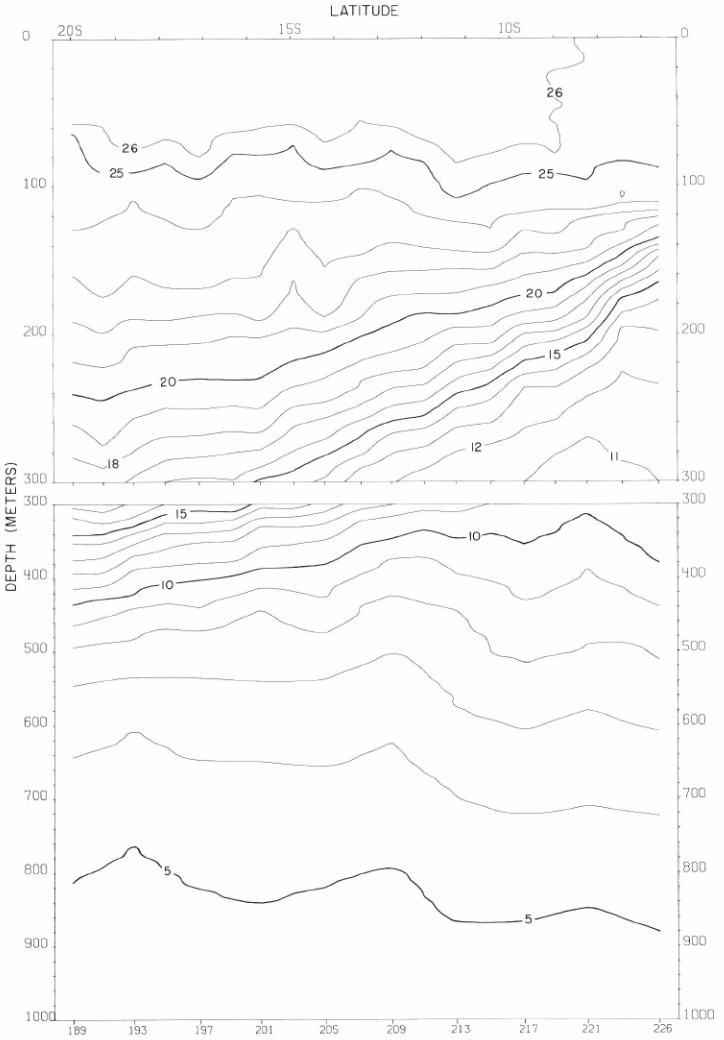

FIGURE 11-T-v4.—Vertical distribution of temperature (°C.) along 126° W. from 19°59′ S. to 6°38′ S., February 16-21, 1967.

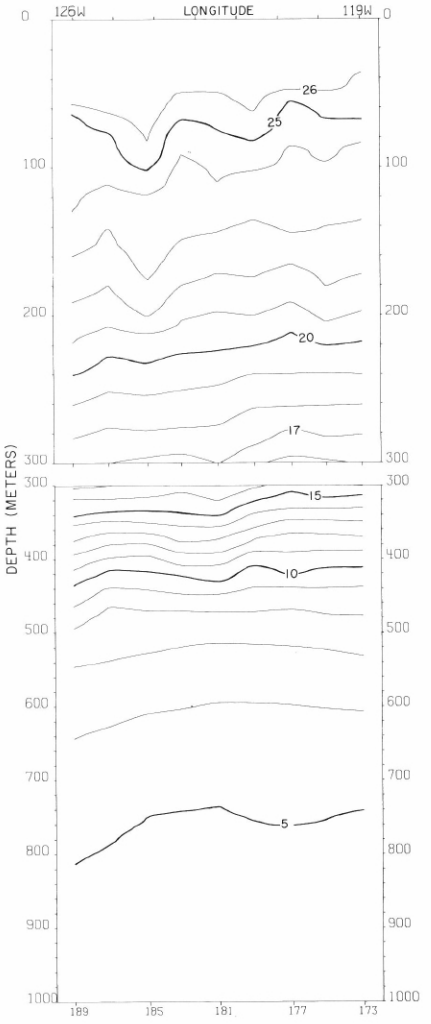

FIGURE 11-T-v3.—Vertical distribution of temperature (°C.) along 20° S., February 14-16, 1967.

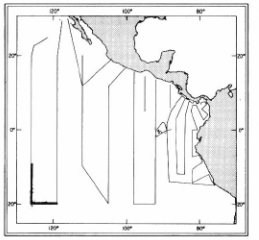

11-T-v3.

11-T-v4.

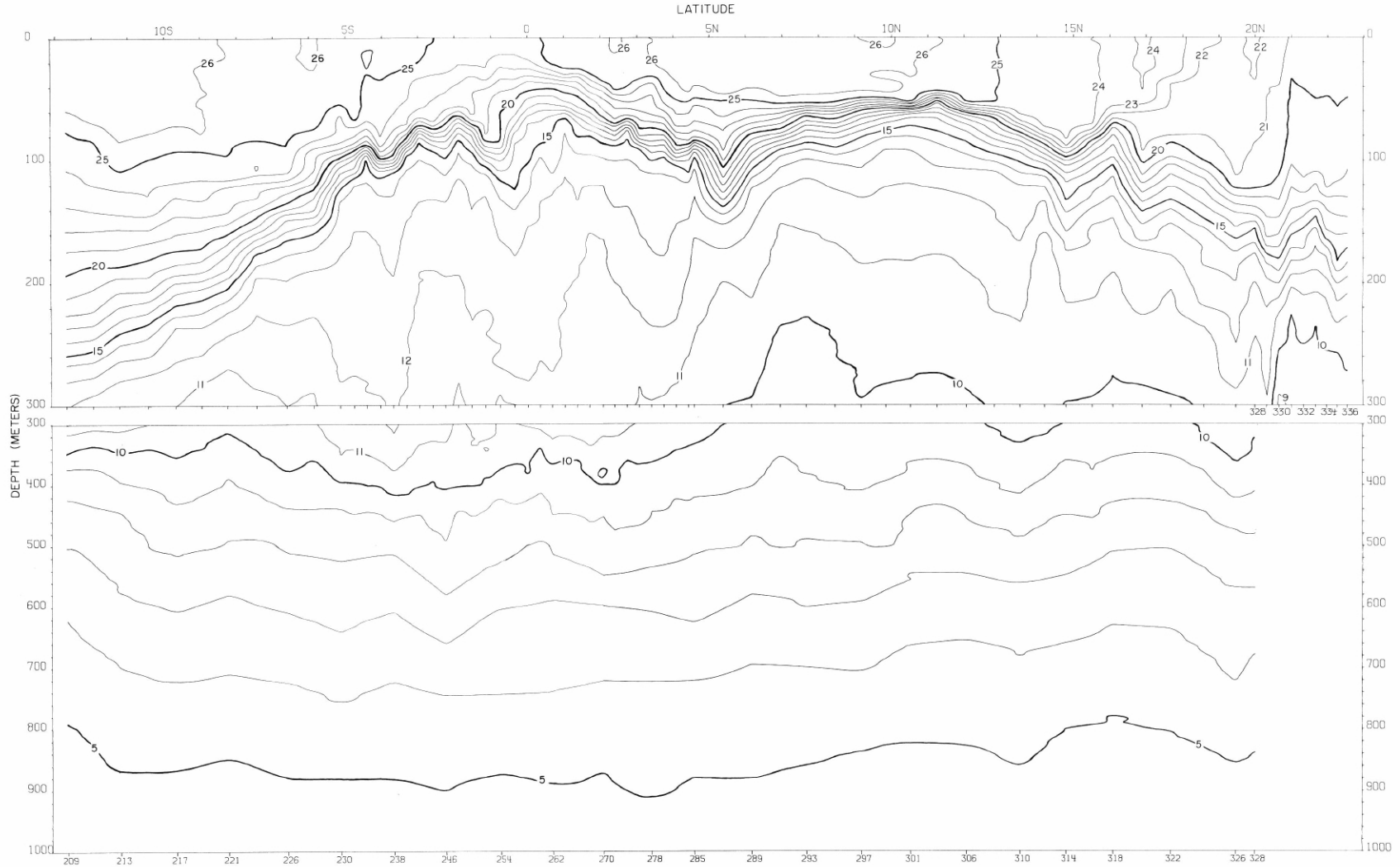

FIGURE 11-T-v5.—Vertical distribution of temperature (°C.) along 126° W. from 12°42′ S. to 22°33′ N., February 19-March 3, 1967.

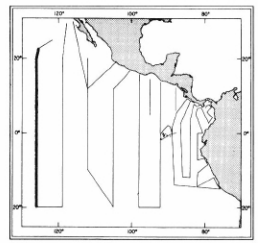

11-T-v5.

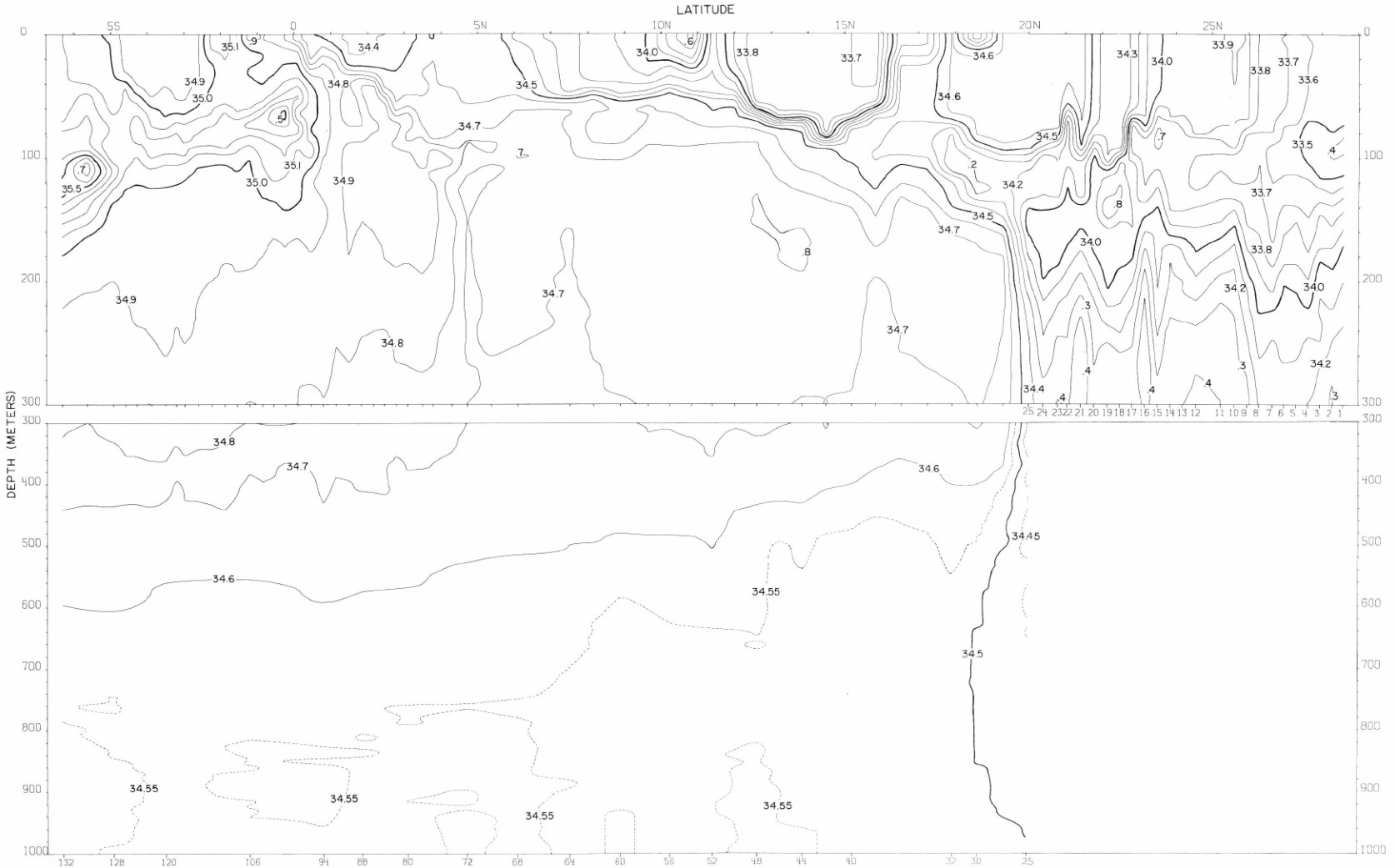

FIGURE 11-S-v1.—Vertical distribution of salinity (‰) along 119° W. from 28°36′ N. to 6°21′ S., January 25-February 9, 1967. The data from Stations 1-24 were not calibrated against Nansen cast data.

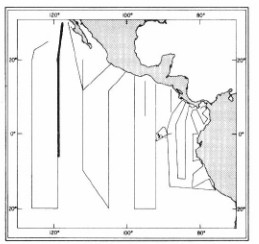

11-S-v1.

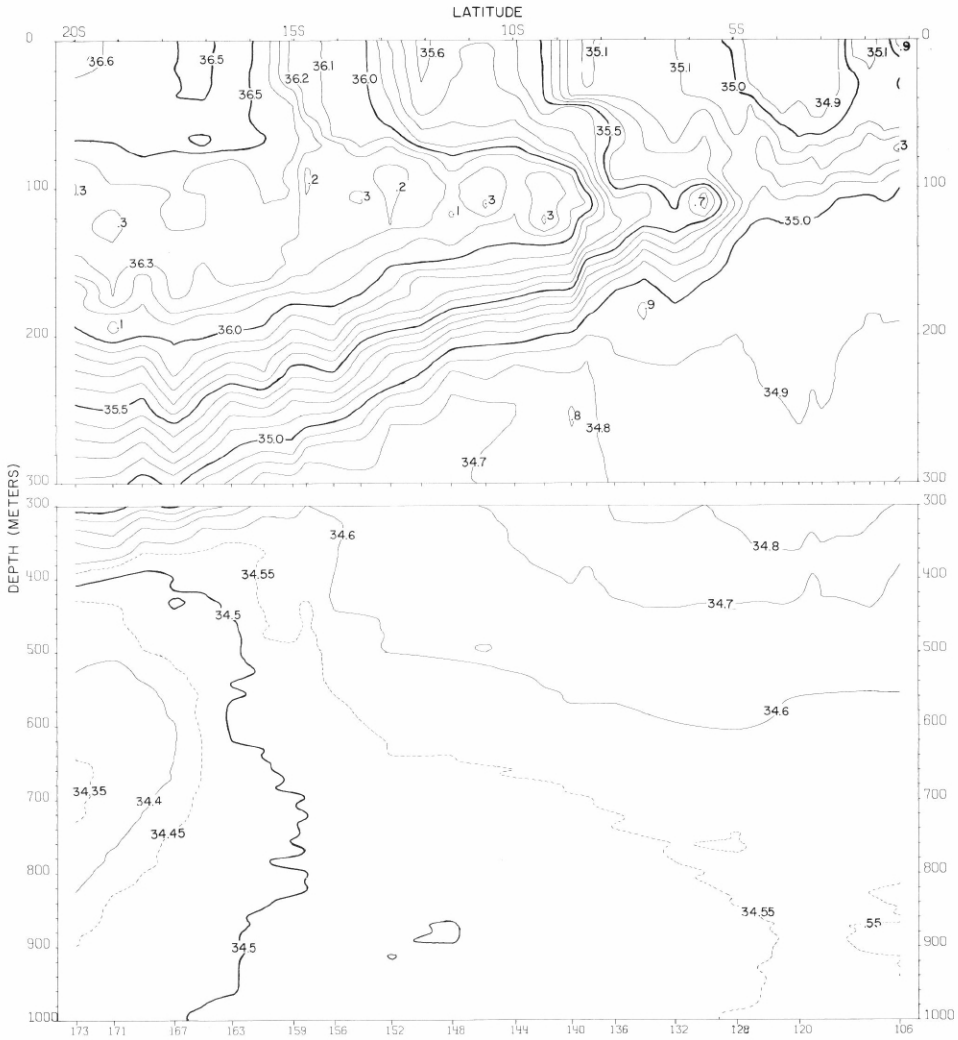

FIGURE 11-S-v2.—Vertical distribution of salinity (‰) along 119° W. from 1°14′ S. to 20°00′ S., February 7-14, 1967.

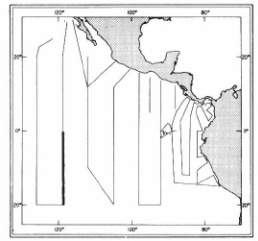

11-S-v2.

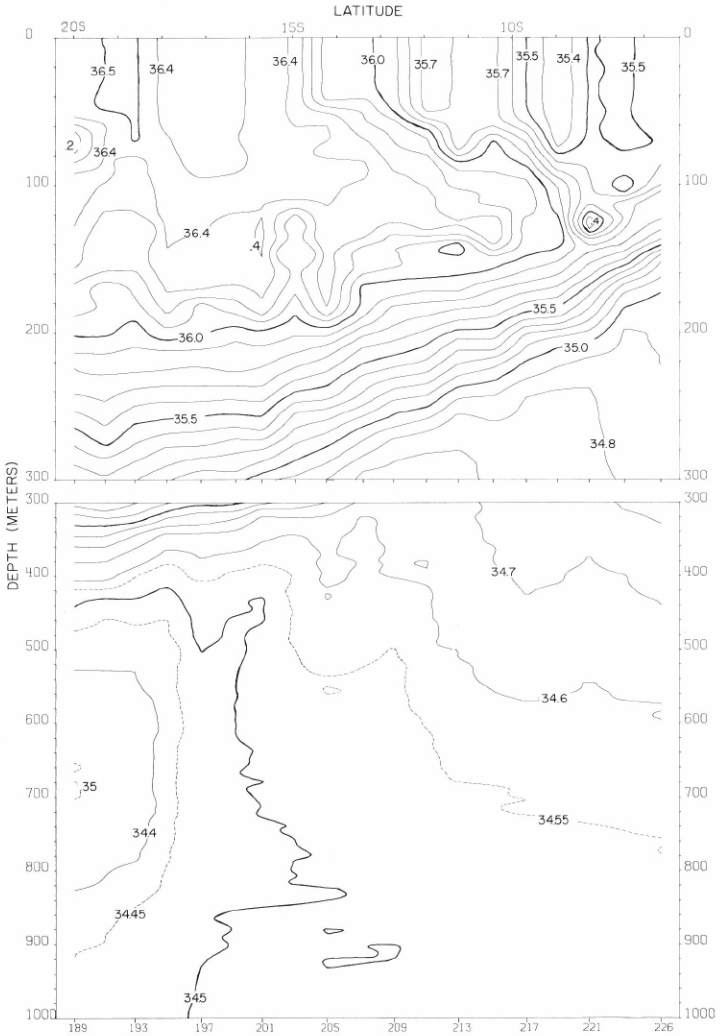

FIGURE 11-S-v4.—Vertical distribution of salinity (‰) along 126° W. from 19°59′ S. to 6°38′ S., February 16-21, 1967.

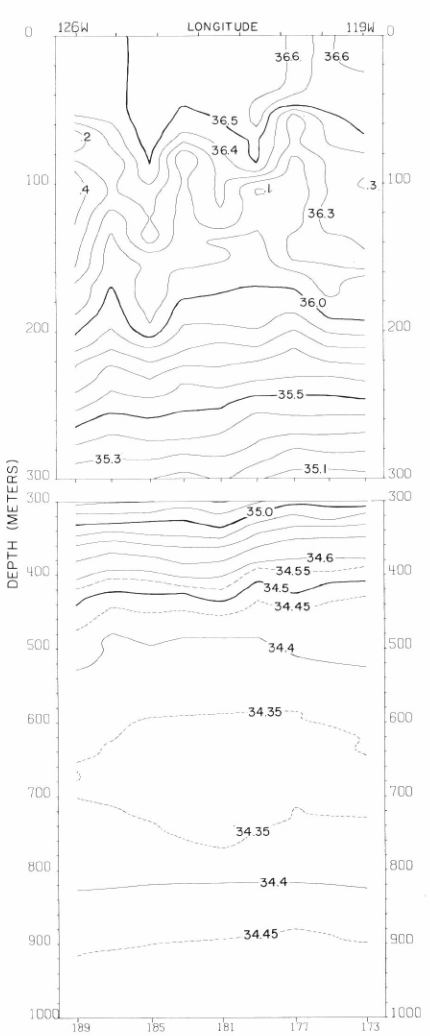

FIGURE 11-S-v3.—Vertical distribution of salinity (‰) along 20° S., February 14-16, 1967.

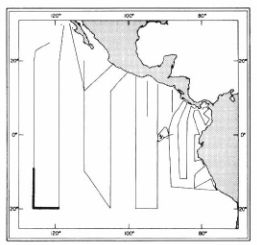

11-S-v3.

11-S-v4.

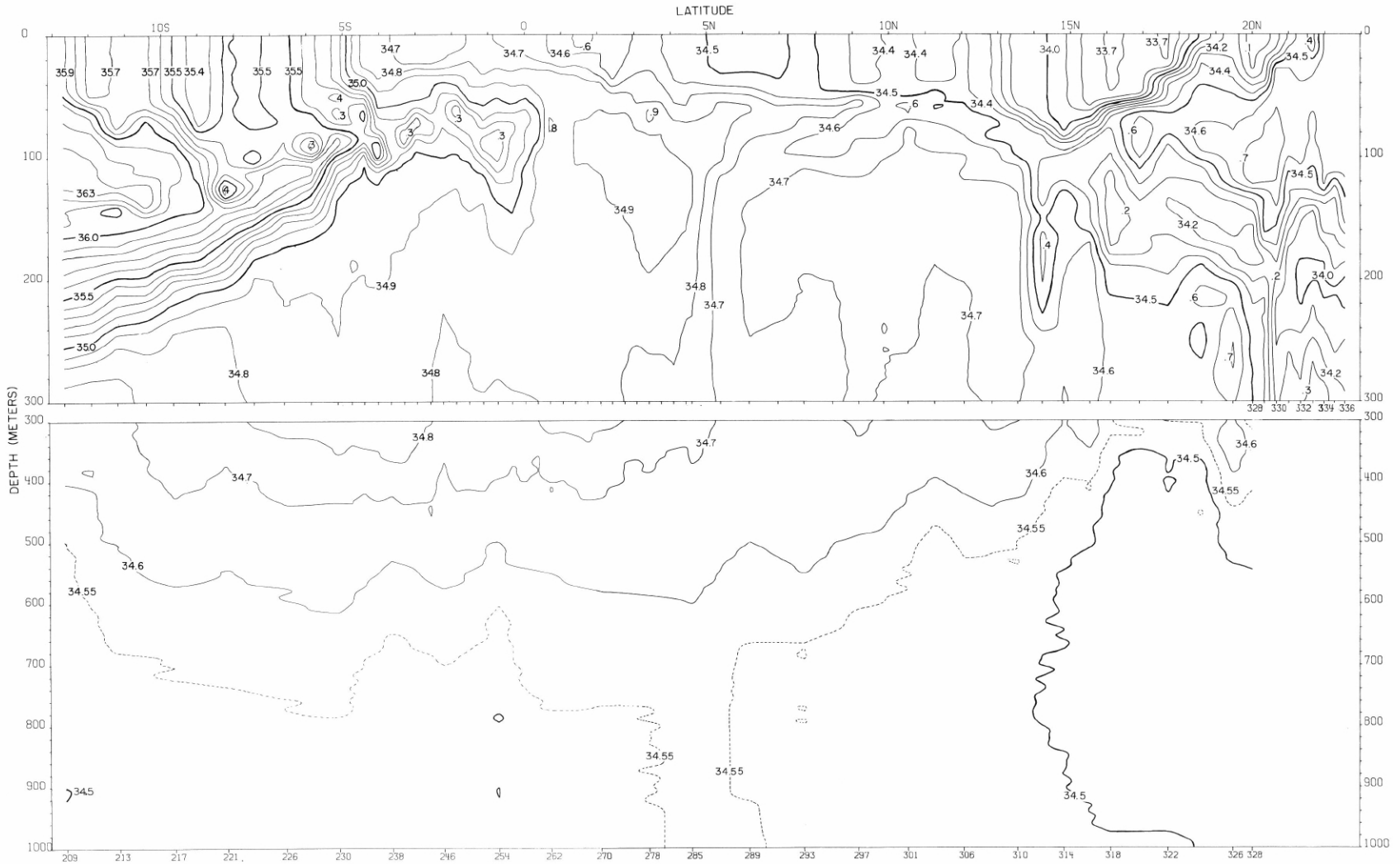

FIGURE 11-S-v5.—Vertical distribution of salinity (‰) along 126° W. from 12°42′ S. to 22°33′ N., February 19-March 3, 1967.

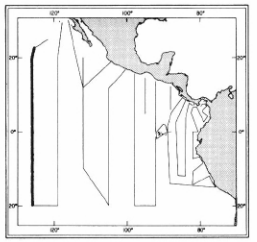

11-S-v5.

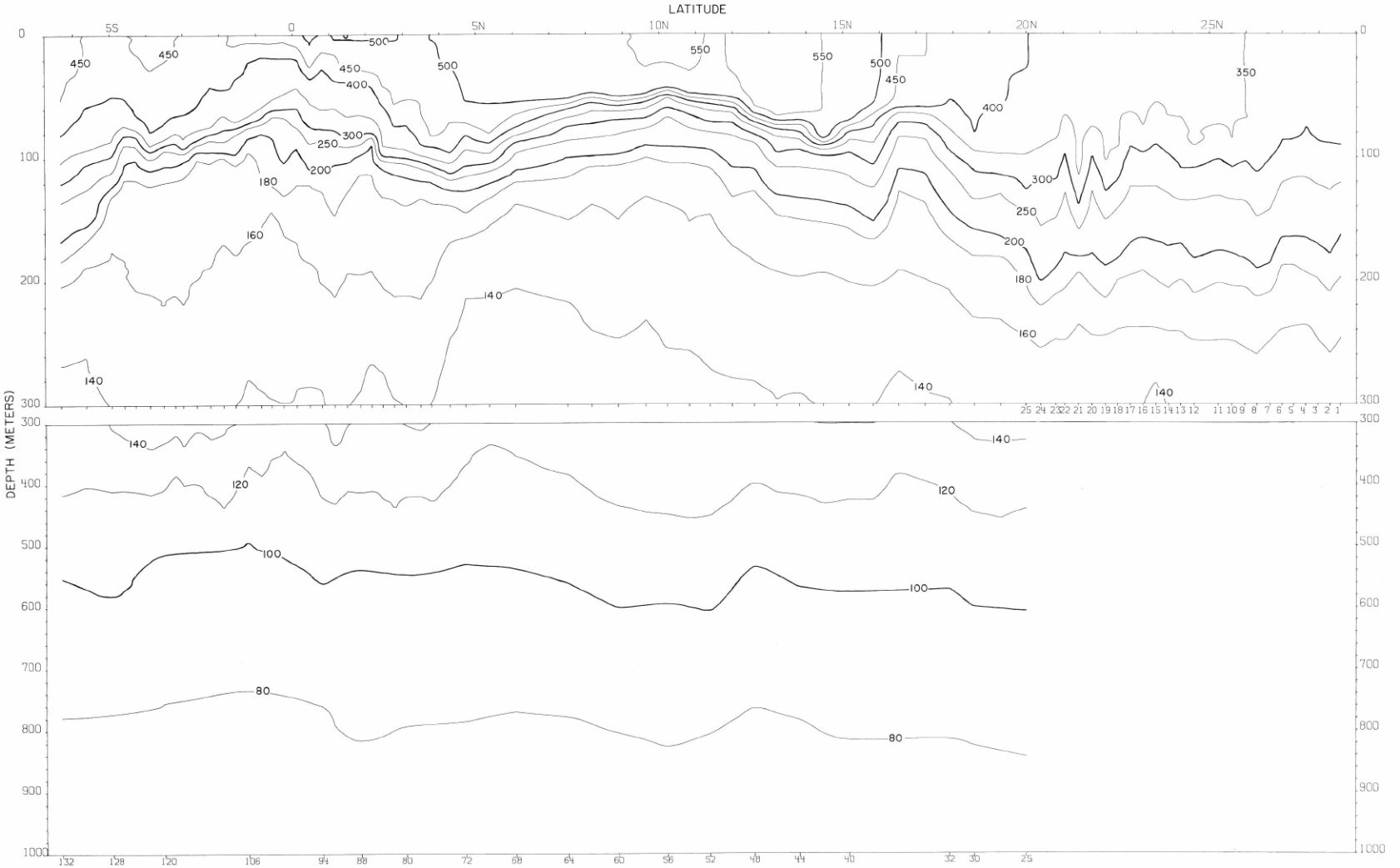

FIGURE 11-δ-v1.—Vertical distribution of thermosteric anomaly, δ_T, (cl./t.) along 119° W. from 28°36′ N. to 6°21′ S., January 25-February 9, 1967. The temperature and salinity data from Stations 1-24 were not calibrated against Nansen cast data.

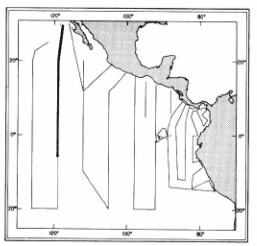

11-δ-v1.

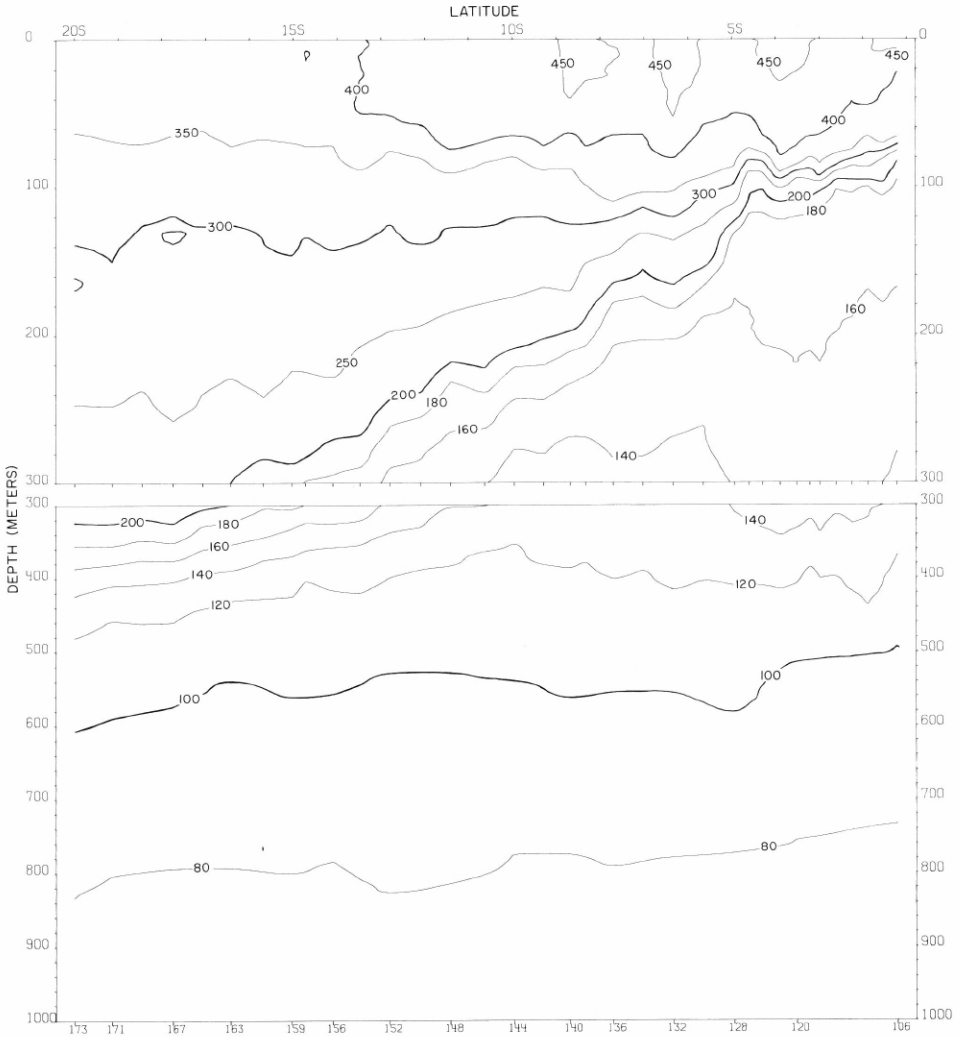

FIGURE 11-δ-v2.—Vertical distribution of thermosteric anomaly, δ_T, (cl./t.) along 119° W. from 1°14′ S. to 20°00′ S., February 7-14, 1967.

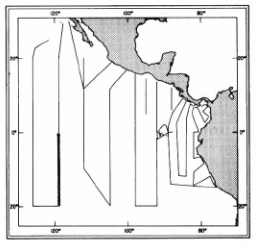

11-δ-v2.

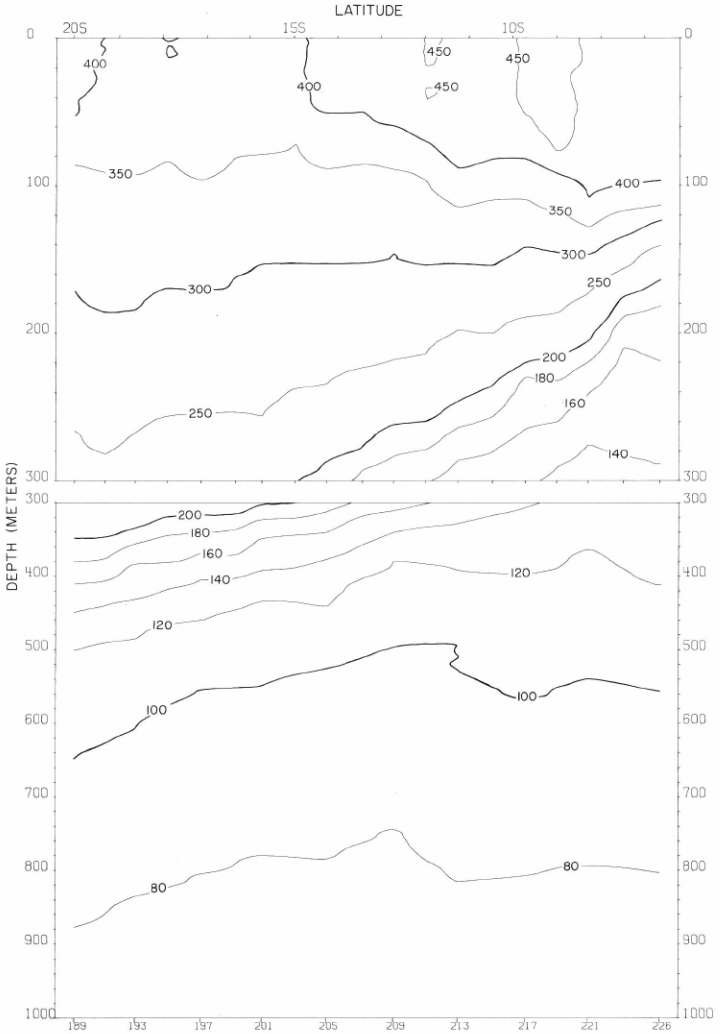

FIGURE 11-δ-v4.—Vertical distribution of thermosteric anomaly, δ_T, (cl./t.) along 126° W. from 19°59′ S. to 6°38′ S., February 16-21, 1967.

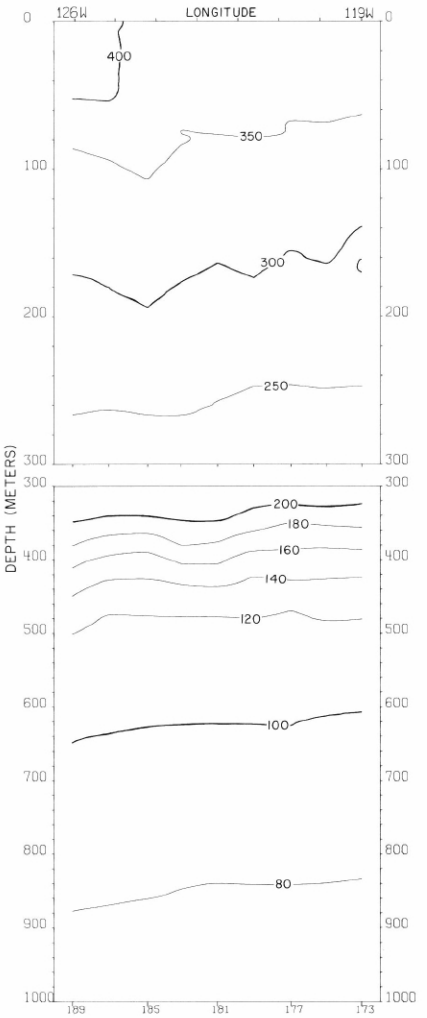

FIGURE 11-δ-v3.—Vertical distribution of thermosteric anomaly, δ_T, (cl./t.) along 20° S., February 14-16, 1967.

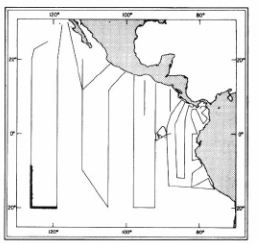

11-δ-v3.

11-δ-v4.

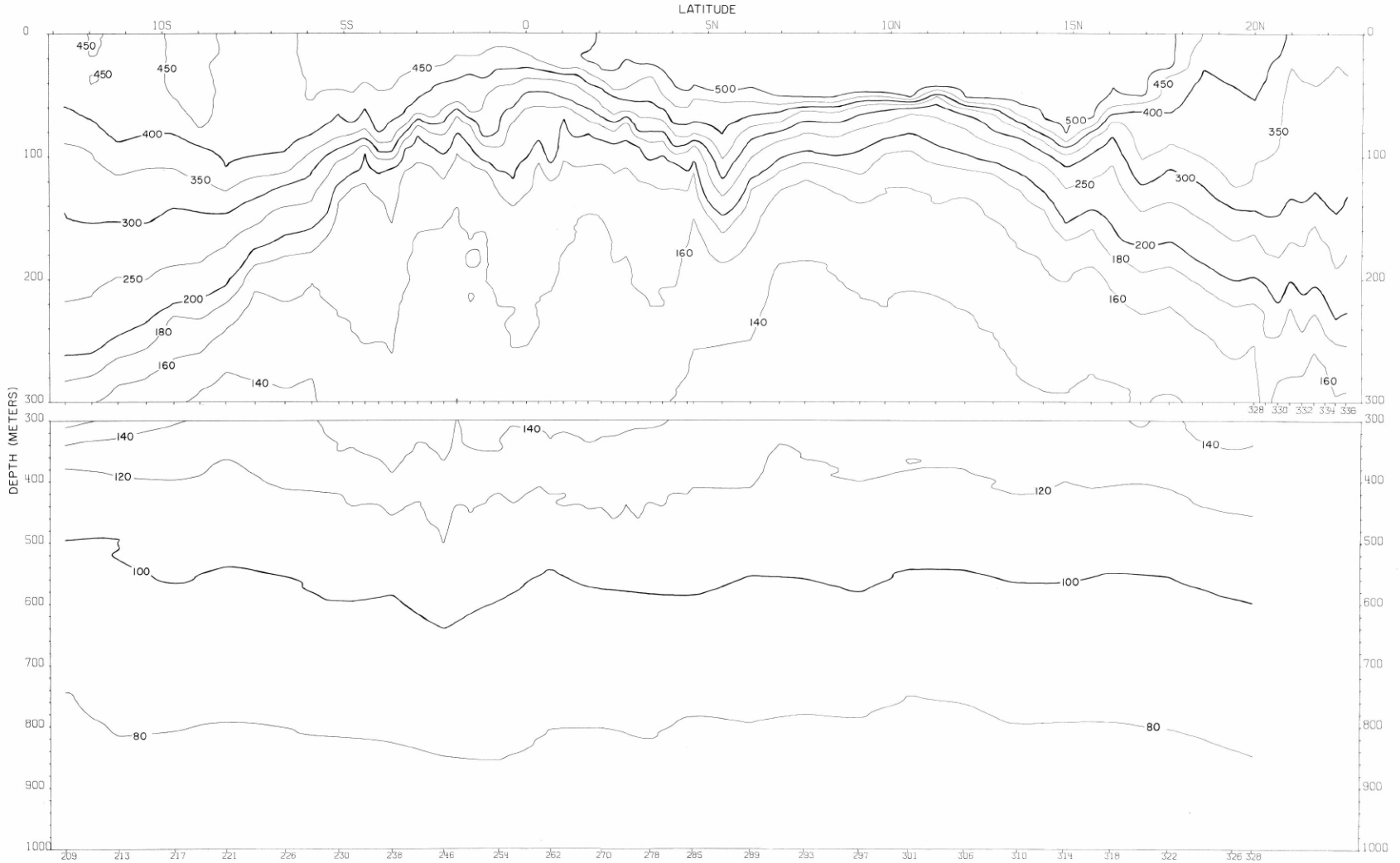

FIGURE 11-δ-v5.—Vertical distribution of thermosteric anomaly, δ_T, (cl./t.) along 126° W. from 12°42′ S. to 22°33′ N., February 19-March 3, 1967.

11-δ-v5.

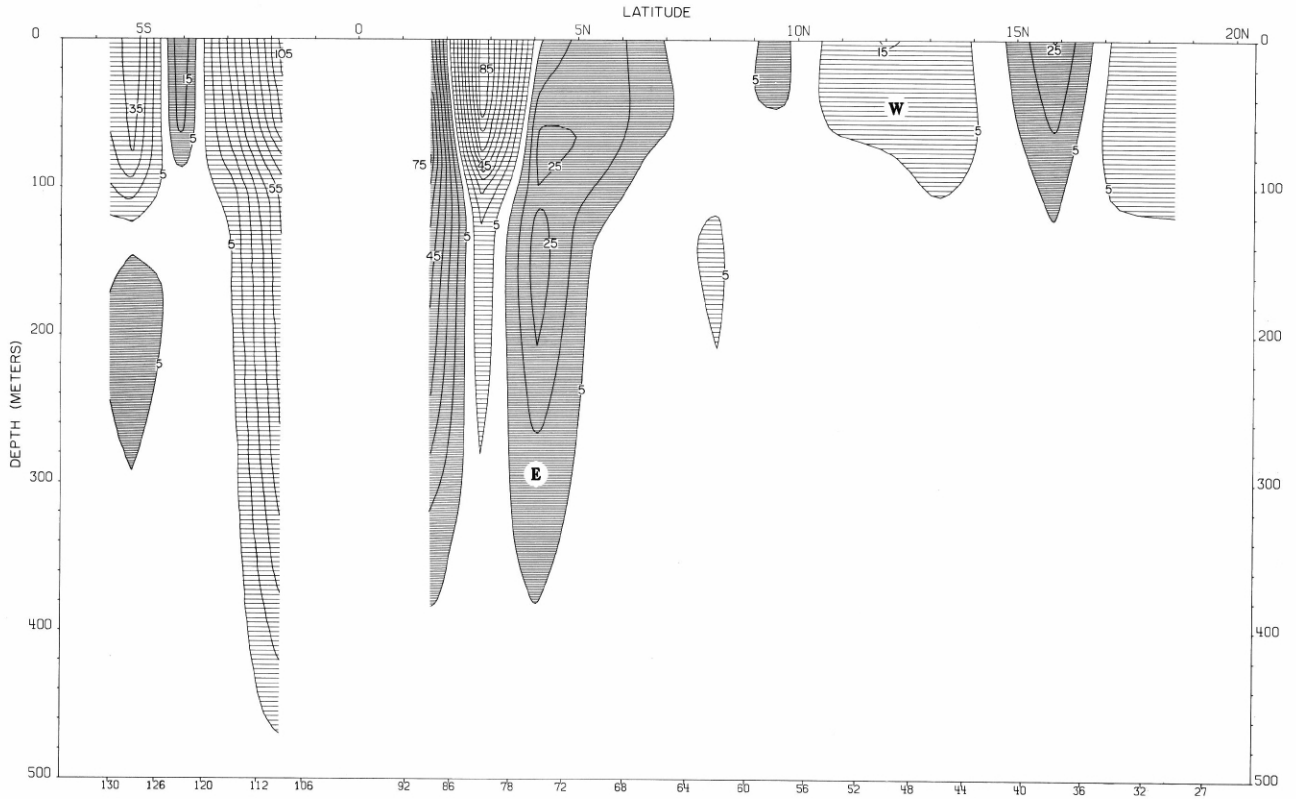

FIGURE 11-G-v1.—Vertical distribution of the zonal component of geostrophic velocity (cm./sec.), relative to 500 db., along 119° W. from 19°19′ N. to 5°40′ S., January 29-February 9, 1967. Dark shading indicates eastward flow with a velocity greater than 5 cm./sec.; light shading indicates westward flow with a velocity greater than 5 cm./sec.

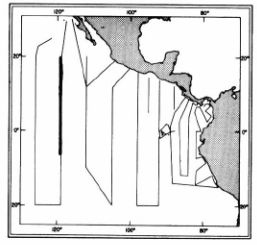

11-G-v1.

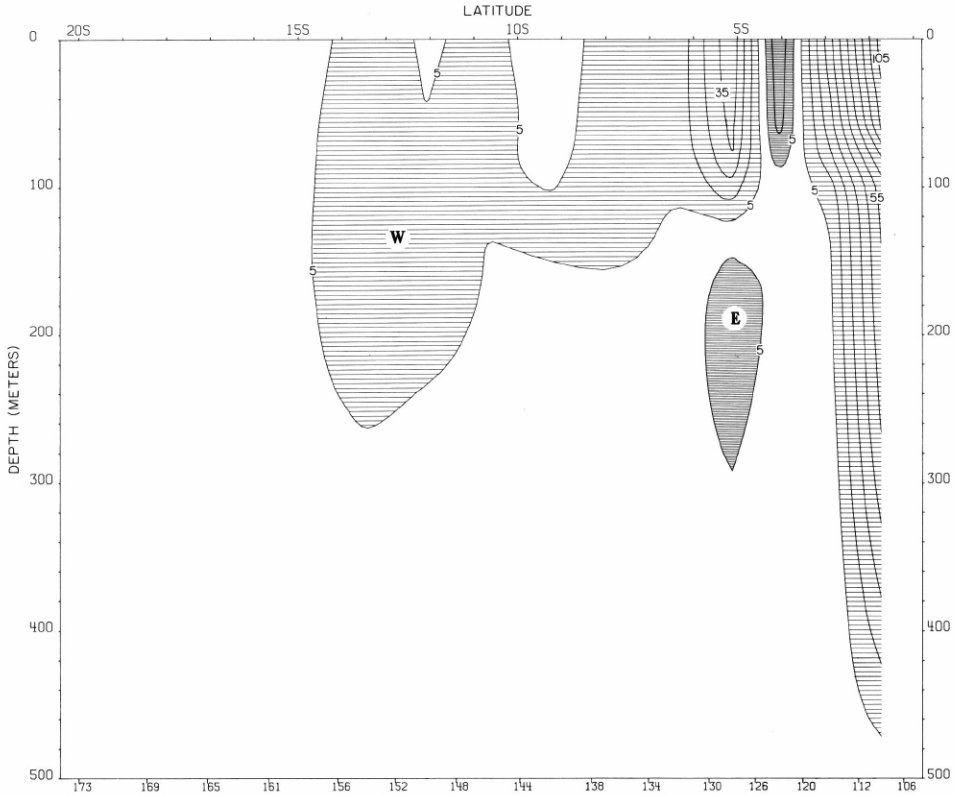

FIGURE 11-G-v2.—Vertical distribution of the zonal component of geostrophic velocity (cm./sec.), relative to 500 db., along 119° W. from 1°14′ S. to 20°00′ S., February 7-14, 1967. Dark shading indicates eastward flow with a velocity greater than 5 cm./sec.; light shading indicates westward flow with a velocity greater than 5 cm./sec.

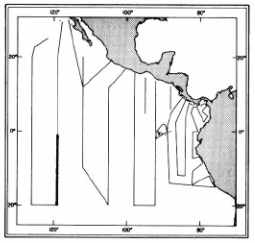

11-G-v2.

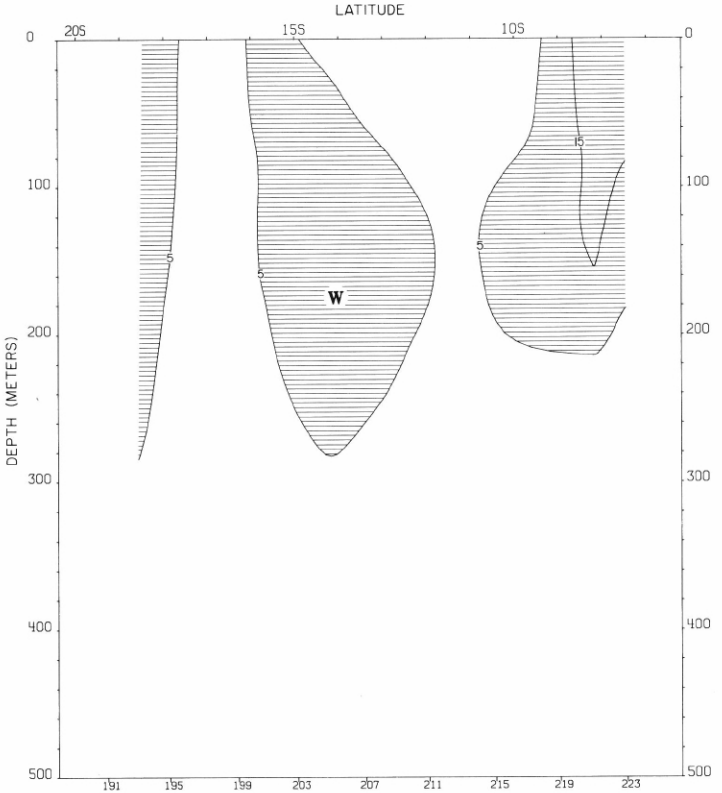

FIGURE 11-G-v4.—Vertical distribution of the zonal component of geostrophic velocity (cm./sec.), relative to 500 db., along 126° W. from 19°59′ S. to 6°38′ S., February 16-21, 1967. Dark shading indicates eastward flow with a velocity greater than 5 cm./sec.; light shading indicates westward flow with a velocity greater than 5 cm./sec.

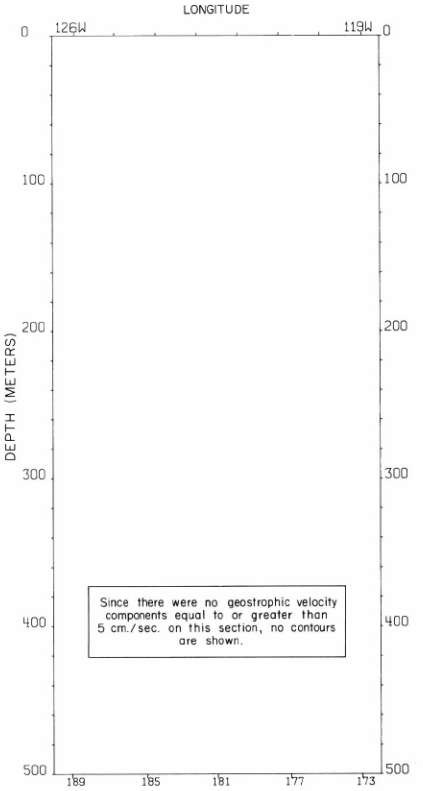

FIGURE 11-G-v3.—Vertical distribution of the meridional component of geostrophic velocity (cm./sec.), relative to 500 db., along 20° S., February 14-16, 1967. Since there were no geostrophic velocity components equal to or greater than 5 cm./sec. on this section, no contours are shown.

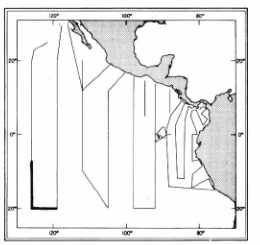

11-G-v3.

11-G-v4.

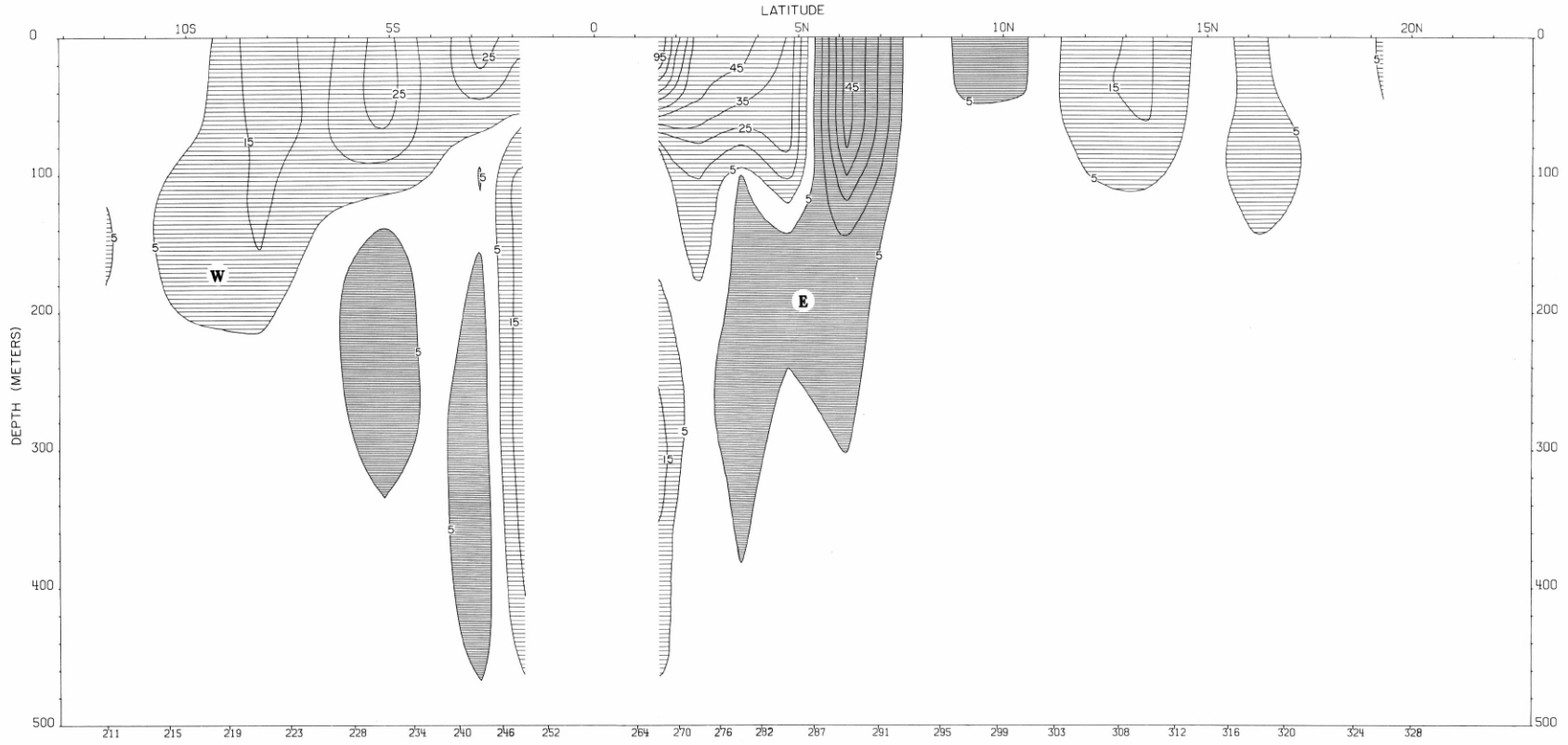

FIGURE 11-G-v5.—Vertical distribution of the zonal component of geostrophic velocity (cm./sec.), relative to 500 db., along 126° W. from 11°57′ S. to 20°01′ N., February 19-March 2, 1967. Dark shading indicates eastward flow with a velocity greater than 5 cm./sec.; light shading indicates westward flow with a velocity greater than 5 cm./sec.

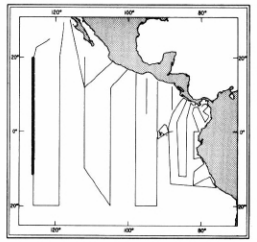

11-G-v5.

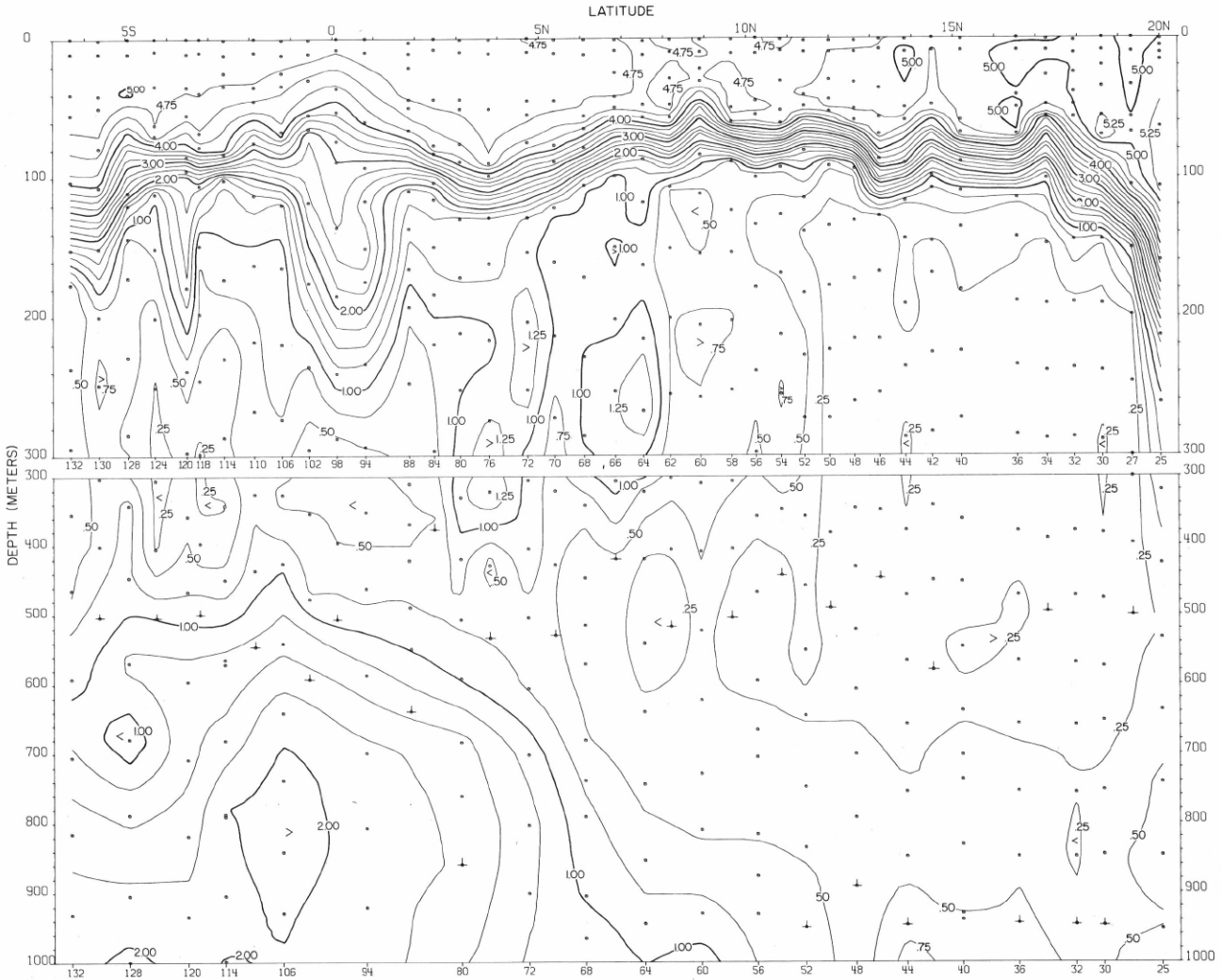

FIGURE 11-O2-v1.—Vertical distribution of oxygen (ml./l.) along 119° W. from 20°00′ N. to 6°21′ S., January 28-February 9, 1967.

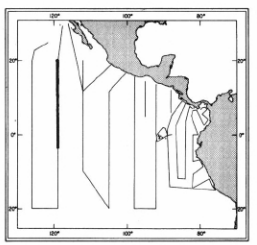

11-O2-v1.

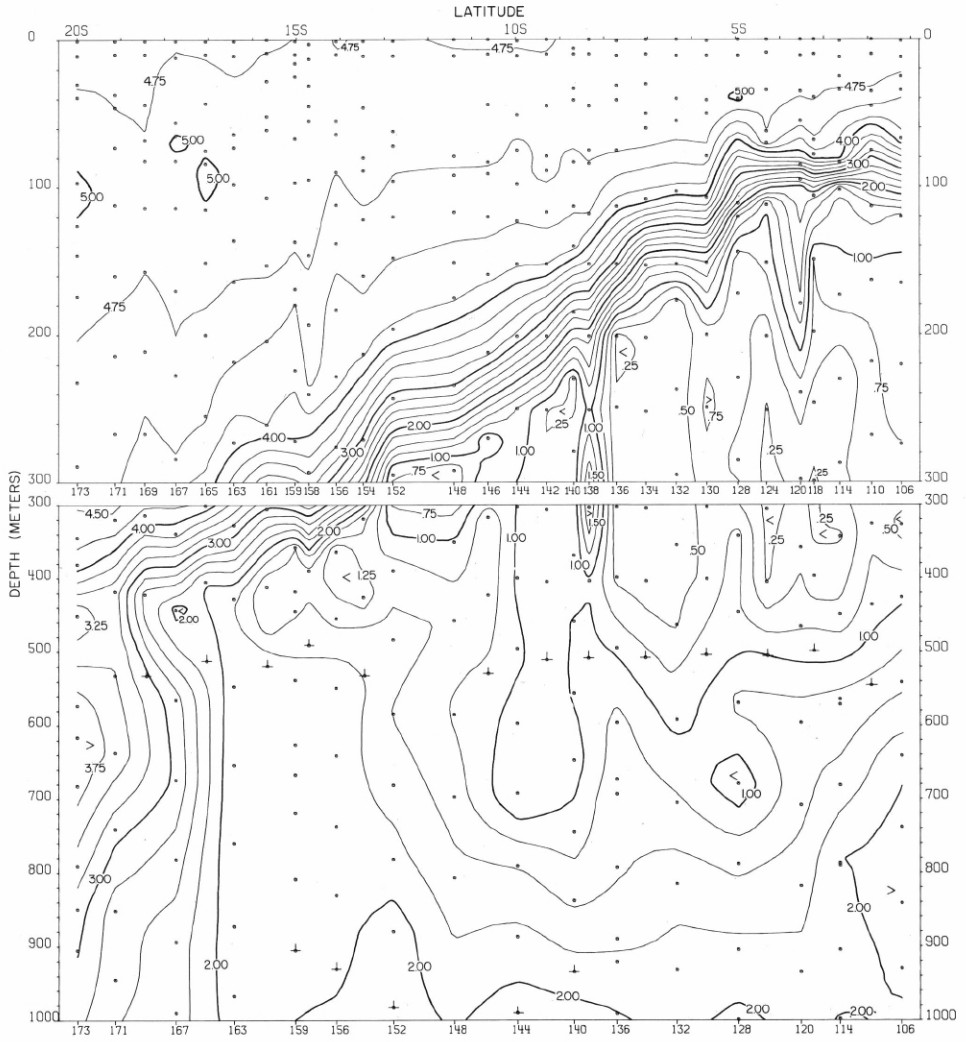

FIGURE 11-O2-v2.—Vertical distribution of oxygen (ml./l.) along 119° W. from 1°14′ S. to 20°00′ S., February 7-14, 1967.

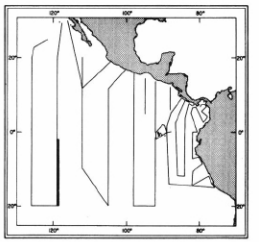

11-O2-v2.

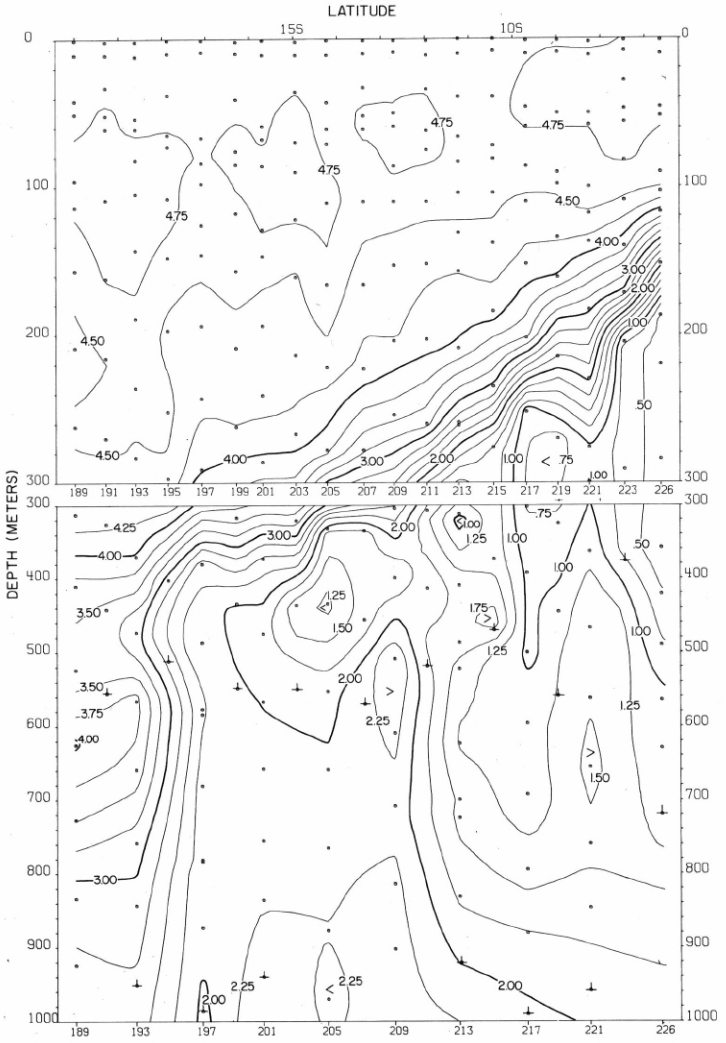

FIGURE 11-O2-v4.—Vertical distribution of oxygen (ml./l.) along 126° W. from 19°59′ S. to 6°38′ S., February 16-21, 1967.

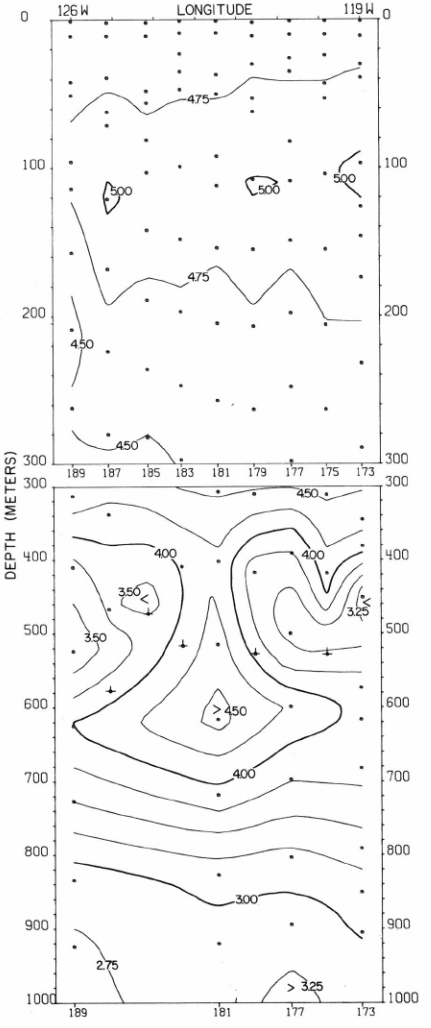

FIGURE 11-O2-v3.—Vertical distribution of oxygen (ml./l.) along 20° S., February 14-16, 1967.

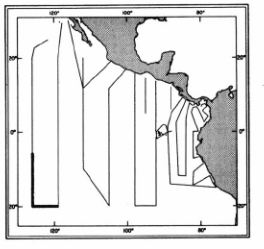

11-O2-v3.

11-O2-v4.

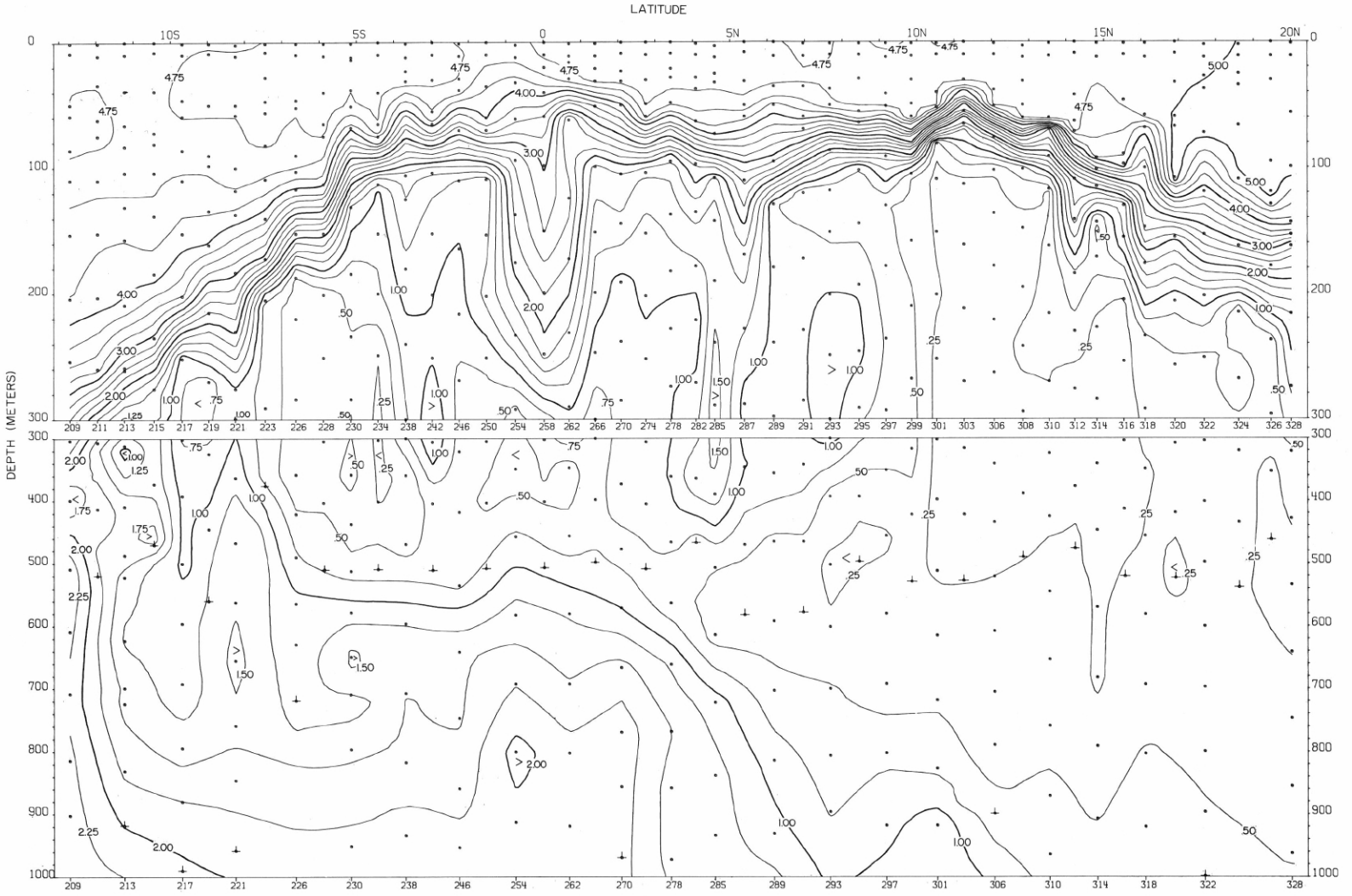

FIGURE 11-O_2-v5.—Vertical distribution of oxygen (ml./l.) along 126° W. from 12°42′ S. to 20°01′ N., February 19-March 2, 1967.

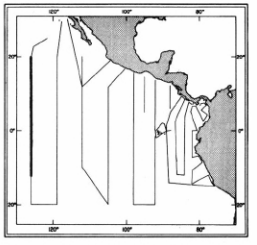

11-O_2-v5.

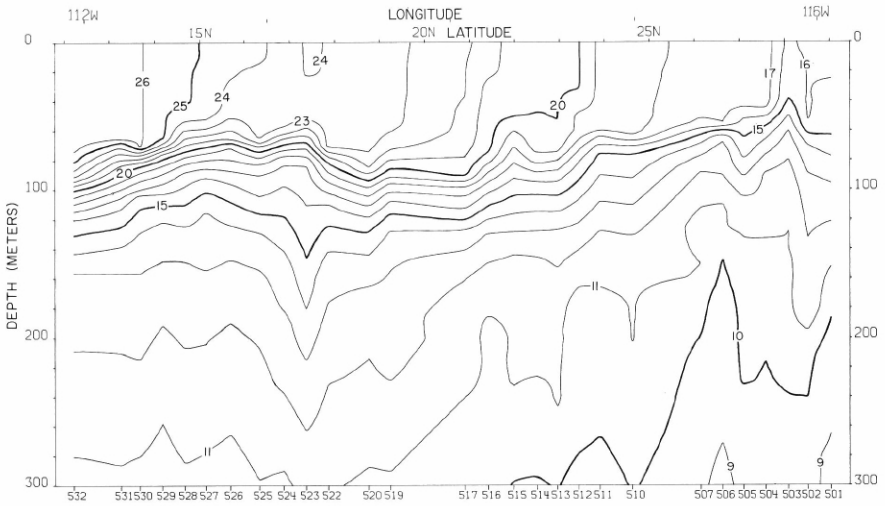

FIGURE 12-T-v1.—Vertical distribution of temperature (°C.) along a section from 29° N. near the coast of Baja California to 12° N., 112° W., February 8-12, 1967. These data were not calibrated against Nansen cast data.

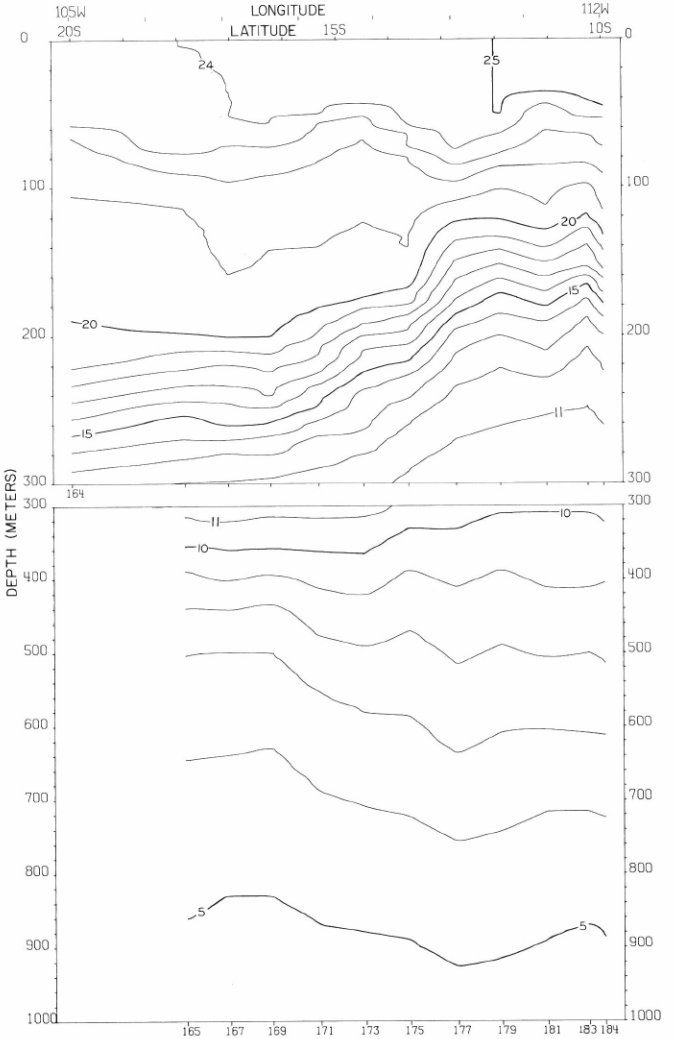

FIGURE 12-T-v5.—Vertical distribution of temperature (°C.) along a southeast-northwest section from 20° S., 105° W. to 10° S., 112° W., March 6-9, 1967.

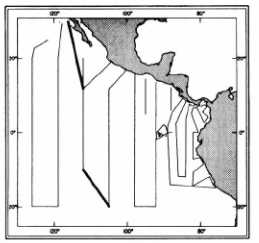

12-T-v1.

12-T-v5.

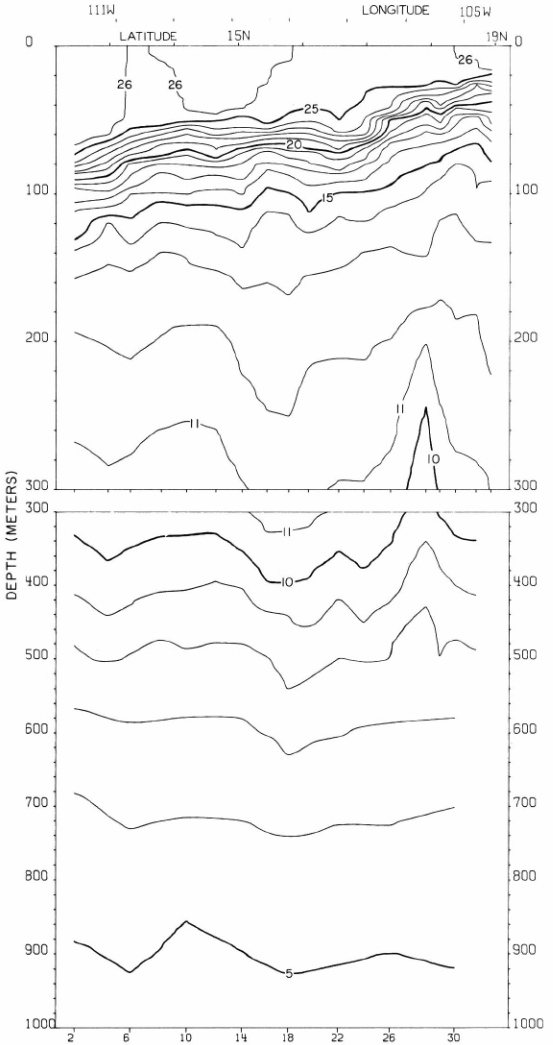

FIGURE 12-T-v2.—Vertical distribution of temperature (°C.) along a section from 12° N., 112° W. to Manzanillo, February 12-16, 1967.

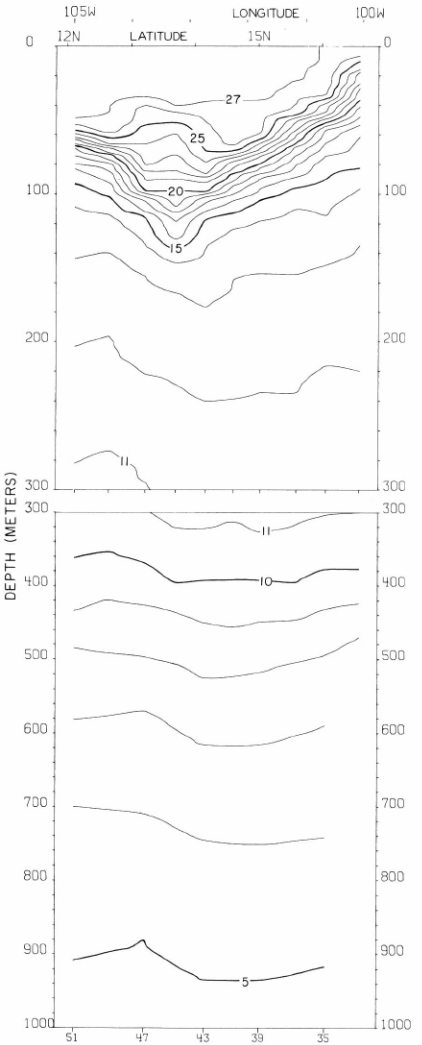

FIGURE 12-T-v3.—Vertical distribution of temperature (°C.) along a section from Acapulco to 12° N., 105° W., February 19-21, 1967.

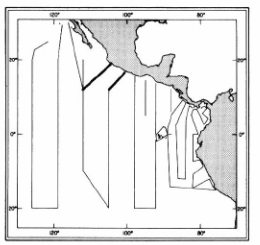

12-T-v2.

12-T-v3.

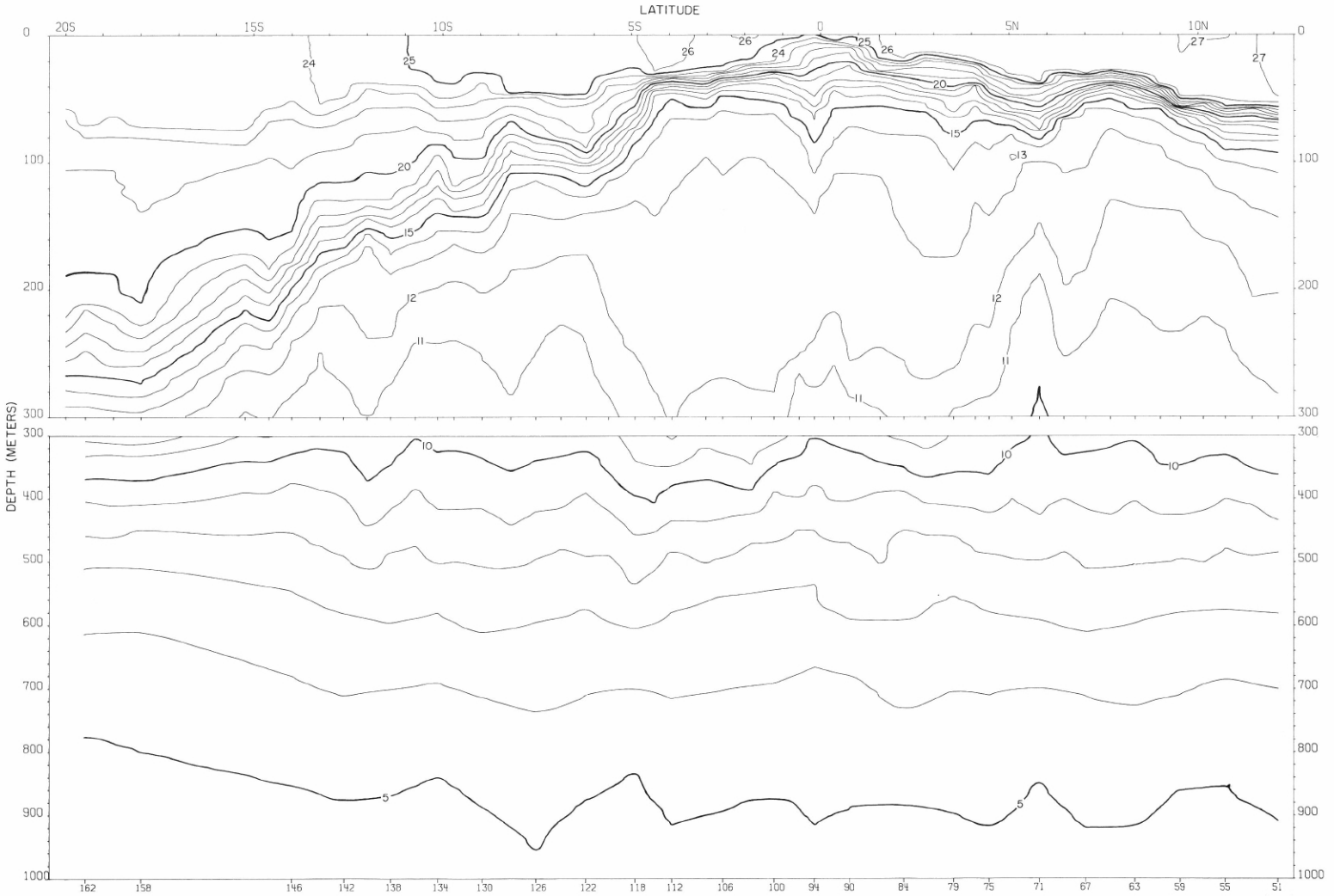

FIGURE 12-T-v4. — Vertical distribution of temperature (°C.) along 105° W., February 21-March 6, 1967.

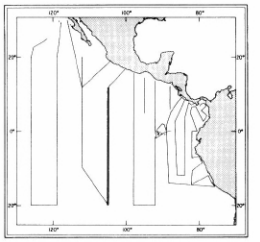

12-T-v4.

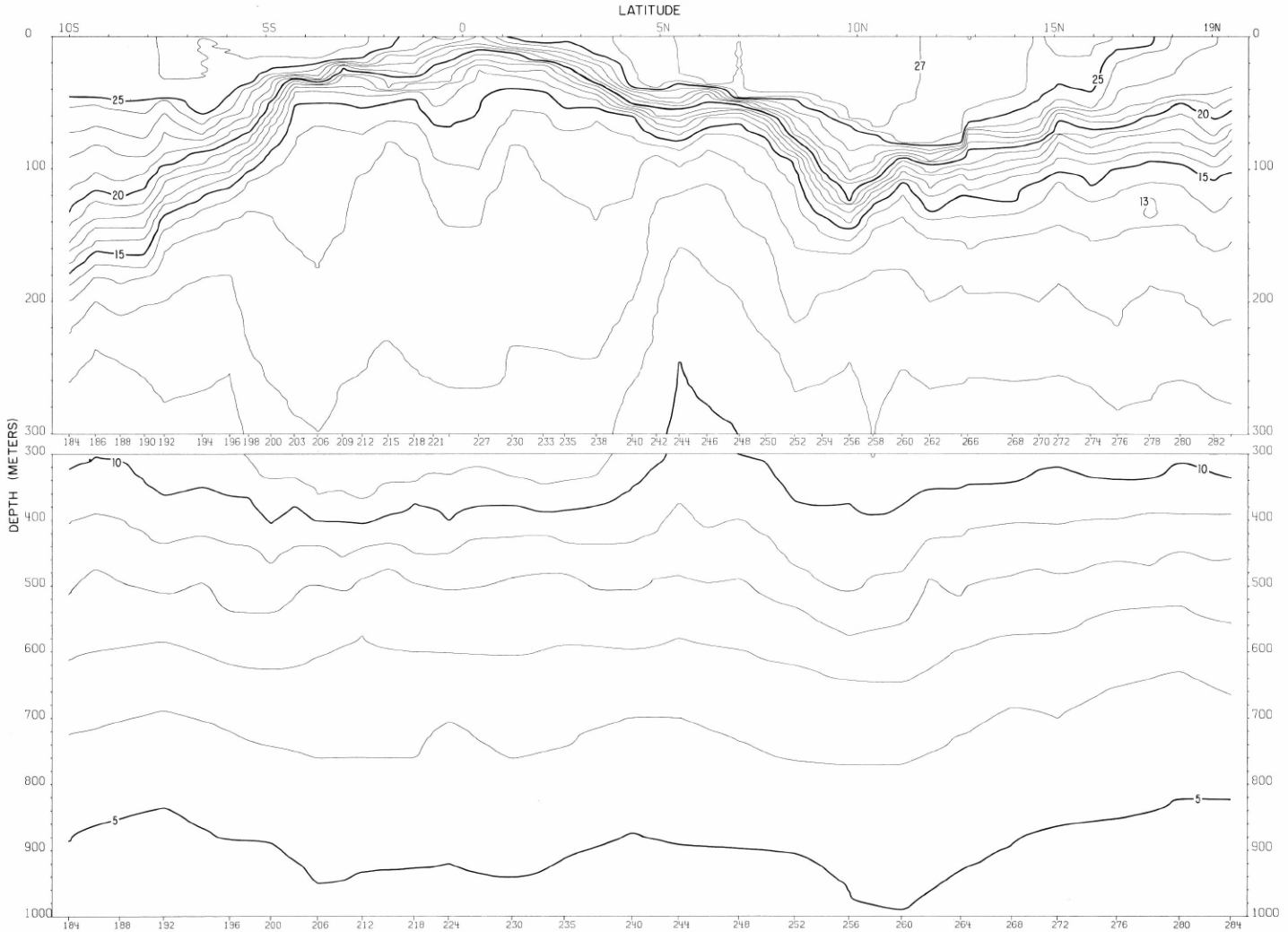

FIGURE 12-T-v6. — Vertical distribution of temperature (°C.) along 112° W., March 9-21, 1967.

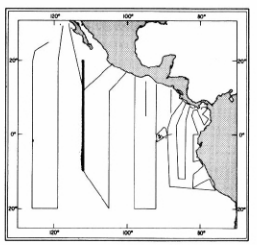

12-T-v6.

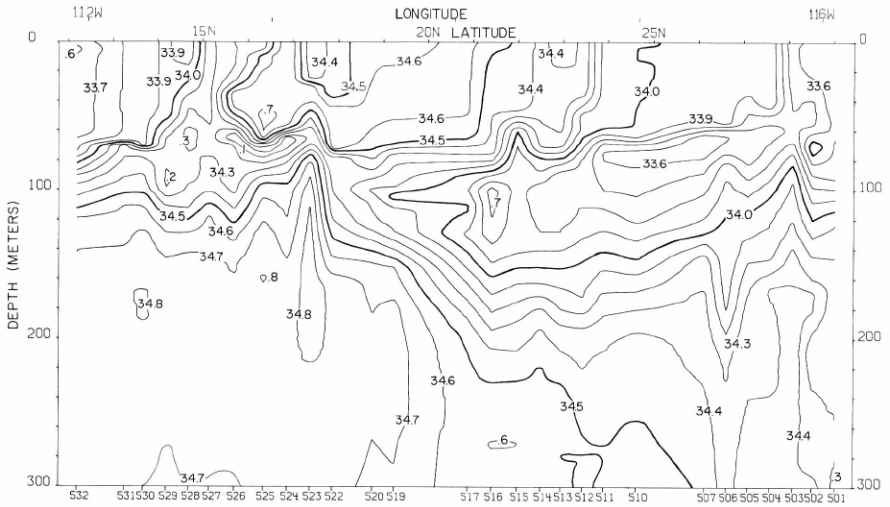

FIGURE 12-S-v1.—Vertical distribution of salinity (‰) along a section from 29° N. near the coast of Baja California to 12° N., 112° W., February 8-12, 1967. These data were not calibrated against Nansen cast data.

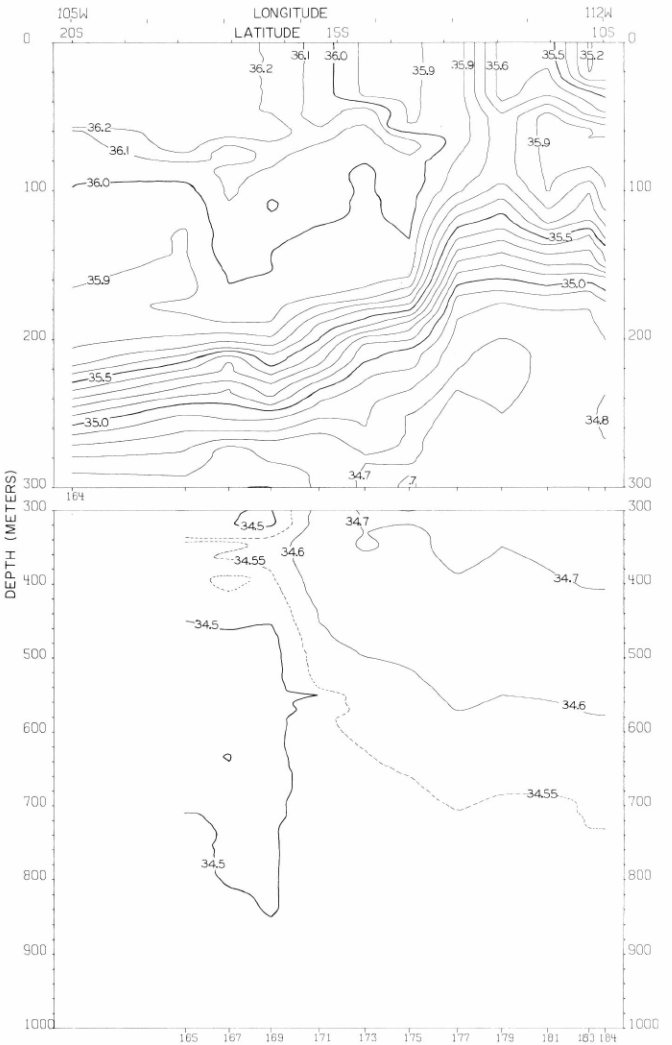

FIGURE 12-S-v5.—Vertical distribution of salinity (‰) along a southeast-northwest section from 20° S., 105° W. to 10° S., 112° W., March 6-9, 1967.

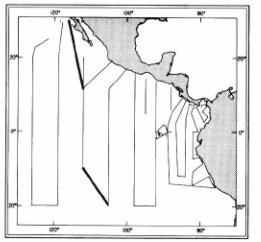

12-S-v1.

12-S-v5.

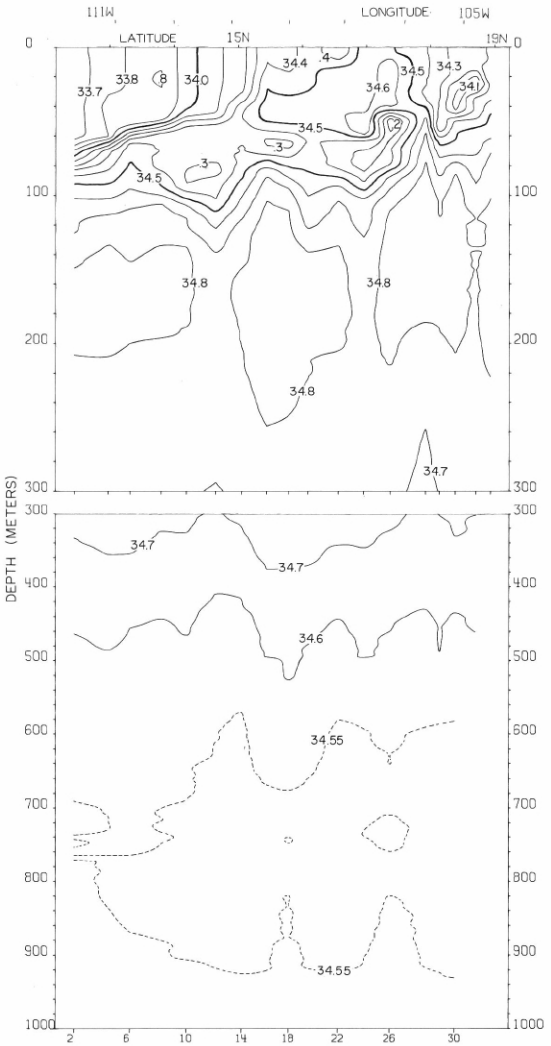

FIGURE 12-S-v2.—Vertical distribution of salinity (‰) along a section from 12° N., 112° W. to Manzanillo, February 12-16, 1967.

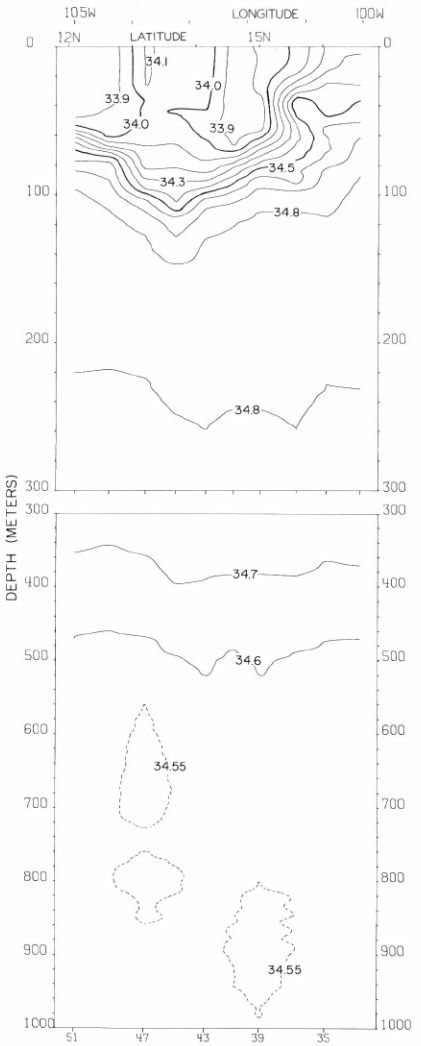

FIGURE 12-S-v3.—Vertical distribution of salinity (‰) along a section from Acapulco to 12° N., 105° W., February 19-21, 1967.

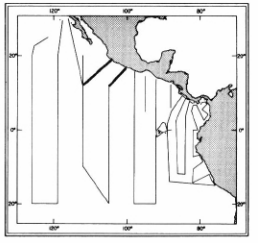

12-S-v2.

12-S-v3.

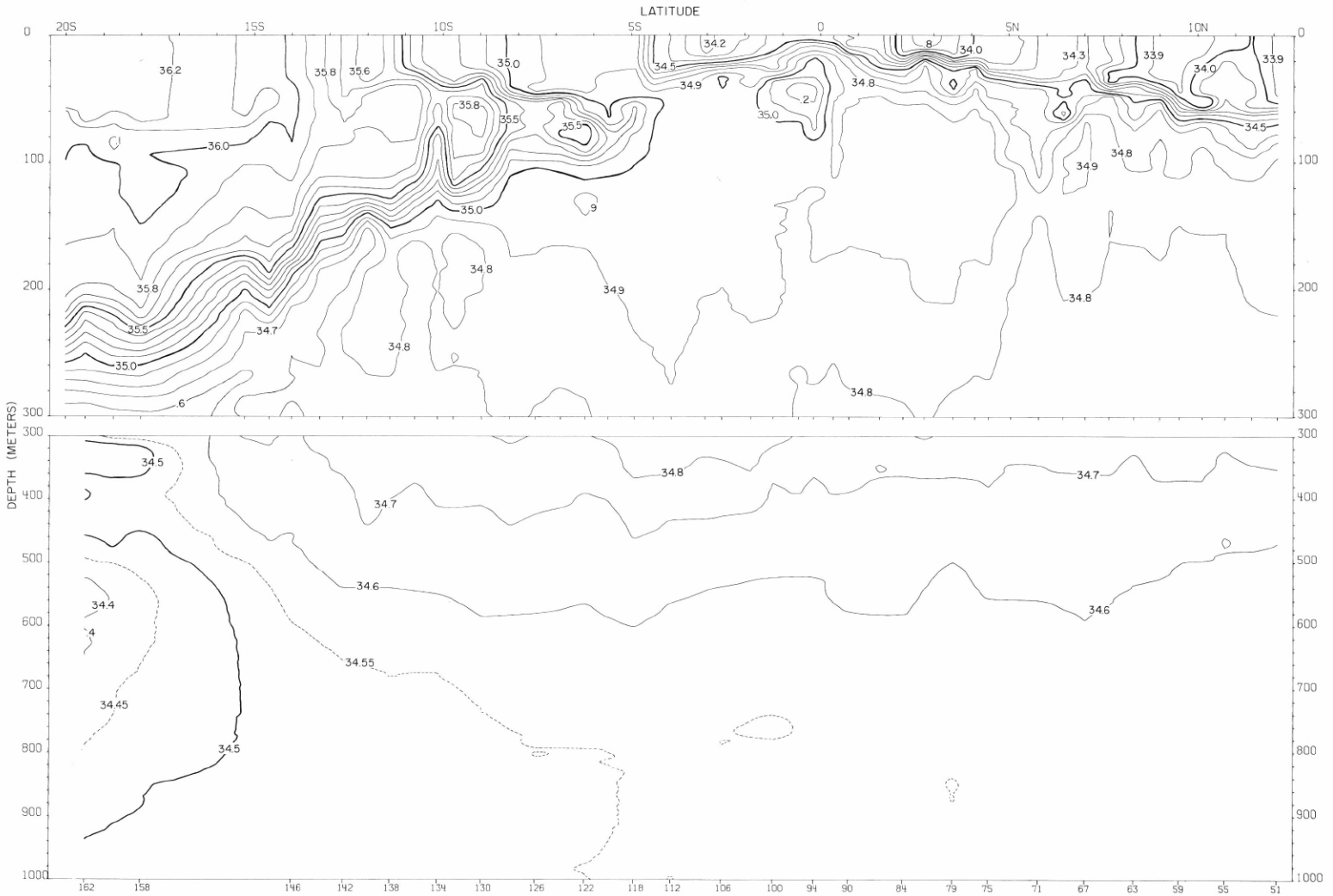

FIGURE 12-S-v4.—Vertical distribution of salinity (‰) along 105° W., February 21-March 6, 1967.

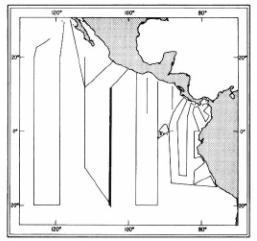

12-S-v4.

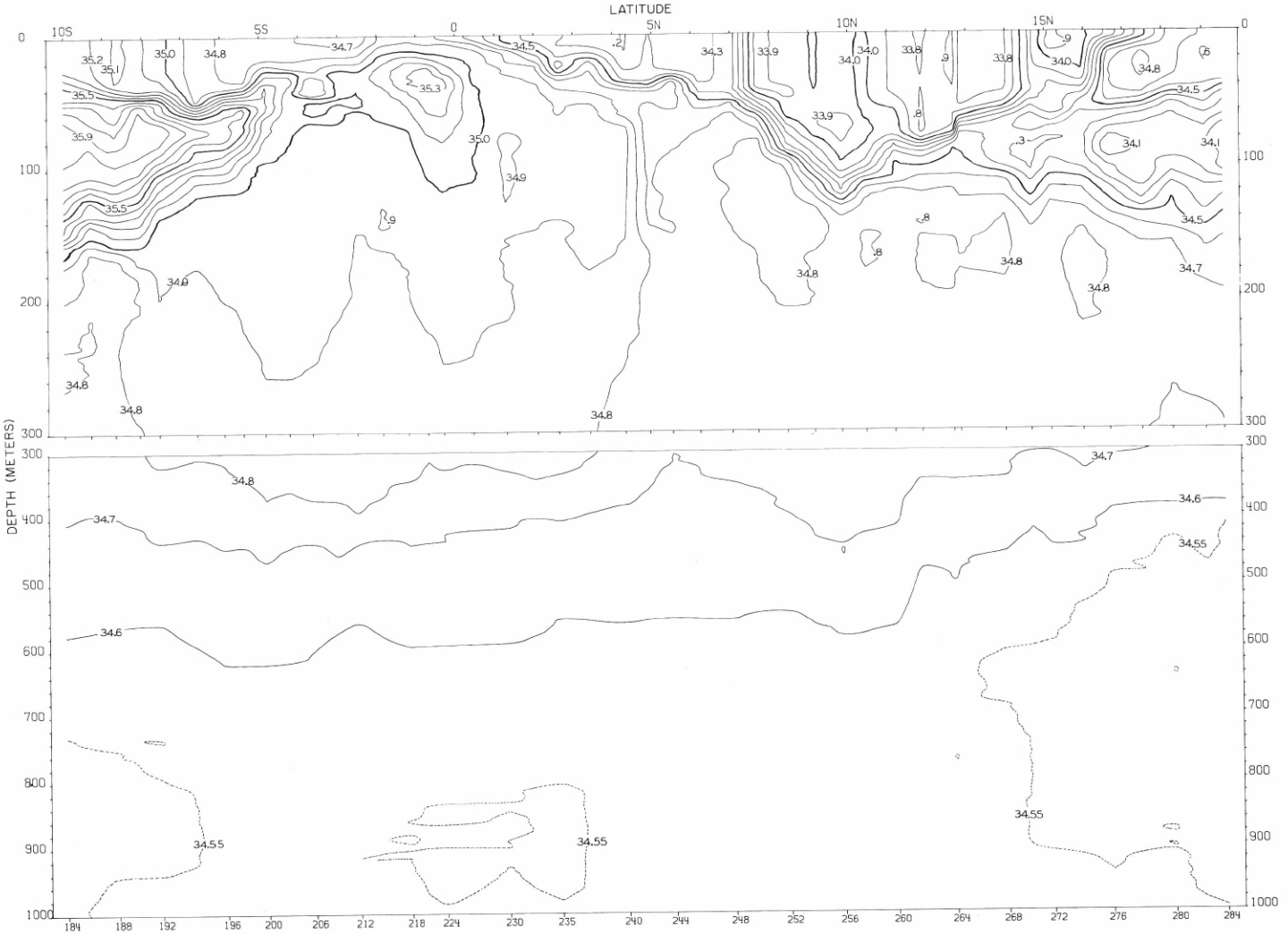

FIGURE 12-S-v6.—Vertical distribution of salinity (‰) along 112° W., March 9-21, 1967.

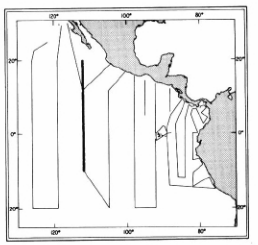

12-S-v6.

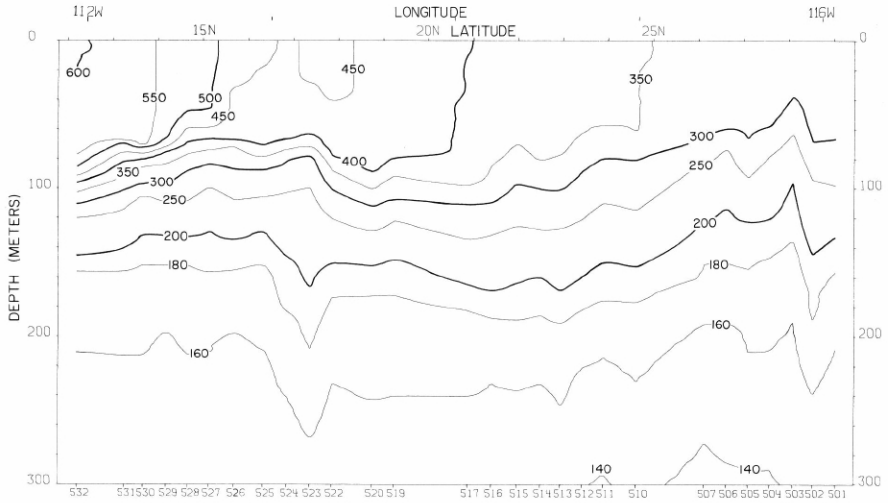

FIGURE 12-δ-v1.—Vertical distribution of thermosteric anomaly, δ_T, (cl./t.) along a section from 29° N. near the coast of Baja California to 12° N., 112° W., February 8-12, 1967. The temperature and salinity data from these stations were not calibrated against Nansen cast data.

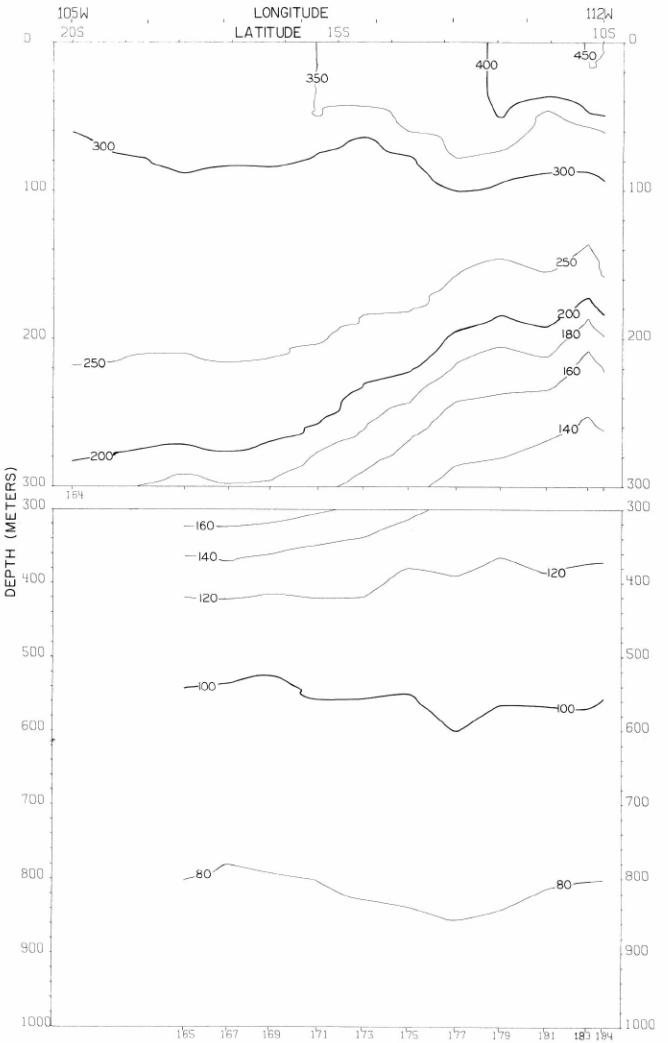

FIGURE 12-δ-v5.—Vertical distribution of thermosteric anomaly, δ_T, (cl./t.) along a southeast-northwest section from 20° S., 105° W. to 10° S., 112° W., March 6-9, 1967.

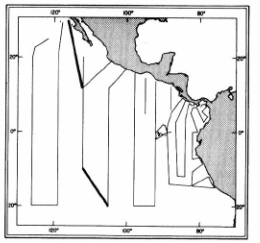

12-δ-v1.

12-δ-v5.

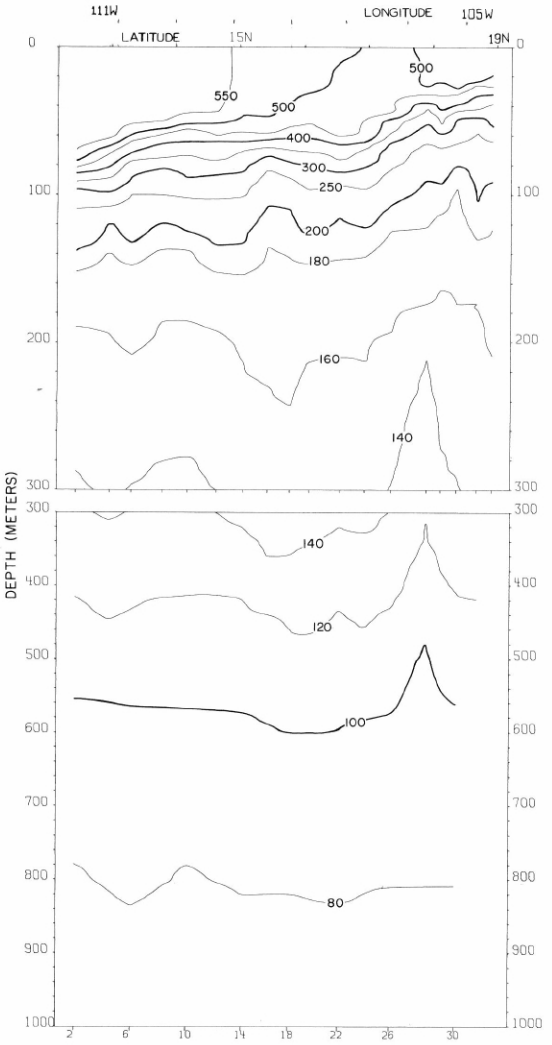

FIGURE 12-δ-v2.—Vertical distribution of thermosteric anomaly, δ_T, (cl./t.) along a section from 12° N., 112° W. to Manzanillo, February 12-16, 1967.

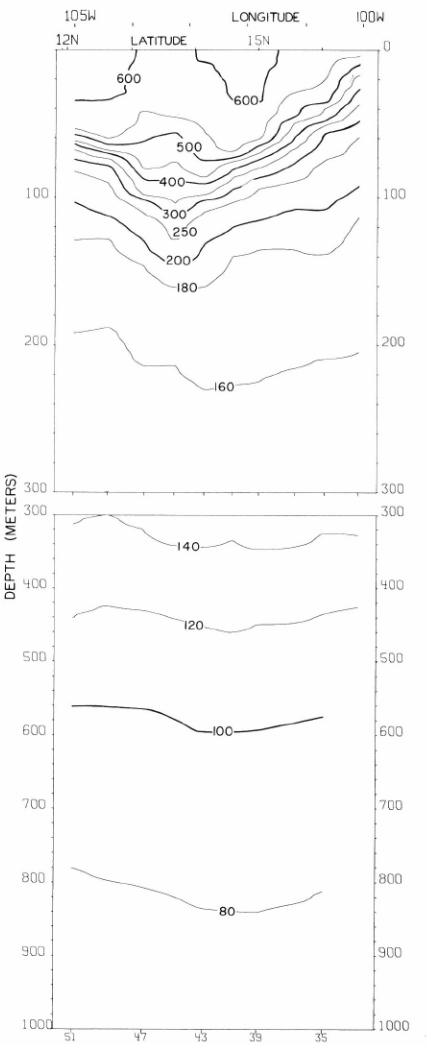

FIGURE 12-δ-v3.—Vertical distribution of thermosteric anomaly, δ_T, (cl./t.) along a section from Acapulco to 12° N., 105° W., February 19-21, 1967.

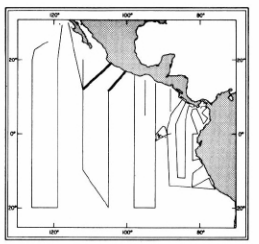

12-δ-v2.

12-δ-v3.

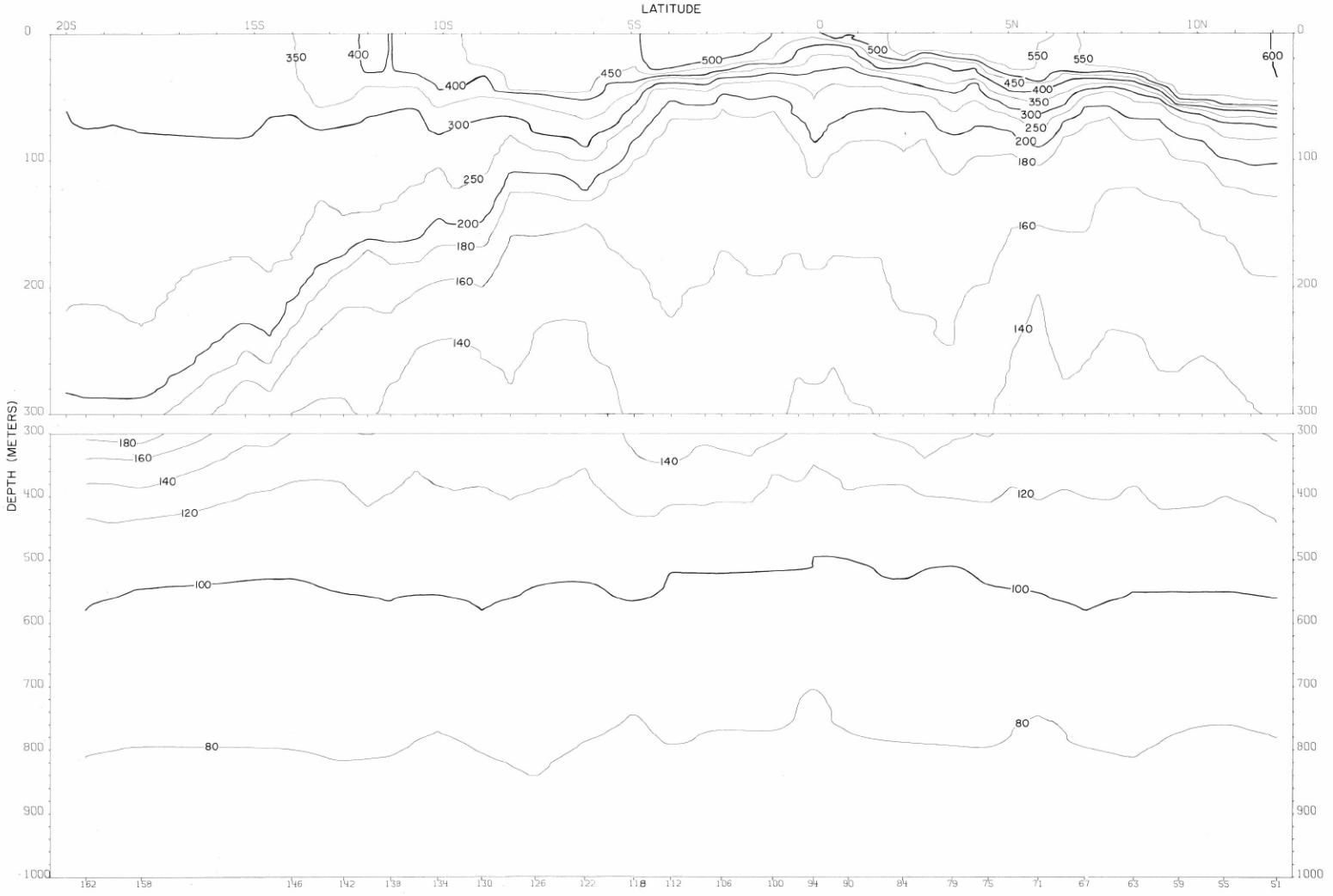

FIGURE 12-δ-v4.—Vertical distribution of thermosteric anomaly, δ_T, (cl./t.) along 105° W., February 21-March 6, 1967.

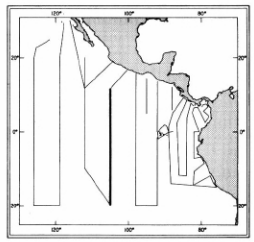

12-δ-v4.

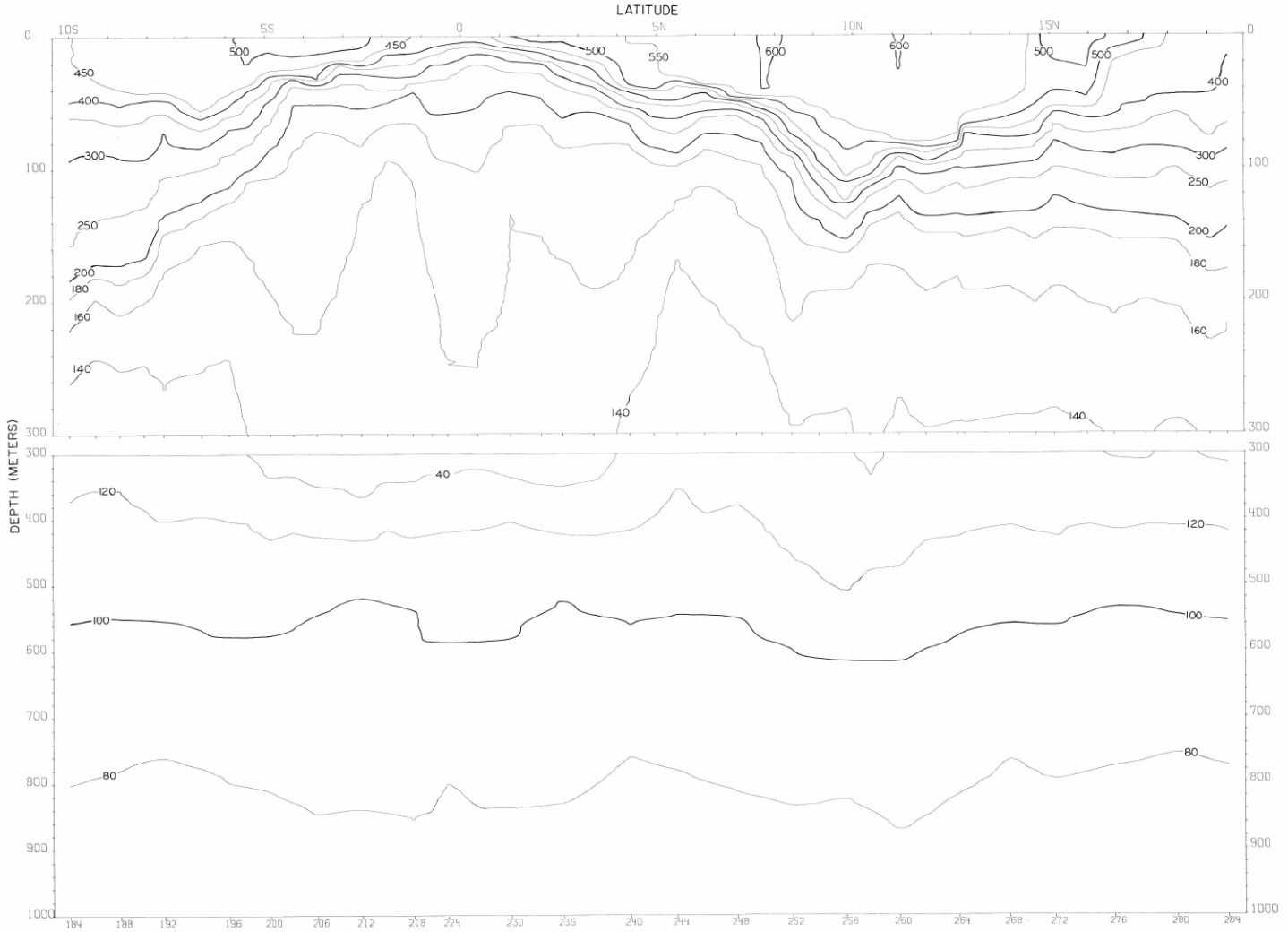

FIGURE 12-δ-v6.—Vertical distribution of thermosteric anomaly, δ_T, (cl./t.) along 112° W., March 9-21, 1967.

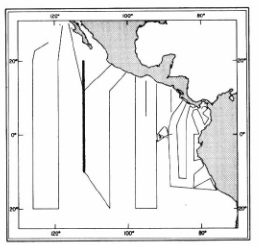

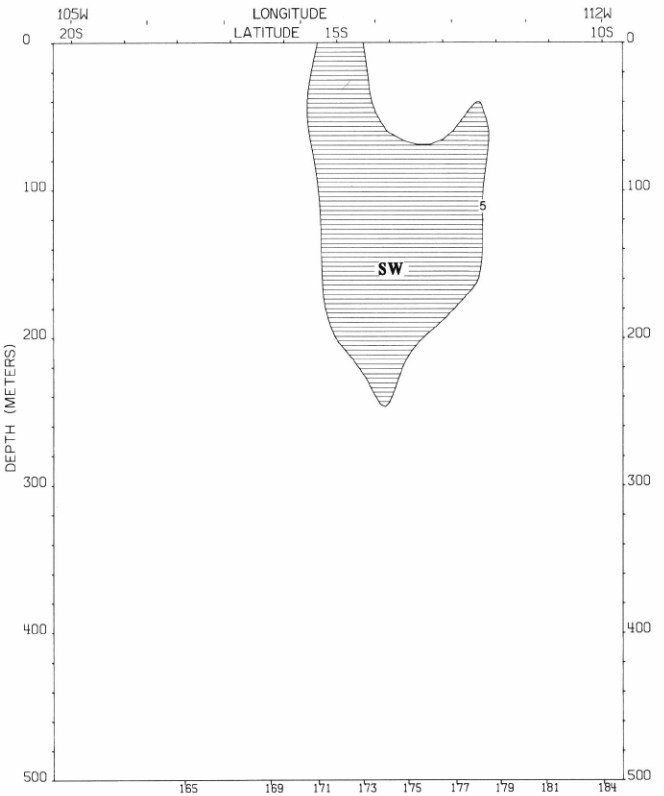

FIGURE 12-G-v5.—Vertical distribution of the component of geostrophic velocity (cm./sec.), relative to 500 db., normal to a section from 20° S., 105° W. to 10° S., 112° W., March 6-9, 1967. Dark shading indicates flow toward the northeast with a velocity greater than 5 cm./sec.; light shading indicates flow toward the southwest with a velocity greater than 5 cm./sec.

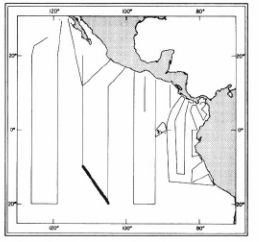

12-G-v5.

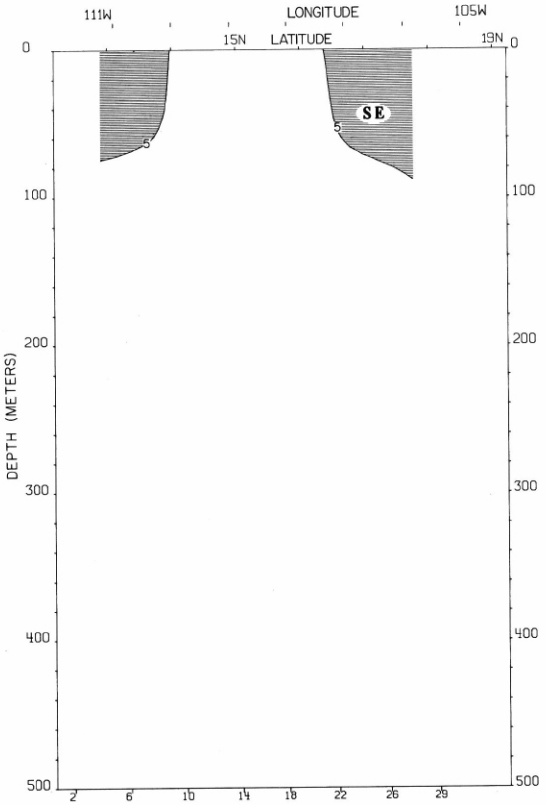

FIGURE 12-G-v2.—Vertical distribution of the component of geostrophic velocity (cm./sec.), relative to 500 db., normal to a section from 12° N., 112° W. to Manzanillo, February 12-16, 1967. Dark shading indicates flow toward the southeast with a velocity greater than 5 cm./sec.; light shading indicates flow toward the northwest with a velocity greater than 5 cm./sec.

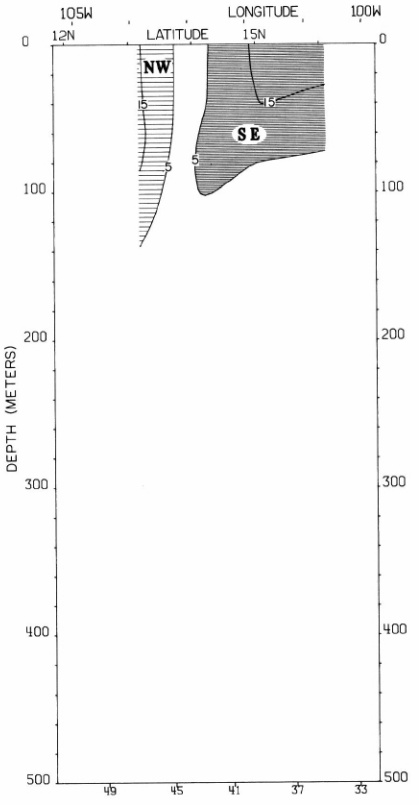

FIGURE 12-G-v3.—Vertical distribution of the component of geostrophic velocity (cm./sec.), relative to 500 db., normal to a section from Acapulco to 12° N., 105° W., February 19-21, 1967. Dark shading indicates flow toward the southeast with a velocity greater than 5 cm./sec.; light shading indicates flow toward the northwest with a velocity greater than 5 cm./sec.

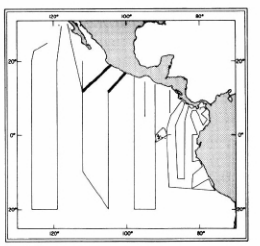

12-G-v2.

12-G-v3.

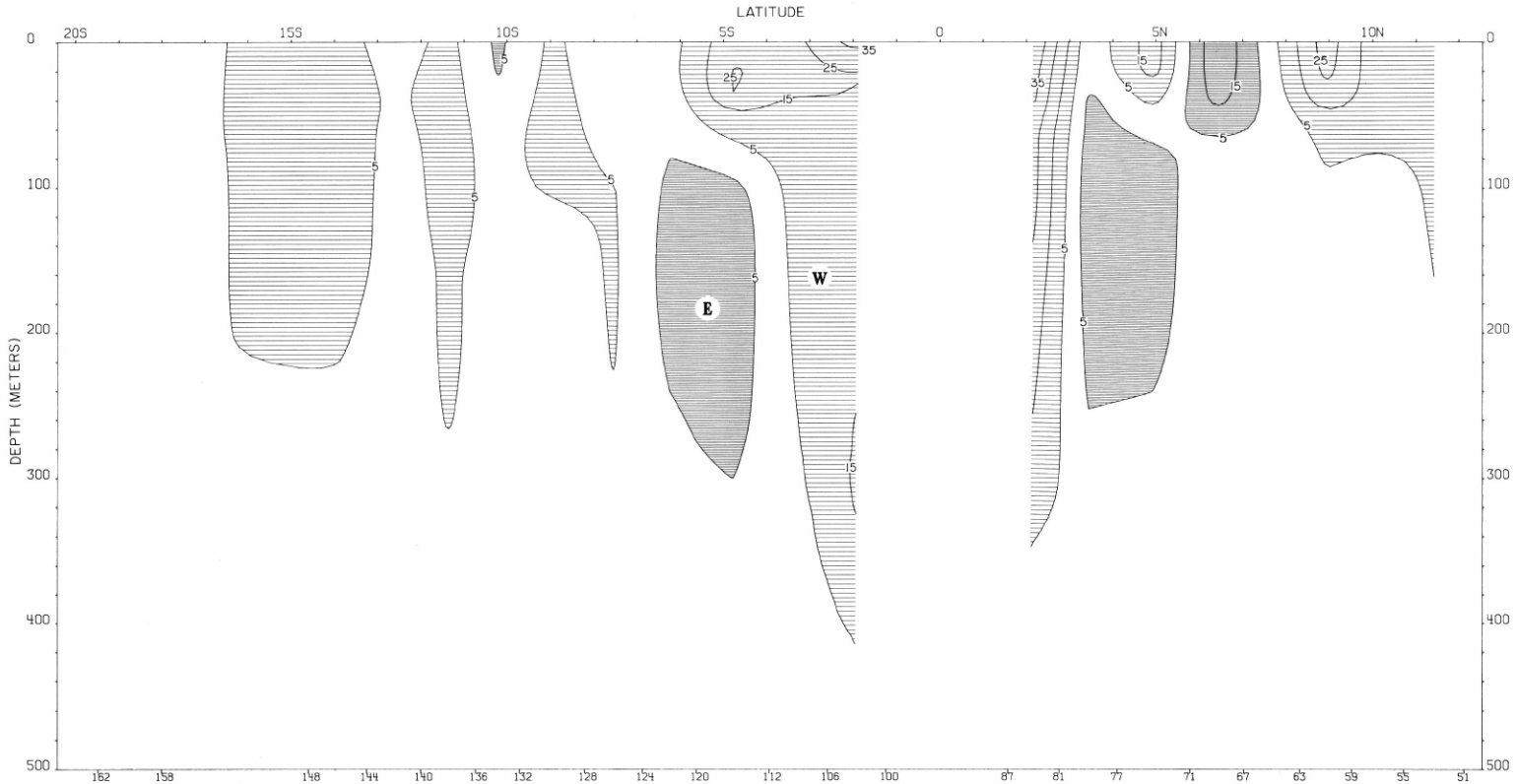

FIGURE 12-G-v4.—Vertical distribution of the zonal component of geostrophic velocity (cm./sec.), relative to 500 db., along 105° W., February 21-March 6, 1967. Dark shading indicates eastward flow with a velocity greater than 5 cm./sec.; light shading indicates westward flow with a velocity greater than 5 cm./sec.

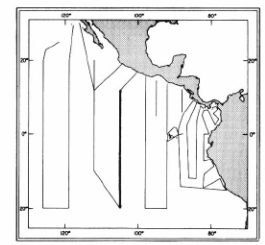

12-G-v4.

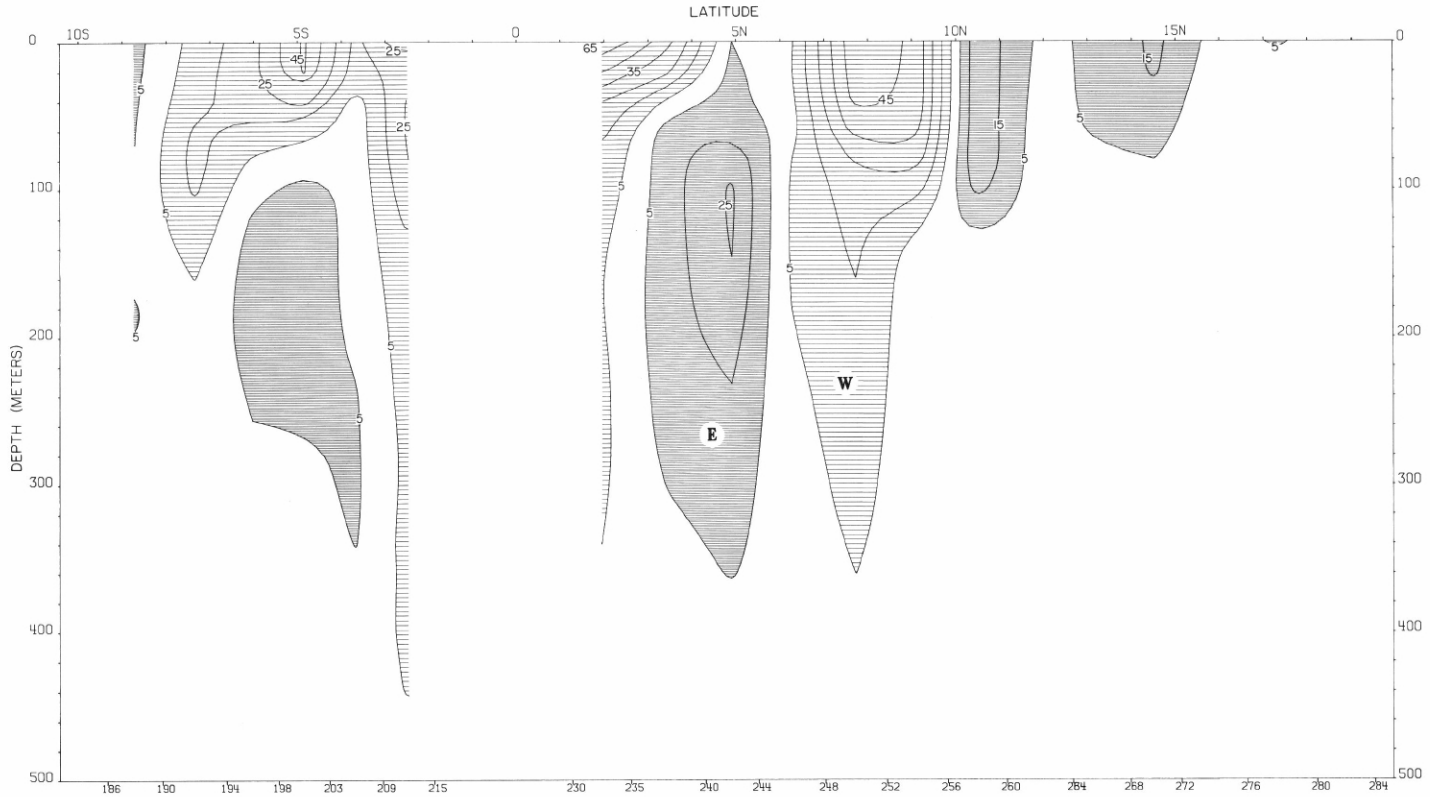

FIGURE 12-G-v6.—Vertical distribution of the zonal component of geostrophic velocity (cm./sec.), relative to 500 db., along 112° W., March 9-21, 1967. Dark shading indicates eastward flow with a velocity greater than 5 cm./sec.; light shading indicates westward flow with a velocity greater than 5 cm./sec.

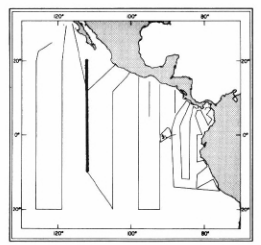

12-G-v6.

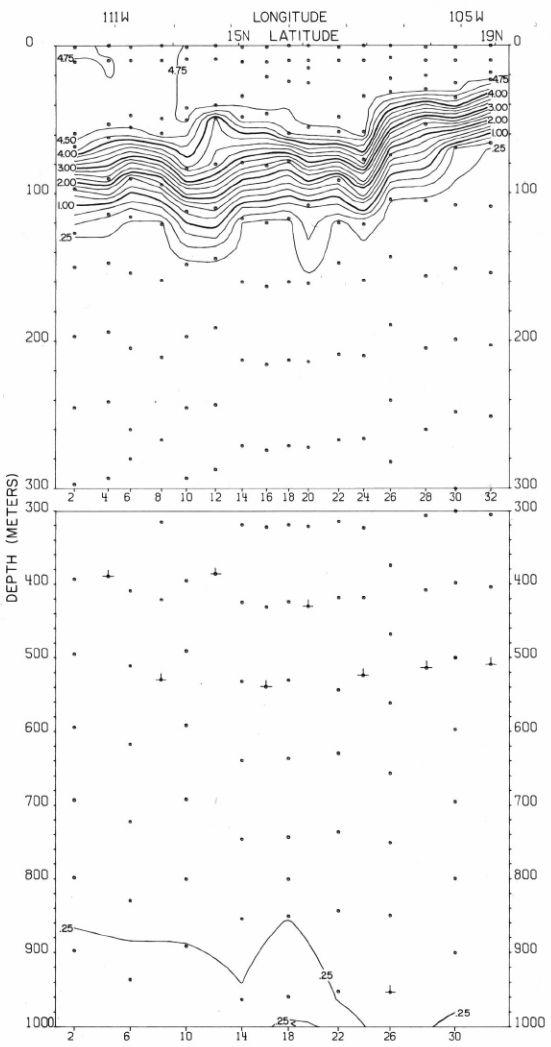

FIGURE 12-O_2-v2.—Vertical distribution of oxygen (ml./l.) along a section from 12° N., 112° W. to Manzanillo, February 12-16, 1967.

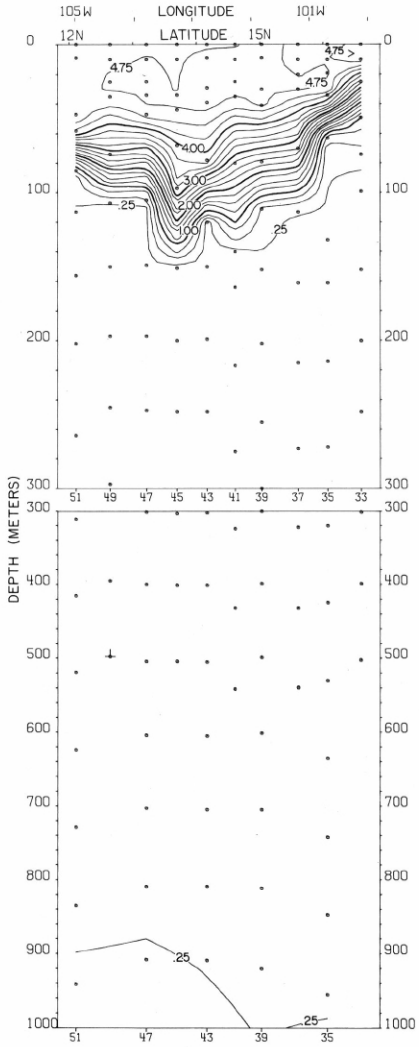

FIGURE 12-O_2-v3.—Vertical distribution of oxygen (ml./l.) along a section from Acapulco to 12° N., 105° W., February 19-21, 1967.

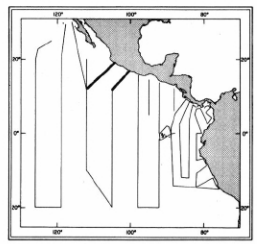

12-O_2-v2.

12-O_2-v3.

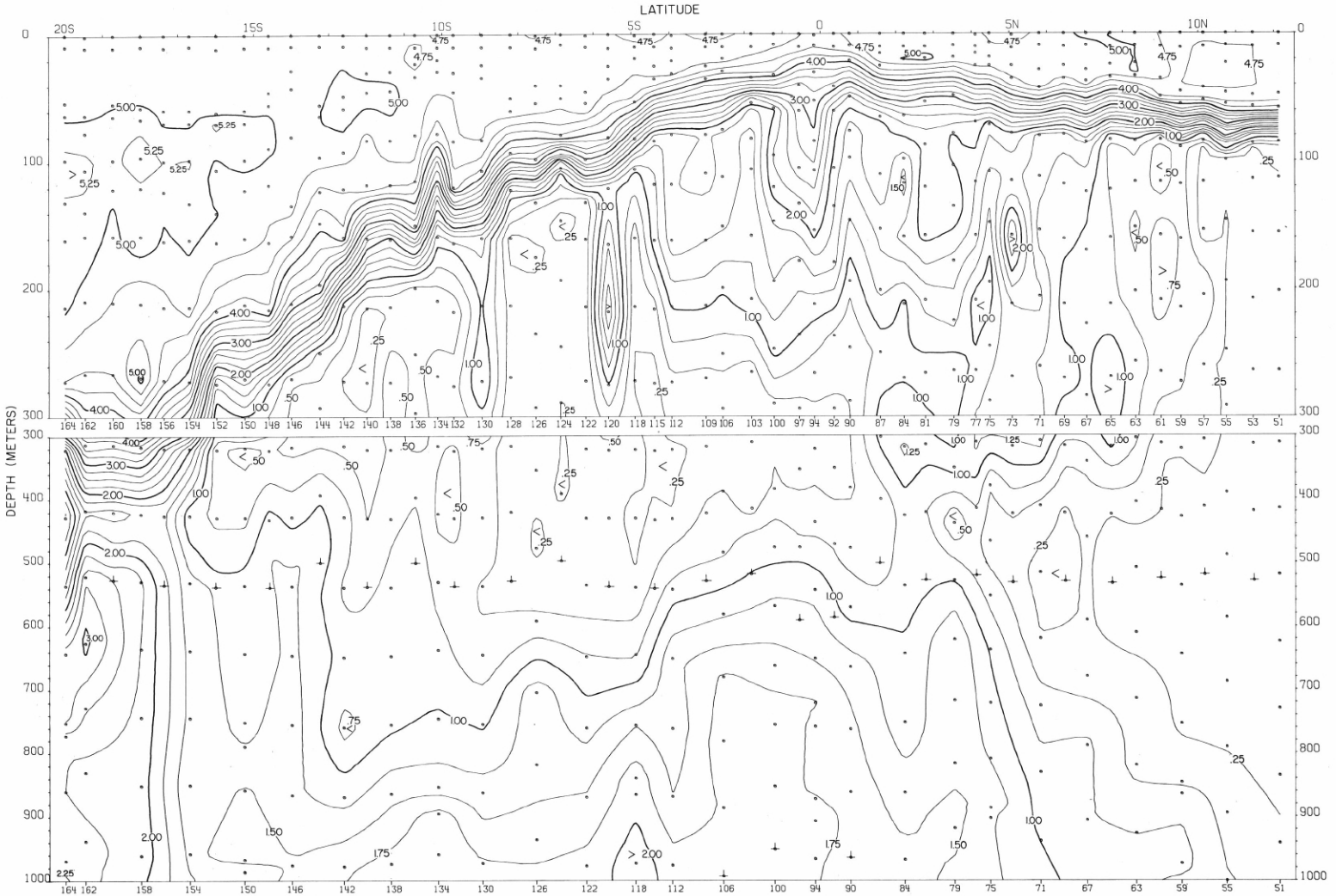

FIGURE 12-O_2-v4.—Vertical distribution of oxygen (ml./l.) along 105° W., February 21-March 6, 1967.

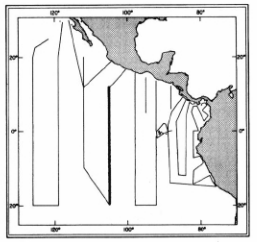

12-O_2-v4.

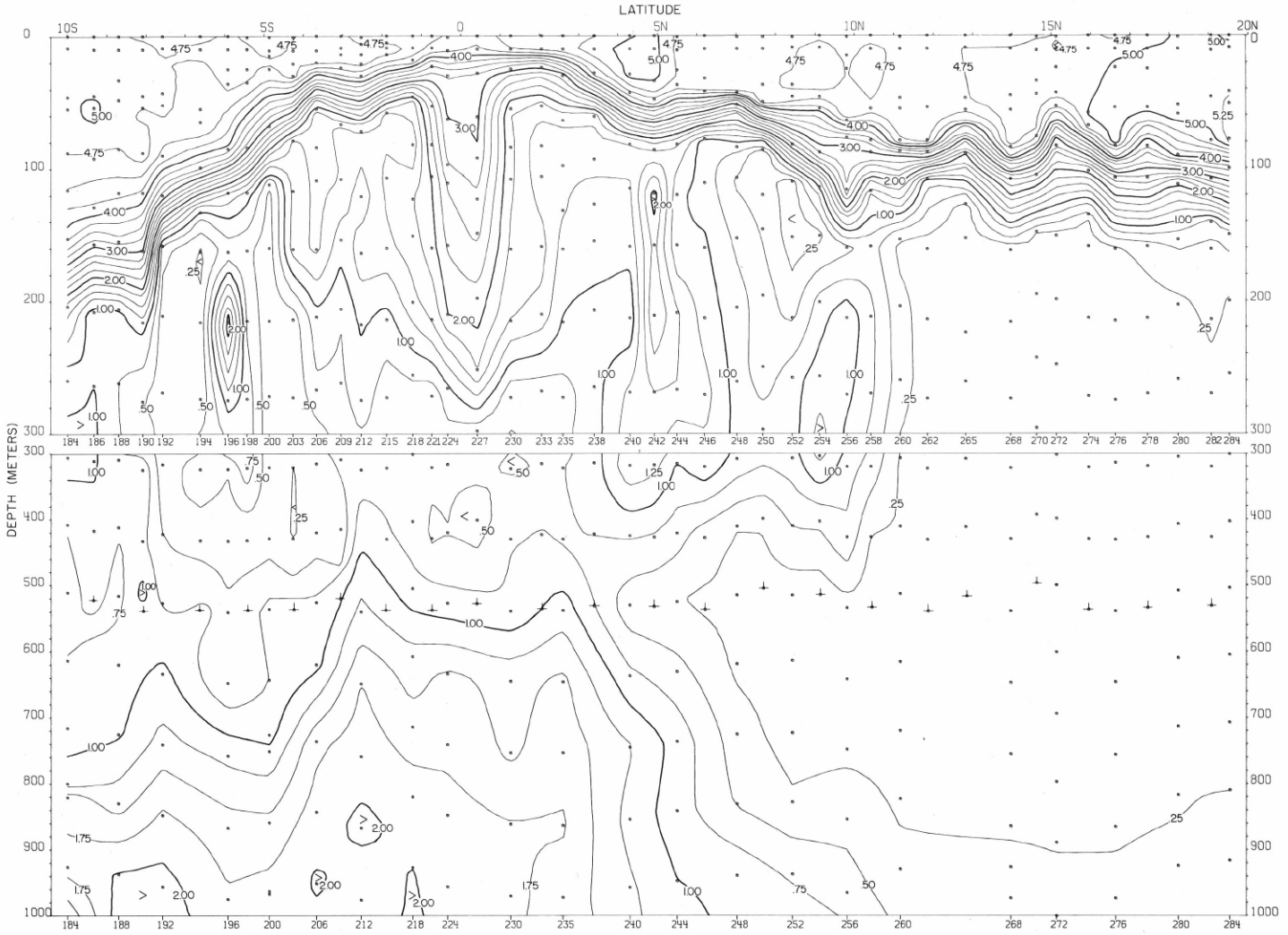

FIGURE 12-O2-v6.—Vertical distribution of oxygen (ml./l.) along 112° W., March 9-21, 1967.

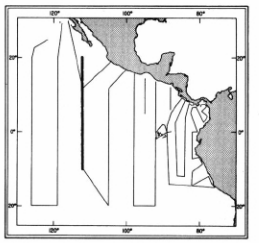

12-O2-v6.

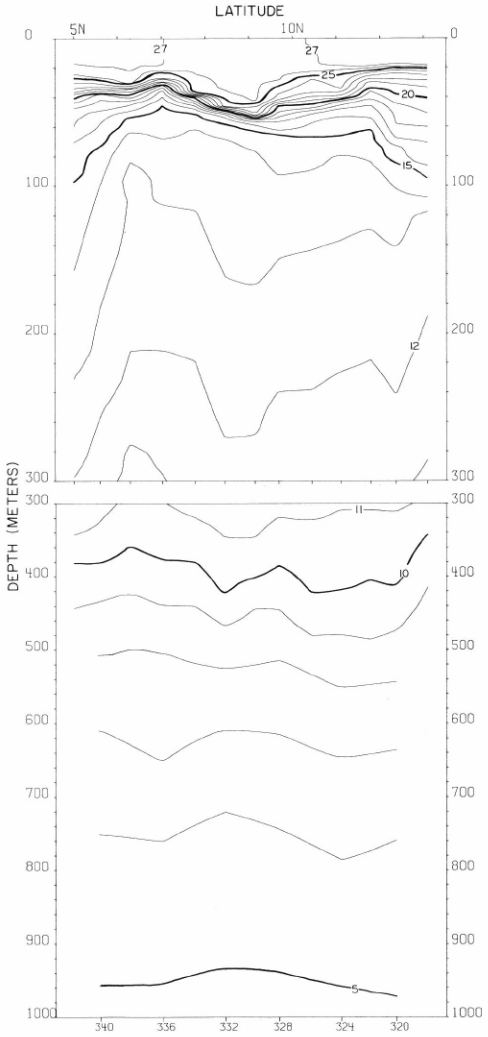

FIGURE 13-T-v6.—Vertical distribution of temperature (°C.) along 95° W., March 17-20, 1967. These contours are based on STD data read from analog traces.

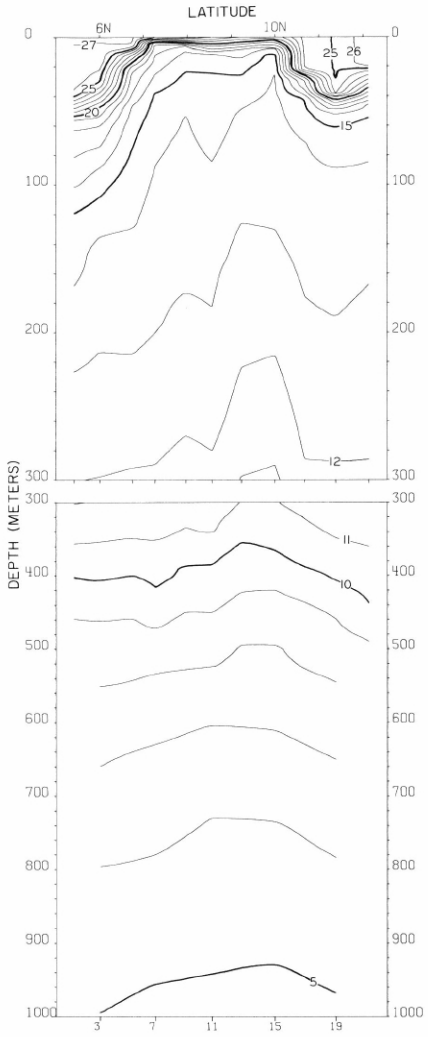

FIGURE 13-T-v1.—Vertical distribution of temperature (°C.) along 88° W., February 1-4, 1967. These contours are based on STD data read from analog traces.

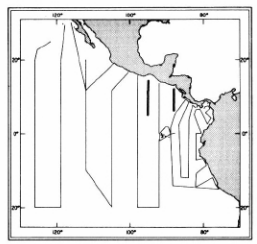

13-T-v1.

13-T-v6.

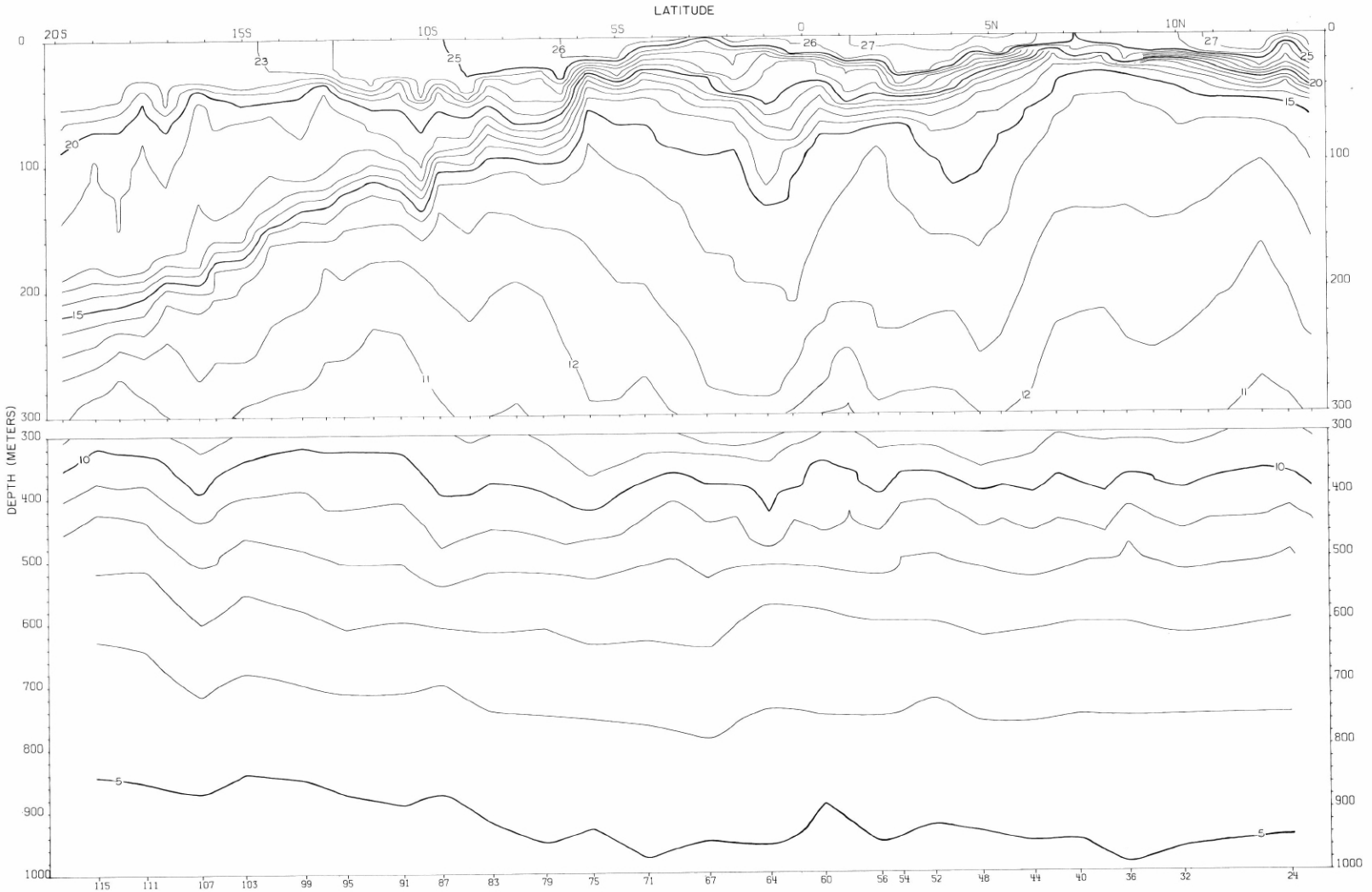

FIGURE 13-T-v2.—Vertical distribution of temperature (°C.) along 92° W., February 7-21, 1967. These contours are based on STD data read from analog traces.

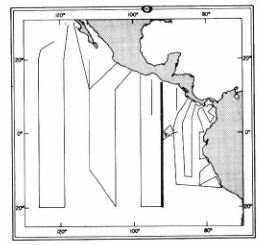

13-T-v2.

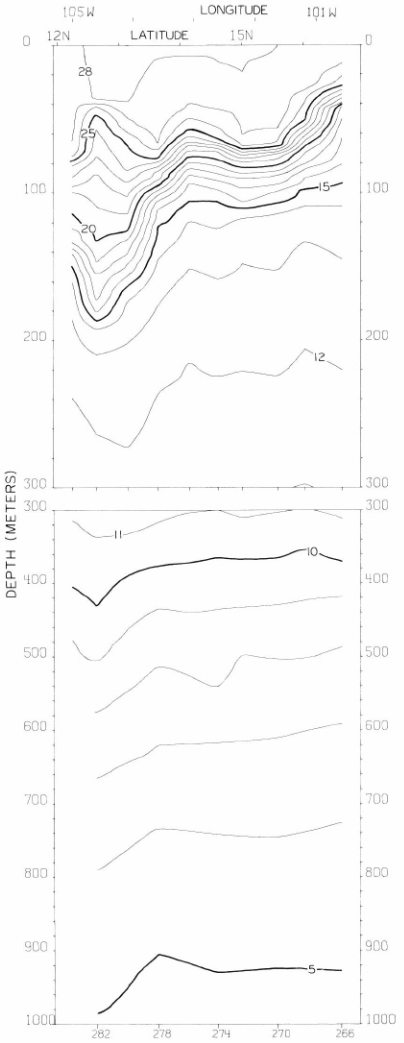

FIGURE 13-T-v5.—Vertical distribution of temperature (°C.) along a section from Acapulco to 12° N., 105° W., March 13-15, 1967. These contours are based on STD data read from analog traces.

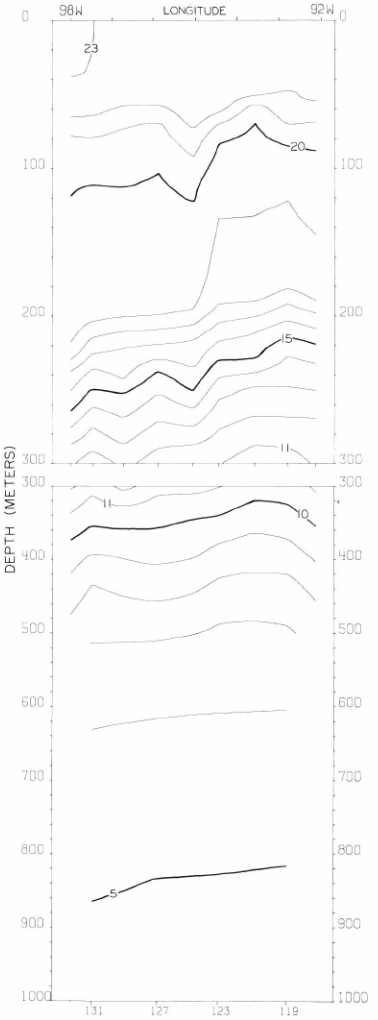

FIGURE 13-T-v3.—Vertical distribution of temperature (°C.) along 20° S., February 21-23, 1967. These contours are based on STD data read from analog traces.

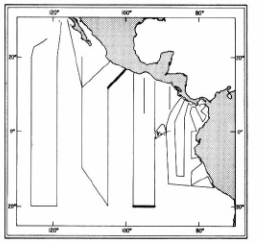

13-T-v3.

13-T-v5.

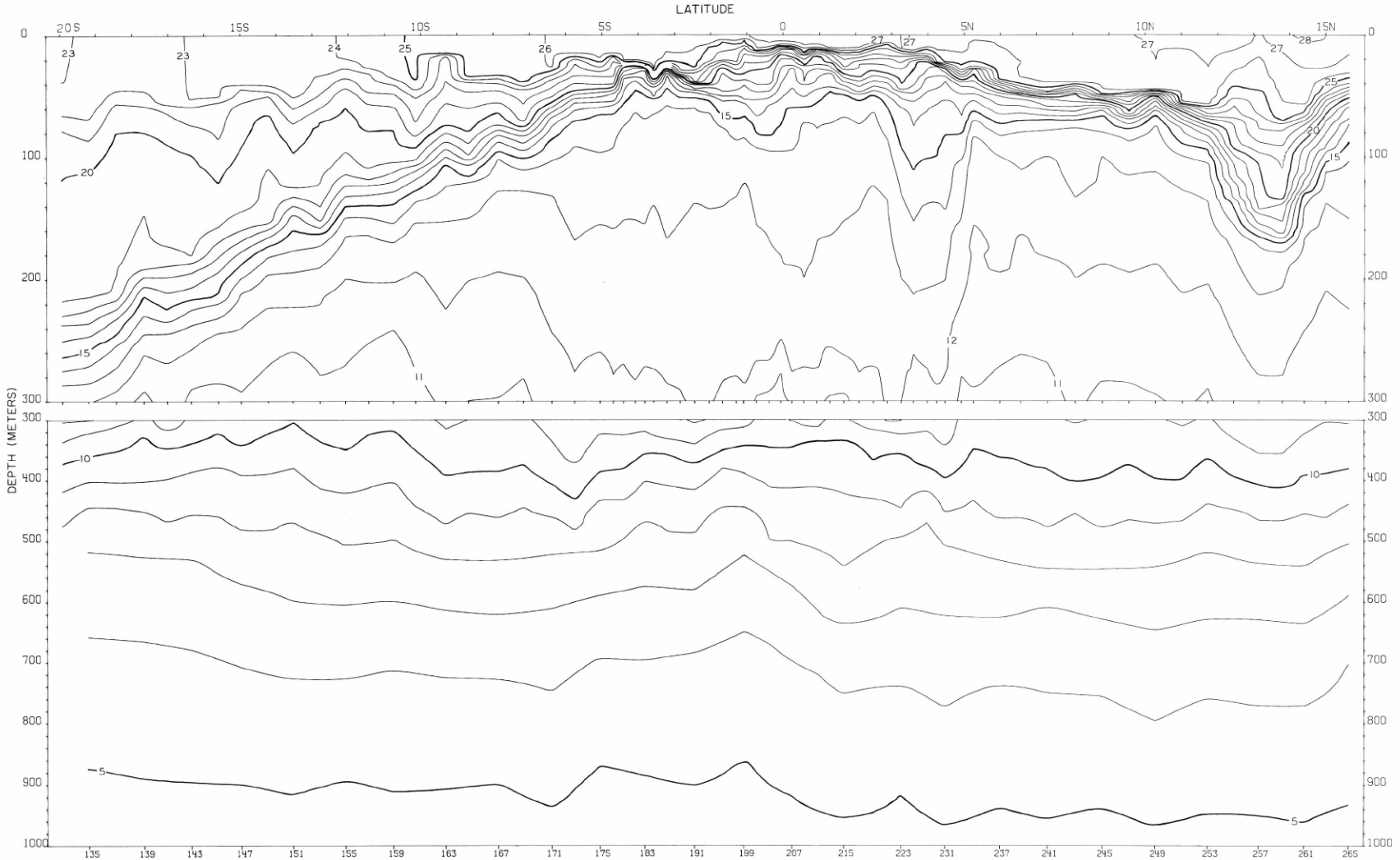

FIGURE 13-T-v4.—Vertical distribution of temperature (°C.) along 98° W., February 23-March 8, 1967. These contours are based on STD data read from analog traces.

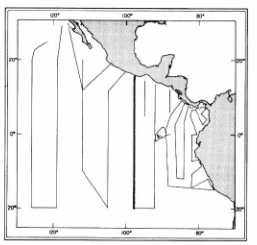

13-T-v4.

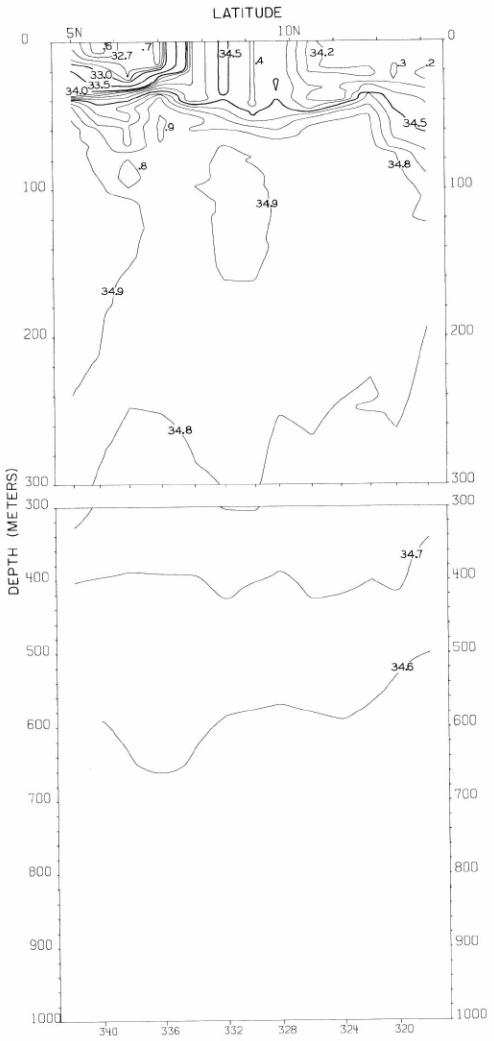

FIGURE 13-S-v6.—Vertical distribution of salinity (‰) along 95° W., March 17-20, 1967. These contours are based on STD data read from analog traces.

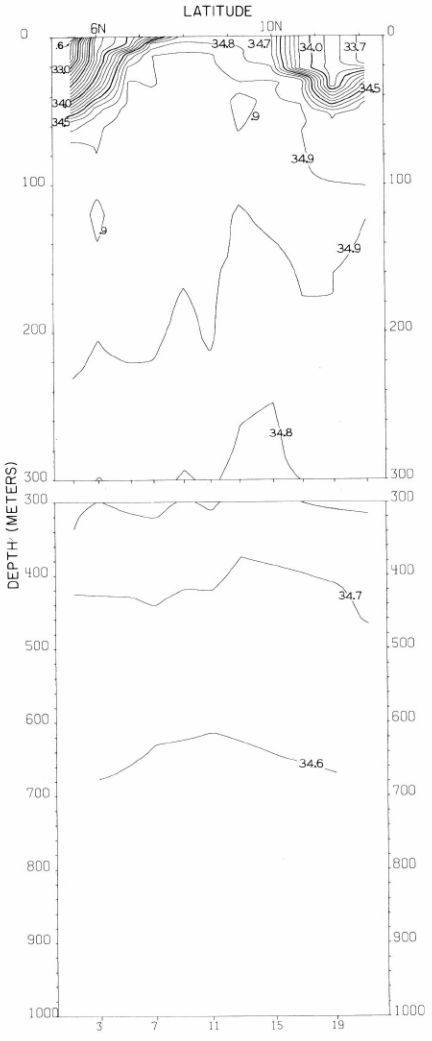

FIGURE 13-S-v1.—Vertical distribution of salinity (‰) along 88° W., February 1-4, 1967. These contours are based on STD data read from analog traces.

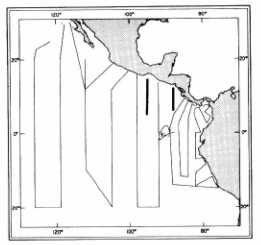

13-S-v1.

13-S-v6.

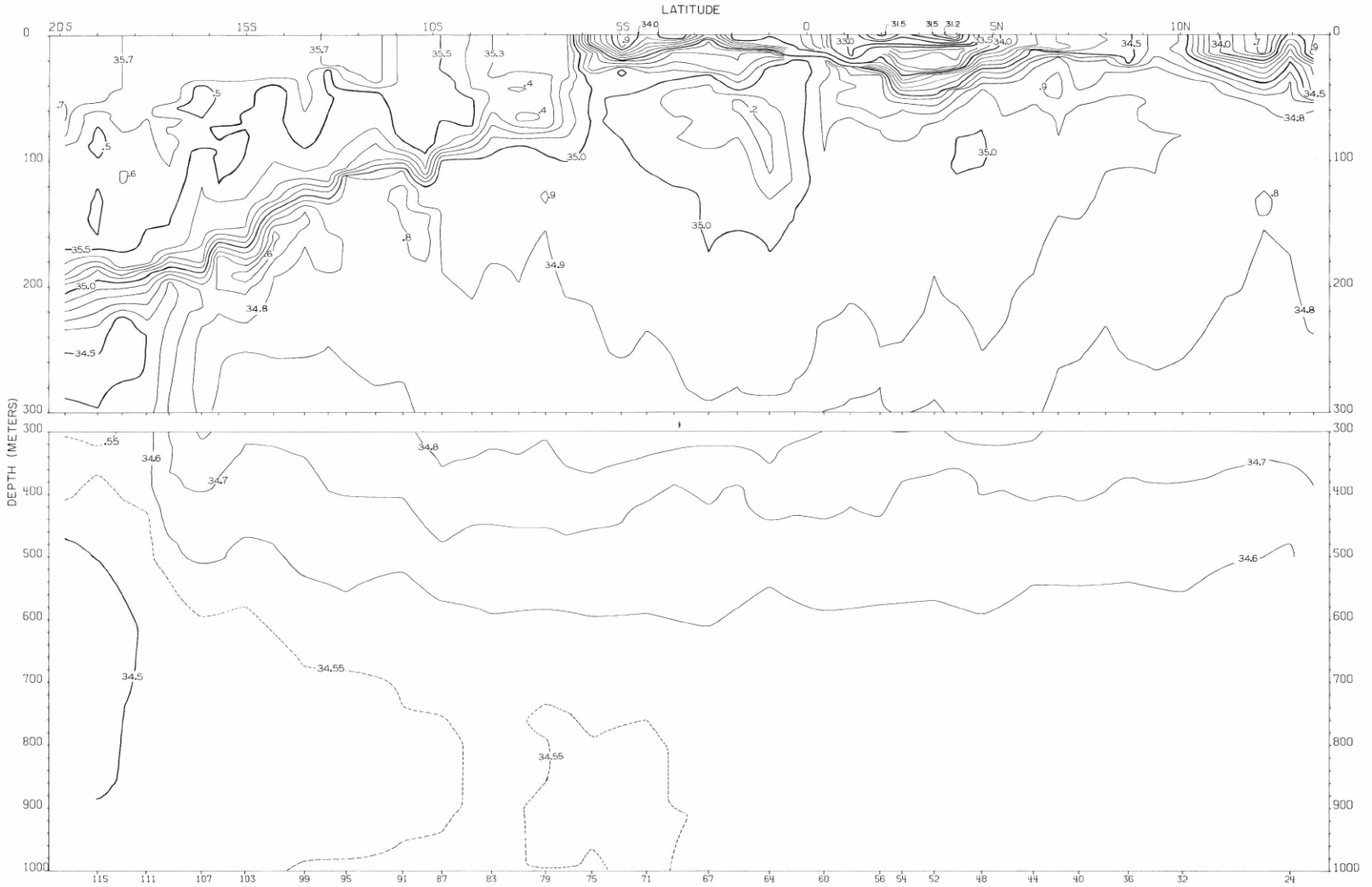

FIGURE 13-S-v2.—Vertical distribution of salinity (‰) along 92° W., February 7-21, 1967. These contours are based on STD data read from analog traces.

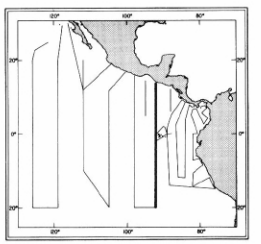

13-S-v2.

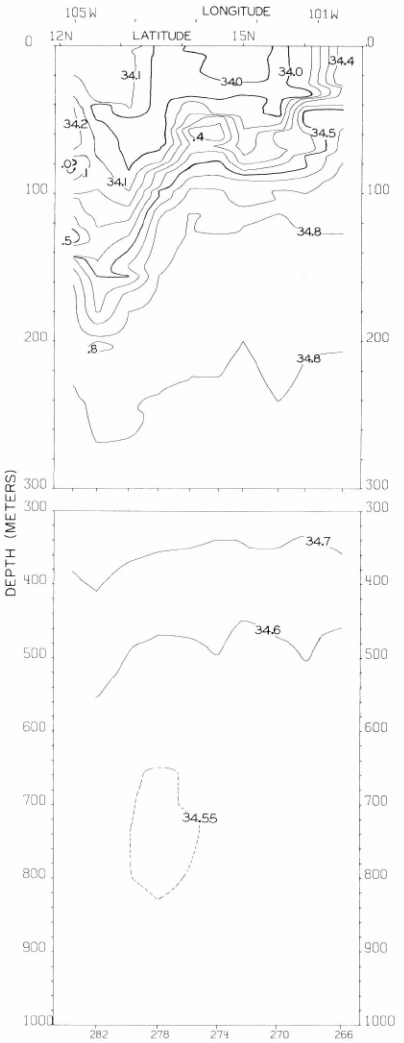

FIGURE 13-S-v5.—Vertical distribution of salinity (‰) along a section from Acapulco to 12° N., 105° W., March 13-15, 1967. These contours are based on STD data read from analog traces.

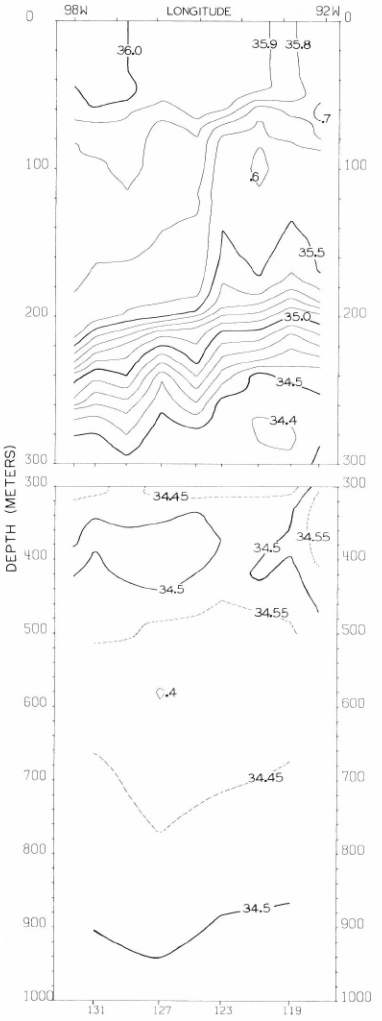

FIGURE 13-S-v3.—Vertical distribution of salinity (‰) along 20° S., February 21-23, 1967. These contours are based on STD data read from analog traces.

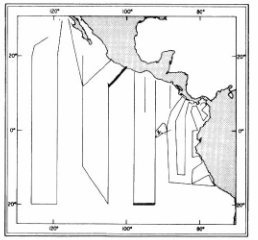

13-S-v3.

13-S-v5.

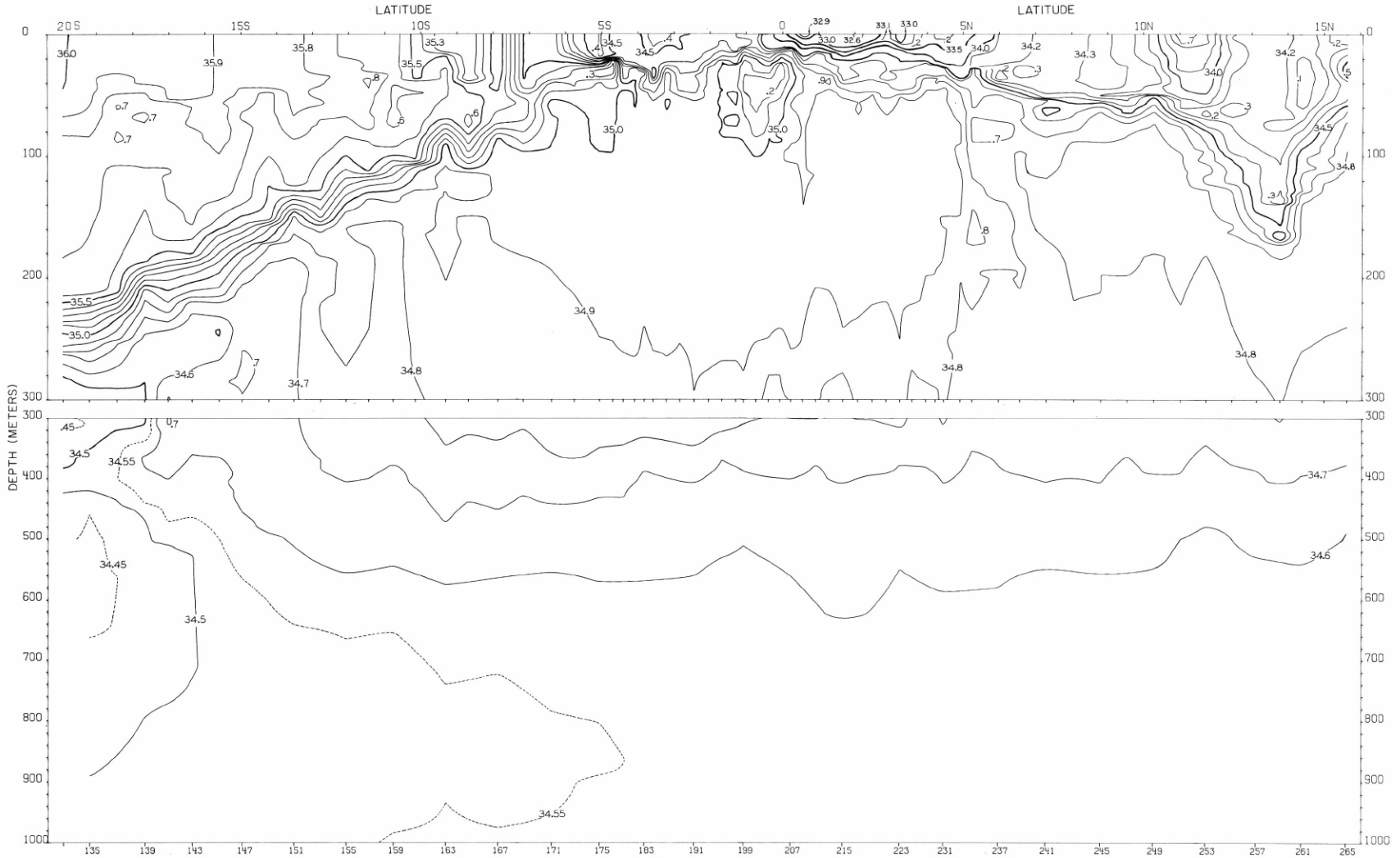

FIGURE 13-S-v4.—Vertical distribution of salinity (‰) along 98° W., February 23-March 8, 1967. These contours are based on STD data read from analog traces.

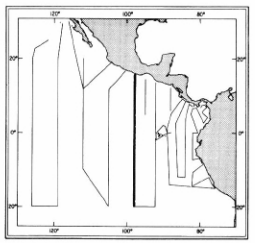

13-S-v4.

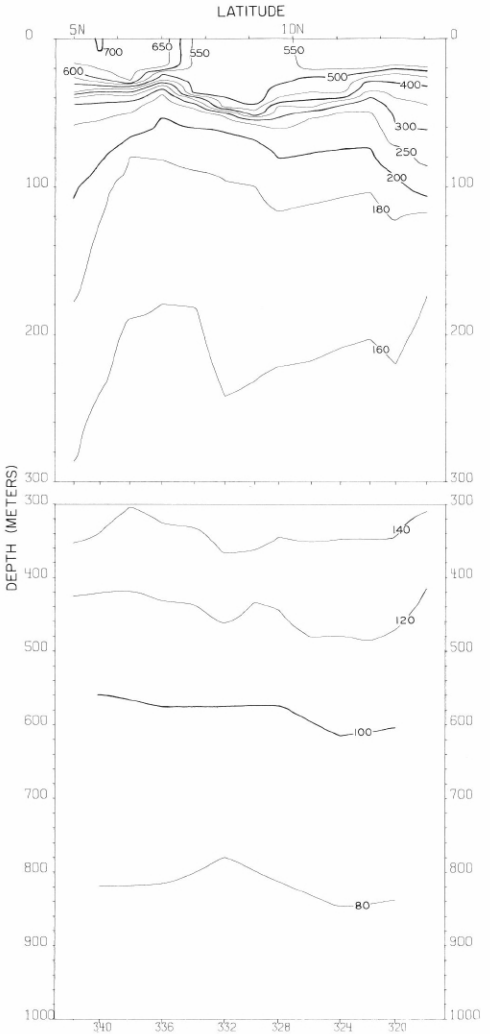

FIGURE 13-δ-v6.—Vertical distribution of thermosteric anomaly, δ_T, (cl./t.) along 95° W., March 17-20, 1967. These contours are based on STD data read from analog traces.

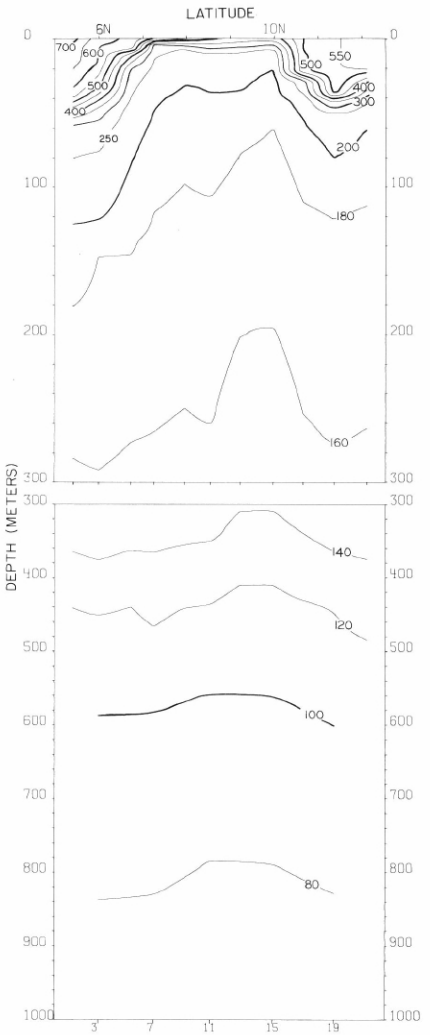

FIGURE 13-δ-v1.—Vertical distribution of thermosteric anomaly, δ_T, (cl./t.), along 88° W., February 1-4, 1967. These contours are based on STD data read from analog traces.

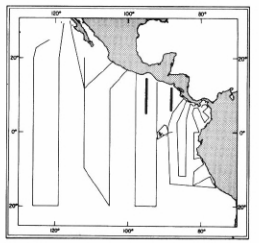

13-δ-v1.

13-δ-v6.

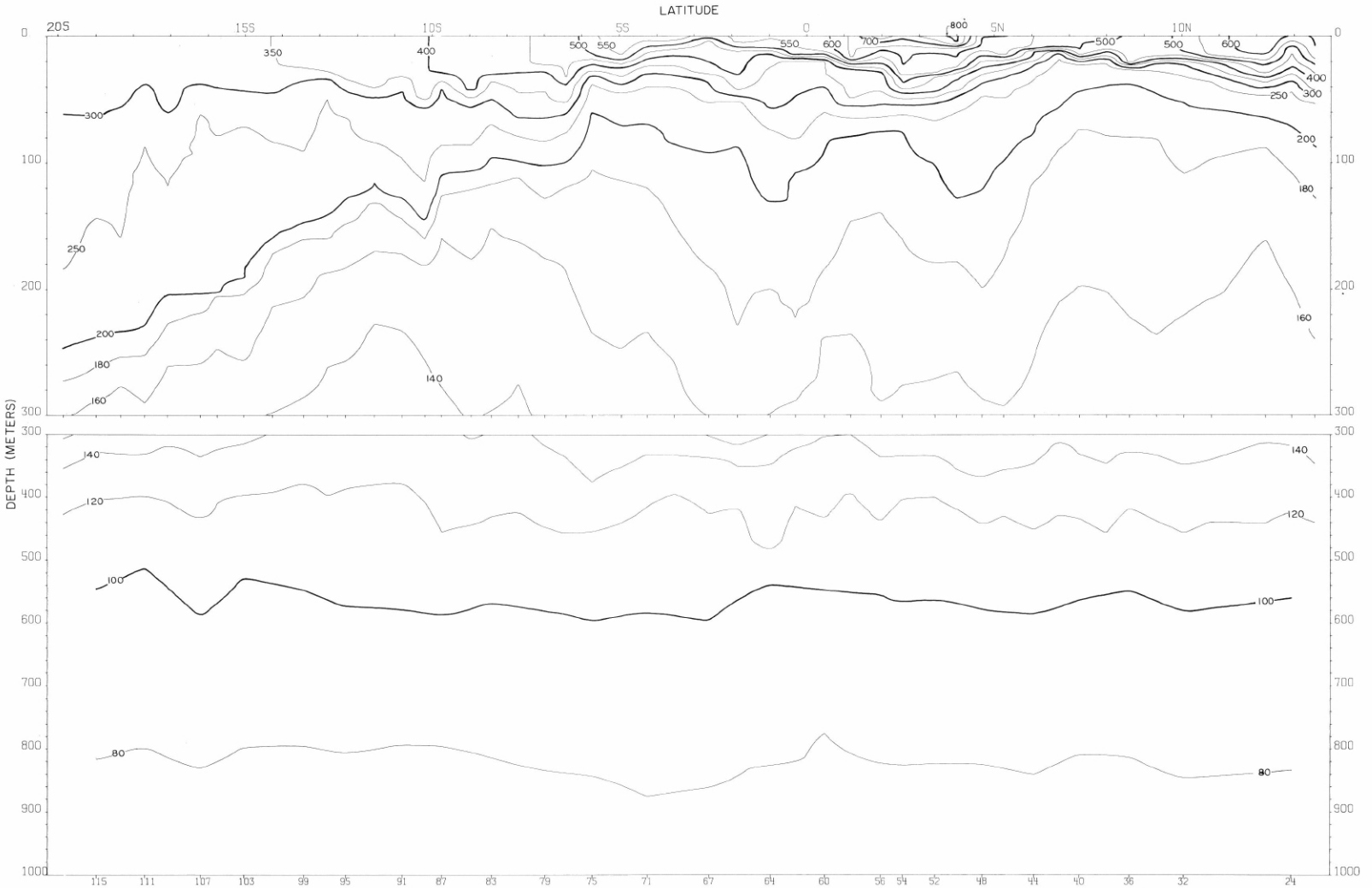

FIGURE 13-δ-v2.—Vertical distribution of thermosteric anomaly, δ_T, (cl./t.) along 92° W., February 7-21, 1967. These contours are based on STD data read from analog traces.

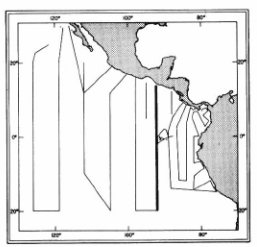

13-δ-v2.

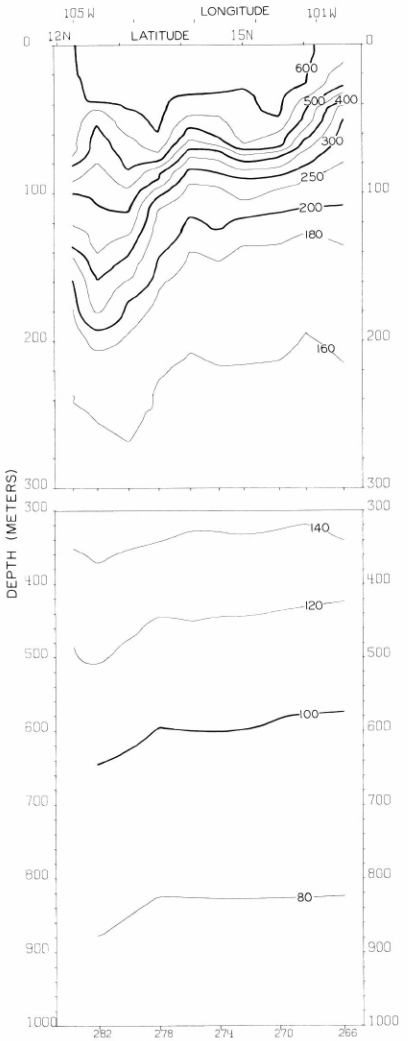

FIGURE 13-δ-v5.—Vertical distribution of thermosteric anomaly, δ_T, (cl./t.) along a section from Acapulco to 12° N., 105° W., March 13-15, 1967. These contours are based on STD data read from analog traces.

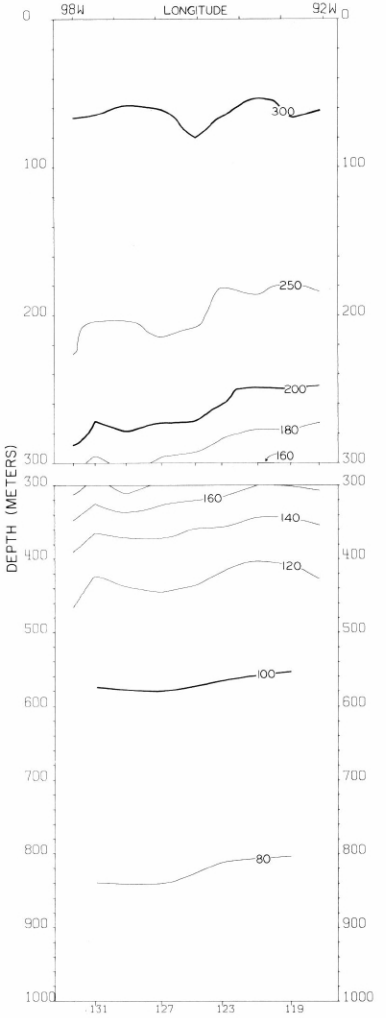

FIGURE 13-δ-v3.—Vertical distribution of thermosteric anomaly, δ_T, (cl./t.) along 20° S., February 21-23, 1967. These contours are based on STD data read from analog traces.

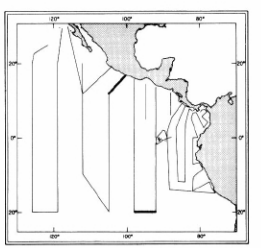

13-δ-v3.

13-δ-v5.

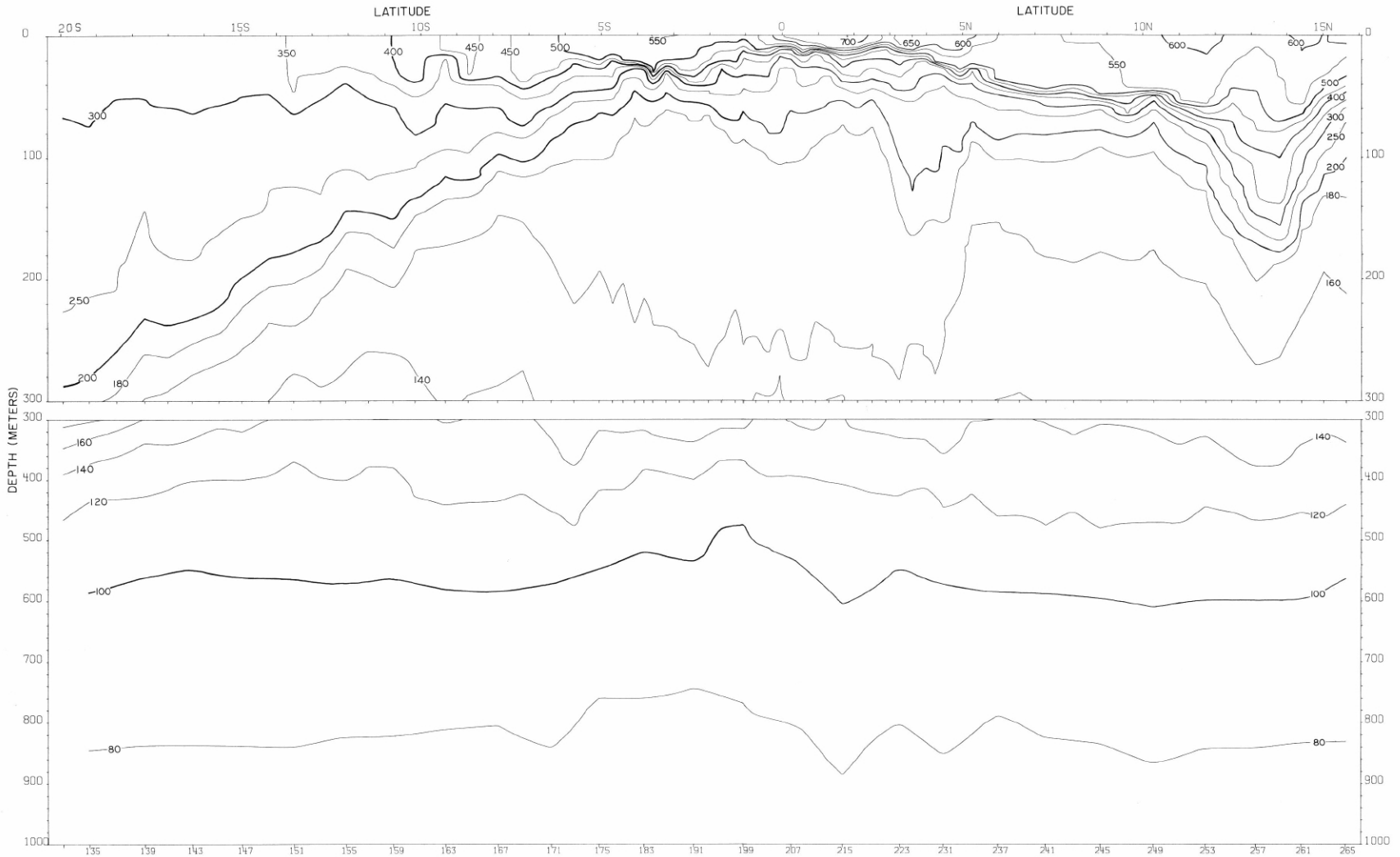

FIGURE 13-δ-v4.—Vertical distribution of thermosteric anomaly, δ_T, (cl./t.) along 98° W., February 23-March 8, 1967. These contours are based on STD data read from analog traces.

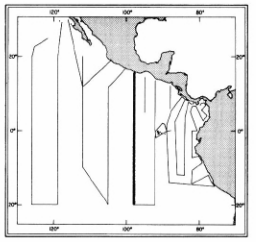

13-δ-v4.

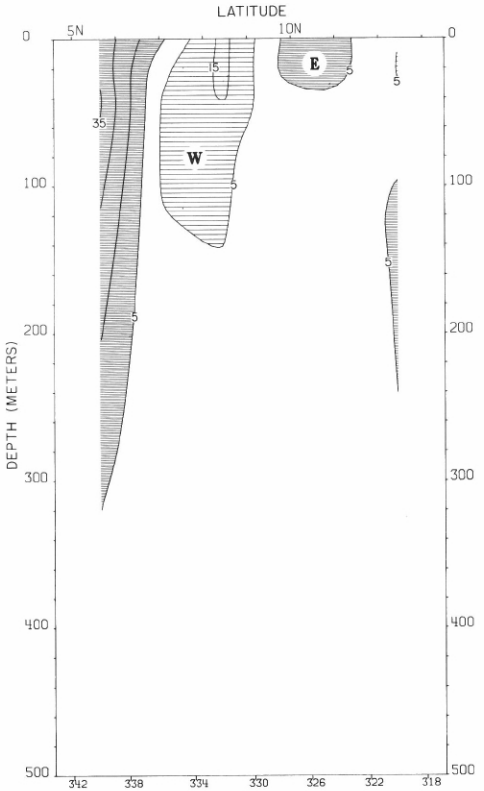

FIGURE 13-G-v6.—Vertical distribution of the zonal component of geostrophic velocity (cm./sec.), relative to 500 db., along 95° W., March 17-20, 1967. Dark shading indicates eastward flow with a velocity greater than 5 cm./sec.; light shading indicates westward flow with a velocity greater than 5 cm./sec.

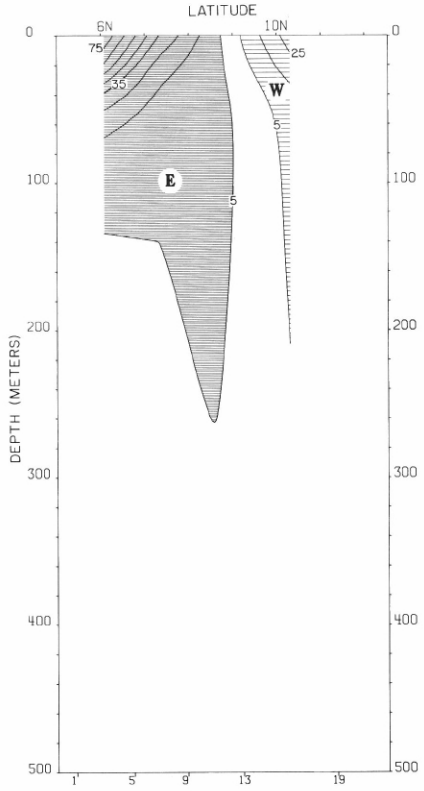

FIGURE 13-G-v1.—Vertical distribution of the zonal component of geostrophic velocity (cm./sec.), relative to 500 db., along 88° W., February 1-4, 1967. Dark shading indicates eastward flow with a velocity greater than 5 cm./sec.; light shading indicates westward flow with a velocity greater than 5 cm./sec.

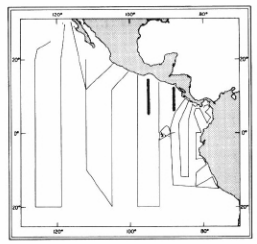

13-G-v1.

13-G-v6.

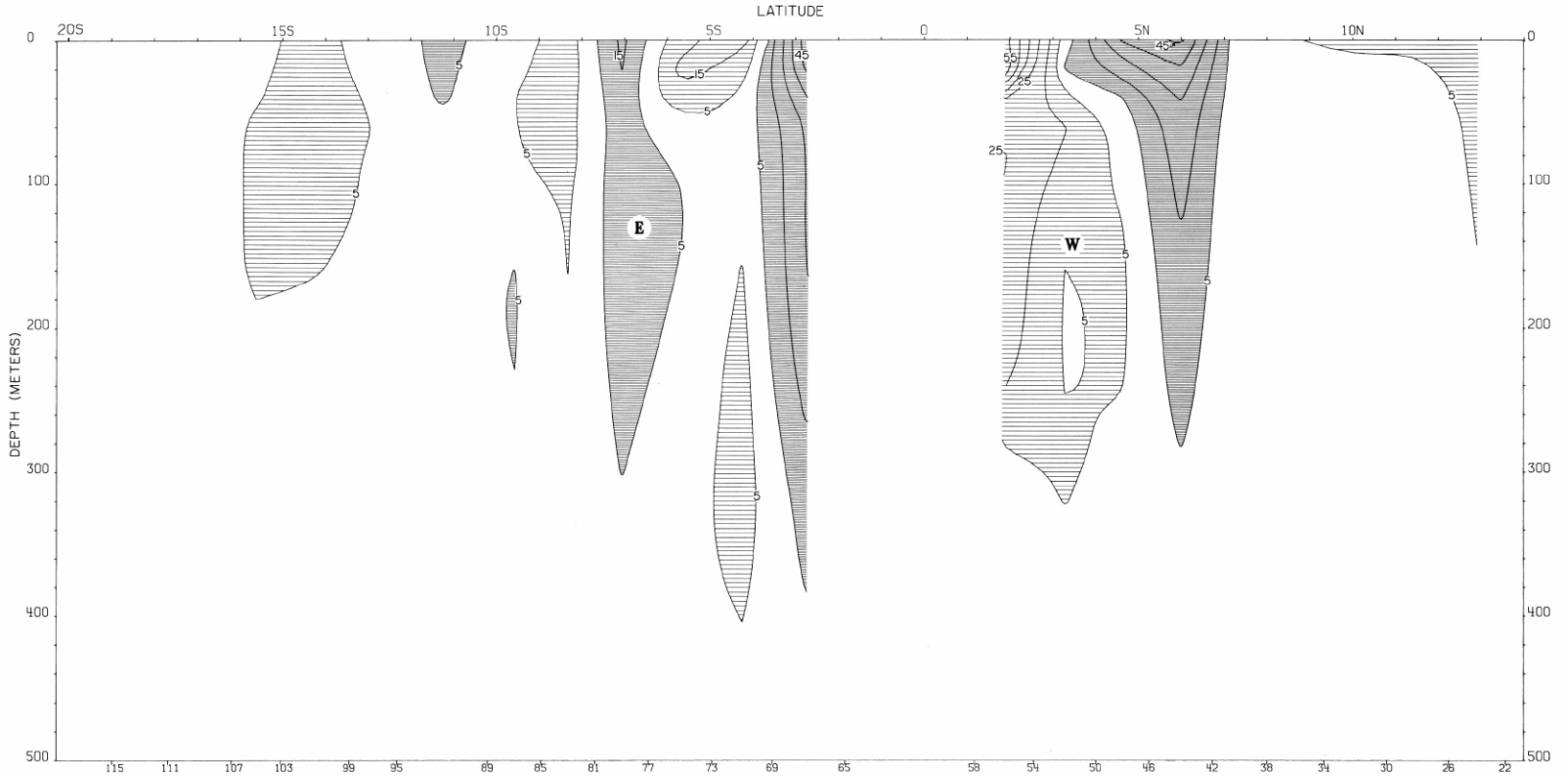

FIGURE 13-G-v2.—Vertical distribution of the zonal component of geostrophic velocity (cm./sec.), relative to 500 db., along 92° W., February 7-21, 1967. Dark shading indicates eastward flow with a velocity greater than 5 cm./sec.; light shading indicates westward flow with a velocity greater than 5 cm./sec.

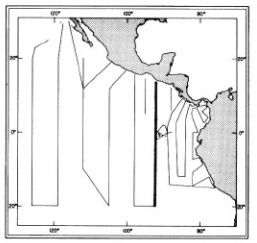

13-G-v2.

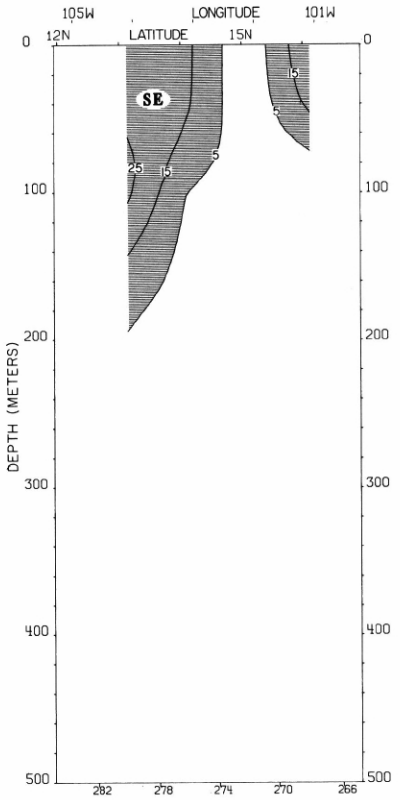

FIGURE 13-G-v5.—Vertical distribution of the component of geostrophic velocity (cm./sec.), relative to 500 db., normal to a section from Acapulco to 12° N., 105° W., March 13-15, 1967. Dark shading indicates flow toward the southeast with a velocity greater than 5 cm./sec.; light shading indicates flow toward the northwest with a velocity greater than 5 cm./sec.

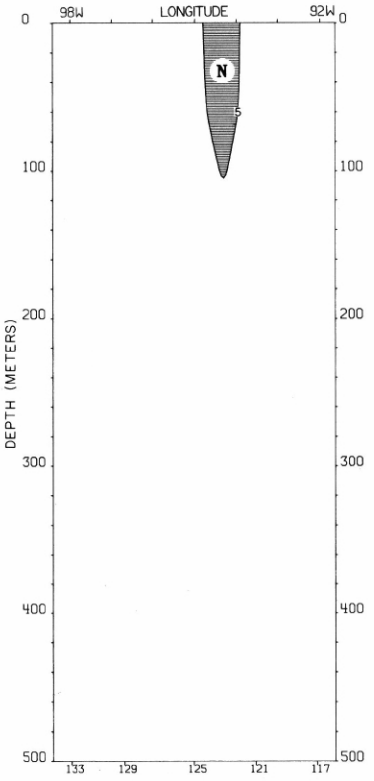

FIGURE 13-G-v3.—Vertical distribution of the meridional component of geostrophic velocity (cm./sec.), relative to 500 db., along 20° S., February 21-23, 1967. Dark shading indicates northward flow with a velocity greater than 5 cm./sec.; light shading indicates southward flow with a velocity greater than 5 cm./sec.

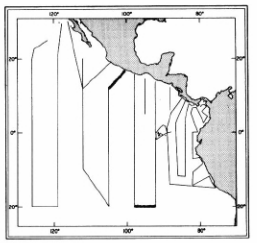

13-G-v3.

13-G-v5.

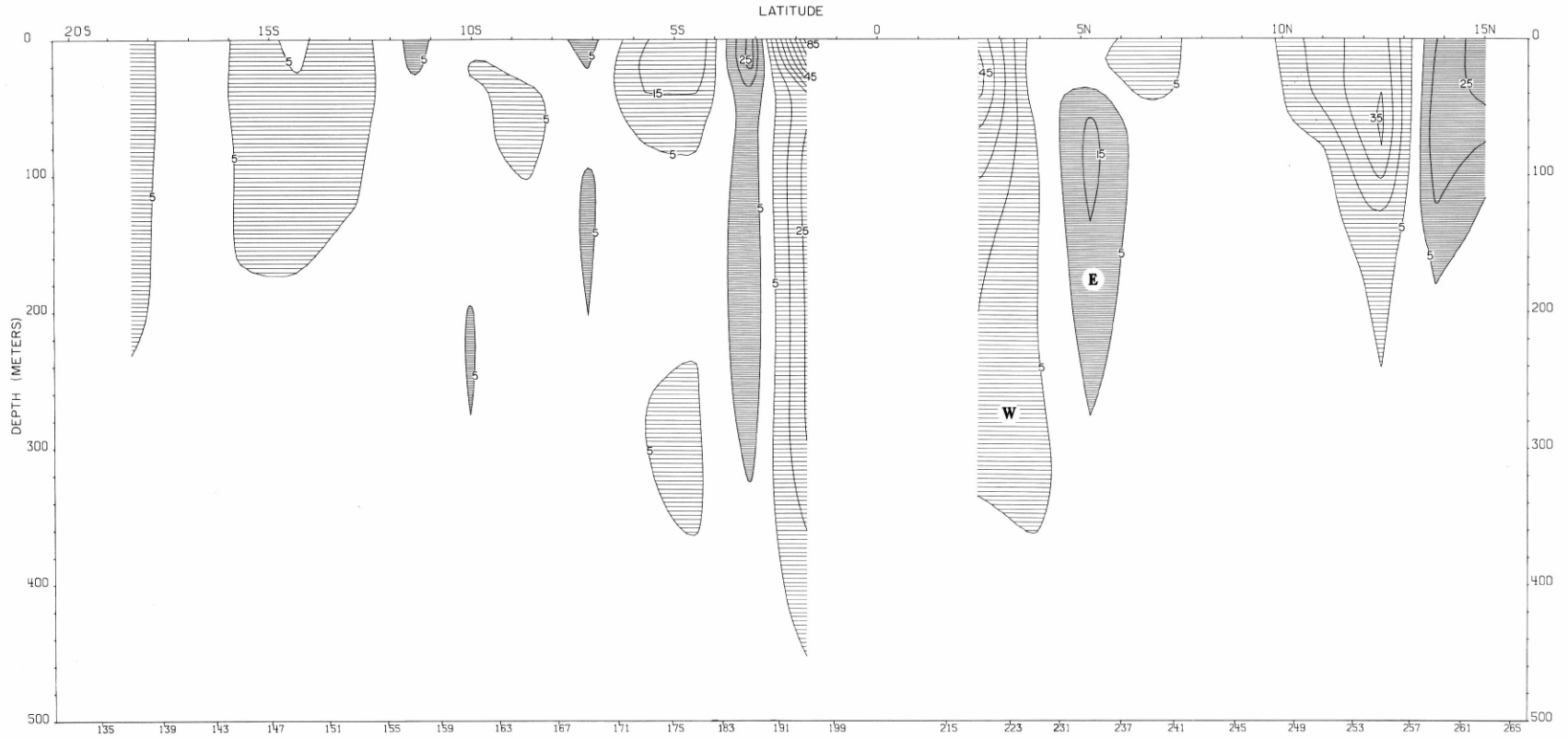

FIGURE 13-G-v4.—Vertical distribution of the zonal component of geostrophic velocity (cm./sec.), relative to 500 db., along 98° W., February 23-March 8, 1967. Dark shading indicates eastward flow with a velocity greater than 5 cm./sec.; light shading indicates westward flow with a velocity greater than 5 cm./sec.

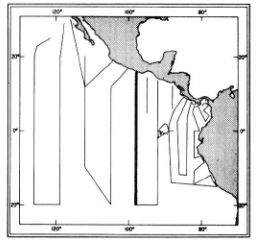

13-G-v4.

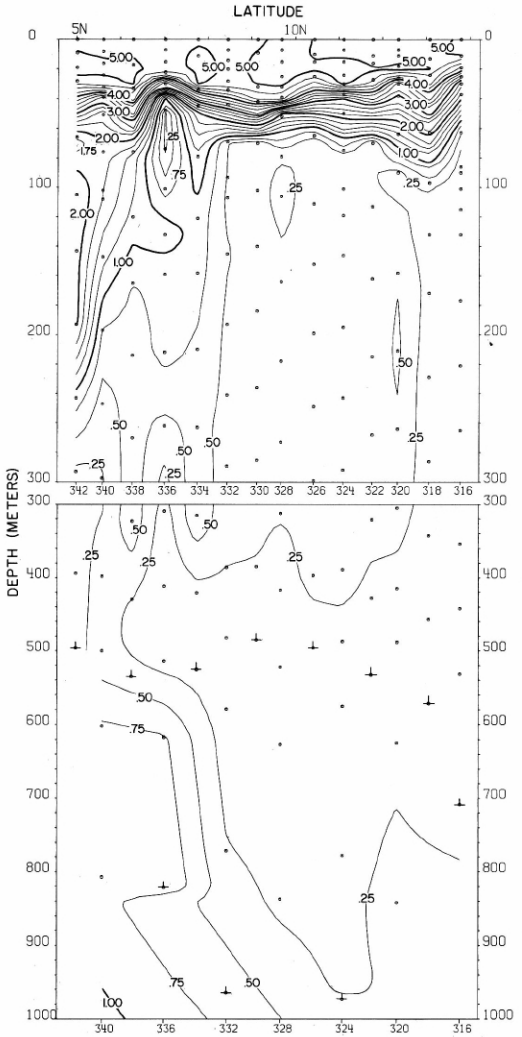

FIGURE 13-O2-v6.—Vertical distribution of oxygen (ml./l.) along 95° W., March 17-20, 1967.

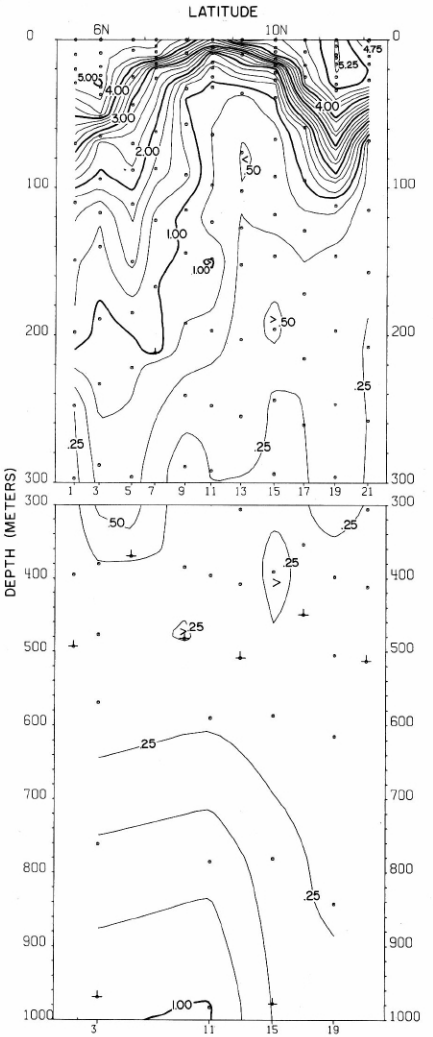

FIGURE 13-O2-v1.—Vertical distribution of oxygen (ml./l.) along 88° W., February 1-4, 1967.

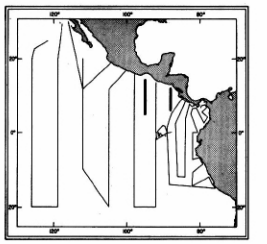

13-O2-v1.

13-O2-v6.

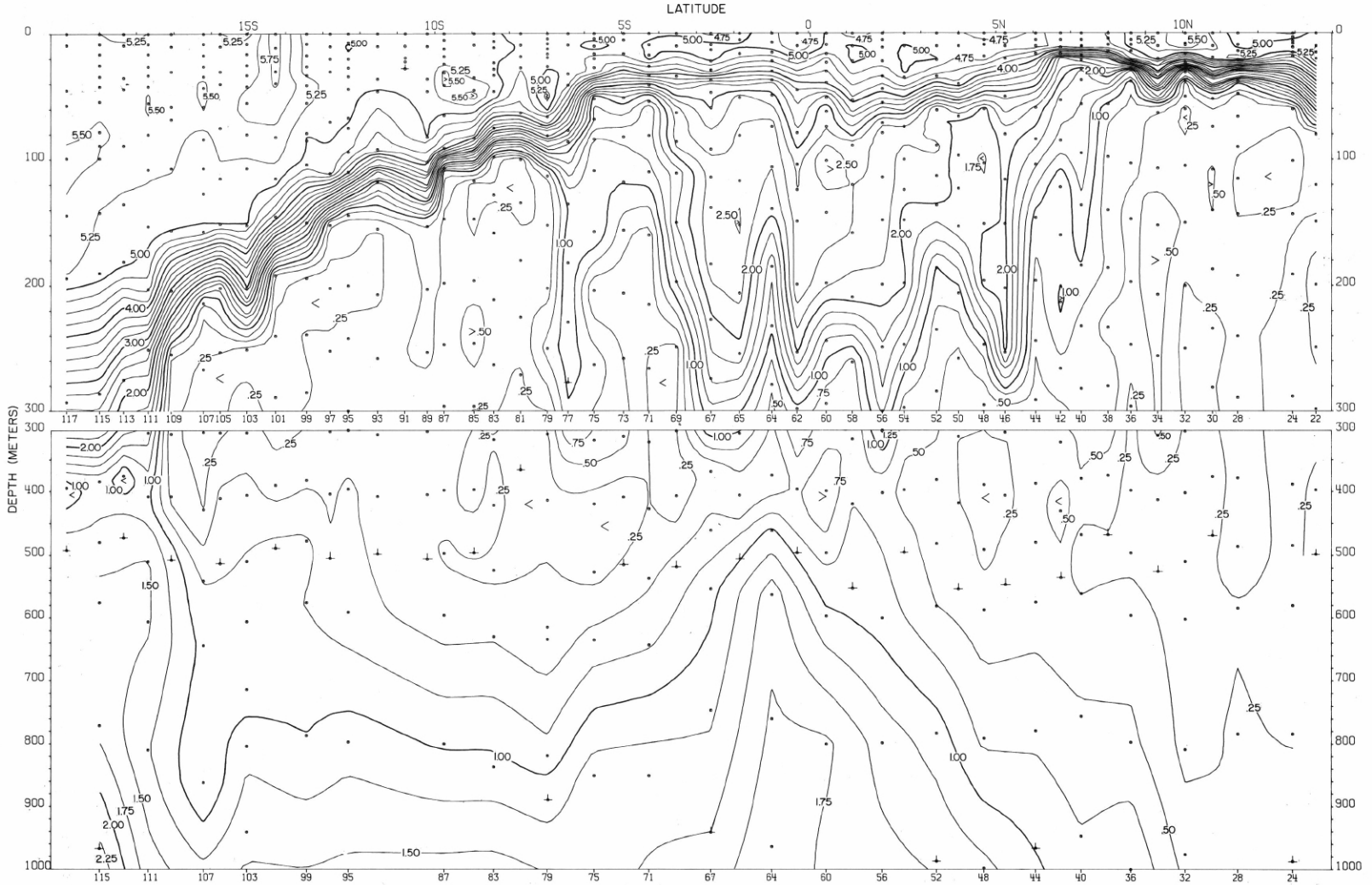

FIGURE 13-O2-v2.—Vertical distribution of oxygen (ml./l.) along 92° W., February 7-21, 1967.

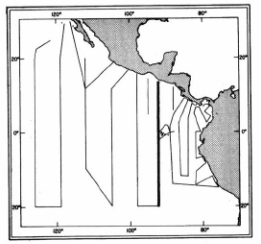

13-O2-v2.

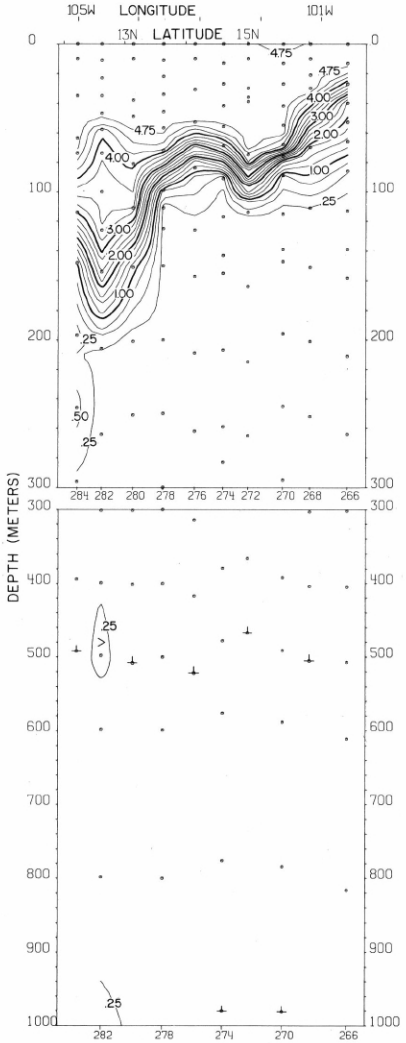

FIGURE 13-O_2-v5.—Vertical distribution of oxygen (ml./l.) along a section from Acapulco to 12° N., 105° W., March 13-15, 1967.

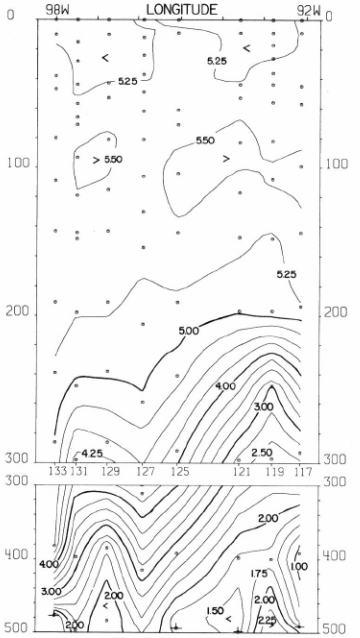

FIGURE 13-O_2-v3.—Vertical distribution of oxygen (ml./l.) along 20° S., February 21-23, 1967.

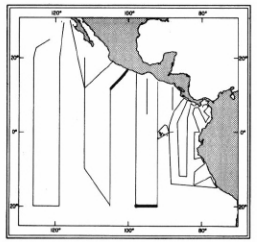

13-O_2-v3.

13-O_2-v5.

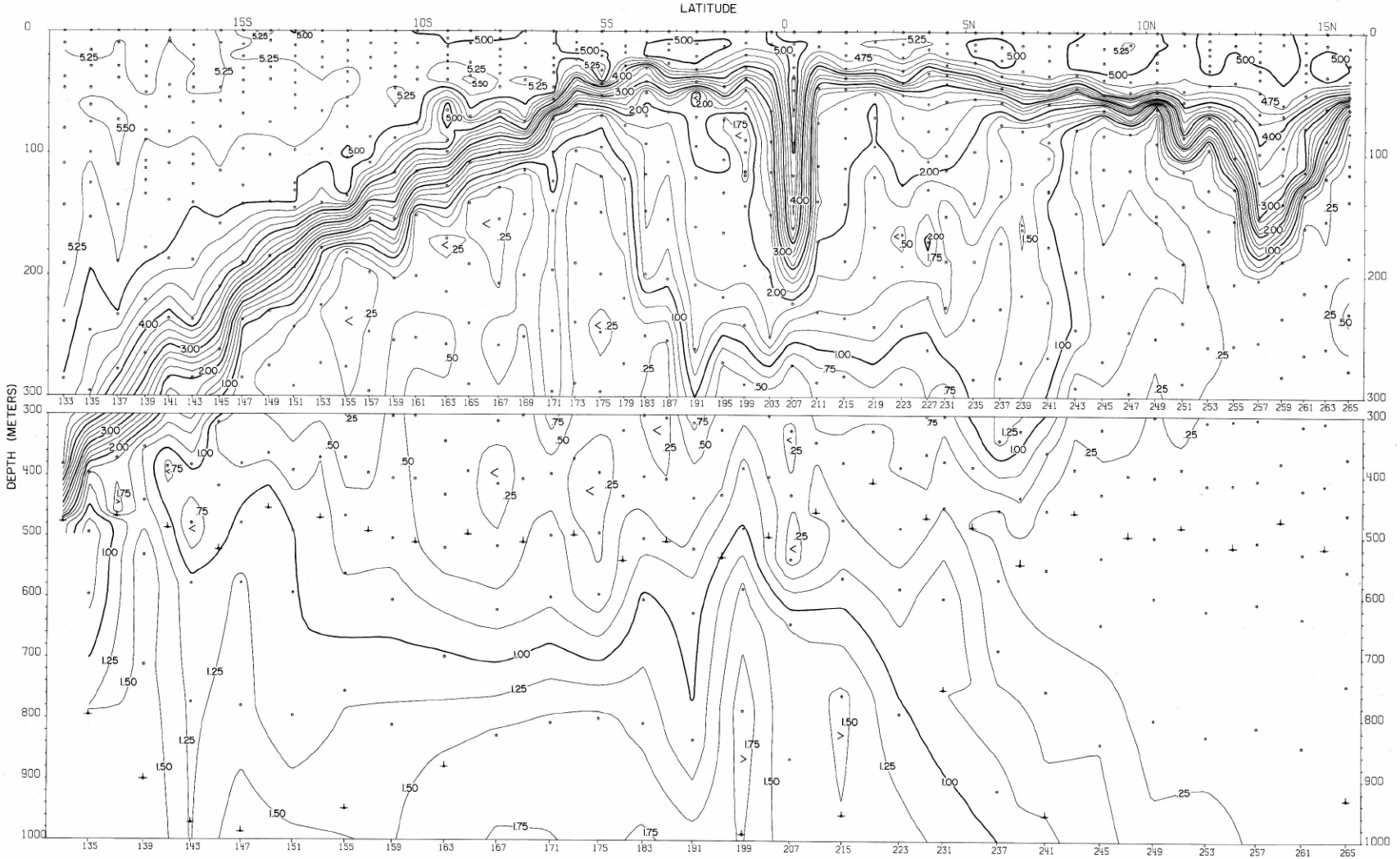

FIGURE 13-O_2-v4.—Vertical distribution of oxygen (ml./l.) along 98° W., February 23-March 8, 1967.

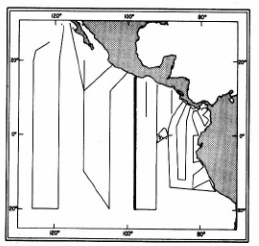

13-O_2-v4.

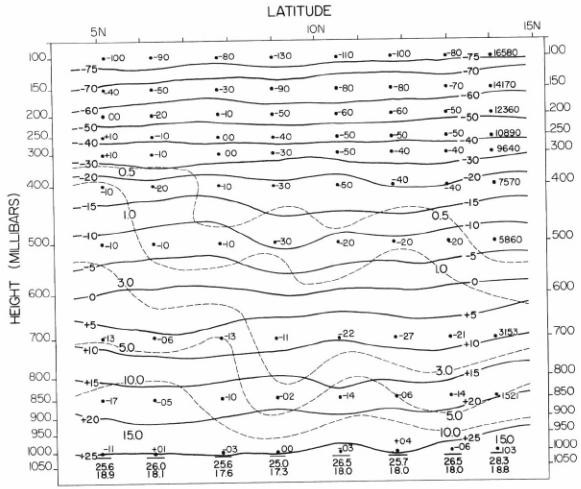

FIGURE 13-UA-v6.—Vertical section of the atmosphere along 95° W., March 16-20, 1967. Solid lines are isotherms of air temperature (°C.). Dashed lines are isopleths of mixing ratio of the air (g./kg.). Surface air temperature is plotted above surface mixing ratio and below a base line representing the surface pressure (mb.). The computed height (m.) of each standard pressure surface is plotted for the northernmost radiosonde station of the section. At other stations the difference of computed height minus the corresponding height at the northern station is shown at each standard level.

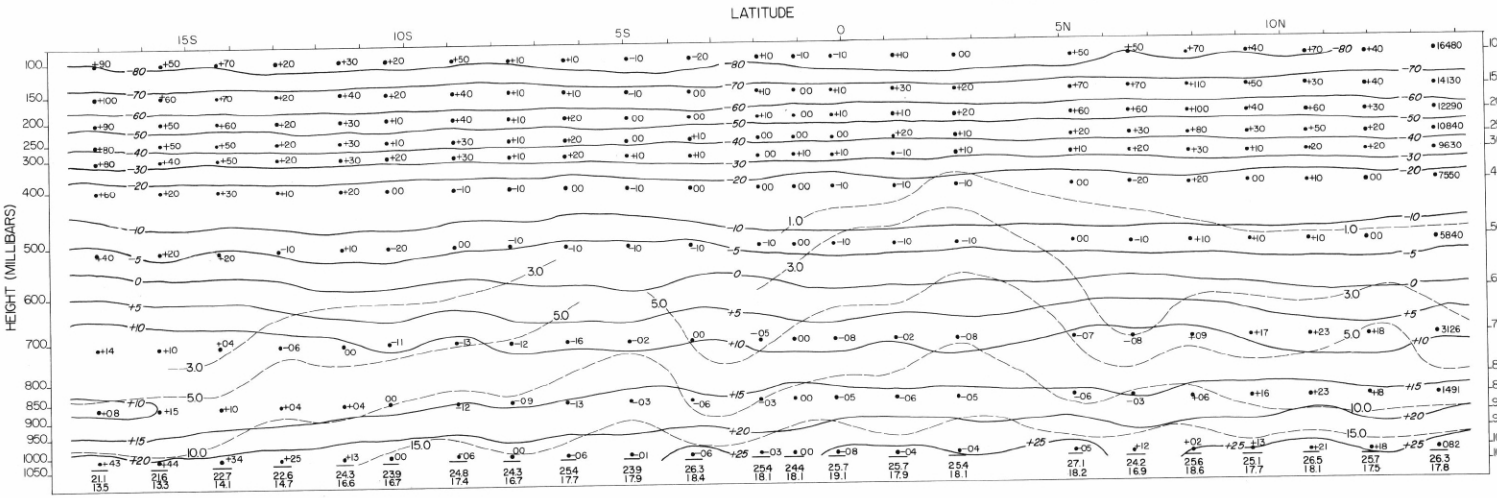

FIGURE 13-UA-v2.—Vertical section of the atmosphere along 92° W., February 8-22, 1967. Solid lines are isotherms of air temperature (°C.). Dashed lines are isopleths of mixing ratio of the air (g./kg.). Surface air temperature is plotted above surface mixing ratio and below a base line representing the surface pressure (mb.). The computed height (m.) of each standard pressure surface is plotted for the northernmost radiosonde station of the section. At other stations the difference of computed height minus the corresponding height at the northern station is shown at each standard level.

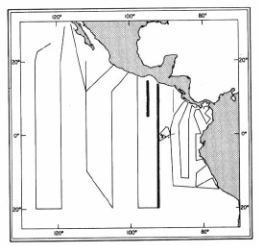

13-UA-v2.

13-UA-v6.

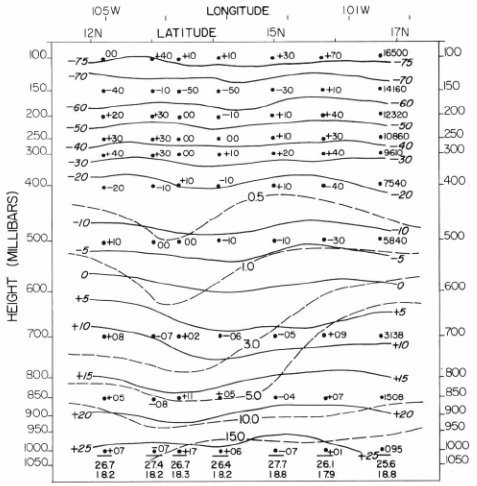

FIGURE 13-UA-v5.—Vertical section of the atmosphere along a line from Acapulco to 12° N., 105° W., March 9 and 13-15, 1967. Solid lines are isotherms of air temperature (°C.). Dashed lines are isopleths of mixing ratio of the air (g./kg.). Surface air temperature is plotted above surface mixing ratio and below a base line representing the surface pressure (mb.). The computed height (m.) of each standard pressure surface is plotted for the northernmost radiosonde station of the section. At other stations the difference of computed height minus the corresponding height at the northern station is shown at each standard level.

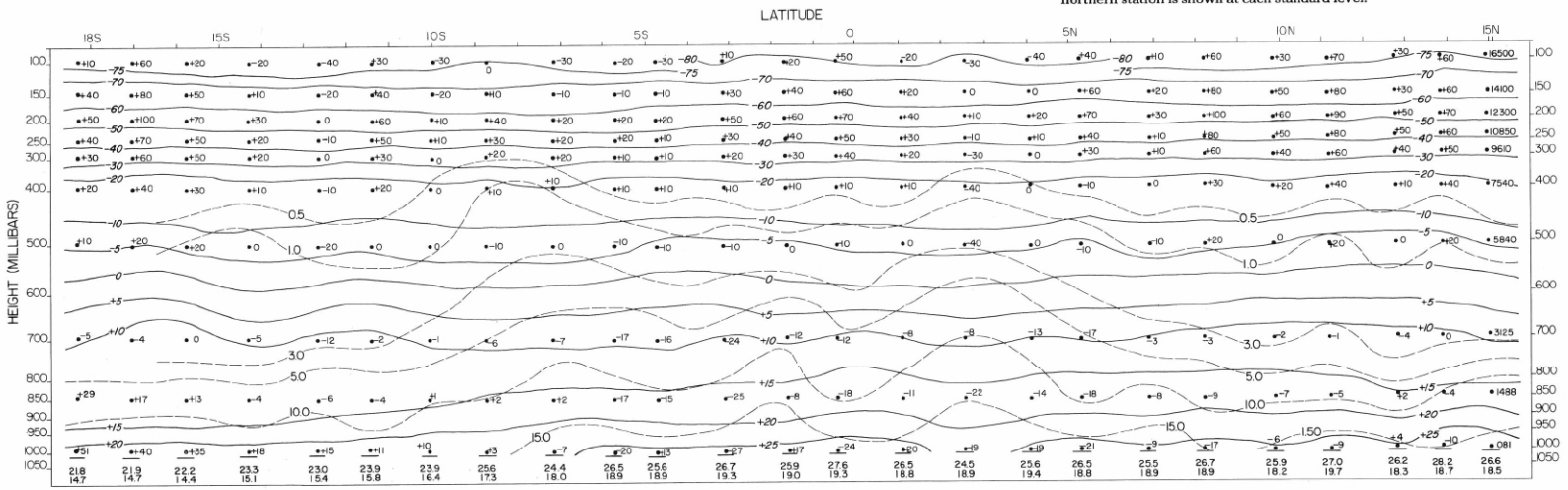

FIGURE 13-UA-v4.—Vertical section of the atmosphere along 98° W., February 23-March 8, 1967. Solid lines are isotherms of air temperature (°C.). Dashed lines are isopleths of mixing ratio of the air (g./kg.). Surface air temperature is plotted above surface mixing ratio and below a base line representing the surface pressure (mb.). The computed height (m.) of each standard pressure surface is plotted for the northernmost radiosonde station of the section. At other stations the difference of computed height minus the corresponding height at the northern station is shown at each standard level.

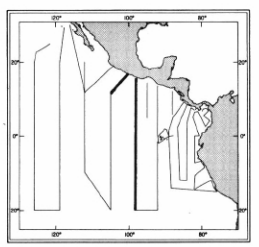

13-UA-v4.

13-UA-v5.

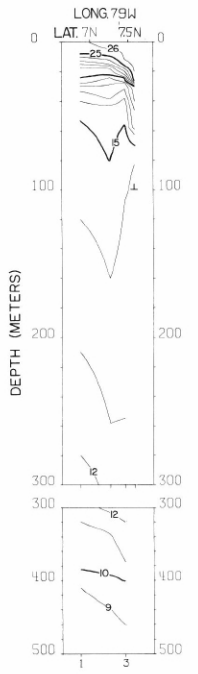

FIGURE 14-T-v1.—Vertical distribution of temperature (°C.) along a southwest-northeast section in the northern portion of the Panama Bight from 79°44′ W. to 78°43′ W., January 31, 1967. These contours are based on STD data read principally from analog traces.

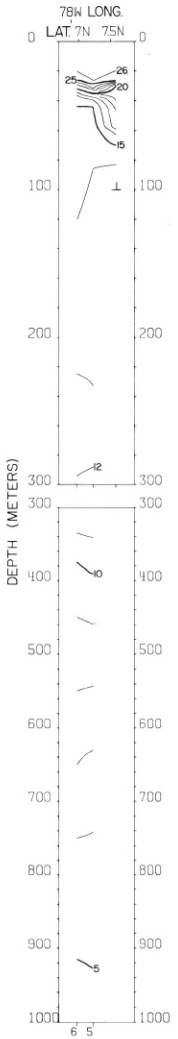

FIGURE 14-T-v2.—Vertical distribution of temperature (°C.) along a section in the Panama Bight near the coasts of Panama and Colombia from 7°35′ N. to 6°58′ N., January 31-February 1, 1967. These contours are based on STD data read principally from analog traces.

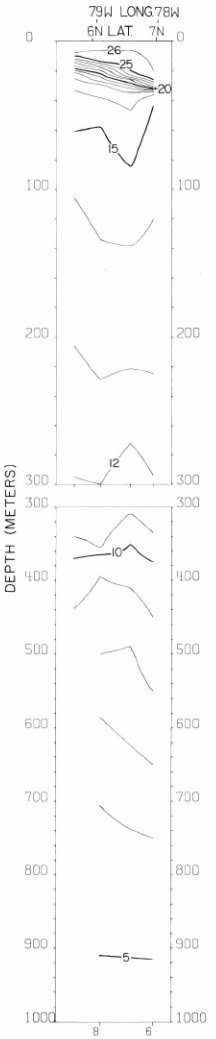

FIGURE 14-T-v3.—Vertical distribution of temperature (°C.) along a northeast-southwest section in the Panama Bight from the coast of Colombia to 5°43′ N., 79°22′ W., February 1, 1967. These contours are based on STD data read principally from analog traces.

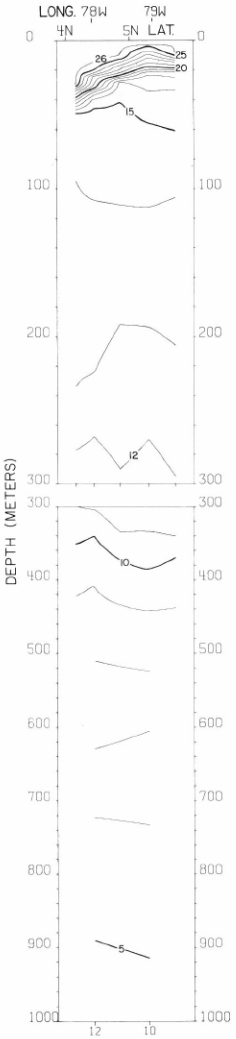

FIGURE 14-T-v4.—Vertical distribution of temperature (°C.) along a northwest-southeast section in the central portion of the Panama Bight from 5°43′ N., 79°22′ W. to the coast of Colombia, February 1-2, 1967. These contours are based on STD data read principally from analog traces.

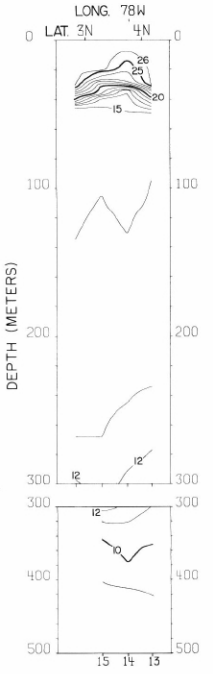

FIGURE 14-T-v5.—Vertical distribution of temperature (°C.) along a section in the Panama Bight near the coast of Colombia from 4°10′ N. to 2°45′ N., February 2-3, 1967. These contours are based on STD data read principally from analog traces.

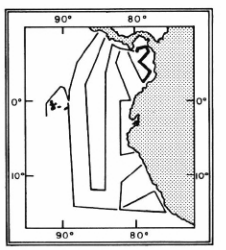

14-T-v1.

14-T-v2.

14-T-v3.

14-T-v4.

14-T-v5.

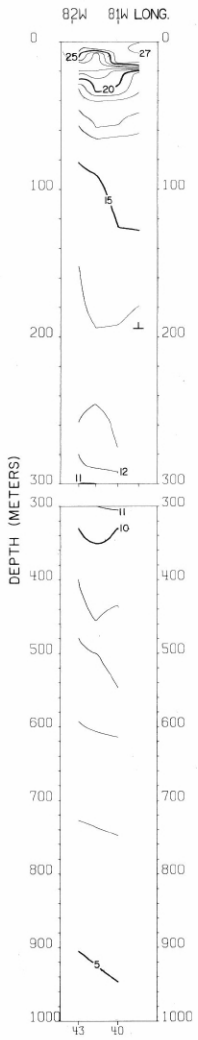

FIGURE 14-T-v9.—Vertical distribution of temperature (°C.) along the Equator from the coast of Ecuador to 81°54′ W., February 8-9, 1967. These contours are based on STD data read principally from analog traces.

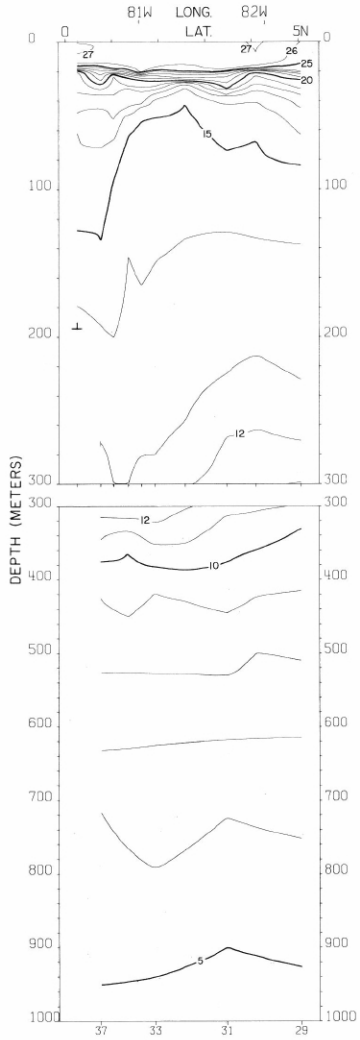

FIGURE 14-T-v8.—Vertical distribution of temperature (°C.) along a northwest-southeast section from 5°03′ N., 82°18′ W. to the coast of Ecuador, February 6-8, 1967. These contours are based on STD data read principally from analog traces.

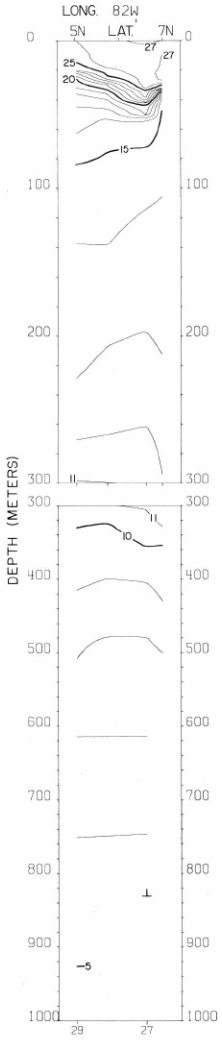

FIGURE 14-T-v7.—Vertical distribution of temperature (°C.) along a northeast-southwest section from Isla Coiba, Panama to 5°03′ N., 82°18′ W., February 5-6, 1967. These contours are based on STD data read principally from analog traces.

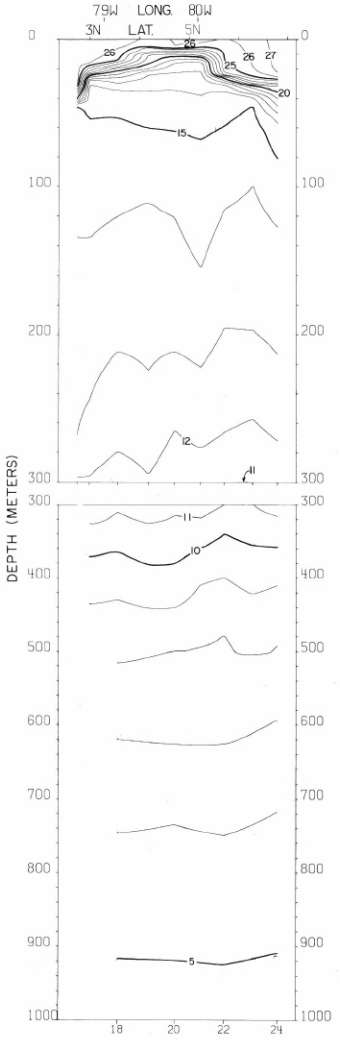

FIGURE 14-T-v6.—Vertical distribution of temperature (°C.) along a southeast-northwest section across the Panama Bight from the coast of Colombia to Peninsula de Azuero, Panama, February 3-5, 1967. These contours are based on STD data read principally from analog traces.

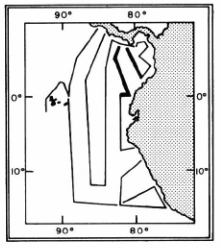

14-T-v6.

14-T-v7.

14-T-v8.

14-T-v9.

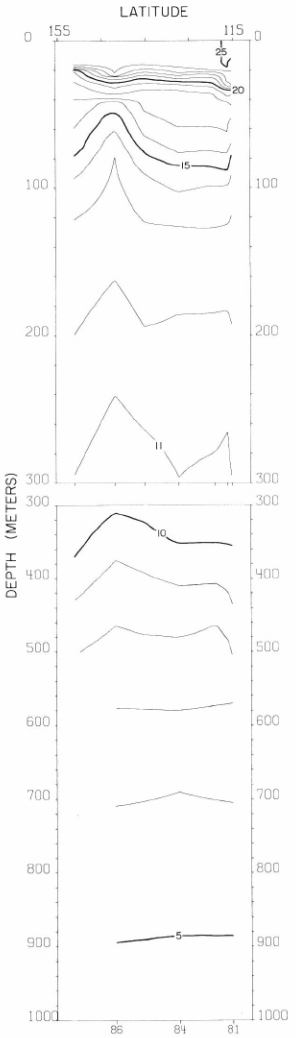

FIGURE 14-T-v13.—Vertical distribution of temperature (°C.) along 81°46′ W. from 11°02′ S. to 14°37′ S., February 14-15, 1967. These contours are based on STD data read principally from analog traces.

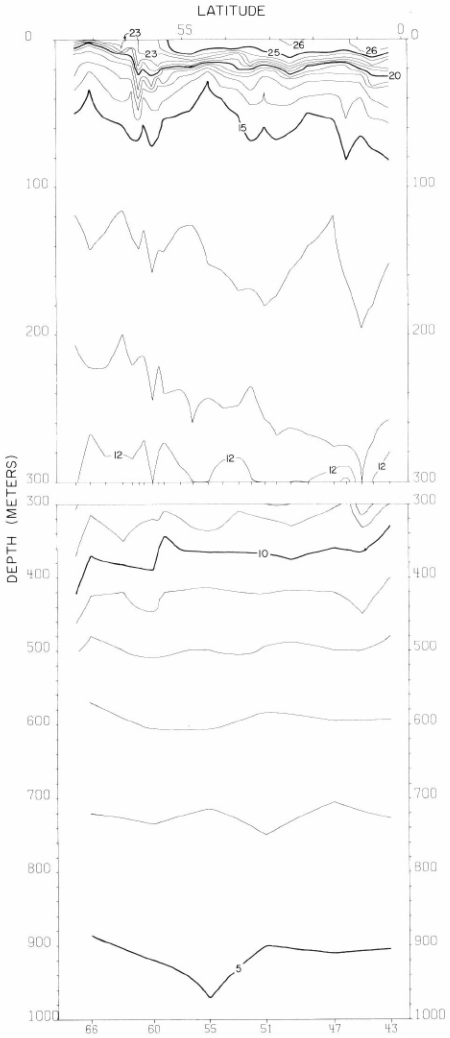

FIGURE 14-T-v10.—Vertical distribution of temperature (°C.) along 82° W. from 0°18′ S. to 7°27′ S., February 9-11, 1967. These contours are based on STD data read principally from analog traces.

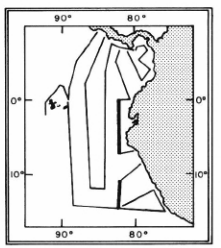

14-T-v10.

14-T-v13.

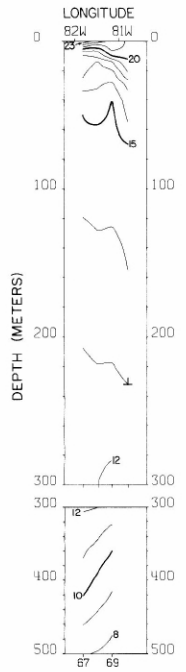

FIGURE 14-T-v11.—Vertical distribution of temperature (°C.) along 7°15′ S. from 81°50′ W. to the coast of Peru, February 11-12, 1967. These contours are based on STD data read principally from analog traces.

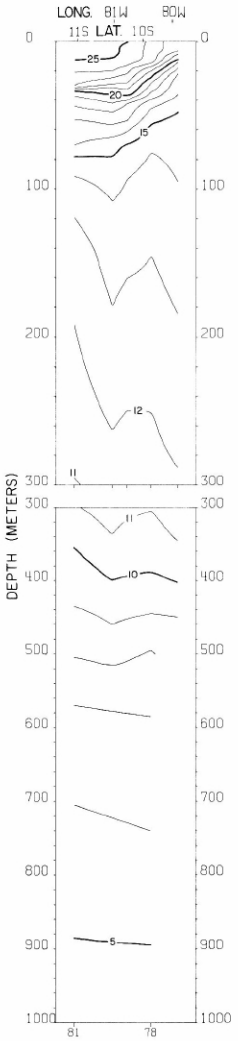

FIGURE 14-T-v12.—Vertical distribution of temperature (°C.) along a northeast-southwest section from the coast of Peru to 11° S., 81°46′ W., February 13-14, 1967. These contours are based on STD data read principally from analog traces.

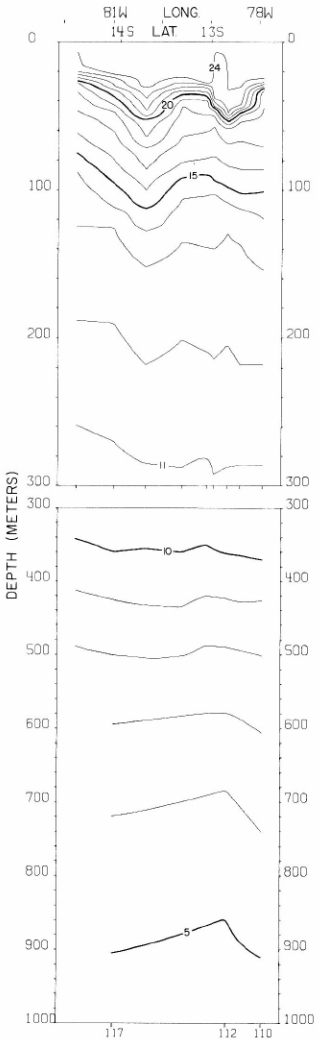

FIGURE 14-T-v16.—Vertical distribution of temperature (°C.) along a northeast-southwest section from the coast of Peru to 14°30′ S., 81°43′ W., February 24-25, 1967. These contours are based on STD data read principally from analog traces.

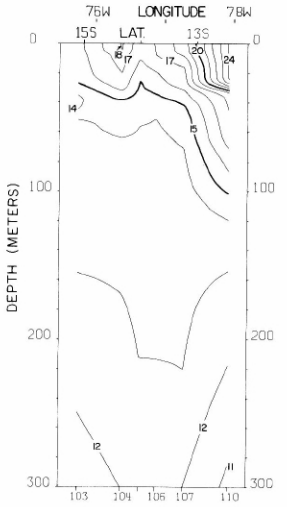

FIGURE 14-T-v15.—Vertical distribution of temperature (°C.) along the coast of Peru from 15°07′ S. to 12°27′ S., February 17-24, 1967. These contours are based on STD data read principally from analog traces.

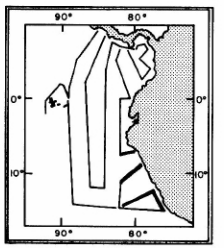

14-T-v11.

14-T-v12.

14-T-v15.

14-T-v16.

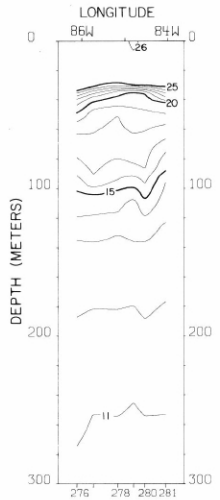

FIGURE 14-T-v25.—Vertical distribution of temperature (°C.) along 12° S., March 25-26, 1967. These contours are based on STD data read principally from analog traces.

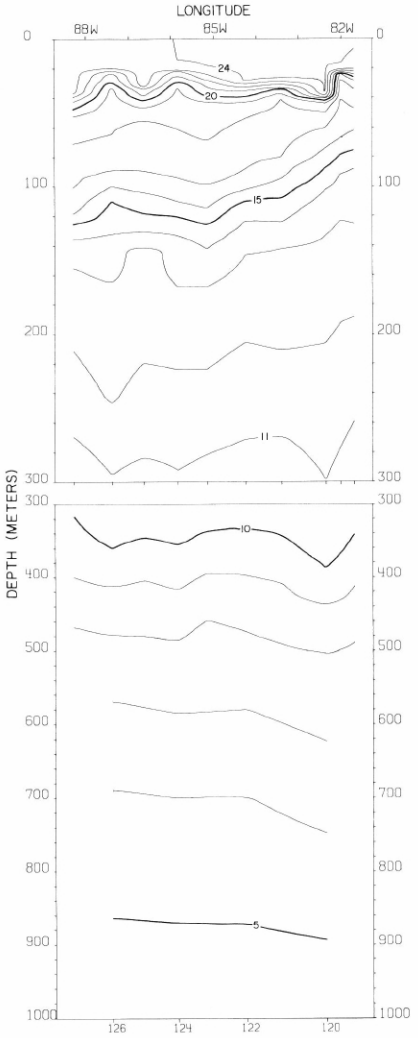

FIGURE 14-T-v17.—Vertical distribution of temperature (°C.) along 14°30′ S. from 81°43′ W. to 88°17′ W., February 25-27, 1967. These contours are based on STD data read principally from analog traces.

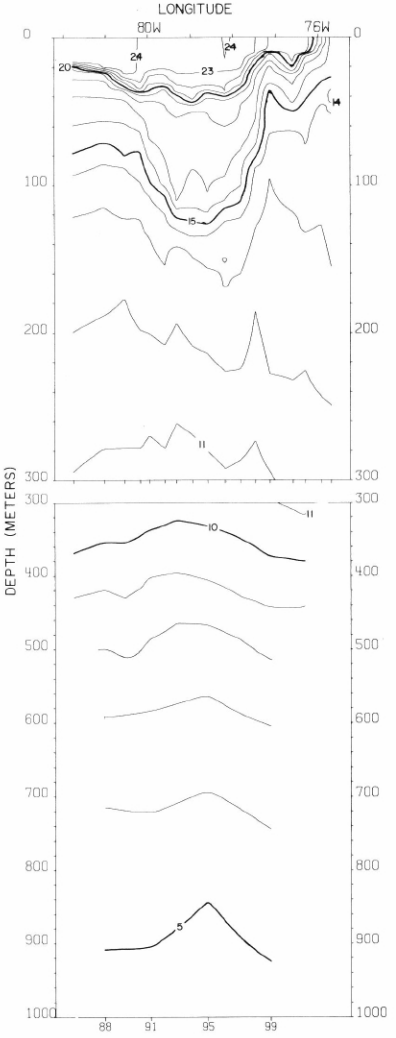

FIGURE 14-T-v14.—Vertical distribution of temperature (°C.) along 15° S. from 81°46′ W. to the coast of Peru, February 15-17, 1967. These contours are based on STD data read principally from analog traces.

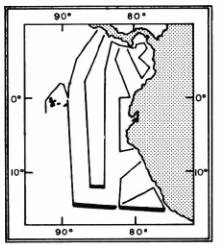

14-T-v14.

14-T-v17.

14-T-v25.

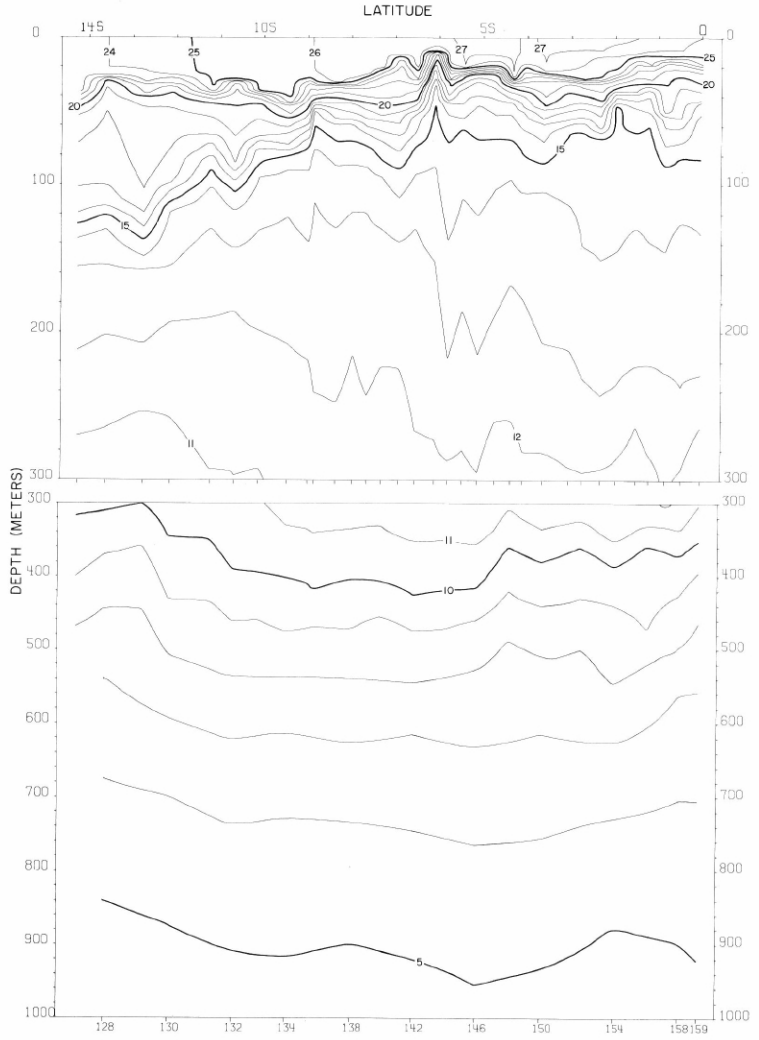

FIGURE 14-T-v18.—Vertical distribution of temperature (°C.) along 88°46′ W., February 27-March 4, 1967. These contours are based on STD data read principally from analog traces.

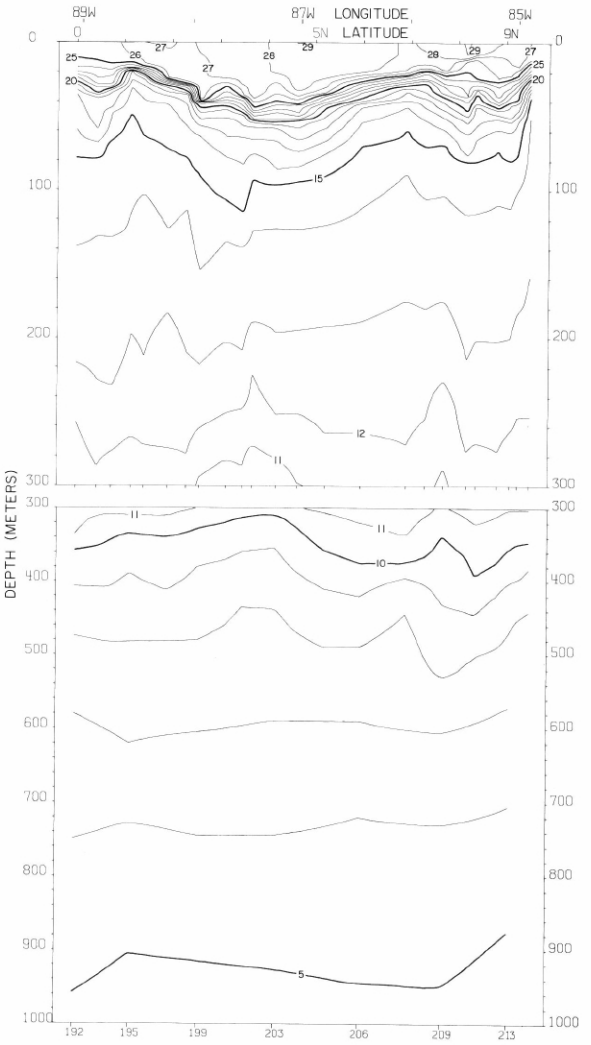

FIGURE 14-T-v22.—Vertical distribution of temperature (°C.) along a southwest-northeast section from the Equator at 89°03′ W. to Puntarenas, March 11-15, 1967. These contours are based on STD data read principally from analog traces.

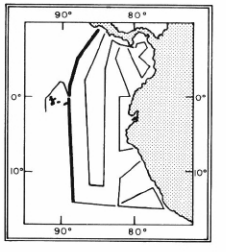

14-T-v18.

14-T-v22.

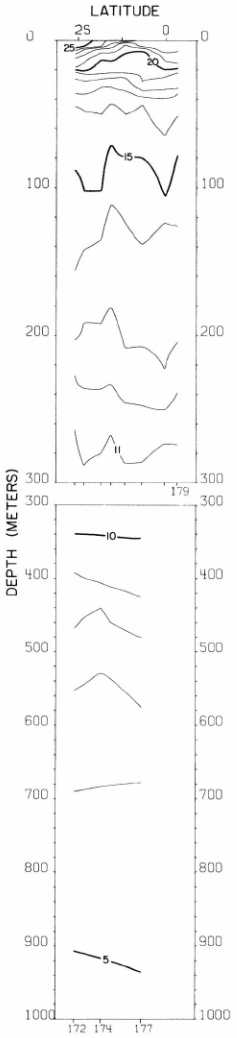

FIGURE 14-T-v19.—Vertical distribution of temperature (°C.) along 92° W., west of the Galapagos Islands, March 8-9, 1967. These contours are based on STD data read principally from analog traces.

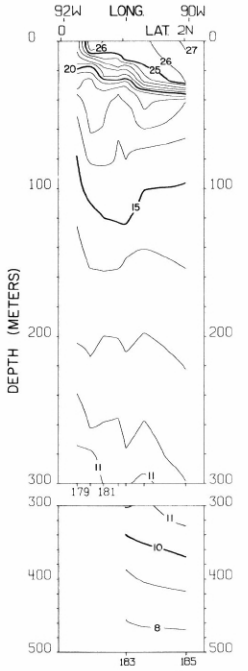

FIGURE 14-T-v20.—Vertical distribution of temperature (°C.) along a section north of the Galapagos Islands, from 0°16′ N., 91°47′ W. to 2°01′ N., 90°03′ W., March 9-10, 1967. These contours are based on STD data read principally from analog traces.

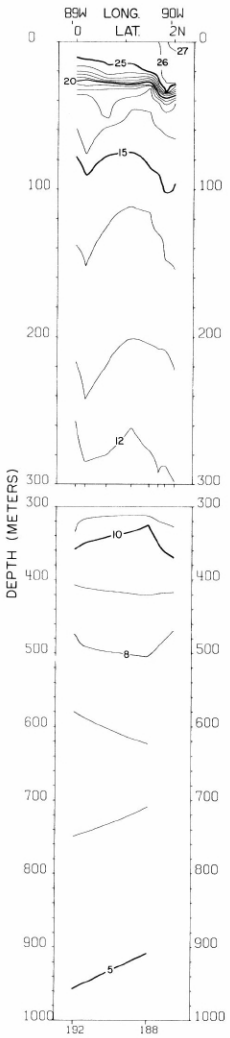

FIGURE 14-T-v21.—Vertical distribution of temperature (°C.) along a section northeast of the Galapagos Islands, from 2°01′ N., 90°03′ W. to the Equator at 89°03′ W., March 11, 1967. These contours are based on STD data read principally from analog traces.

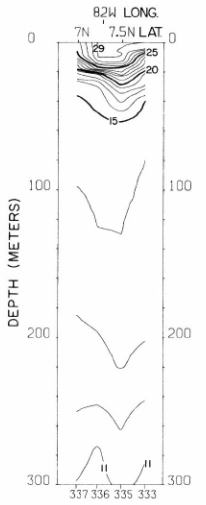

FIGURE 14-T-v28.—Vertical distribution of temperature (°C.) along the coast of Panama from 82°50′ W. to 81°28′ W., April 2, 1967. These contours are based on STD data read principally from analog traces.

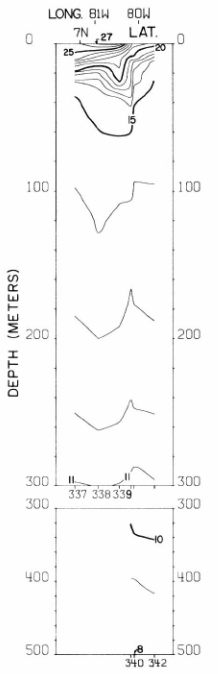

FIGURE 14-T-v29.—Vertical distribution of temperature (°C.) along the coast of Panama from 81°28′ W. to 79°38′ W., April 2-3, 1967. These contours are based on STD data read principally from analog traces.

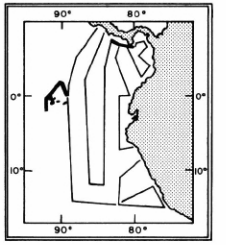

14-T-v19.

14-T-v20.

14-T-v21.

14-T-v28.

14-T-v29.

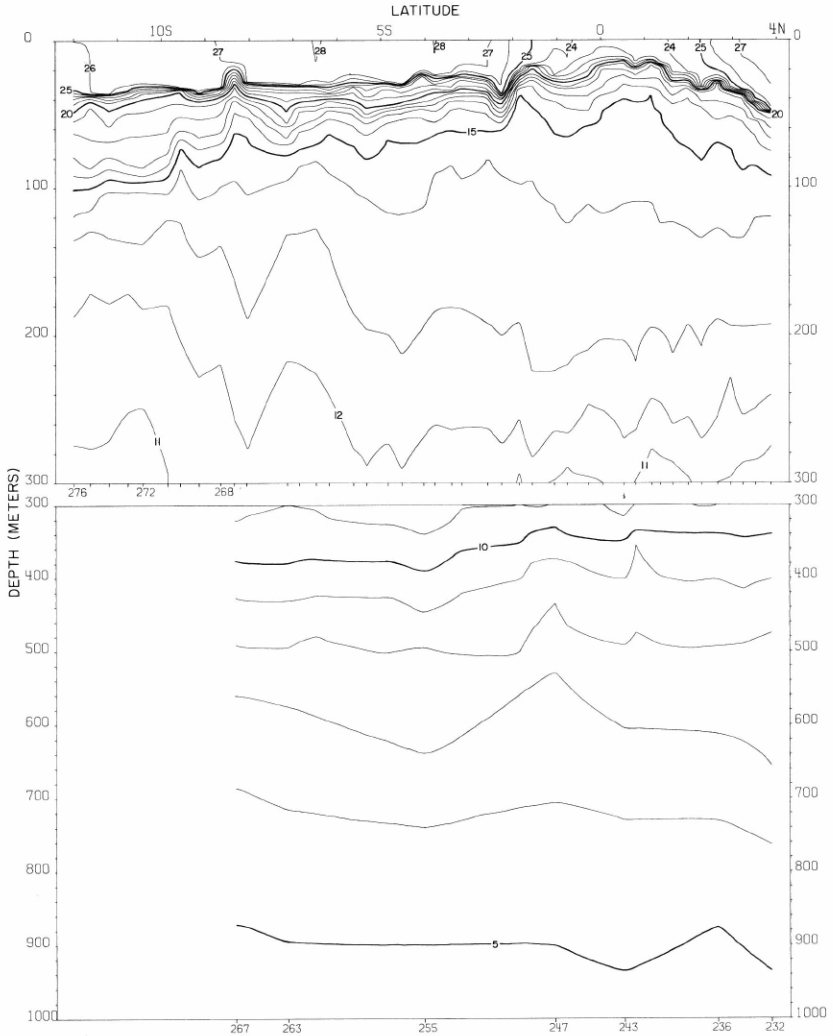

FIGURE 14-T-v24.—Vertical distribution of temperature (°C.) along 86°19′ W., March 20-25, 1967. These contours are based on STD data read principally from analog traces.

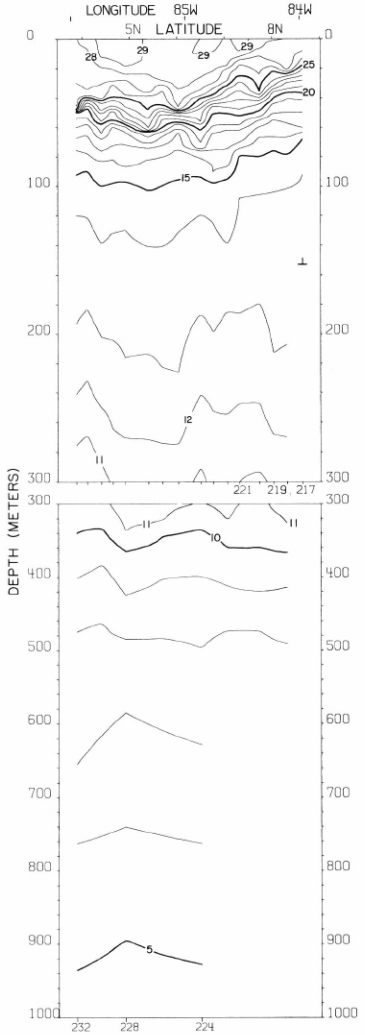

FIGURE 14-T-v23.—Vertical distribution of temperature (°C.) along a northeast-southwest section from the coast of Costa Rica to 3°52′ N., 85°57′ W., March 18-20, 1967. These contours are based on STD data read principally from analog traces.

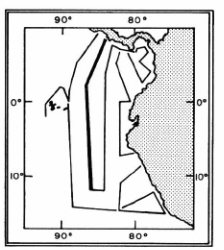

14-T-v23.

14-T-v24.

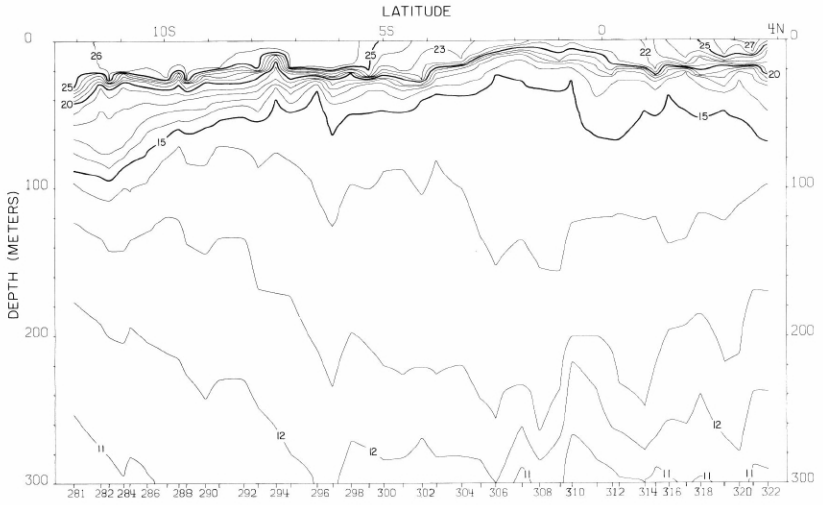

FIGURE 14-T-v26.—Vertical distribution of temperature (°C.) along 84° W., March 26-31, 1967. These contours are based on STD data read principally from analog traces.

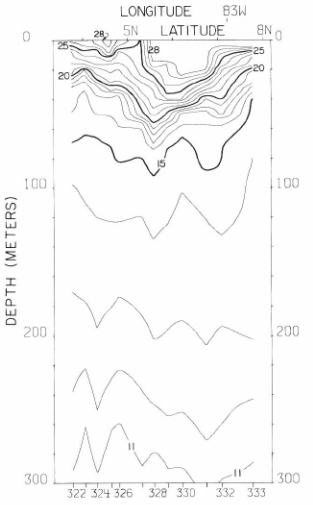

FIGURE 14-T-v27.—Vertical distribution of temperature (°C.) along a southwest-northeast section from 3°45′ N., 83°48′ W. to Punta Burica, Costa Rica-Panama, March 31-April 2, 1967. These contours are based on STD data read principally from analog traces.

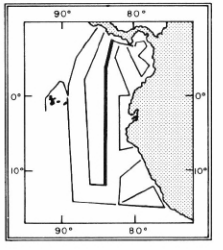

14-T-v26.

14-T-v27.

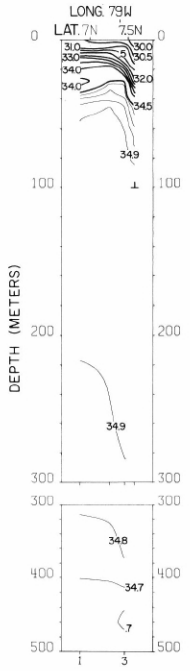

FIGURE 14-S-v1.—Vertical distribution of salinity (‰) along a southwest-northeast section in the northern portion of the Panama Bight from 79°44′ W. to 78°43′ W., January 31, 1967. These contours are based on STD data read principally from analog traces.

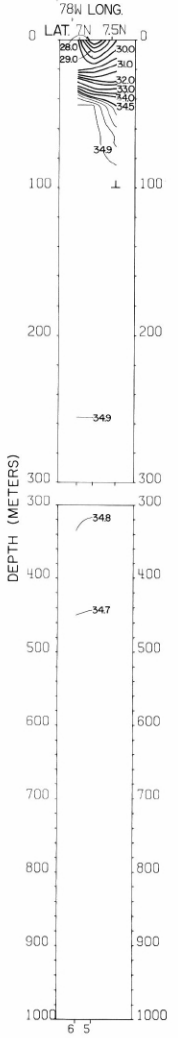

FIGURE 14-S-v2.—Vertical distribution of salinity (‰) along a section in the Panama Bight near the coasts of Panama and Colombia from 7°35′ N. to 6°58′ N., January 31-February 1, 1967. These contours are based on STD data read principally from analog traces.

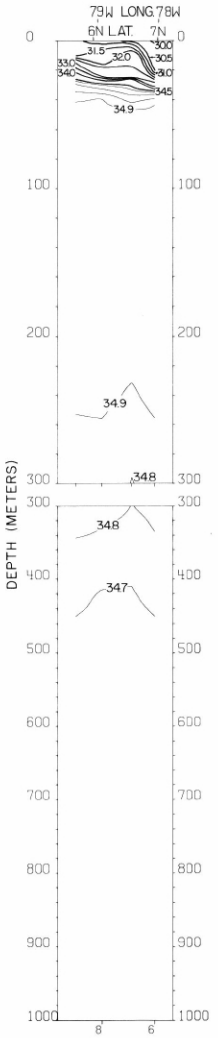

FIGURE 14-S-v3.—Vertical distribution of salinity (‰) along a northeast-southwest section in the Panama Bight from the coast of Colombia to 5°43′ N., 79°22′ W., February 1, 1967. These contours are based on STD data read principally from analog traces.

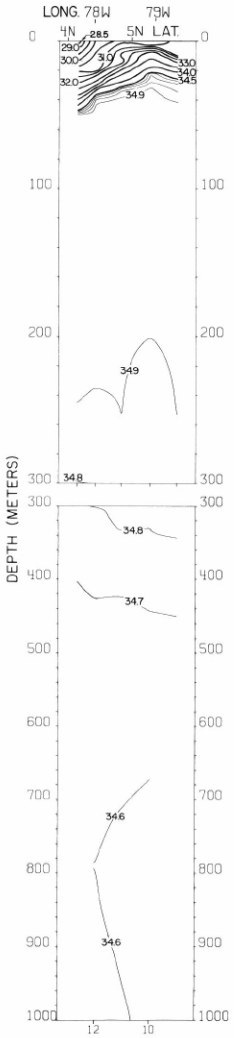

FIGURE 14-S-v4.—Vertical distribution of salinity (‰) along a northwest-southeast section in the central portion of the Panama Bight from 5°43′ N., 79°22′ W. to the coast of Colombia, February 1-2, 1967. These contours are based on STD data read principally from analog traces.

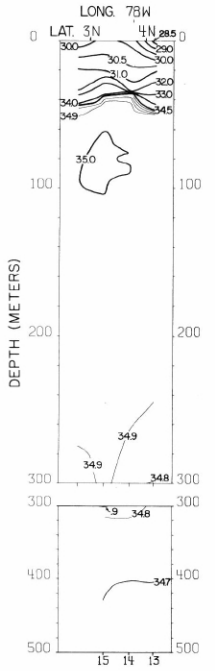

FIGURE 14-S-v5.—Vertical distribution of salinity (‰) along a section in the Panama Bight near the coast of Colombia from 4°10′ N. to 2°45′ N., February 2-3, 1967. These contours are based on STD data read principally from analog traces.

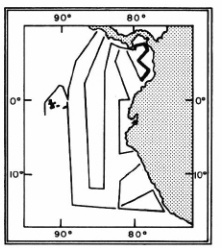

14-S-v1.

14-S-v2.

14-S-v3.

14-S-v4.

14-S-v5.

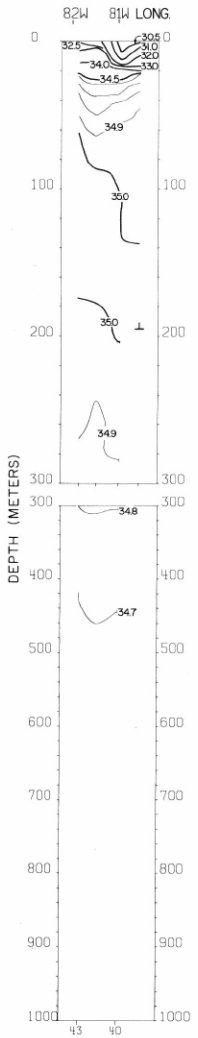

FIGURE 14-S-v9.—Vertical distribution of salinity (‰) along the Equator from the coast of Ecuador to 81°54′ W., February 8-9, 1967. These contours are based on STD data read principally from analog traces.

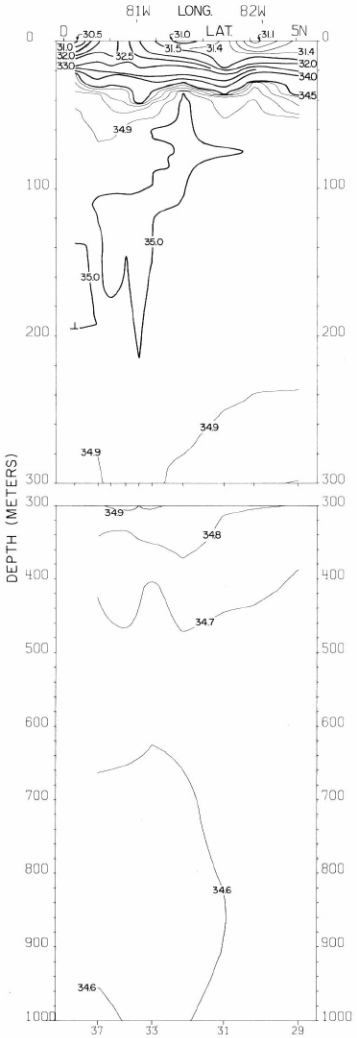

FIGURE 14-S-v8.—Vertical distribution of salinity (‰) along a northwest-southeast section from 5°03′ N., 82°18′ W. to the coast of Ecuador, February 6-8, 1967. These contours are based on STD data read principally from analog traces.

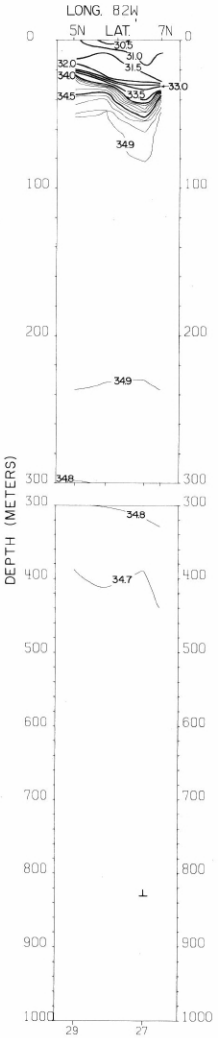

FIGURE 14-S-v7.—Vertical distribution of salinity (‰) along a northeast-southwest section from Isla Coiba, Panama to 5°03′ N., 82°18′ W., February 5-6, 1967. These contours are based on STD data read principally from analog traces.

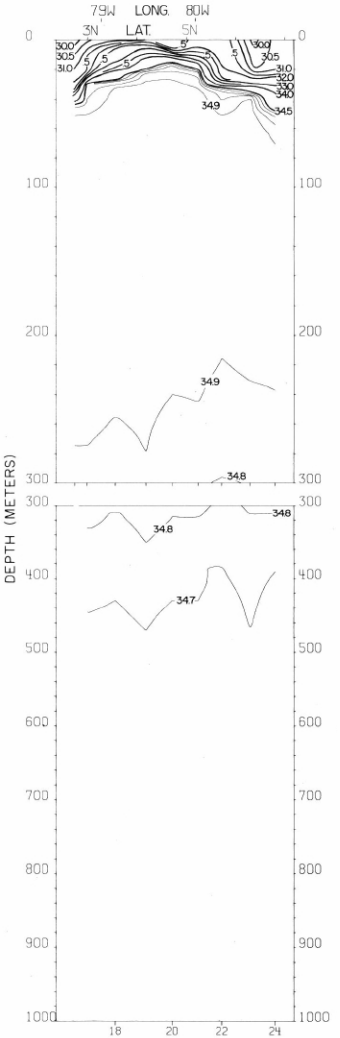

FIGURE 14-S-v6.—Vertical distribution of salinity (‰) along a southeast-northwest section across the Panama Bight from the coast of Colombia to Peninsula de Azuero, Panama, February 3-5, 1967. These contours are based on STD data read principally from analog traces.

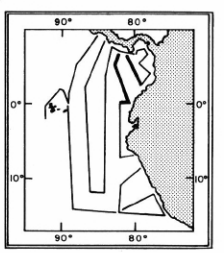

14-S-v6.

14-S-v7.

14-S-v8.

14-S-v9.

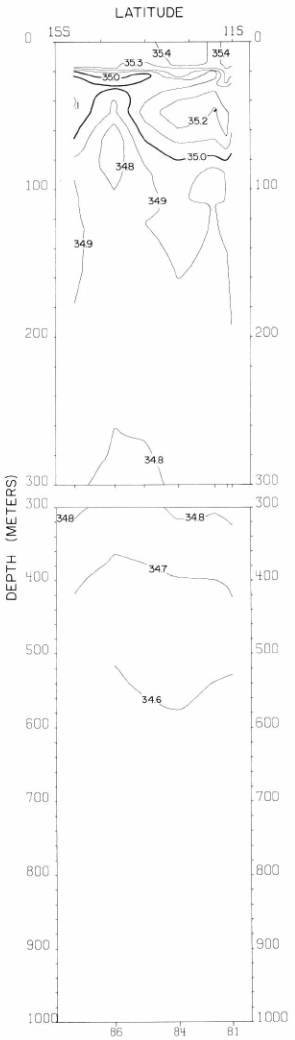

FIGURE 14-S-v13.—Vertical distribution of salinity (‰) along 81°46′ W. from 11°02′ S. to 14°37′ S., February 14-15, 1967. These contours are based on STD data read principally from analog traces.

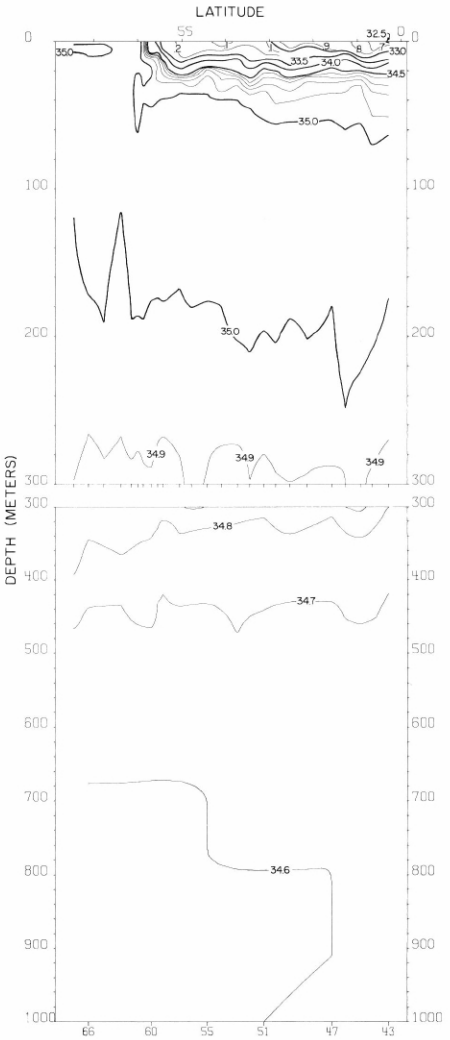

FIGURE 14-S-v10.—Vertical distribution of salinity (‰) along 82° W. from 0°18′ S. to 7°27′ S., February 9-11, 1967. These contours are based on STD data read principally from analog traces.

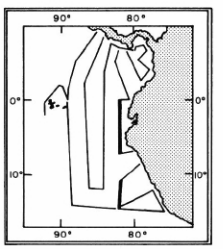

14-S-v10.

14-S-v13.

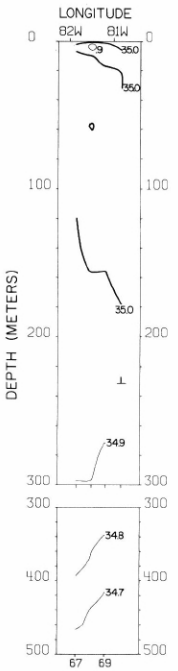

FIGURE 14-S-v11.—Vertical distribution of salinity (‰) along 7°15′ S. from 81°50′ W. to the coast of Peru, February 11-12, 1967. These contours are based on STD data read principally from analog traces.

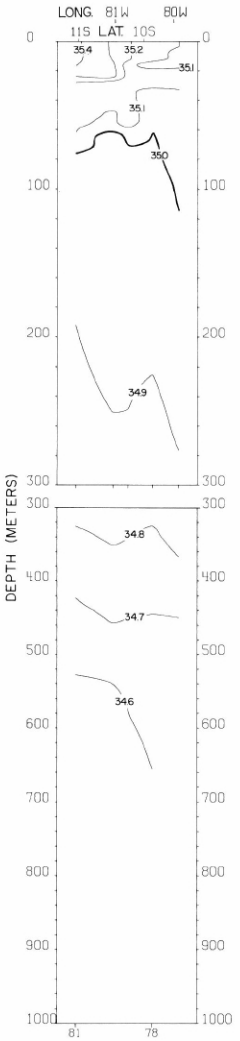

FIGURE 14-S-v12.—Vertical distribution of salinity (‰) along a northeast-southwest section from the coast of Peru to 11° S., 81°46′ W., February 13-14, 1967. These contours are based on STD data read principally from analog traces.

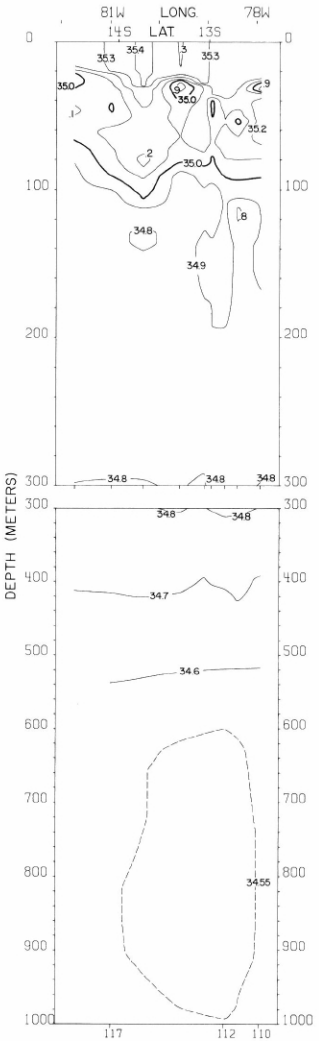

FIGURE 14-S-v16.—Vertical distribution of salinity (‰) along a northeast-southwest section from the coast of Peru to 14°30′ S., 81°43′ W., February 24-25, 1967. These contours are based on STD data read principally from analog traces.

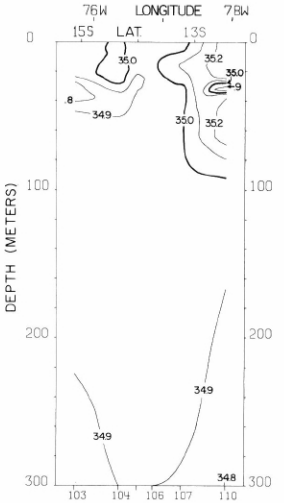

FIGURE 14-S-v15.—Vertical distribution of salinity (‰) along the coast of Peru from 15°07′ S. to 12°27′ S., February 17-24, 1967. These contours are based on STD data read principally from analog traces.

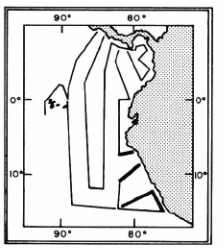

14-S-v11.

14-S-v12.

14-S-v15.

14-S-v16.

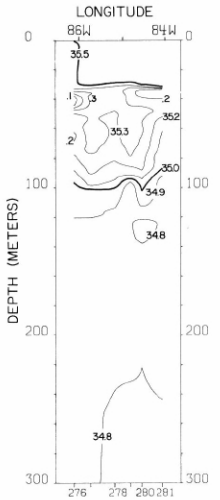

FIGURE 14-S-v25.—Vertical distribution of salinity (‰) along 12° S., March 25-26, 1967. These contours are based on STD data read principally from analog traces.

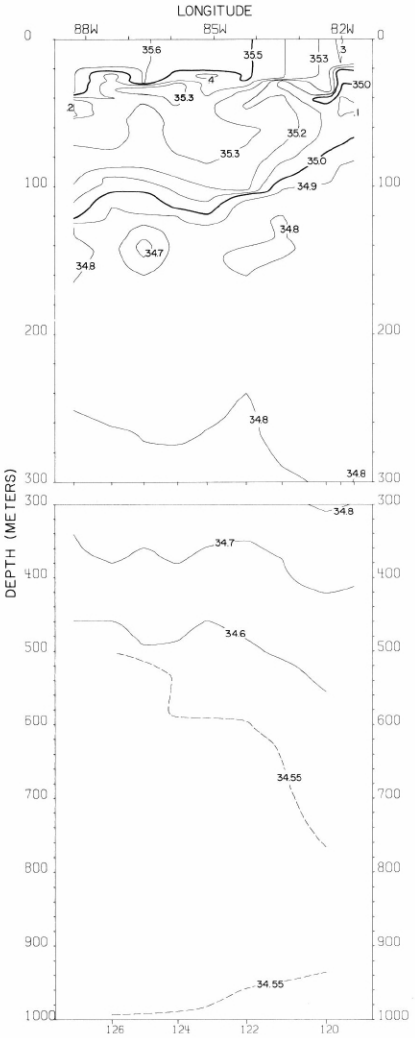

FIGURE 14-S-v17.—Vertical distribution of salinity (‰) along 14°30′ S. from 81°43′ W. to 88°17′ W., February 25-27, 1967. These contours are based on STD data read principally from analog traces.

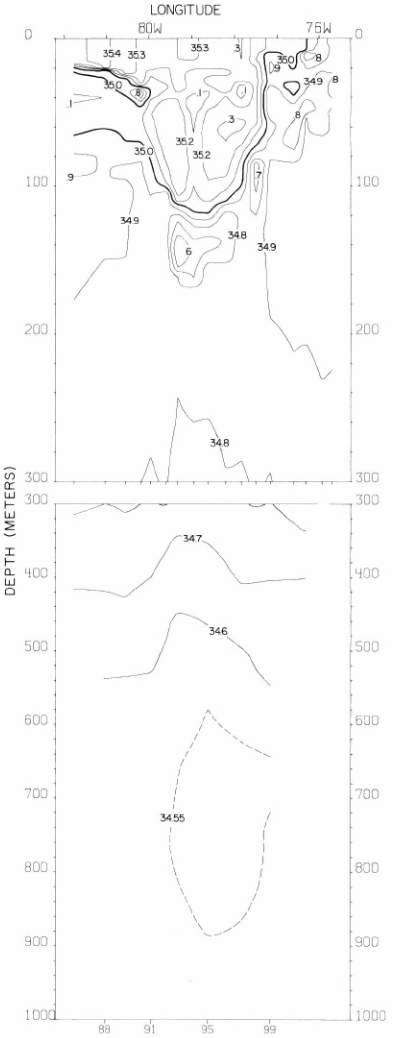

FIGURE 14-S-v14.—Vertical distribution of salinity (‰) along 15° S. from 81°46′ W. to the coast of Peru, February 15-17, 1967. These contours are based on STD data read principally from analog traces.

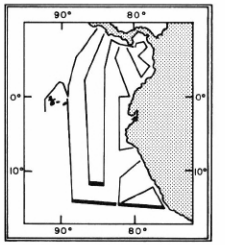

14-S-v14.

14-S-v17.

14-S-v25.

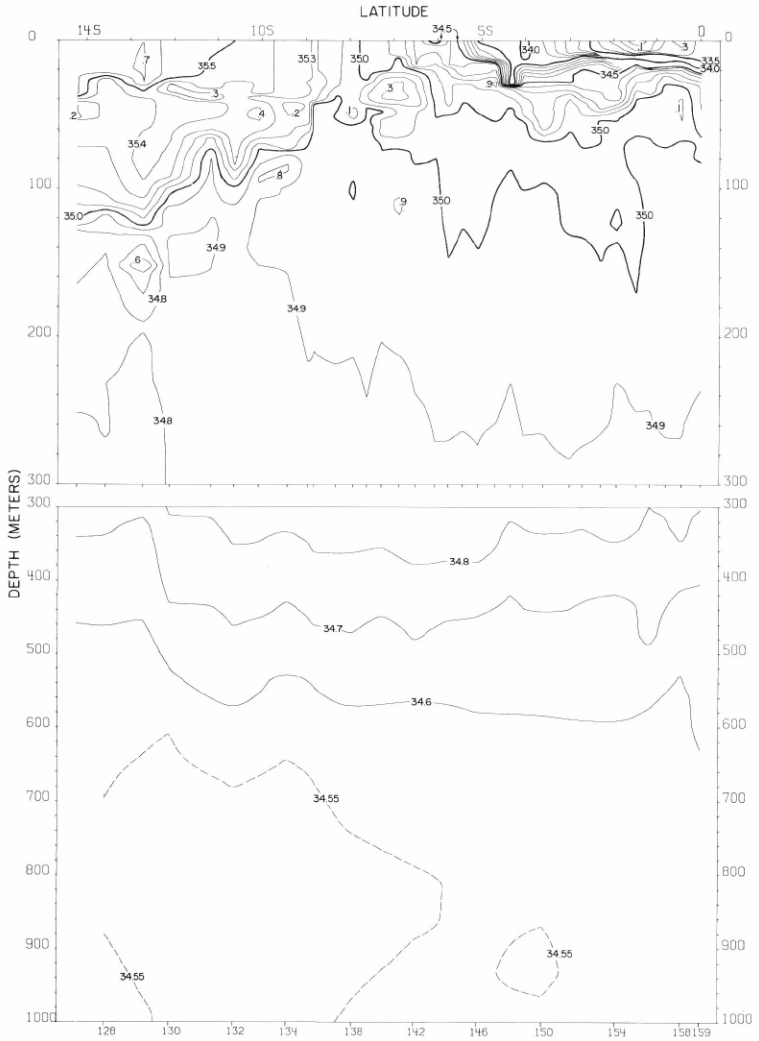

FIGURE 14-S-v18.—Vertical distribution of salinity (‰) along 88°46′ W., February 27-March 4, 1967. These contours are based on STD data read principally from analog traces.

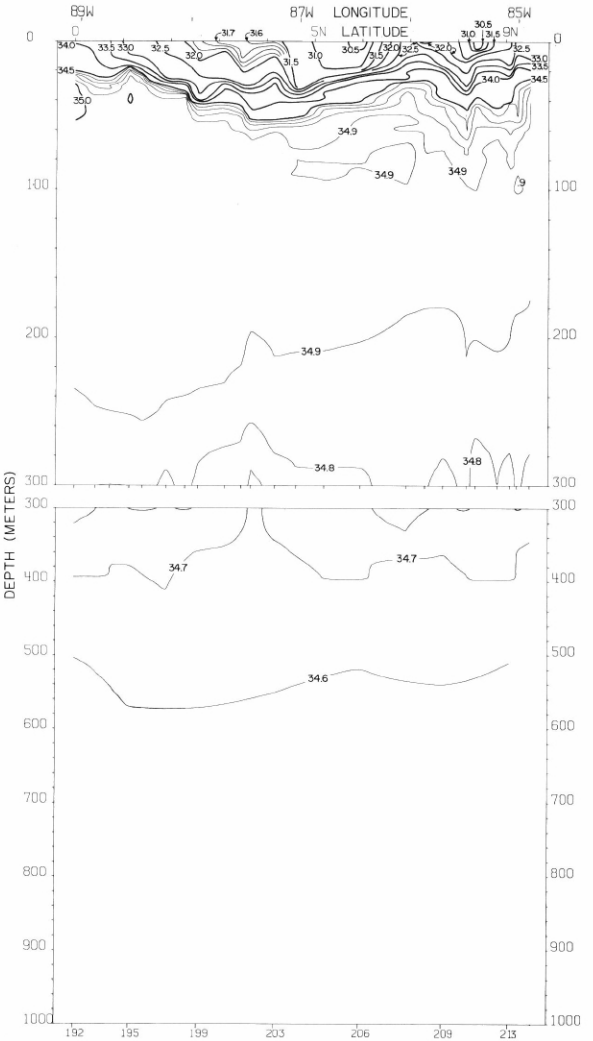

FIGURE 14-S-v22.—Vertical distribution of salinity (‰) along a southwest-northeast section from the Equator at 89°03′ W. to Puntarenas, March 11-15, 1967. These contours are based on STD data read principally from analog traces.

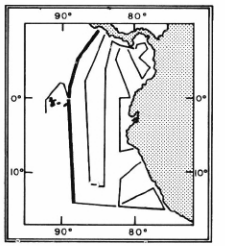

14-S-v18.

14-S-v22.

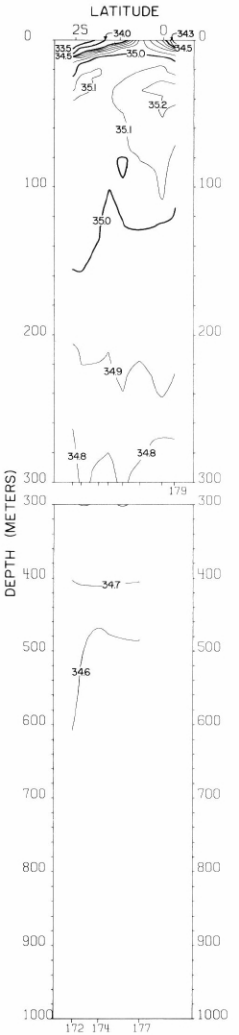

FIGURE 14-S-v19.—Vertical distribution of salinity (‰) along 92° W., west of the Galapagos Islands, March 8-9, 1967. These contours are based on STD data read principally from analog traces.

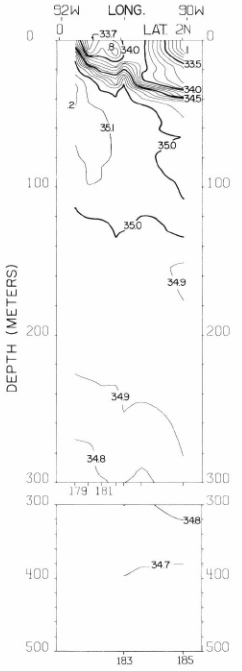

FIGURE 14-S-v20.—Vertical distribution of salinity (‰) along a section north of the Galapagos Islands, from 0°16′ N., 91°47′ W. to 2°01′ N., 90°03′ W., March 9-10, 1967. These contours are based on STD data read principally from analog traces.

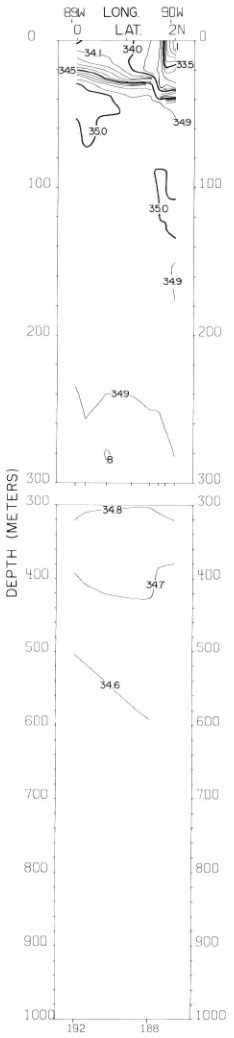

FIGURE 14-S-v21.—Vertical distribution of salinity (‰) along a section northeast of the Galapagos Islands, from 2°01′ N., 90°03′ W. to the Equator at 89°03′ W., March 11, 1967. These contours are based on STD data read principally from analog traces.

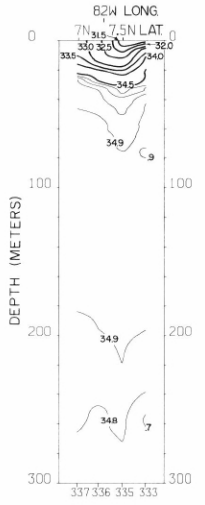

FIGURE 14-S-v28.—Vertical distribution of salinity (‰) along the coast of Panama from 82°50′ W. to 81°28′ W., April 2, 1967. These contours are based on STD data read principally from analog traces.

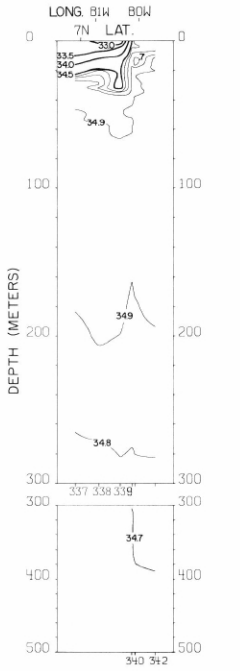

FIGURE 14-S-v29.—Vertical distribution of salinity (‰) along the coast of Panama from 81°28′ W. to 79°38′ W., April 2-3, 1967. These contours are based on STD data read principally from analog traces.

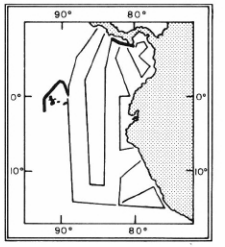

14-S-v19.

14-S-v20.

14-S-v21.

14-S-v28.

14-S-v29.

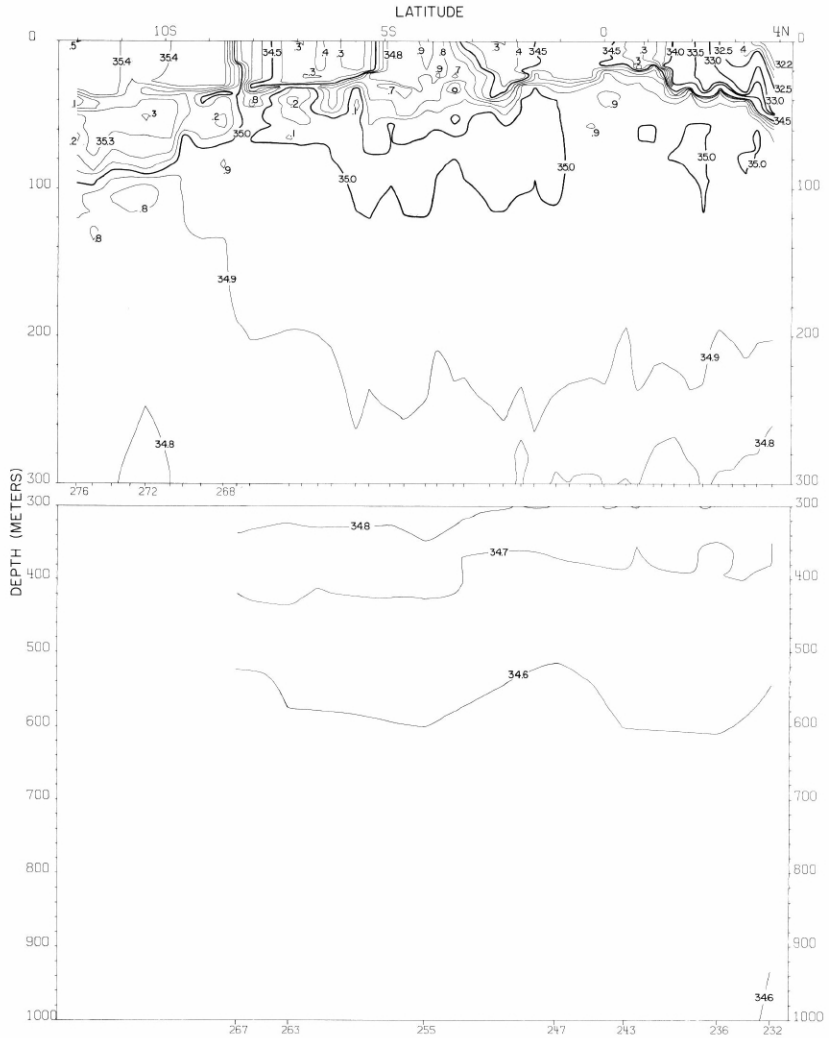

FIGURE 14-S-v24.—Vertical distribution of salinity (‰) along 86°19′ W., March 20-25, 1967. These contours are based on STD data read principally from analog traces.

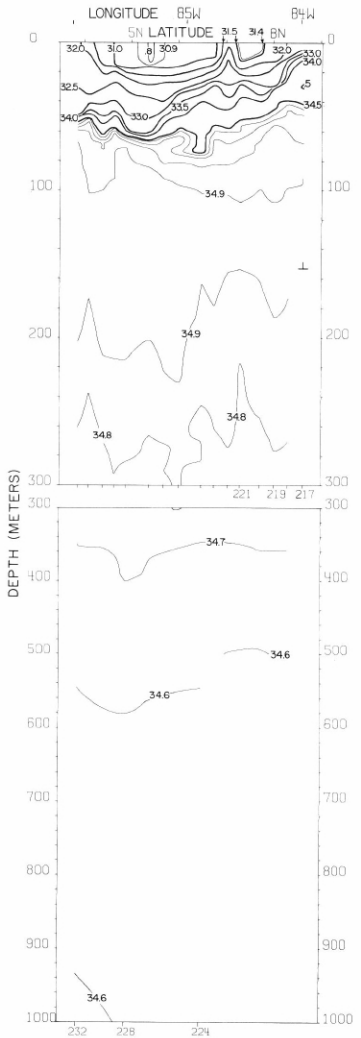

FIGURE 14-S-v23.—Vertical distribution of salinity (‰) along a northeast-southwest section from the coast of Costa Rica to 3°52′ N., 85°57′ W., March 18-20, 1967. These contours are based on STD data read principally from analog traces.

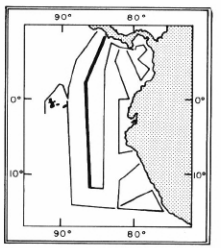

14-S-v23.

14-S-v24.

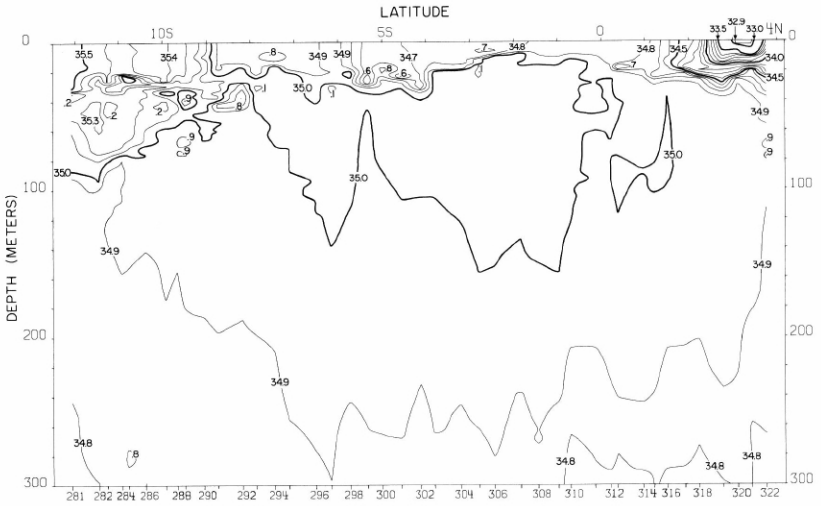

FIGURE 14-S-v26.—Vertical distribution of salinity (‰) along 84° W., March 26-31, 1967. These contours are based on STD data read principally from analog traces.

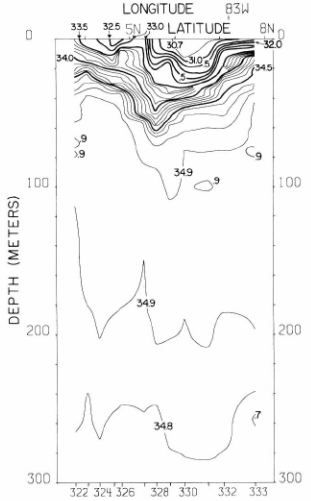

FIGURE 14-S-v27.—Vertical distribution of salinity (‰) along a southwest-northeast section from 3°45′ N., 83°48′ W. to Punta Burica, Costa Rica-Panama, March 31-April 2, 1967. These contours are based on STD data read principally from analog traces.

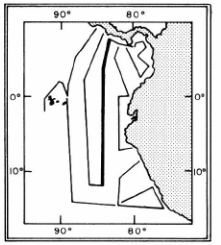

14-S-v26.

14-S-v27.

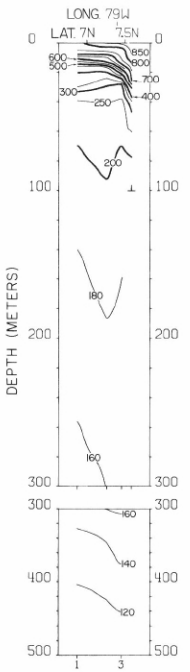

FIGURE 14-δ-v1.—Vertical distribution of thermosteric anomaly, δ_T, (cl./t.) along a southwest-northeast section in the northern portion of the Panama Bight from 79°44′ W. to 78°43′ W., January 31, 1967. These contours are based on STD data read principally from analog traces.

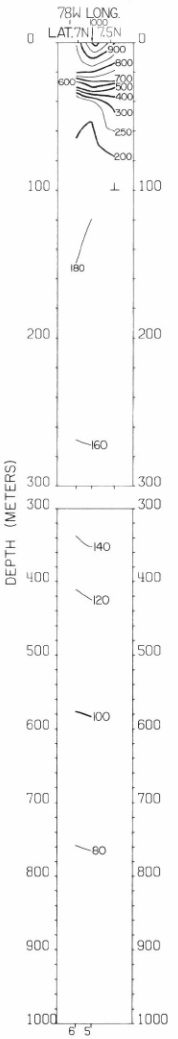

FIGURE 14-δ-v2.—Vertical distribution of thermosteric anomaly, δ_T, (cl./t.) along a section in the Panama Bight near the coasts of Panama and Colombia from 7°35′ N. to 6°58′ N., January 31-February 1, 1967. These contours are based on STD data read principally from analog traces.

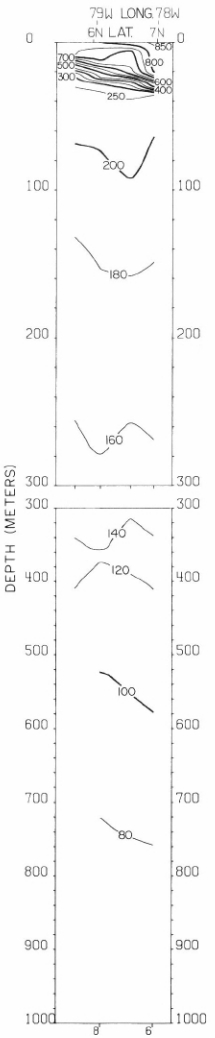

FIGURE 14-δ-v3.—Vertical distribution of thermosteric anomaly, δ_T, (cl./t.) along a northeast-southwest section in the Panama Bight from the coast of Colombia to 5°43′ N., 79°22′ W., February 1, 1967. These contours are based on STD data read principally from analog traces.

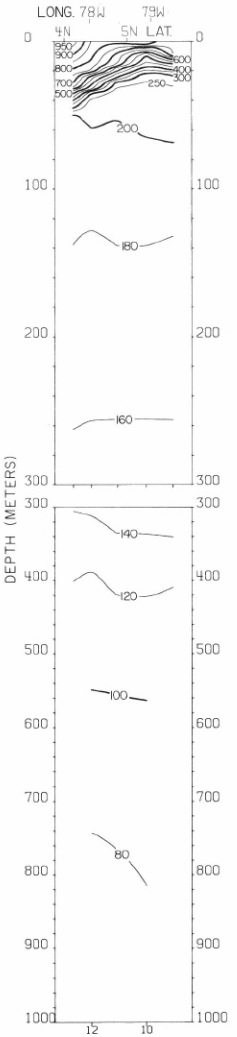

FIGURE 14-δ-v4.—Vertical distribution of thermosteric anomaly, δ_T, (cl./t.) along a northwest-southeast section in the central portion of the Panama Bight from 5°43′ N., 79°22′ W. to the coast of Colombia, February 1-2, 1967. These contours are based on STD data read principally from analog traces.

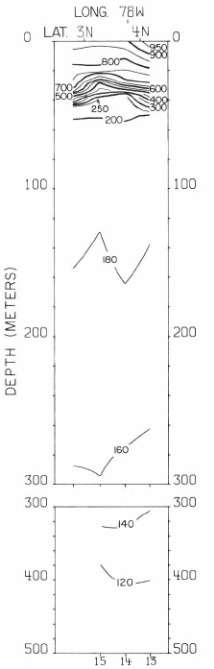

FIGURE 14-δ-v5.—Vertical distribution of thermosteric anomaly, δ_T, (cl./t.) along a section in the Panama Bight near the coast of Colombia from 4°10′ N. to 2°45′ N., February 2-3, 1967. These contours are based on STD data read principally from analog traces.

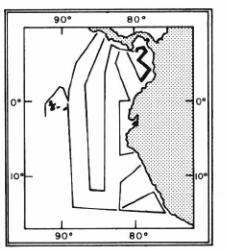

14-δ-v1.

14-δ-v2.

14-δ-v3.

14-δ-v4.

14-δ-v5.

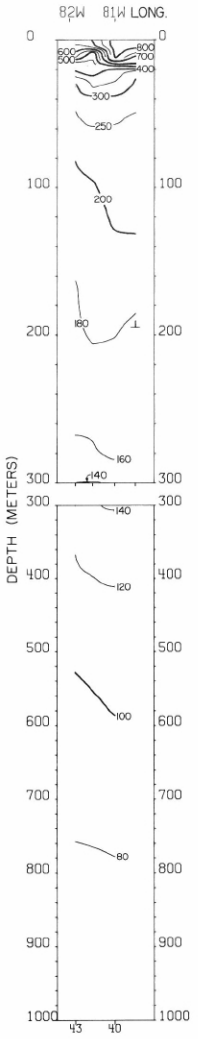

FIGURE 14-δ-v9.—Vertical distribution of thermosteric anomaly, δ_T, (cl./t.) along the Equator from the coast of Ecuador to 81°54′ W., February 8-9, 1967. These contours are based on STD data read principally from analog traces.

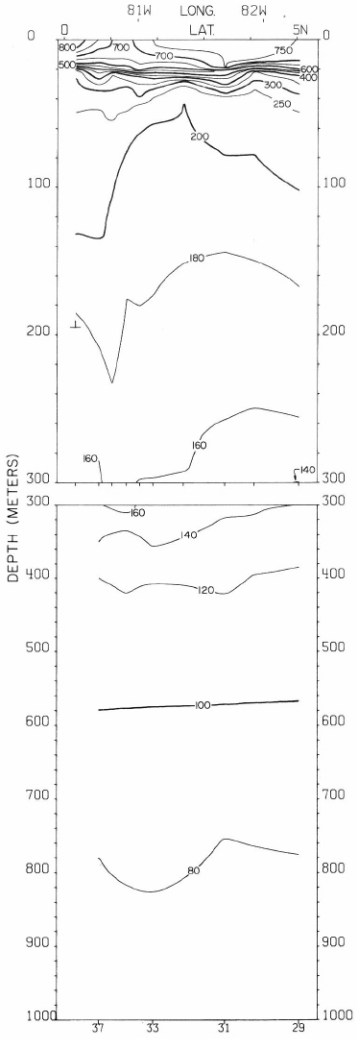

FIGURE 14-δ-v8.—Vertical distribution of thermosteric anomaly, δ_T, (cl./t.) along a northwest-southeast section from 5°03′ N., 82°18′ W. to the coast of Ecuador, February 6-8, 1967. These contours are based on STD data read principally from analog traces.

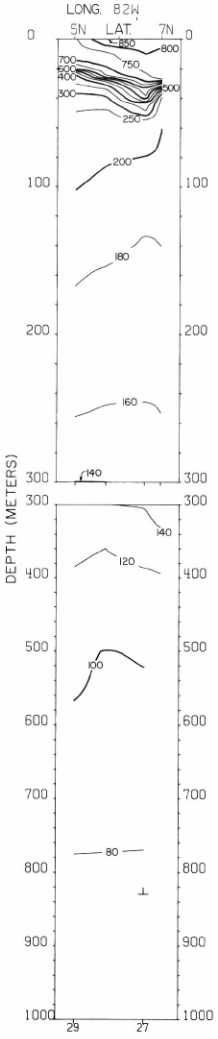

FIGURE 14-δ-v7.—Vertical distribution of thermosteric anomaly, δ_T, (cl./t.) along a northeast-southwest section from Isla Coiba, Panama to 5°03′ N., 82°18′ W., February 5-6, 1967. These contours are based on STD data read principally from analog traces.

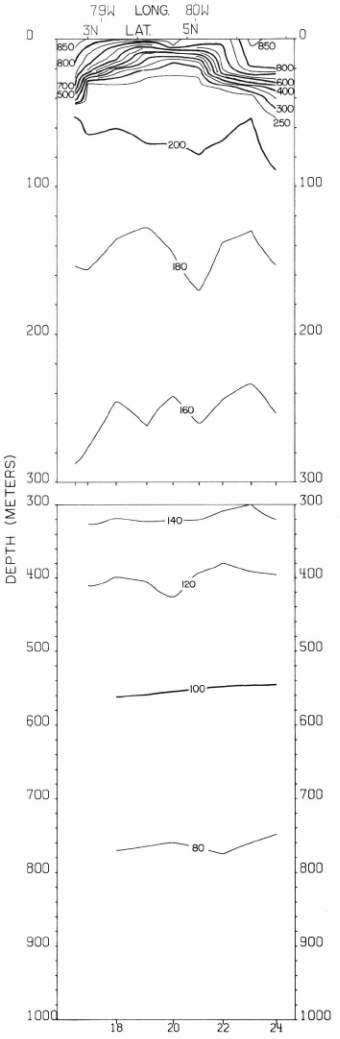

FIGURE 14-δ-v6.—Vertical distribution of thermosteric anomaly, δ_T, (cl./t.) along a southeast-northwest section across the Panama Bight from the coast of Colombia to Peninsula de Azuero, Panama, February 3-5, 1967. These contours are based on STD data read principally from analog traces.

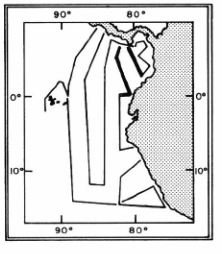

14-δ-v6.

14-δ-v7.

14-δ-v8.

14-δ-v9.

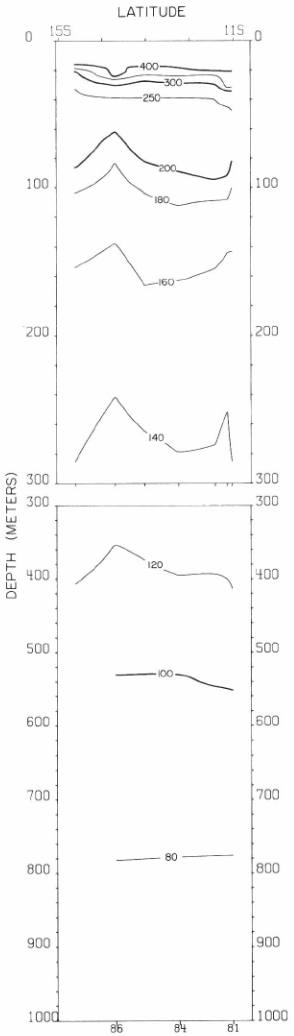

FIGURE 14-δ-v13.—Vertical distribution of thermosteric anomaly, δ_T, (cl./t.) along 81°46′ W. from 11°02′ S. to 14°37′ S., February 14-15, 1967. These contours are based on STD data read principally from analog traces.

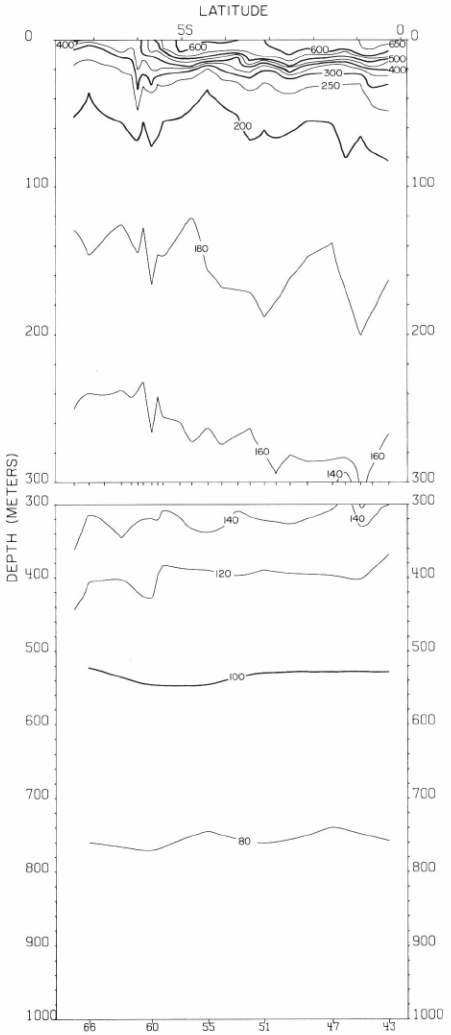

FIGURE 14-δ-v10.—Vertical distribution of thermosteric anomaly, δ_T, (cl./t.) along 82° W. from 0°18′ S. to 7°27′ S., February 9-11, 1967. These contours are based on STD data read principally from analog traces.

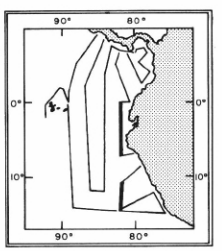

14-δ-v10.

14-δ-v13.

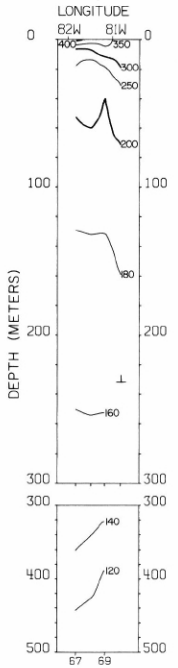

FIGURE 14-δ-v11.—Vertical distribution of thermosteric anomaly, δ_T, (cl./t.) along 7°15′ S. from 81°50′ W. to the coast of Peru, February 11-12, 1967. These contours are based on STD data read principally from analog traces.

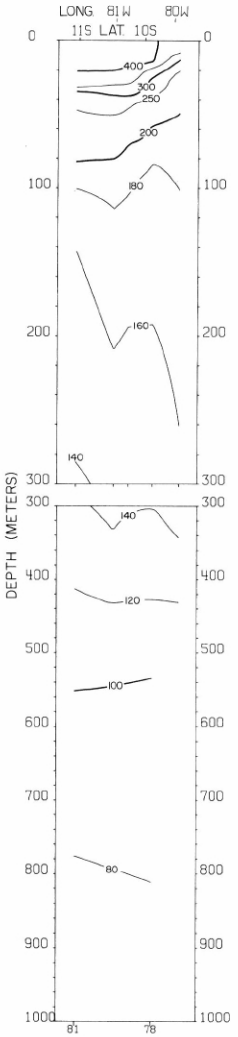

FIGURE 14-δ-v12.—Vertical distribution of thermosteric anomaly, δ_T, (cl./t.) along a northeast-southwest section from the coast of Peru to 11° S., 81°46′ W., February 13-14, 1967. These contours are based on STD data read principally from analog traces.

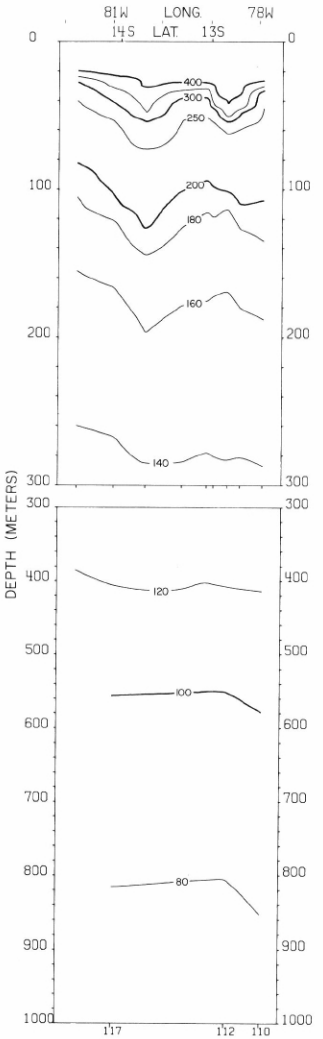

FIGURE 14-δ-v16.—Vertical distribution of thermosteric anomaly, δ_T, (cl./t.) along a northeast-southwest section from the coast of Peru to 14°30′ S., 81°43′ W., February 24-25, 1967. These contours are based on STD data read principally from analog traces.

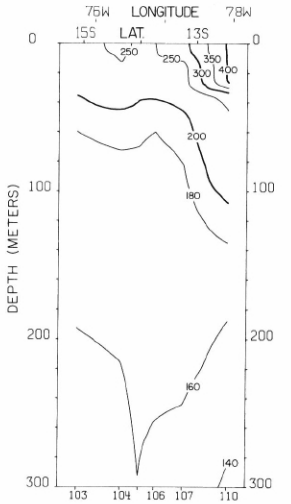

FIGURE 14-δ-v15.—Vertical distribution of thermosteric anomaly, δ_T, (cl./t.) along the coast of Peru from 15°07′ S. to 12°27′ S., February 17-24, 1967. These contours are based on STD data read principally from analog traces.

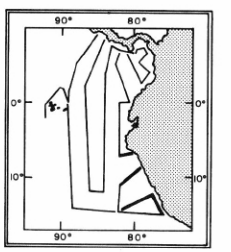

14-δ-v11.

14-δ-v12.

14-δ-v15.

14-δ-v16.

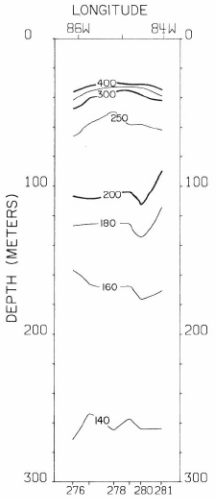

FIGURE 14-δ-v25.—Vertical distribution of thermosteric anomally, δ_T, (cl./t.) along 12° S., March 25-26, 1967. These contours are based on STD data read principally from analog traces.

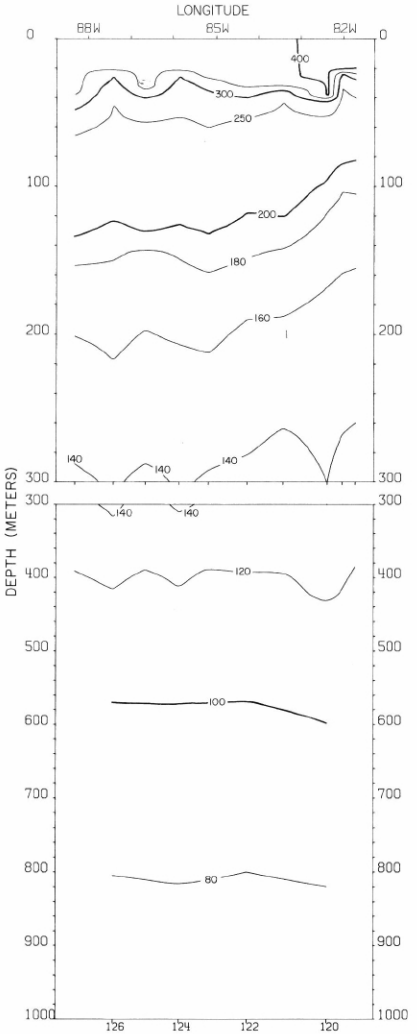

FIGURE 14-δ-v17.—Vertical distribution of thermosteric anomaly, δ_T, (cl./t.) along 14°30′ S. from 81°43′ W. to 88°17′ W., February 25-27, 1967. These contours are based on STD data read principally from analog traces.

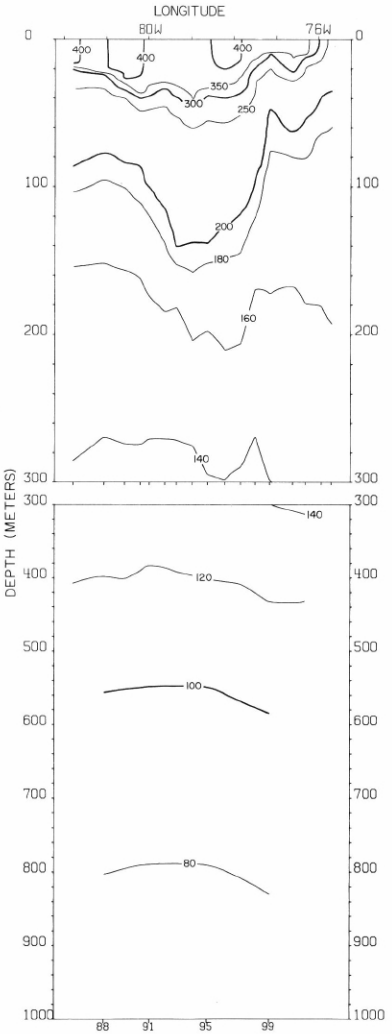

FIGURE 14-δ-v14.—Vertical distribution of thermosteric anomaly, δ_T, (cl./t.) along 15° S. from 81°46′ W. to the coast of Peru, February 15-16, 1967. These contours are based on STD data read principally from analog traces.

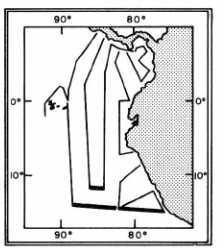

14-δ-v14.

14-δ-v17.

14-δ-v25.

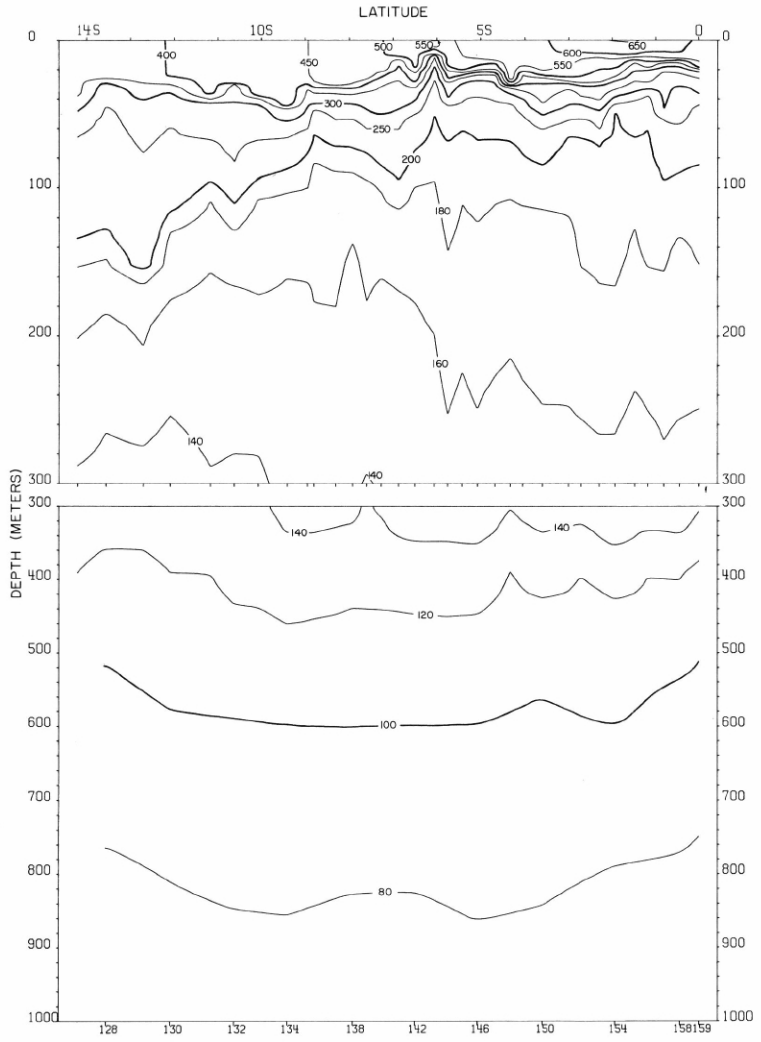

FIGURE 14-δ-v18.—Vertical distribution of thermosteric anomaly, δ_T, (cl./t.) along 88°46′ W., February 27-March 4, 1967. These contours are based on STD data read principally from analog traces.

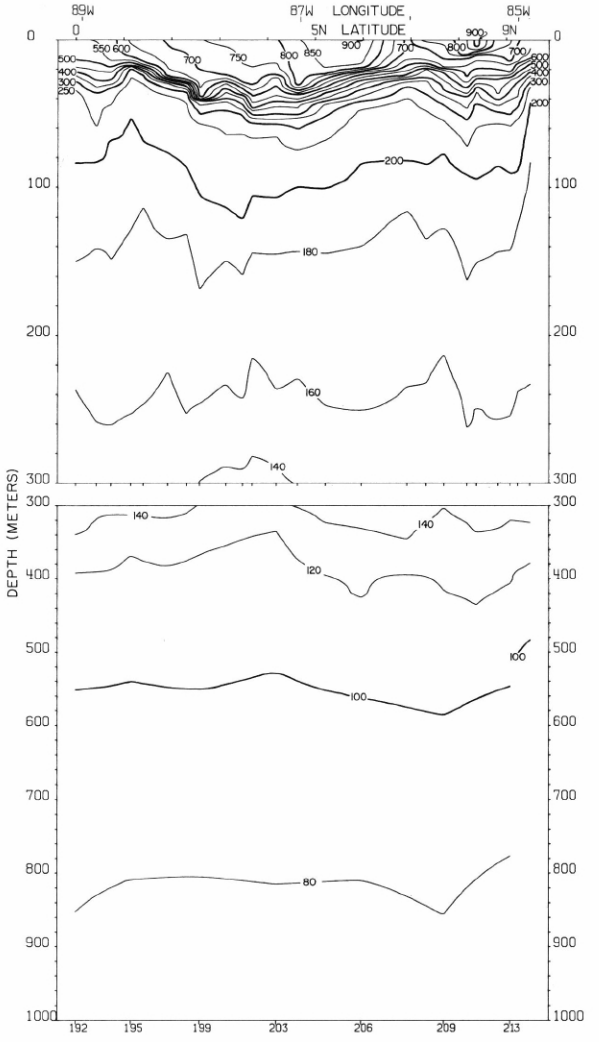

FIGURE 14-δ-v22.—Vertical distribution of thermosteric anomaly, δ_T, (cl./t.) along a southwest-northeast section from the Equator at 89°03′ W. to Puntarenas, March 11-15, 1967. These contours are based on STD data read principally from analog traces.

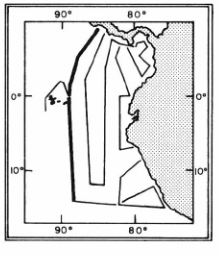

14-δ-v18.

14-δ-v22.

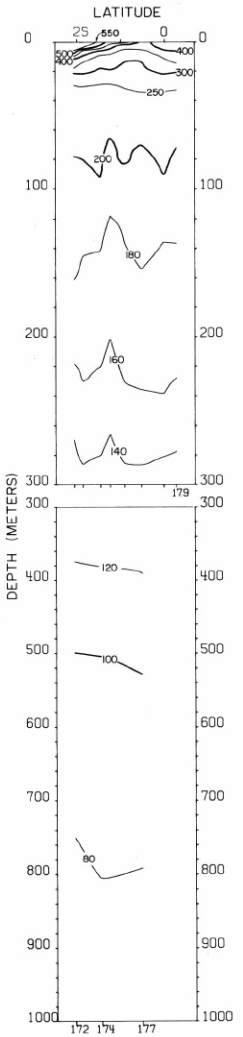

FIGURE 14-δ-v19.—Vertical distribution of thermosteric anomaly, δ_T, (cl./t.) along 92° W., west of the Galapagos Islands, March 8-9, 1967. These contours are based on STD data read principally from analog traces.

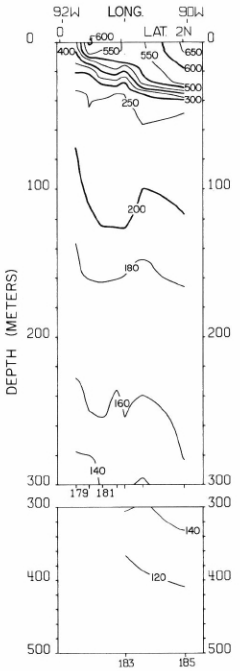

FIGURE 14-δ-v20.—Vertical distribution of thermosteric anomaly, δ_T, (cl./t.) along a section north of the Galapagos Islands, from 0°16′ N., 91°47′ W. to 2°01′ N., 90°03′ W., March 9-10, 1967. These contours are based on STD data read principally from analog traces.

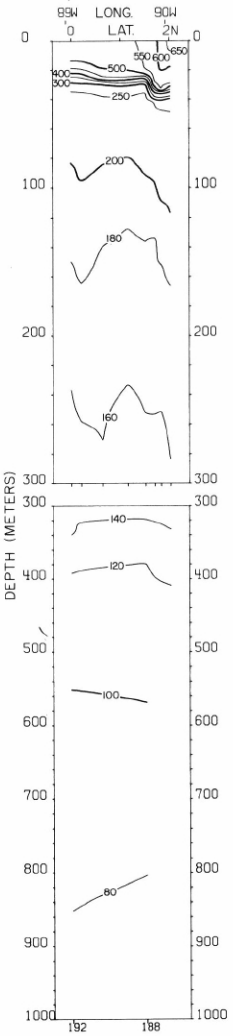

FIGURE 14-δ-v21.—Vertical distribution of thermosteric anomaly, δ_T, (cl./t.) along a section northeast of the Galapagos Islands, from 2°01′ N., 90°03′ W. to the Equator at 89°03′ W., March 11, 1967. These contours are based on STD data read principally from analog traces.

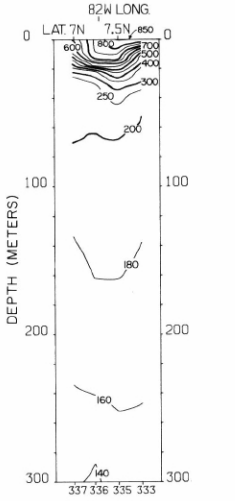

FIGURE 14-δ-v28.—Vertical distribution of thermosteric anomaly, δ_T, (cl./t.) along the coast of Panama from 82°50′ W. to 81°28′ W., April 2, 1967. These contours are based on STD data read principally from analog traces.

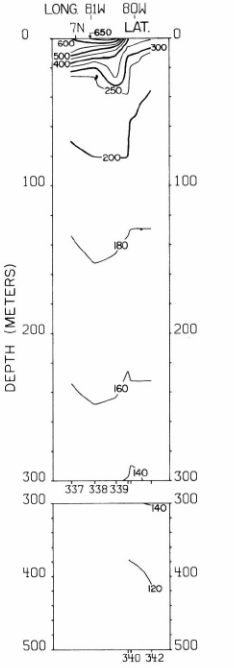

FIGURE 14-δ-v29.—Vertical distribution of thermosteric anomaly, δ_T, (cl./t.) along the coast of Panama from 81°28′ W. to 79°38′ W., April 2-3, 1967. These contours are based on STD data read principally from analog traces.

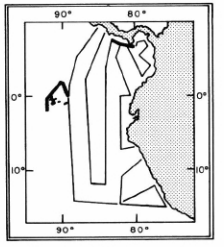

14-δ-v19.

14-δ-v20.

14-δ-v21.

14-δ-v28.

14-δ-v29.

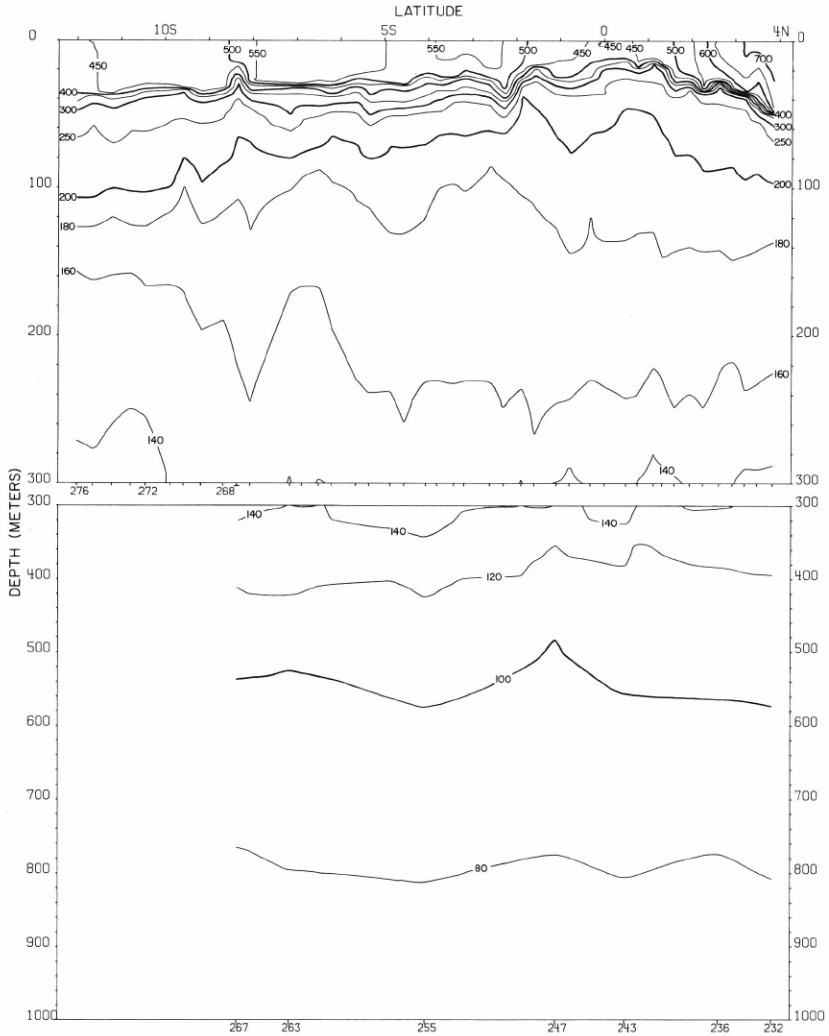

FIGURE 14-δ-v24.—Vertical distribution of thermosteric anomaly, δ_T, (cl./t.) along 86°19′ W., March 20-25, 1967. These contours are based on STD data read principally from analog traces.

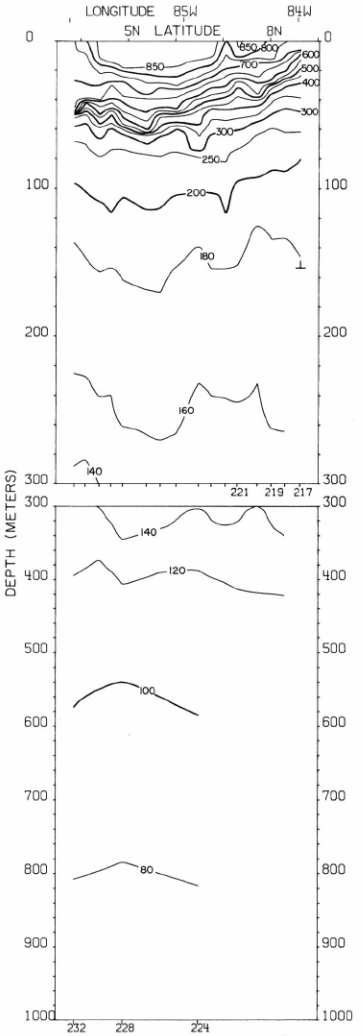

FIGURE 14-δ-v23.—Vertical distribution of thermosteric anomaly, δ_T, (cl./t.) along a northeast-southwest section from the coast of Costa Rica to 3°52′ N., 85°57′ W., March 18-20, 1967. These contours are based on STD data read principally from analog traces.

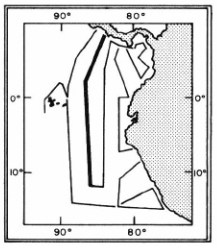

14-δ-v23.

14-δ-v24.

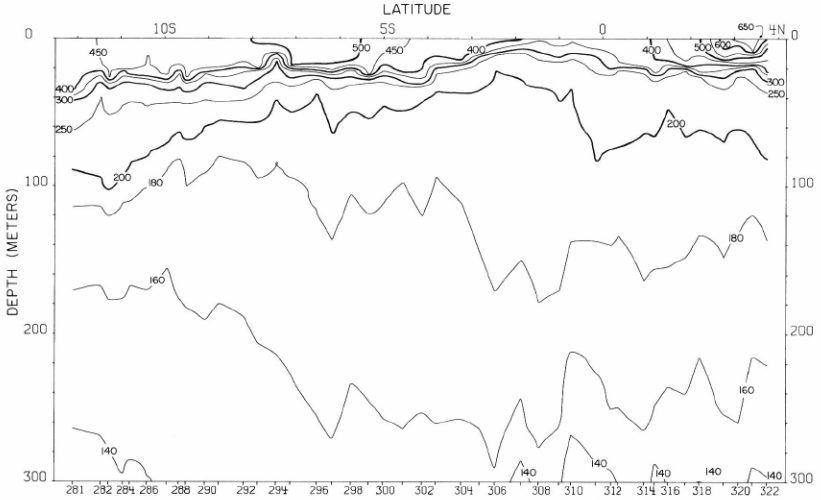

FIGURE 14-δ-v26.—Vertical distribution of thermosteric anomaly, δ_T, (cl./t.) along 84° W., March 26-31, 1967. These contours are based on STD data read principally from analog traces.

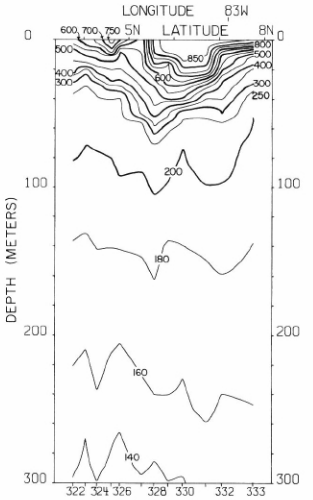

FIGURE 14-δ-v27.—Vertical distribution of thermosteric anomaly, δ_T, (cl./t.) along a southwest-northeast section from 3°45′ N., 83°48′ W. to Punta Burica, Costa Rica-Panama, March 31-April 2, 1967. These contours are based on STD data read principally from analog traces.

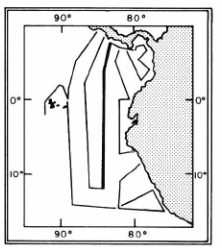

14-δ-v26.

14-δ-v27.

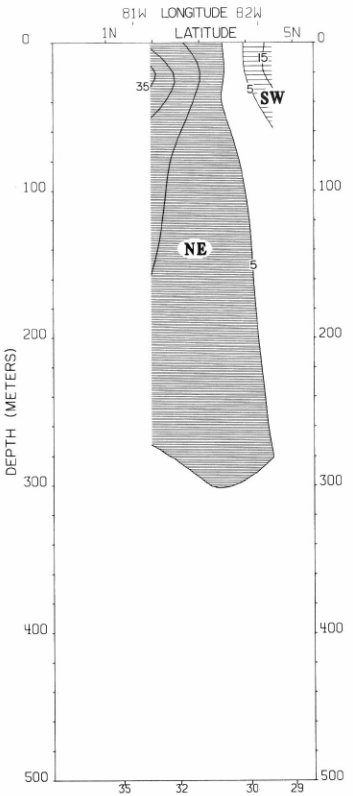

FIGURE 14-G-v8.—Vertical distribution of the component of geostrophic velocity (cm./sec.), relative to 500 db., normal to a northwest-southeast section from 5°03′N., 82°18′ W. to the coast of Ecuador, February 6-7, 1967. Dark shading indicates flow toward the northeast with a velocity greater than 5 cm./sec.; light shading indicates flow toward the southwest with a velocity greater than 5 cm./sec.

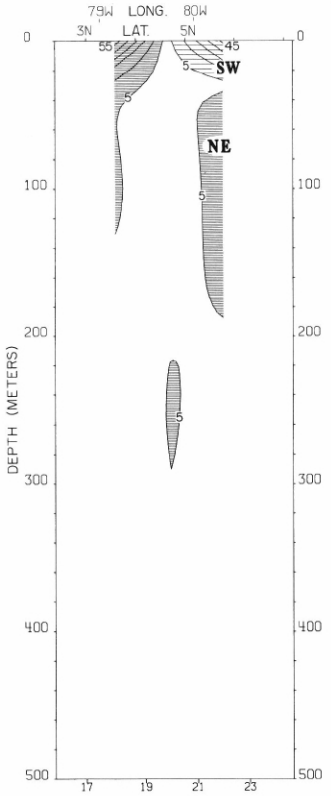

FIGURE 14-G-v6.—Vertical distribution of the component of geostrophic velocity (cm./sec.), relative to 500 db., normal to a southeast-northwest section across the Panama Bight from the coast of Colombia to Peninsula de Azuero, Panama, February 3-5, 1967. Dark shading indicates flow toward the northeast with a velocity greater than 5 cm./sec.; light shading indicates flow toward the southwest with a velocity greater than 5 cm./sec.

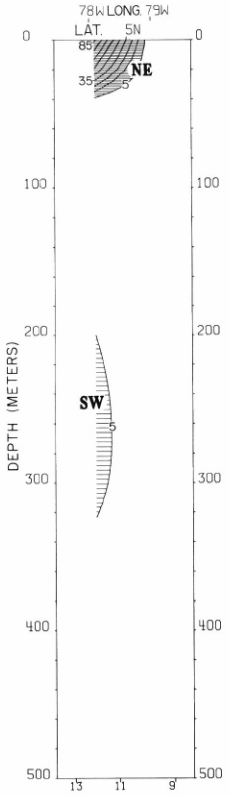

FIGURE 14-G-v4.—Vertical distribution of the component of geostrophic velocity (cm./sec.), relative to 500 db., normal to a northwest-southeast section in the central portion of the Panama Bight from 5°43′ N., 79°22′ W. to the coast of Colombia, February 1-2, 1967. Dark shading indicates flow toward the northeast with a velocity greater than 5 cm./sec.; light shading indicates flow toward the southwest with a velocity greater than 5 cm./sec.

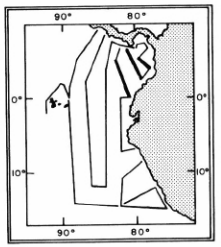

14-G-v4.

14-G-v6.

14-G-v8.

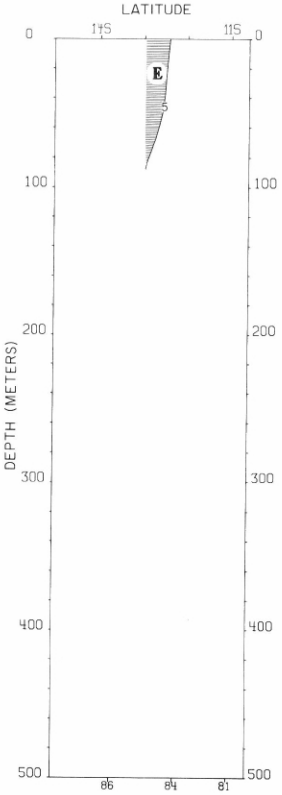

FIGURE 14-G-v13.—Vertical distribution of the zonal component of geostrophic velocity (cm./sec.), relative to 500 db., along 81°46′ W. from 11°02′ S. to 13°42′ S., February 14-15, 1967. Dark shading indicates eastward flow with a velocity greater than 5 cm./sec.

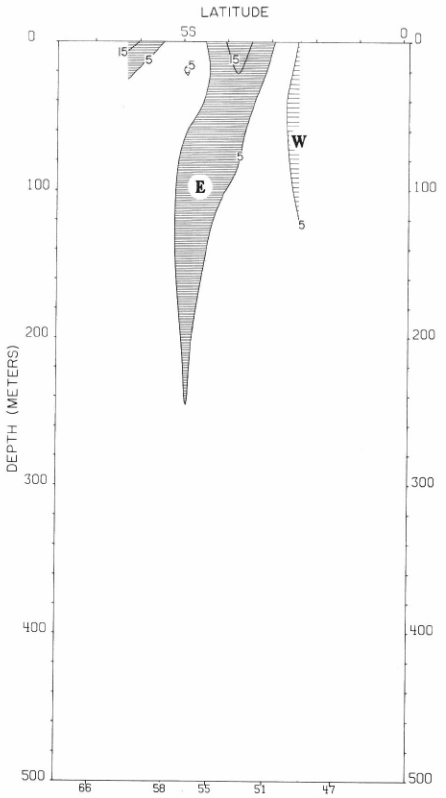

FIGURE 14-G-v10.—Vertical distribution of the zonal component of geostrophic velocity (cm./sec.), relative to 500 db., along 82° W. from 1°35′ S. to 7°07′S., February 9-11, 1967. Dark shading indicates eastward flow with a velocity greater than 5 cm./sec.; light shading indicates westward flow with a velocity greater than 5 cm./sec.

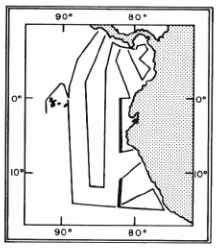

14-G-v10.

14-G-v13.

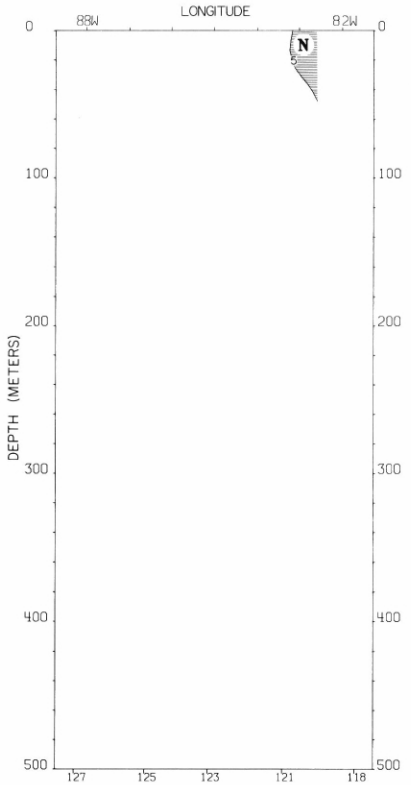

FIGURE 14-G-v17.—Vertical distribution of the meridional component of geostrophic velocity (cm./sec.), relative to 500 db., along 14°30′ S. from 81°43′ W. to 88°17′ W., February 25-27, 1967. Dark shading indicates northward flow with a velocity greater than 5 cm./sec.

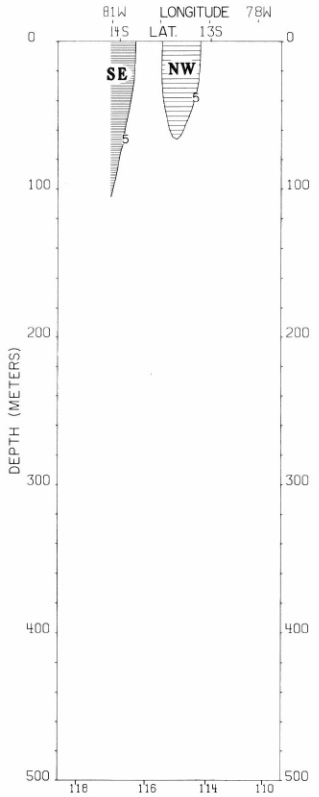

FIGURE 14-G-v16.—Vertical distribution of the component of geostrophic velocity (cm./sec.), relative to 500 db., normal to a northeast-southwest section from the coast of Peru to 14°30′ S., 81°43′ W., February 24-25, 1967. Dark shading indicates flow toward the southeast with a velocity greater than 5 cm./sec.; light shading indicates flow toward the northwest with a velocity greater than 5 cm./sec.

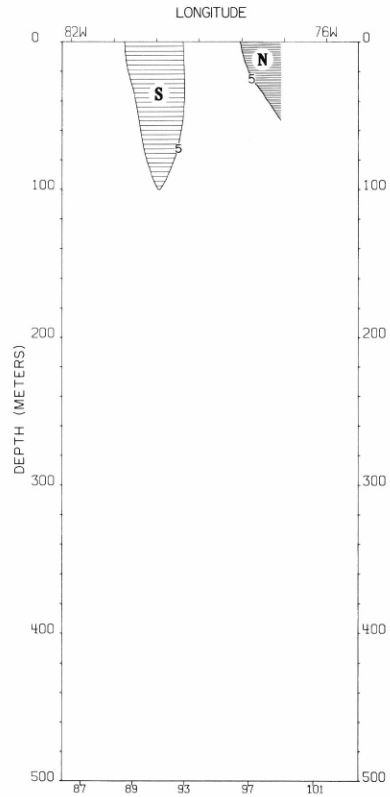

FIGURE 14-G-v14.—Vertical distribution of the meridional component of geostrophic velocity (cm./sec.), relative to 500 db., along 15° S. from 81°46′W. to the coast of Peru, February 15-17, 1967. Dark shading indicates northward flow with a velocity greater than 5 cm./sec.; light shading indicates southward flow with a velocity greater than 5 cm./sec.

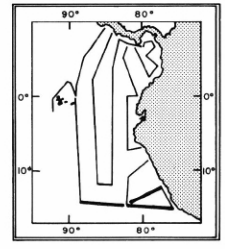

14-G-v14.

14-G-v16.

14-G-v17.

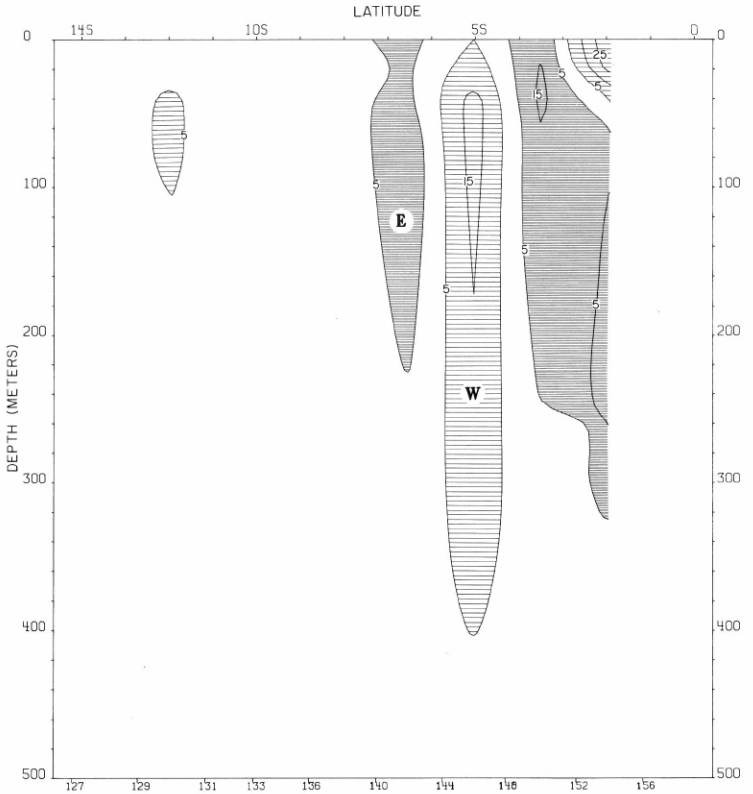

FIGURE 14-G-v18.—Vertical distribution of the zonal component of geostrophic velocity (cm./sec.), relative to 500 db., along 88°46′ W., February 27-March 4, 1967. Dark shading indicates eastward flow with a velocity greater than 5 cm./sec.; light shading indicates westward flow with a velocity greater than 5 cm./sec.

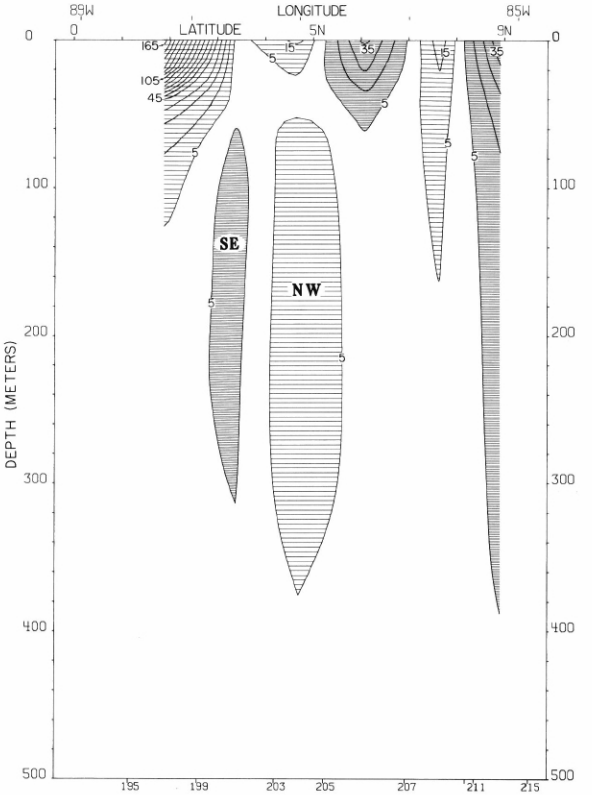

FIGURE 14-G-v22.—Vertical distribution of the component of geostrophic velocity (cm./sec.), relative to 500 db., normal to a southwest-northeast section from 1°22′ N., 89°02′ W. to Puntarenas, March 12-15, 1967. Dark shading indicates flow toward the southeast with a velocity greater than 5 cm./sec.; light shading indicates flow toward the northwest with a velocity greater than 5 cm./sec.

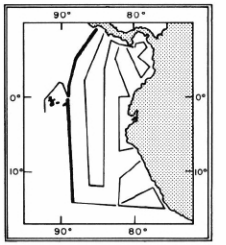

14-G-v18.

14-G-v22.

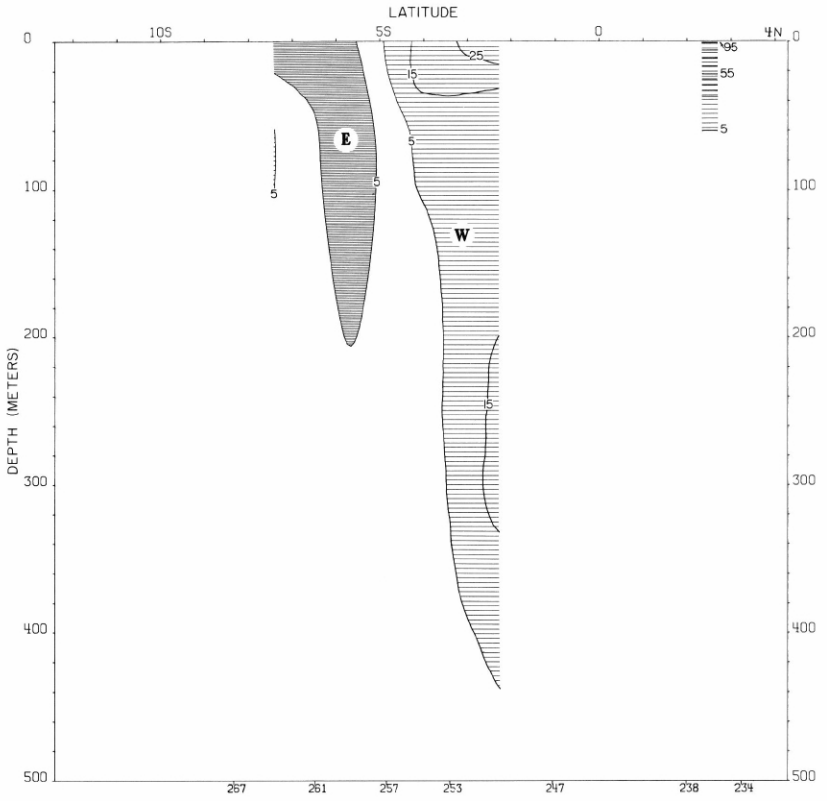

FIGURE 14-G-v24.—Vertical distribution of the zonal component of geostrophic velocity (cm./sec.), relative to 500 db., along 86°19′ W., March 20-24, 1967. Dark shading indicates eastward flow with a velocity greater than 5 cm./sec.; light shading indicates westward flow with a velocity greater than 5 cm./sec.

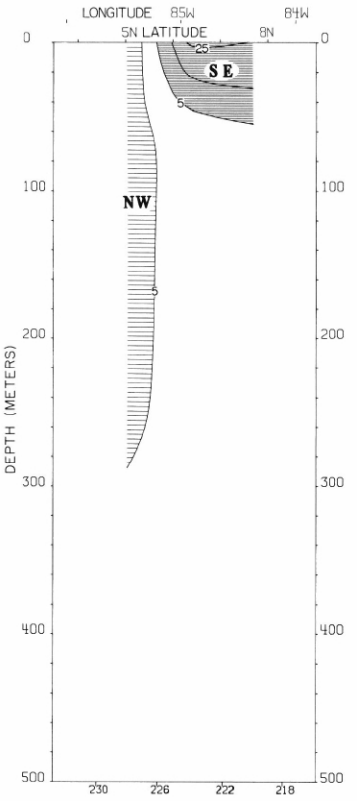

FIGURE 14-G-v23.—Vertical distribution of the component of geostrophic velocity (cm./sec.), relative to 500 db., normal to a northeast-southwest section from the coast of Costa Rica to 4°25′ N., 85°47′ W., March 18-19, 1967. Dark shading indicates flow toward the southeast with a velocity greater than 5 cm./sec.; light shading indicates flow toward the northwest with a velocity greater than 5 cm./sec.

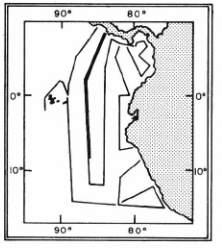

14-G-v23.

14-G-v24.

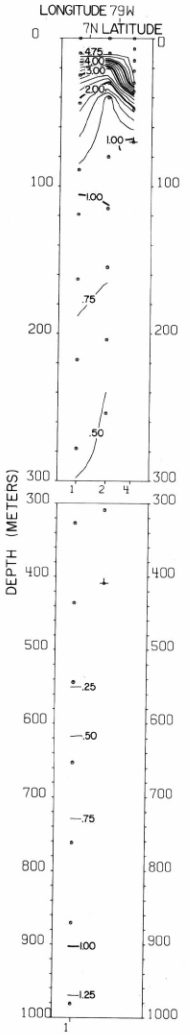

FIGURE 14-O₂-v1.—Vertical distribution of oxygen (ml./l.) along a southwest-northeast section in the northern portion of the Panama Bight from 79°44′ W. to 78°43′ W., January 31, 1967.

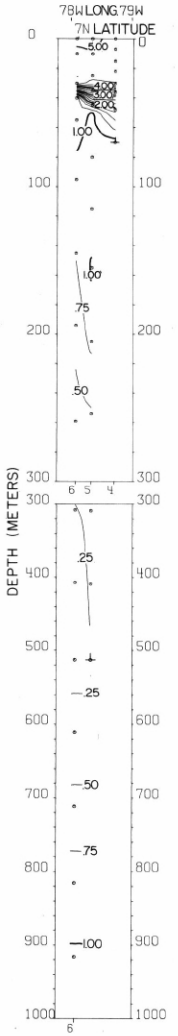

FIGURE 14-O₂-v2.—Vertical distribution of oxygen (ml./l.) along a section in the Panama Bight near the coasts of Panama and Colombia from 7°35′ N. to 6°58′ N., January 31-February 1, 1967.

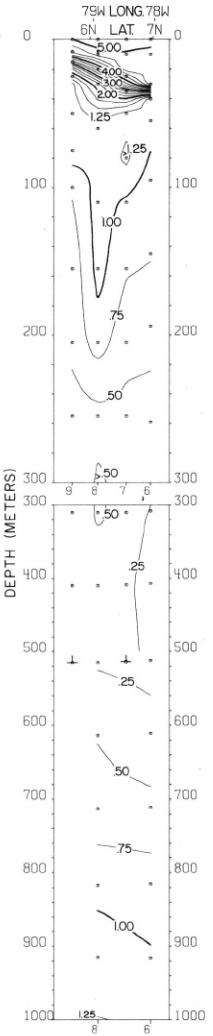

FIGURE 14-O₂-v3.—Vertical distribution of oxygen (ml./l.) along a northeast-southwest section in the Panama Bight from the coast of Colombia to 5°43′ N., 79°22′ W., February 1, 1967.

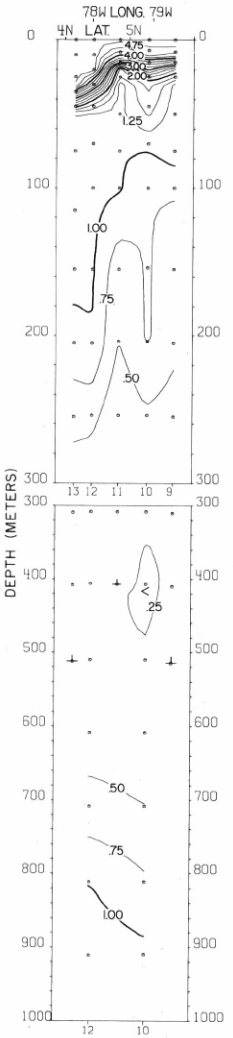

FIGURE 14-O₂-v4.—Vertical distribution of oxygen (ml./l.) along a northwest-southeast section in the central portion of the Panama Bight from 5°43′ N., 79°22′ W. to the coast of Colombia, February 1-2, 1967.

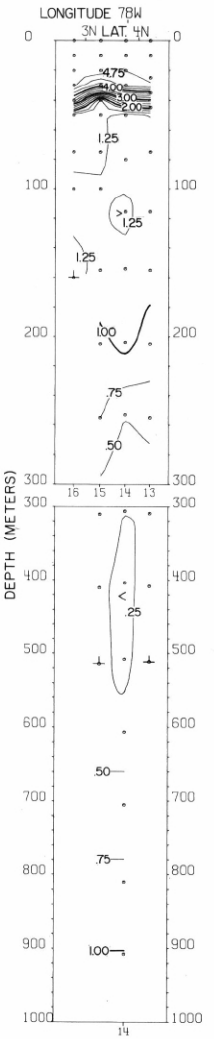

FIGURE 14-O₂-v5.—Vertical distribution of oxygen (ml./l.) along a section in the Panama Bight near the coast of Colombia from 4°10′ N. to 2°45′ N., February 2-3, 1967.

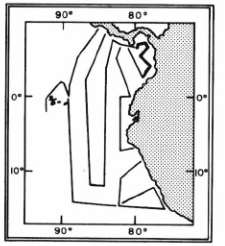

14-O₂-v1.

14-O₂-v2.

14-O₂-v3.

14-O₂-v4.

14-O₂-v5.

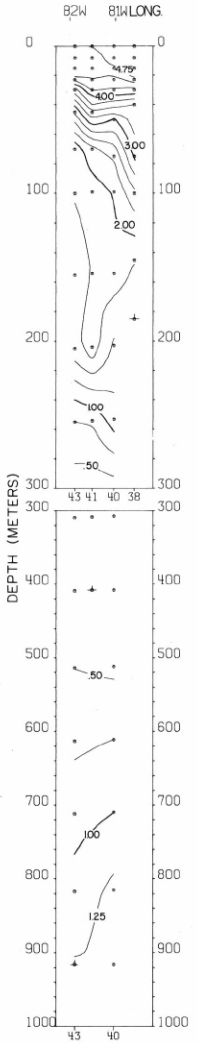

FIGURE 14-O_2-v9.—Vertical distribution of oxygen (ml./l.) along the Equator from the coast of Ecuador to 81°54′ W., February 8-9, 1967.

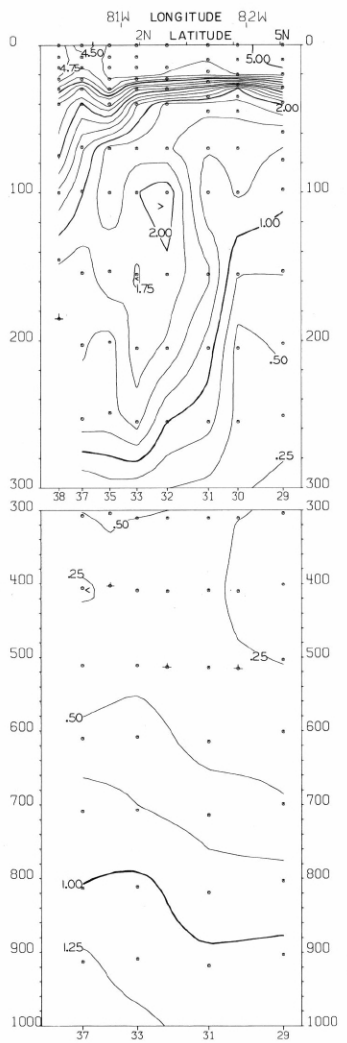

FIGURE 14-O_2-v8.—Vertical distribution of oxygen (ml./l.) along a northwest-southeast section from 5°03′ N., 82°18′ W. to the coast of Ecuador, February 6-8, 1967.

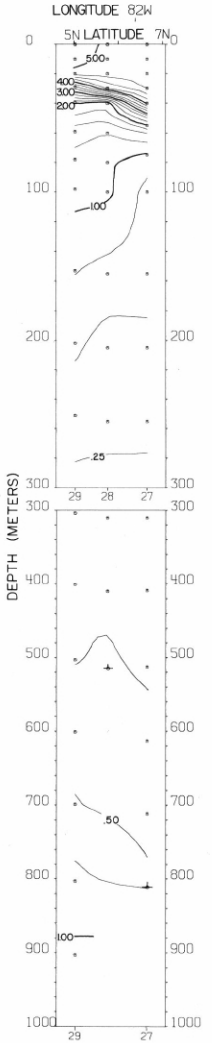

FIGURE 14-O_2-v7.—Vertical distribution of oxygen (ml./l.) along a northeast-southwest section from Isla Coiba, Panama, to 5°03′ N., 82°18′ W., February 5-6, 1967.

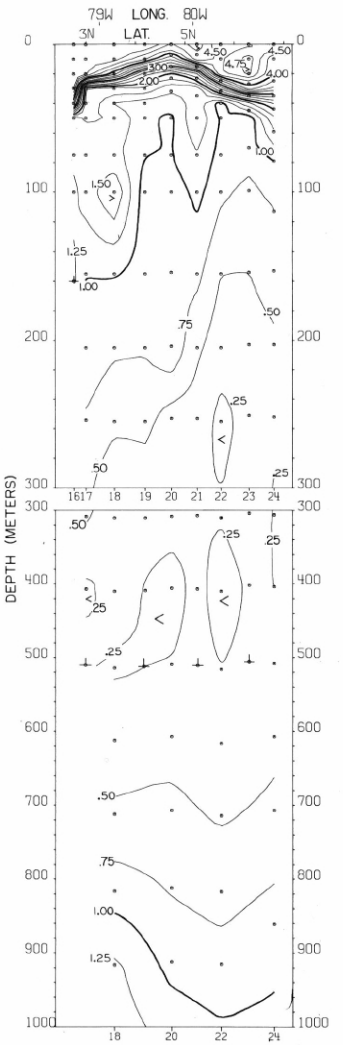

FIGURE 14-O_2-v6.—Vertical distribution of oxygen (ml./l.) along a southeast-northwest section across the Panama Bight from the coast of Colombia to Peninsula de Azuero, Panama, February 3-5, 1967.

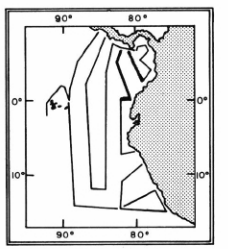

14-O_2-v6.

14-O_2-v7.

14-O_2-v8.

14-O_2-v9.

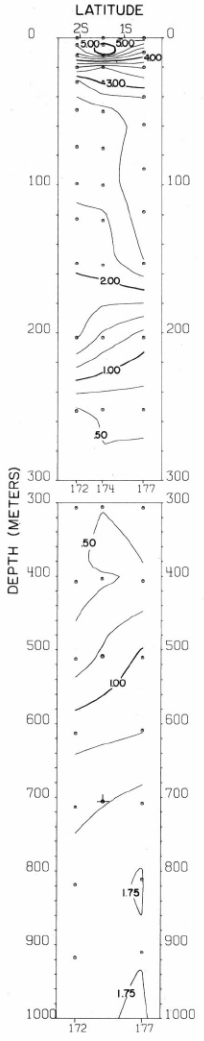

FIGURE 14-O₂-v19. — Vertical distribution of oxygen (ml./l.) along 92° W., west of the Galapagos Islands, March 8-9, 1967.

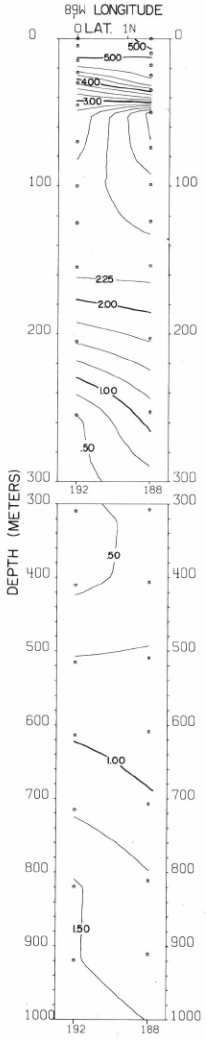

FIGURE 14-O₂-v21. — Vertical distribution of oxygen (ml./l.) along a section northeast of the Galapagos Islands, from 1°33′ N., 89°44′ W. to the Equator at 89°03′ W., March 11, 1967.

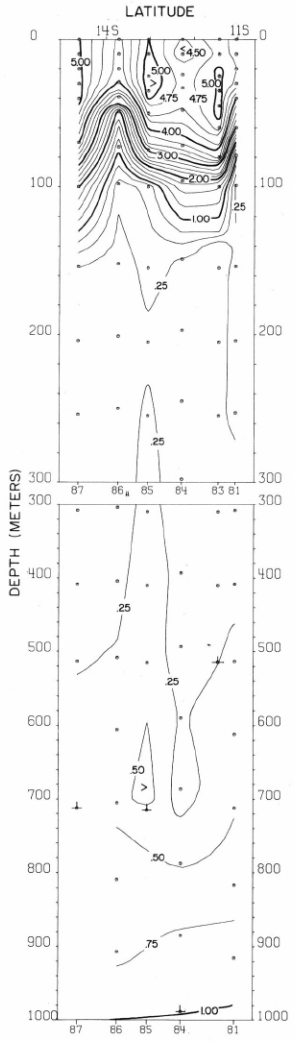

FIGURE 14-O₂-v13.—Vertical distribution of oxygen (ml./l.) along 81°46′ W. from 11°02′ S. to 14°37′ S., February 14-15, 1967.

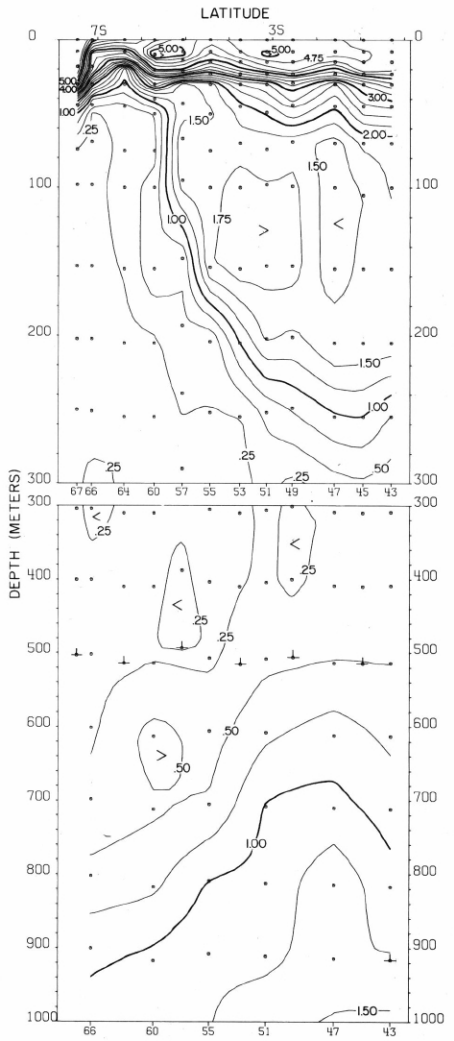

FIGURE 14-O₂-v10.—Vertical distribution of oxygen (ml./l.) along 82° W. from 0°18′ S. to 7°27′ S., February 9-11, 1967.

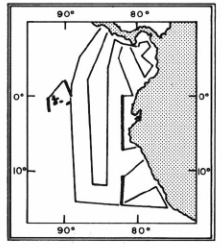

14-O₂-v10.

14-O₂-v13.

14-O₂-v19.

14-O₂-v21.

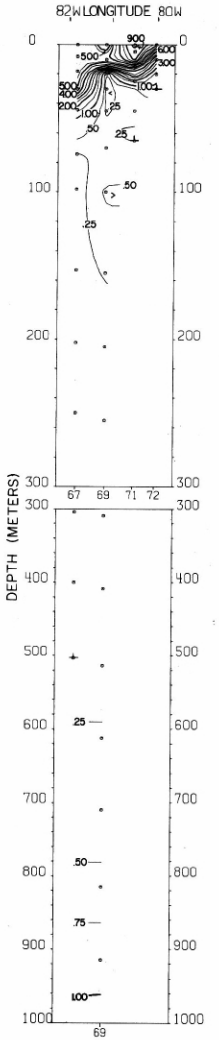

FIGURE 14-O2-v11.—Vertical distribution of oxygen (ml./l.) along 7°15′ S. from 81°50′ W. to the coast of Peru, February 11-12, 1967.

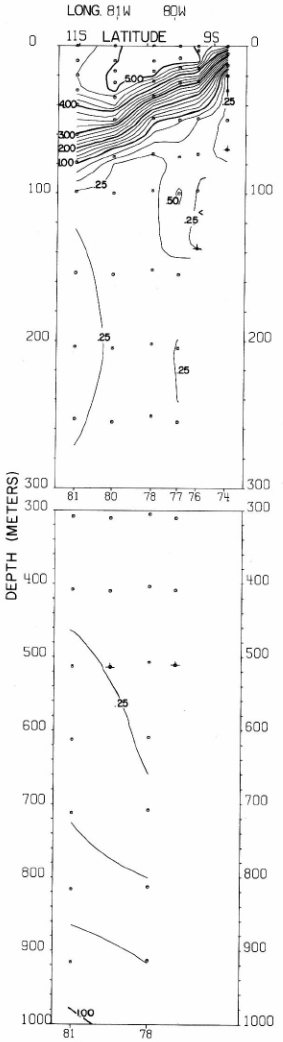

FIGURE 14-O2-v12.—Vertical distribution of oxygen (ml./l.) along a northeast-southwest section from the coast of Peru to 11° S., 81°46′ W., February 13-14, 1967.

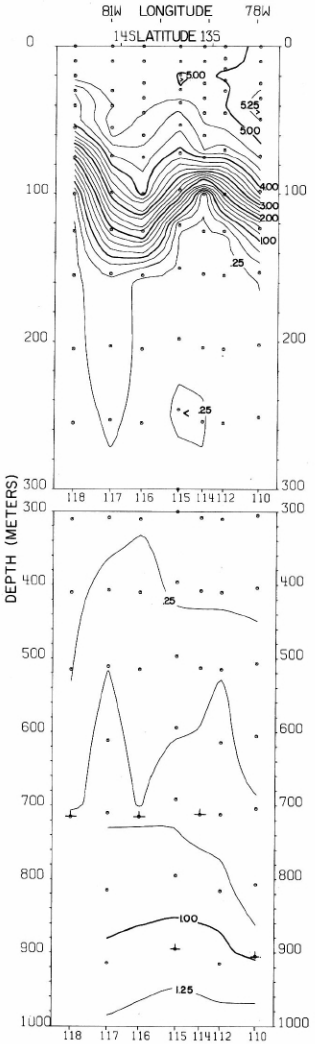

FIGURE 14-O2-v16.—Vertical distribution of oxygen (ml./l.) along a northeast-southwest section from the coast of Peru to 14°30′ S., 81°43′ W., February 24-25, 1967.

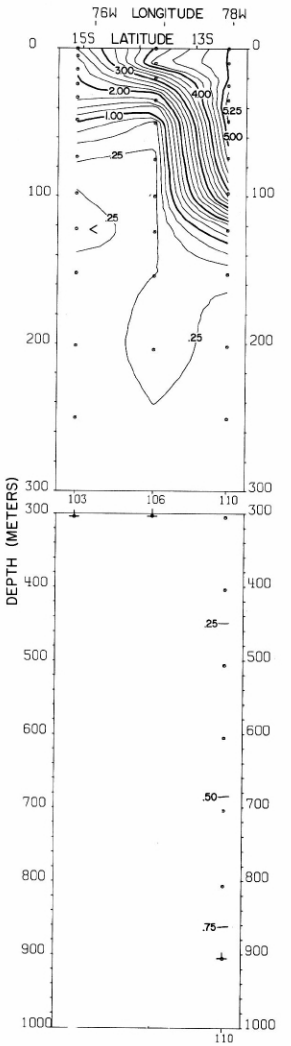

FIGURE 14-O2-v15.—Vertical distribution of oxygen (ml./l.) along the coast of Peru from 15°07′ S. to 12°27′ S., February 17-24, 1967.

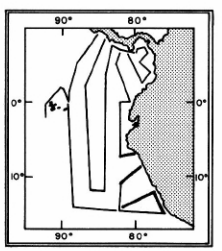

14-O2-v11.

14-O2-v12.

14-O2-v15.

14-O2-v16.

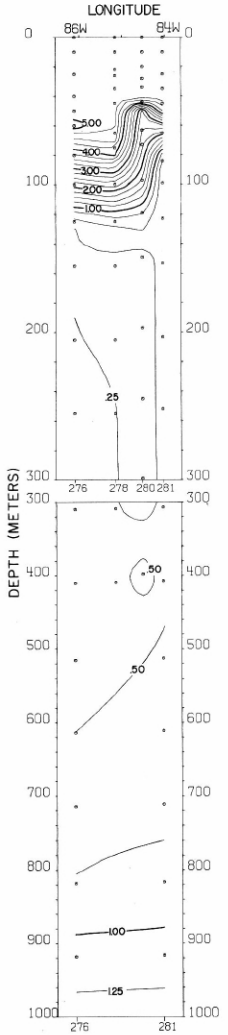

FIGURE 14-O₂-v25.—Vertical distribution of oxygen (ml./l.) along 12° S., March 25-26, 1967.

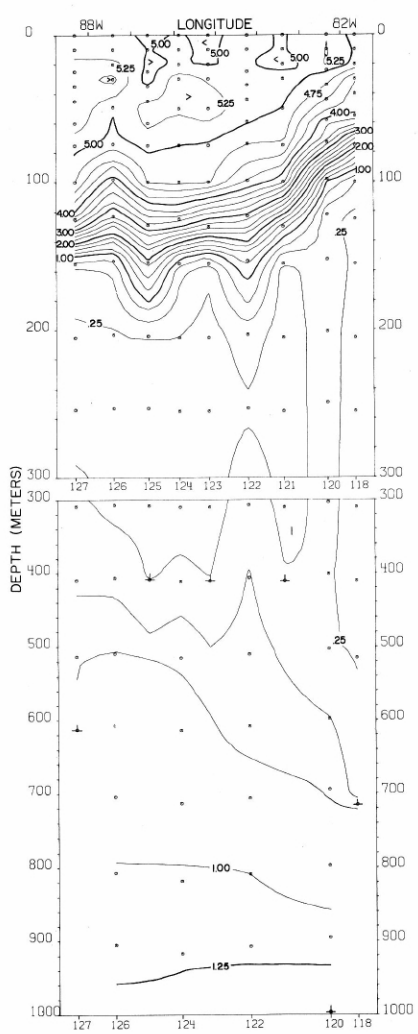

FIGURE 14-O₂-v17.—Vertical distribution of oxygen (ml./l.) along 14°30′ S. from 81°43′ W. to 88°17′ W., February 25-27, 1967.

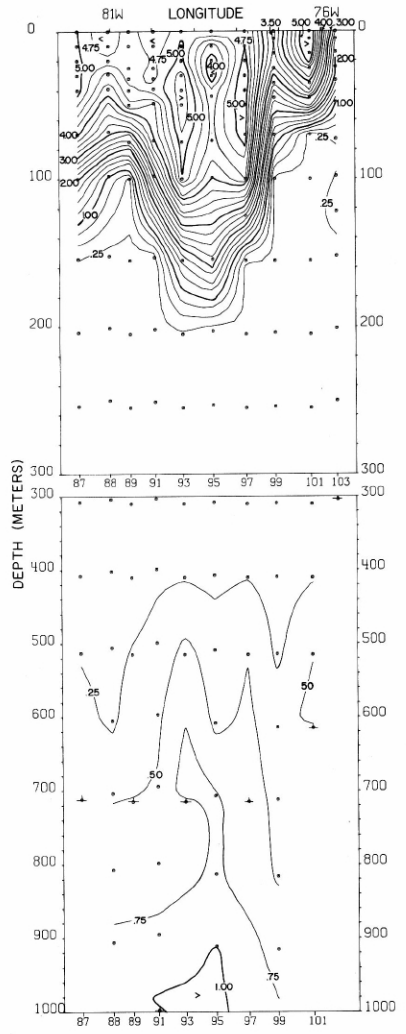

FIGURE 14-O₂-v14.—Vertical distribution of oxygen (ml./l.) along 15° S. from 81°46′ W., to the coast of Peru, February 15-17, 1967.

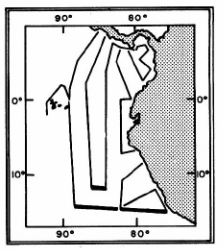

14-O₂-v14.

14-O₂-v17.

14-O₂-v25.

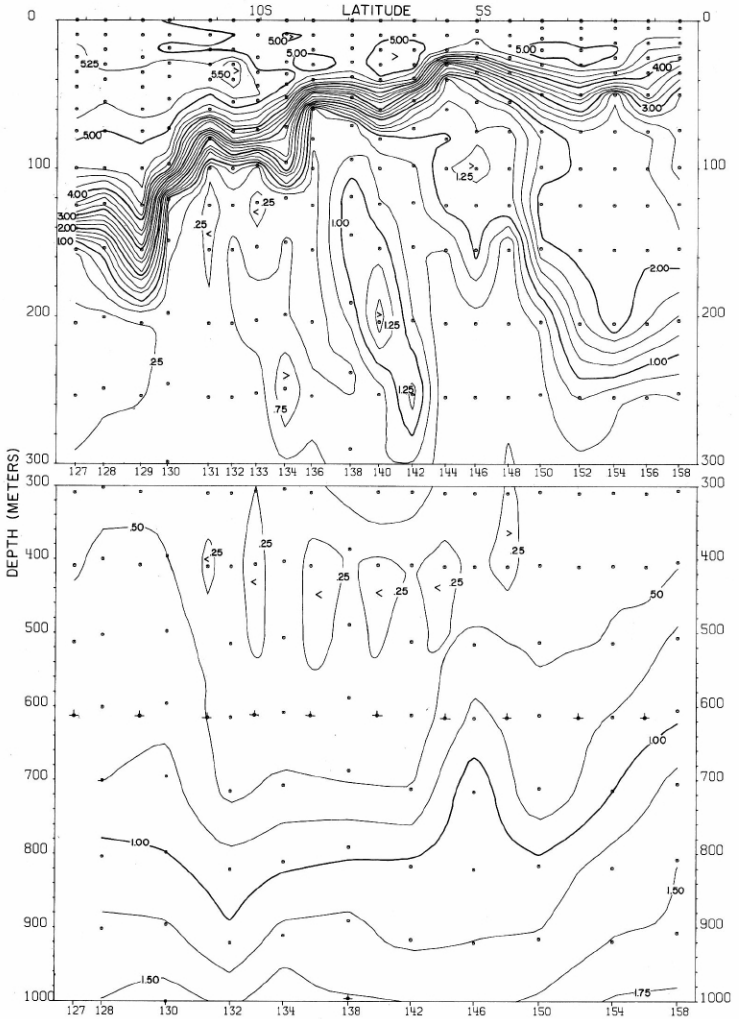

FIGURE 14-O2-v18.—Vertical distribution of oxygen (ml./l.) along 88°46′W., February 27-March 4, 1967.

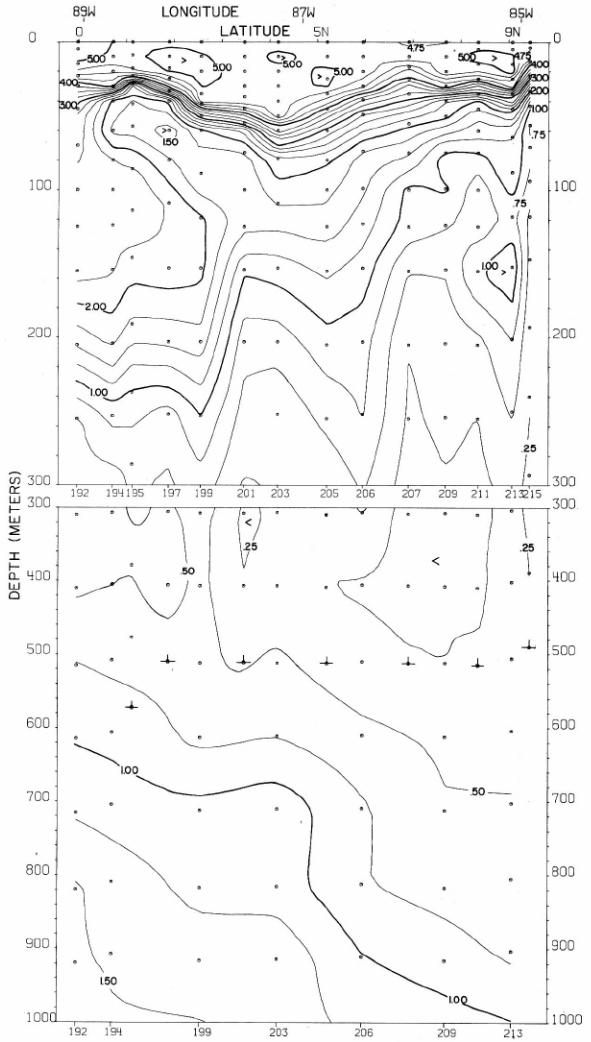

FIGURE 14-O2-v22.—Vertical distribution of oxygen (ml./l.) along a southwest-northeast section from the Equator at 89°03′ W. to Puntarenas, March 11-15, 1967.

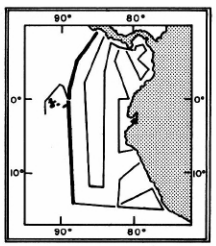

14-O2-v18.

14-O2-v22.

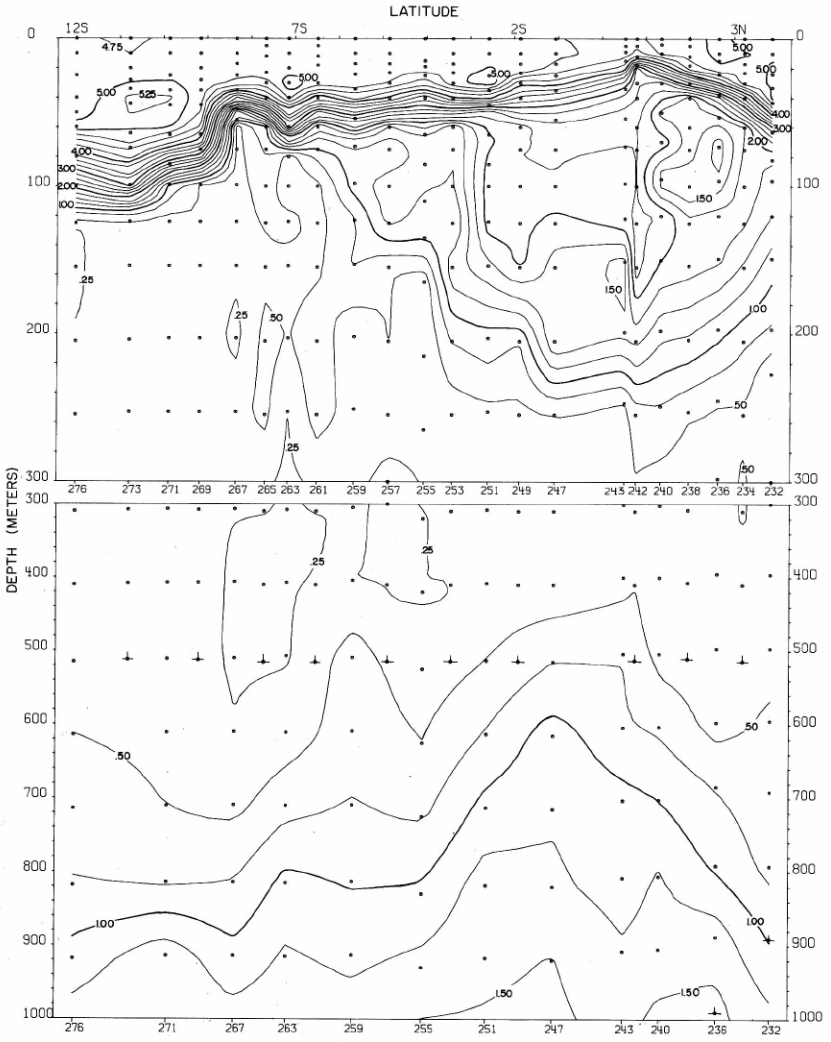

FIGURE 14-O₂-v24.—Vertical distribution of oxygen (ml./l.) along 86°19′ W., March 20-25, 1967.

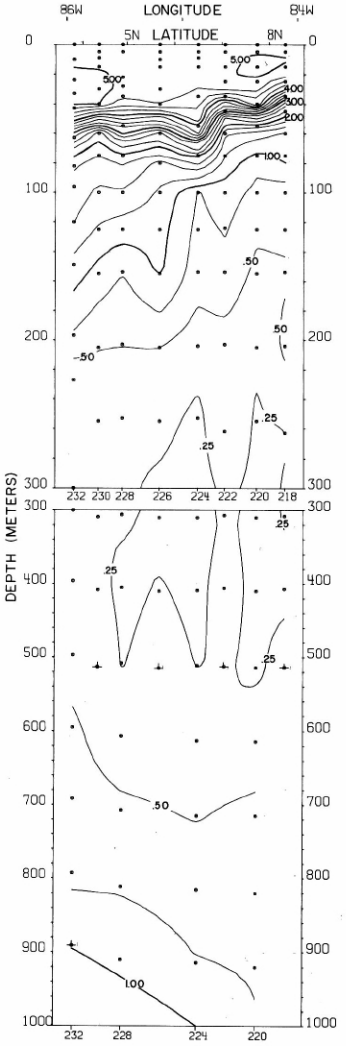

FIGURE 14-O₂-v23.—Vertical distribution of oxygen (ml./l.) along a northeast-southwest section from the coast of Costa Rica to 3°52′ N., 85°57′ W., March 18-20, 1967.

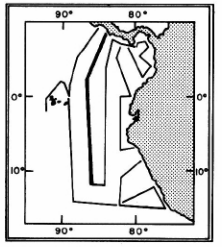

14-O₂-v23.

14-O₂-v24.

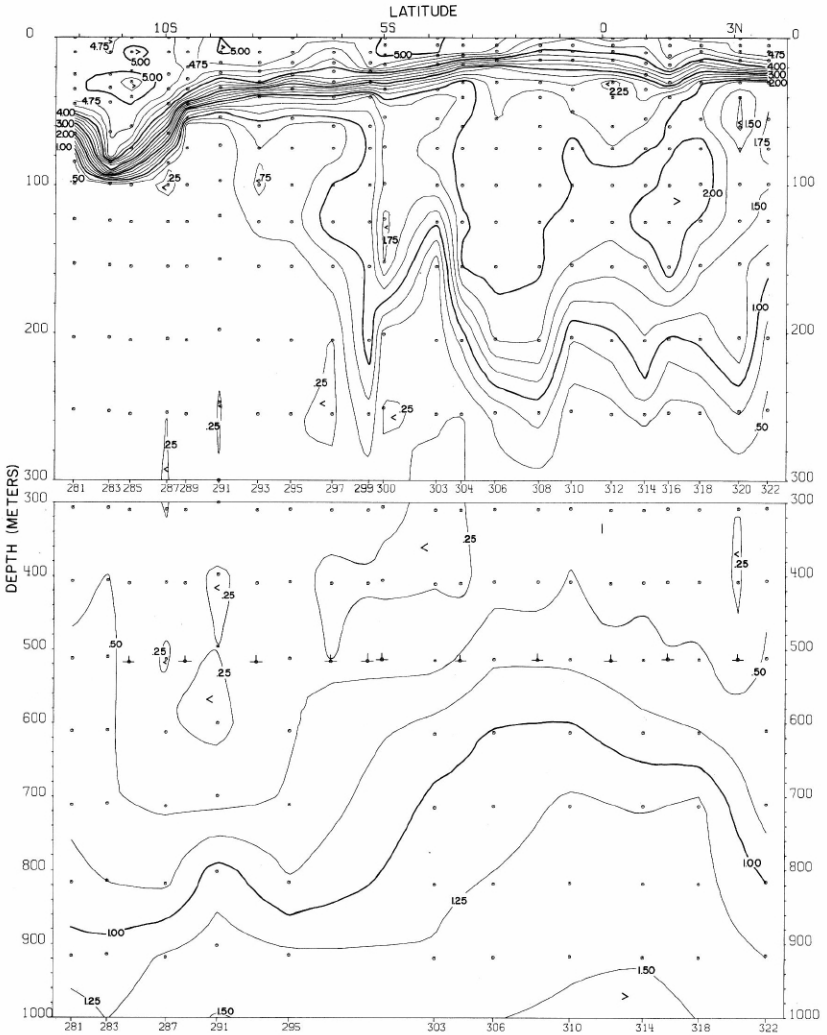

FIGURE 14-O₂-v26.—Vertical distribution of oxygen (ml./l.) along 84° W., March 26-31, 1967.

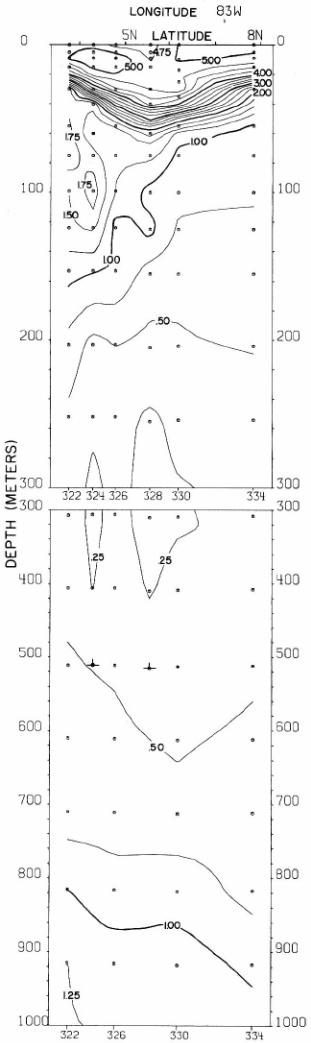

FIGURE 14-O₂-v27.—Vertical distribution of oxygen (ml./l.) along a southwest-northeast section from 3°45′ N., 83°48′ W. to Punta Burica, Costa Rica-Panama, March 31-April 2, 1967.

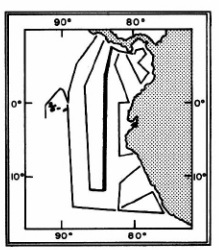

14-O₂-v26.

14-O₂-v27.